In Situ Composites of Compatibilized Polypropylene / Liquid Crystalline Polymer Blends

by

Hugh J. O'Donnell

Dissertation submitted to the Faculty of the

Virginia Polytechnic Institute and State University

in partial fulfillment of the requirements for the degree of

DOCTOR OF PHILOSOPHY

in

Chemical Engineering

APPROVED:

Dr. Donald G. Baird, Chairman

Dr. William L. Conger

Dr. Richey M. Davis

Dr. Ronald Kander

Dr. Garth L. Wilkes

December, 1993
Blacksburg, Virginia

IN SITU COMPOSITES OF COMPATIBILIZED POLYPROPYLENE / LIQUID CRYSTALLINE POLYMER BLENDS

by

Hugh J. O'Donnell

Committe Chairman: Donald G. Baird

Chemical Engineering

(ABSTRACT)

Methods of processing polypropylene (PP)/ liquid crystalline polymer blends to obtain high mechanical properties from injection molded samples were investigated in this dissertation. Three liquid crystalline polymers (LCPs), two liquid crystalline (LC) copolyesters and one LC poly(ester-amide), were used. The PP/LCP blends were compatibilized with a maleic anhydride grafted polypropylene (MAP) to enhance the mechanical properties. The effect of increasing MAP content on the mechanical properties, morphology, and interfacial tension of injection molded tensile bars and plaques made from blends with 30 wt% LCP was investigated. It was determined that MAP enhances both the tensile strength and modulus, but the tensile strength is increased to a greater degree than the tensile modulus. For the LC copolyesters, the tensile strength appeared to reach a maximum while for the LC poly(ester-amide) the tensile strength increased without limit in the range of MAP contents studied. Simultaneously, a finer dispersion was created as the MAP content was increased. Calculation of the interfacial tension from contact angle measurements indicated that the interfacial tension decreased as MAP was added to the PP matrix. Analysis of the MAP concentration after blending indicated that MAP did not

react with the LCP, but enhanced tensile properties resulted from physical interaction such as hydrogen bonding. This mechanism is consistent with the greater property improvements found in the LC poly(ester-amide) blends where the amide group is expected to undergo stronger hydrogen bonding than the ester group.

Analysis of the injection molding of these blends found that heat transfer and solidification significantly affected the flexural modulus of these blends. Injection molding conditions such as fill time, mold thickness, mold temperature and melt temperature were investigated in three molds of different thicknesses. Different processing relationships were found between the LC copolyesters and the LC poly(ester-amide). For the former LCP blends, the highest moduli were obtained from the thinnest mold in a manner parallel to that of the moduli of neat LCPs. For the latter LCP blends, the highest moduli were obtained in the intermediate thickness mold. The differences between the copolyester and LC poly(ester-amide)s processing / property relationships were related to the melt rheology of the LCPs. For the LC copolyesters, maximum mechanical properties were obtained when the melt temperature was selected so that the storage and loss moduli of the LCP were nearly equal. This equality of storage and loss moduli could not be achieved with the LC poly(ester-amide). In addition, upon cooling, the storage and loss moduli of the LC poly(ester-amide) indicated that rapid solidification occurred while a much lower rate of solidification was indicated for the LC copolyesters. In addition the mechanical properties were sensitive to the rate of cooling as indicated by the Graetz number. It was speculated that attainment of the highest mechanical properties was related to the LCP being deformed during the filling stage followed by rapid solidification of the LCP morphology upon cessation of flow.

To my wife Cheryl who's love and perseverance made this possible

and

to my children, Jennifer and Ashley, who hopefully will benefit from this experience.

Anyone who stops learning is old,

whether at twenty or eighty.

Anyone who keeps learning

stays young.

Henry Ford

Acknowledgements

The author wishes to expresses his appreciation to Professor Donald. G. Baird for his help in maintaining my focus on the objectives of this dissertation as well as the many technical discussions that led to the understanding of the topic and the eventual completion of this study. The author would like to express his appreciation to faculty of the chemical engineering, chemistry, and engineering science and mechanics departments who contributed to my eductation of polymer science and engineering. Also, thanks goes to my committee, Professors Conger, Davis, Kander, and Wilkes for contributing helpful suggestions on the direction of this research. Special thanks goes to Professor Love for reading through this dissertation and acting as a substitute during my final examination.

The author would also like to express his appreciation to the following people:

- Dr. Dimitris Collias for many discussions on droplet breakup and any other technical subject in which I needed advice.
- Soon to be Dr. Paulo De Souza for many discussions on the injection molding process as well as many other polymer processes.
- The three musketeers: Tina Handlos for the book of SEMs that I've collected (and for 'some' x-rays); Gerhard for discussions on LCP rheology and the use of optical microscopy; and Mr. Fix-It, Ed Sabol, for the wonders he performed in constructing equipment in the laboratory.

- Will Hartt for the RMS samples he used to run for me. May he find an academic job that only requires ten hours of work a day.
- Robert Young for making my last week in Blacksburg possible. I'm sure you will be a great addition to the laboratory.
- Dr. Jo Ellen Kelly DePorter for her antics and temper that made the lab so entertaining.
- Don Brandom for discussion of those things we don't do in our lab.
- Srivatson 'Watson' Srinivas for the fun we had grading Dr. Beyers papers.
- Wendel Brown for building the mold that made it possible for me to finish. Keep spinning those disks.
- Billy Williams for helping me with all the odds and ends to get things done quickly.
- Dow Chemical for providing financial support during most of my stay at Virginia Tech.

Original Contributions

The following is a list of original contributions made by the author during his study at Virginia Polytechnic Institute and State University:

- PP/LCP blends can be compatibilized with other modified polypropylene polymers which can hydrogen bond. The author proposed an acrylic acid modified polypropylene as well as demonstrated that a hindered phenol modified polypropylene enhances the mechanical properties of the blend.
- The author has shown that maleic anhydride does not directly react with LCP to achieve compatibilization.
- It was shown by the author that maleic anhydride modified polypropylene enhances the mechanical properties of PP/LCP blends, but there is a limitation to the amount of MAP that may be used. The mechanical properties of the PP/LCP blends can either reach a plateau or the properties may decrease if the content of MAP is raised too high.
- The author has shown that cooling and solidification of the LCP during injection molding affects the resulting flexural modulus of a specimen.
- Differences in the processing / property relationships between LC copolyesters and LC poly(ester-amide)s were shown to exist. The author has shown that these differences exist because of differences in the melt rheology and solidification behavior of the LCPs.

Format of Dissertation

This dissertation is written in a journal format. Chapters 3 to 6 are self-contained papers that separately describe the experiments, results and conclusions pertinent to each chapter.

Table of Contents

List of Illustrations

List of Tables

1.0 Introduction

Attainment of superior physical properties from polymers has been the focus of both past and present research. Some of this research has been directed at the synthesis of a more narrow molecular weight distributions and/or more uniform stereochemical configurations. However, attempts to improve the tensile properties of homogeneous polymers via a 'cleaner chemistry' are limited by the ability of the molecular chain to extend and retain an oriented extended conformation until a glassy state and/or semicrystalline state is achieved [1]. Thus, with the exception of gel-spun polyethylene [2,34] most flexible chain thermoplastics can not achieve significantly higher tensile properties.

An alternate means to enhance physical properties is the inclusion of a second phase. For enhanced tensile properties, the inclusion should be of a reinforcing nature. Inorganic fillers such as mica flakes and fiberglass fibers are typically used to increase the tensile properties of polypropylene, PP, nylon, and poly(ethylene terephthlate), PET. Filled polymers offer a low cost option for improved tensile properties that are suitable for thermoplastic processes such as extrusion and injection molding. The disadvantages of processing filled polymer are increased pressures (and hence energy to convey the melt), poor surface finish, erosion of equipment, unsuitability for use in processes such as film blowing or blow molding and limited potential for recycling. In addition, the adhesion between the polymer and filler phases is critical for obtaining the maximum tensile properties. Reactive modifiers are frequently added to promote adhesion between the phases via chemical reactions.

A newer method of producing higher property polymers was discovered nearly twenty years ago with the invention of a synthetic liquid crystalline polymer [3]. This wholy aromatic

polyamide polymer named Kevlar® is solution spun into a high performance fiber with tensile strength and modulus of 2.5 GPa and 120 GPa, respectively [2]. These high properties are attributed to the para aromatic structure that creates a nearly rigid rod polymer. This rigid architecture by its nature forms the extended molecular conformation that permits extensive intermolecular hydrogen bonding leading to the high mechanical properties of this polymer. While high properties are obtained from Kevlar®, the high price resulting from high monomer costs and multiple steps necessary to convert a fiber into an end use product are distinct disadvantages. These disadvantages often leave this product as a high cost alternative to reinforcing fibers such as E-glass, graphite, steel, and carbon.

1.1 Thermotropic Liquid Crystalline Polymers

Since the discovery of Kevlar, researchers have invented thermotropic liquid crystalline polymers (LCP). These polymers are created by including moieties that disrupt [19] or create kinks [17] in the otherwise rigid structure. This less than rigid structure leads to a melting point that is lower than the degradation temperature thus permitting melt processing yet offering higher use temperatures than conventional thermoplastics. These polymers offer high mechanical properties, high dimensional stability, and low coefficient of thermal expansion [48]. As a result there is significant interest in understanding and developing these polymers.

Examination of the rheology of these polymers quickly reveals that the rheology of these LCPs is dramatically different from that of thermoplastics. It is commonly stated that LCPs in the mesophase exhibit a three region flow curve that is related to the structure of the mesophase [21]. The rheology is also complicated by both a shear and thermal history dependence [22-30]

that is not observed with thermoplastics. Wissbrun [24], for example, has shown that preheating of a LCP to a temperature higher than the rheological test temperature creates a significant change in the viscosity relative to a sample tested without preheating.

Another difference for LCPs is the close relationship between the type of flow field and the orientation of the LCP. While chain extension always exists in LCPs, it is now recognized that the polymer process must be designed to orient the mesophasic domains. The ability to orient these domains depends upon both the amount of strain and the type of strain [31,36,37]. It has been shown that elongational flows are far superior to shear flows for obtaining orientation of the domains. The orientation has in turn been directly related to the elastic modulus [32,33] as shown in Fig. 1-1. Hence, processes where extensional kinematics can be accentuated should yield the highest properties from a LCP. A theoretical relationship for drawing of fibers relating the draw ratio, DR, to the orientation angle, θ, was derived by Kenig [36]. This simply relationship is shown below

$$\tan\theta = C_1 DR^{-\lambda} \qquad \textbf{(1-1)}$$

where λ is a material constant and its value indicates the relative ease of orienting the polymer. Kenig and coworkers derived other relationships for various shear flows and combined these in one of the only known simple mathematical analysis of injection molding of LCPs [37,38].

In one of the earliest reports of a LCP, Jackson and Kuhfuss [18] studied the dependence of the mechanical properties of a molded copolyester composed of 40 mol% PET and 60 mol % hydroxybenzoic acid (PET/HBA60) to the mold thickness. Two dramatic effects were noted and these results are shown in Fig. 1-2. For moldings of increasingly smaller thicknesses the machine direction flex modulus increases substantially while the transverse direction properties are reduced

slightly. Hence, high mechanical anisotropies exist for this LCP and this is a common property of oriented LCPs. It should also be noted for thick molds that the properties are much lower but they are nearly isotropic. Thus, there is a strong relationship between the mold thickness and the orientation in molds, and this creates not only high mechanical properties but also high mechanical anisotropies.

In a study of the orientation profile through the thickness of the molding it was found that the orientation profile depended upon the rigidity of the LCP [39]. For rigid LCPs containing 36% HBA moieties, a pronouced variation in the orientation from high orientation at the skin and subskin to a local minimum beneath the skin and a global minimum at the core were measured. However, for a more flexible LCP with only 15% HBA a flatter orientation profile was measured which resembled the profile of a thermoplastic molding. These orientation profiles are illustrated in Fig. 1-3. Hence, both experimentally and theoretically, the rigid nature of LCPs leads to dramatic differences in orientation distributions from that found in thermoplastics. These differences must be used advantageously when designing a polymer process.

In a key study of molding LCPs, Garg and Kenig [38] related the flex modulus of the molding to the frozen skin layer where high orientation exists. Using an equation derived by Dietz et al. [16]

$$d=2\left(\frac{T_s-T_W}{T_M-T_W}\right)(\alpha t)^{1/2} \qquad \textbf{(1-2)}$$

where the frozen layer thickness, d, is related to the melt, wall, and solidification temperature (Tm, Tw, and Ts, respectively) and where α is the thermal diffusivity and t is the time the polymer is in contact with the wall during the filling stage. Garg and Kenig varied the mold and

melt temperature to find that the flexural modulus varied directly with the temperature group shown in equation (1-2). Thus, the flex modulus scaled directly with the heat transfer responsible for freezing the orientation created in the fountain flow and high shear stress layers near the wall of the mold. Hence, heat transfer and solidification are important mechanisms for obtaining high properties from injection molded articles.

The mechanical behavior of these anisotropic LCPs may be described by composite theory. The in-plane mechanical properties surprisingly follow simple composite theory for continous unidirectional fiber reinforced lamina as shown by Ide and Chung [35] for a LCP based on HBA and hydroxynaphthoic acid (HNA). Blundell [39] showed that a molding may be mechanically modeled by sectioning a molding into lamina whose properties can be determined from X-ray data and Ward's aggregate model [4]. The modulus of these lamina are then combined using composite theory to match the tensile modulus of the molding. In summary, the mechanical properties of LCPs in moldings are very anisotropic because of the combined effect of fluid flow and solidification on the orientation profiles. However, because of the strong anisotropies the mechanical properties of these materials may be predicted from simple composite theory.

For thermoplastics, anisotropy has been minimized with the creation of biaxial processes like blow molding and film blowing. However, for LCPs fabricated in processes like injection molding, properties are anisotropic with considerably higher properties in the flow direction than in the direction transverse to flow. One exception, however, was created in moldings by control of the flow within the mold. Zachariades and Economy [41] designed a mold with a rotating wall that also translated thus providing a sweezing flow during the filling stage of injection molding. They showed by directing the flow from a center gated mold with the radially spinning and

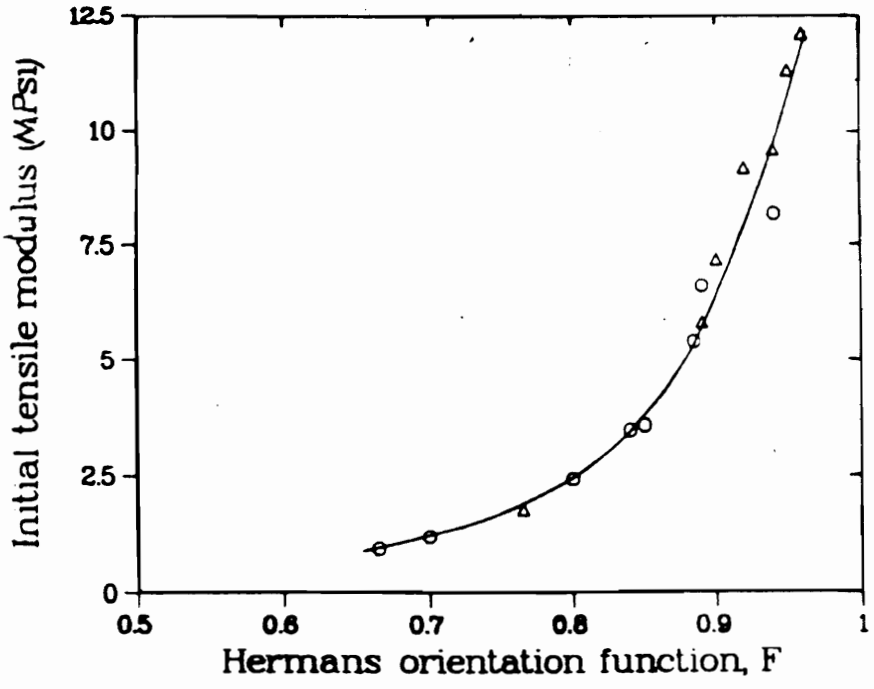

Fig. 1-1. Tensile modulus versus Hermans orientation function for a LCP: ○ standard die; △ new die [33].

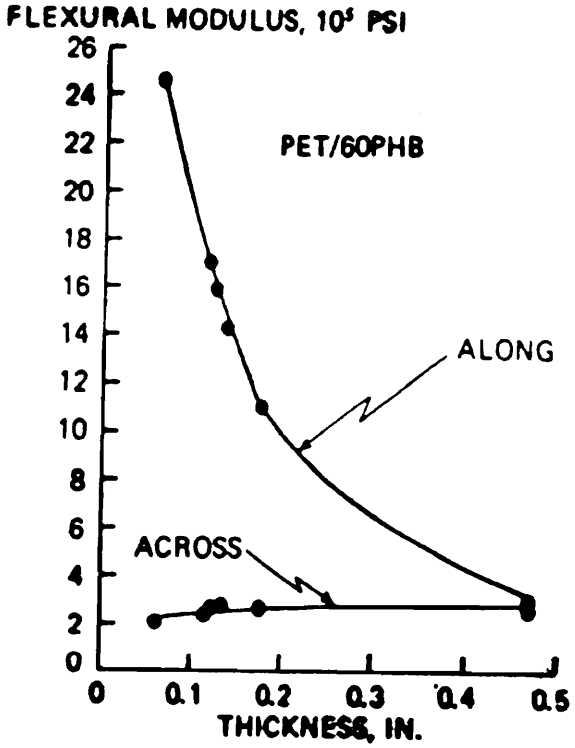

Fig. 1-2. Flex modulus versus mold thickness for machine and transverse properties [18].

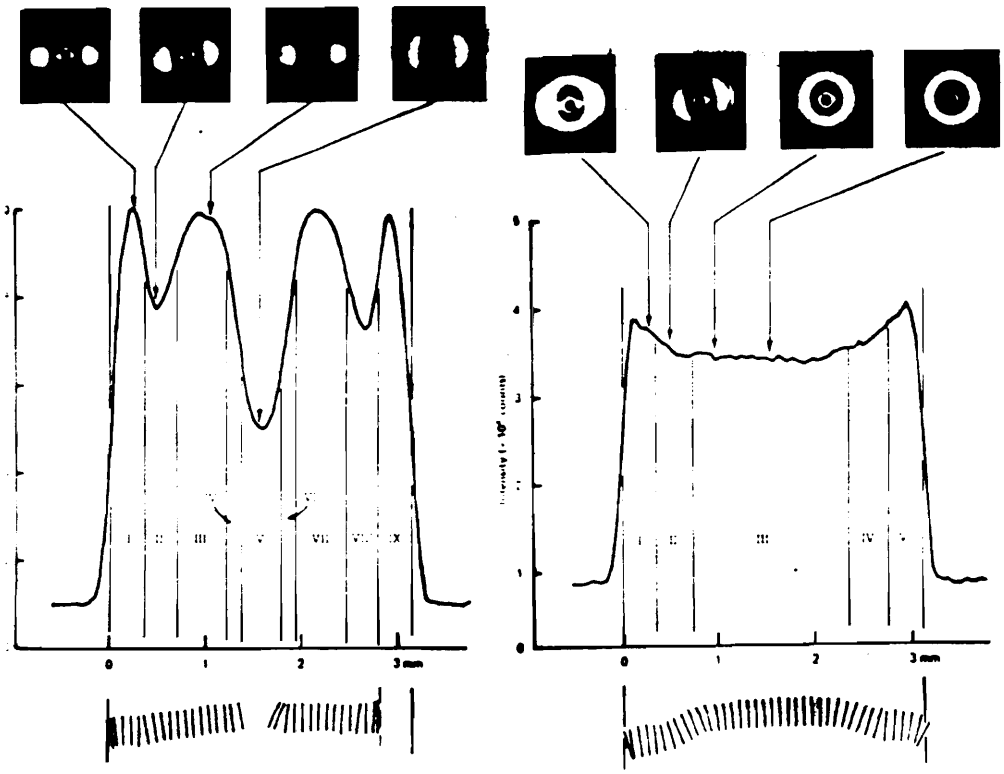

Fig. 1-3. Effect of chain rigidity on the orientation profiles of LCP moldings containing a) 36% HBA and b) 15% HBA [39].

compressing mold wall that triaxial flow and orientation could be obtained. As a result, very strong parts from both thermoplastics and thermotropic polymers were obtained. A similar study of film blowing of hydroxypropyl cellulose (HPC), a LCP, and PS made with a rotating annular film die was reported [40]. This die was capable of producing equal biaxial films of PS. Although equal biaxial properties were not obtained with HPC, the anisotropy was reduced. In summary, LCPs possess high mechanical properties in the flow direction and low properties in the transverse direction. However, if fluid can be forced to flow in multiple directions then this anisotropy can be reduced. Although anisotropy is still a potential weakness, the high properties of LCPs are creating interest for their use in not only neat forms but also in blends.

1.2 LCP Blends: In Situ Composites

The high mechanical properties and ease of processing of LCPs have led to their development as possible replacements for inorganic fillers in thermoplastics resins. This approach is especially attractive where inorganic fillers are not desired (e.g. poor surface finish or equipment erosion) or suitable (e.g. film blowing). LCP reinforcement of thermoplastic resins is accomplished by melt blending during processing with the creation of LCP fibrils within the resin. This morphology and the enhanced properties of these blends has lead to the phrase *in situ composites* to describe these materials.

Many combinations of thermoplastic resins with LCPs have been studied to date. The majority of these studies use polycarbonate (PC), polystyrene (PS), nylon, polyethylene terephthalate (PET), polyether imide (PEI) and polyether ether ketone (PEEK) resins with LCPs commercially obtained from either Hoechst Celanese, Eastman Kodak, or Unitika [42,45-54].

These commercially available LCPs are typically copolyesters or poly(ester-amides) which are primarily composed of aromatic moieties such as HBA or HNA.

One of the greatest advantages of blending LCPs with thermoplastics is the large reduction in viscosity that occurs with the addition of the LCPs [42,45,51,61,62]. The viscosity of these blends can be either intermediate to the two neat polymers [42,62] or lower than either neat polymer [42,61,62]. This drop in viscosity permits filling of intricate molds or permits higher flow rates in extrusion processes.

However, the reinforcement of blends depends on the fibrillation of the dispersed LCP phase. The process of deformation of a dispersed Newtonian phase in a Newtonian matrix has been the subject of considerable experimental and theoretical studies since 1932 [11-15]. The results may be summarized by stating that in shear flow a viscosity ratio near unity allows a droplet to readily deform and break while in extensional flow the viscosity ratio does not greatly affect the ability to deform and break a droplet. In addition, for droplet breakup to occur the hydrodynamic stresses on the surface of the drop must be greater than the restoring interfacial stresses [12,13]. This ratio of stresses is called the Weber, We, or Capillary, Ca, number and is given by the expression $\eta\dot{\gamma}R/\sigma$ where η is the viscosity, $\dot{\gamma}$ is the shear rate, R the radius of the drop, and σ the surface tension. In cases where droplets are deformed into threads, these extended shapes can remain stable in extensional flow fields for long periods of time. However, in the quiescent state these threads can readily break under the action of Rayleigh waves [12,14]. For in situ reinforcement of thermoplastics, LCPs must not only deform into fibers but must also retain this shape until solidification occurs.

Experimentally it is found that LCP blends extruded through short capillary dies develop fibrillar morphologies that reinforce the extruded strands. However, for long capillaries, e.g.

L/D of 40, only droplets emerge from the capillary and the blend is not reinforced with these morphologies [43,45,51,55]. Fibrils may also be produced in drawing processes. However, it has been shown in several studies that the LCP must be able to supercool to the drawing temperature in order for fibrillation and enhanced properties to occur [51,53,59].

Enhancement of mechanical properties also depends on the adhesion between the phases [5-9]. Blends which exhibit enhanced mechanical properties are termed compatible [5,6] and compatibility can occur because of partial miscibility between polymeric components or it can be created with the use of polymeric additives such as block copolymers or reactive polymers [5,7]. Thus, selection of components for blends should consider the ability of components to adhere or to mix at the interphase thereby creating adhesion [10]. Blends which exhibit partial miscibility often have good adhesion and enhanced mechanical properties. However, the mechanical properties of immiscible blends are often poor and these blends display large dispersed phase sizes and fiber pullout upon fracture [42,44,56-58]. A typical example contrasting the mechanical properties of a partially miscible PC and LCP blend versus an immiscible PS and LCP blend is shown in Fig. 1-4. This figure shows that the tensile strength of the partially miscible PC blend exhibits strength equal to or greater than the additivity of the two neat polymers. However, the strength of the immiscible PS blend is low over the entire composition range. While polymeric compatibilizers have been used in thermoplastic blends for some time [5-9] there is only one LCP blend that uses a compatibilizing agent [57,58]. The compatibilizer is a maleic anhydride grafted PP which has successfully enhanced the tensile modulus and strength of polypropylene (PP) with three LCPs. Properties for uncompatibilized and compatibilized PP/Vectra B950 blends are shown in Table 1-1 [58].

The type of mixing can also enhance the mechanical properties of LCP blends. Various

Table 1-1. Tensile properties of PP(MHG)/Vectra B950 blends [58].

Tensile Properties of PP/Vectra B Tensile Bars w/w.o Compatibilization

Materials	Tensile Modulus GPa	Tensile Strength MPa	Elong. Yield %	Tough-ness KJ/cum
PP	1.369	31.24		427 *
PP/Vectra B 80/20	2.876 (0.089)	26.45 (0.34)	2.27	660
PP/Vectra B 80/20 (Comp)	3.295 (0.188)	36.85 (0.98)	2.00	786
PP/Vectra B 70/30	3.674 (0.395)	27.26 (2.28)	1.50	681 *
PP/Vectra B 70/30 (Comp)	5.280 (0.555)	50.31 (1.97)	1.47	370
PP/Vectra B 50/50	6.474 (0.825)	38.78 (4.07)	0.98	675
PP/Vectra B 50/50 (Comp)	7.832 (0.640)	58.69 (6.26)	1.04	362
PP/Vectra B 20/80	12.97 (0.536)	78.23 (7.7)	0.85	568
PP/Vectra B 20/80 (Comp)	14.46 (2.203)	112.0 (6.53)	1.04	777
Vectra B	21.98 (1.543)	227 (32.0)	1.00	1187

Standard Deviations are given in parenthesis.
(Comp) - Compatibilized
Toughness till 3 % indicated by (*)

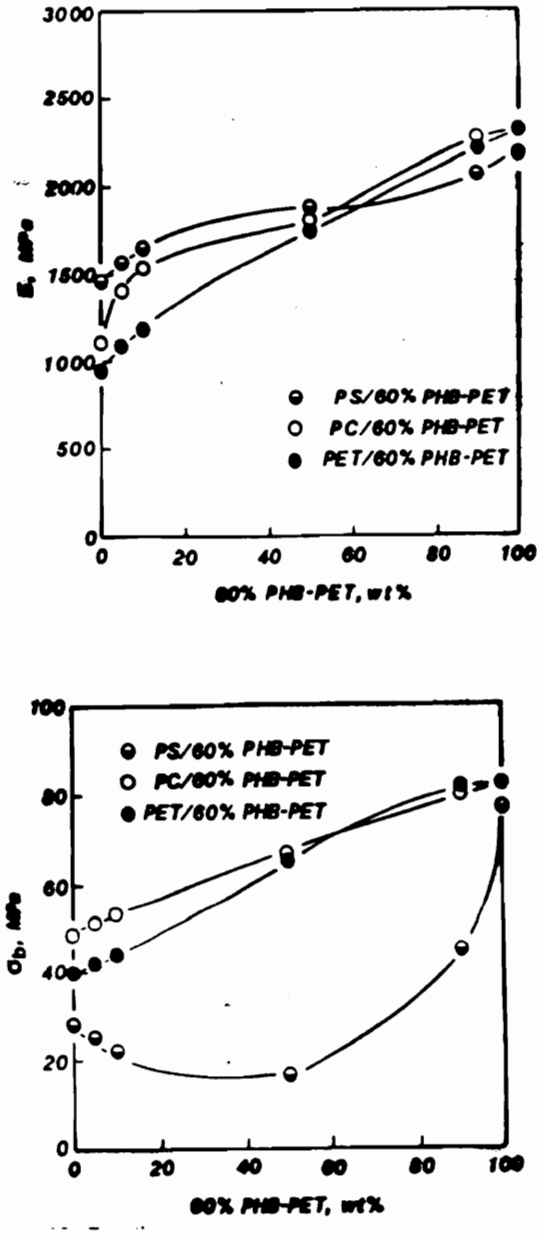

Fig. 1-4 Tensile modulus (a) and tensile strength (b) of PC and PS blends with PET/HBA60 [42].

mixing devices [50,51,59,63] or methods [63,64] have been used resulting in improved properties. For instance, comparison of properties from blends extruded and mixed with a static mixer have shown higher properties than blends mixed in a internal mixer [50,51]. The manner in which an extruder is operated also can result in significant improvements in mechanical properties. For instance, Ko and Wilkes [64] using an extruder connected to a gear pump and a film die showed that the screw speed can significantly change the morphology of the dispersed LCP phase. As the screw speed increased, independently of flow rate, the LCP phase gradually changed from droplets to fibers with corresponding increases in properties. Thus, mixing must be considered when blending a LCP / thermoplastic resin.

1.3 In Situ Composites of Polypropylene

LCP blends offer several advantages over thermoplastic resins or filled thermoplastic resins, and the PP/LCP blends offer these same advantages. Similarly, LCP reinforced PP blends have some of the same disadvantages of other LCP blends. This dissertation will explore the benefits and disadvantages of PP/LCP in situ composites which are fabricated via the injection molding process.

The first advantage of creating LCP blends with PP is that addition of small percentages of LCP to PP may reduce the viscosity of the blend [62]. This can lead to the ability to fill complicated molds or the ability to increase extrusion rates. Hence, there is an interest in using LCP blends for control of thermoplastic resin viscosity almost regardless of mechanical properties [62]. The second advantage is that the LCP can increase the mechanical properties of PP. With the large annual consumption of PP, development of a PP/LCP blend with enhanced properties

can be of great interest to the industrial community. The third advantage is that the use of LCP blends can lead to a higher surface finish compared to filled systems which often exhibit a rough surface appearence. For instance, although blends of PP with LCP do not exhibit good surface appearance these blends can be converted into blends possessing excellent surface finishes through compatibilization. This was demonstrated with an anhydride functionalized PP compatibilizer [57]. The fourth advantage is that LCP blends may offer the opportunity for recycling while additional processing of glass filled systems result in continual fiber breakage and loss of mechanical properties [48]. Hence, the PP/LCP system offers several distinct advantages in comparison to filled PP systems.

There are, however, several disadvantages with the PP/LCP blends. The first disadvantage is common to all LCP blends. This shortcoming is the highly anisotropic nature of in situ composites created during processing. While high tensile properties exist in the machine direction, the tensile properties in the transverse direction can be a fraction of these values. Development of a transversely isotropic material is needed for all in situ composites. The second disadvantage of the PP blends is the limited stability of PP at the processing temperatures required for most LCPs. This limits the range of temperatures and residence times that can be used with these blends. The third disadvantage of these blends is a modulus that does not equal or exceed that of glass-filled PP systems. Development of a process to increase this modulus would greatly enhance the replacement of fiber-filled systems with the LCP blends. The final disadvantage of the PP/LCP blends is that the strength is low compared to the strength of fiber-filled systems. A comparison of the mechanical properties of PP/LCP blends and PP/fiber-filled systems is shown in Table 1-2.

Table 1-2. Comparison of mechanical properties of glass-filled PP and LCP reinforced PP [58].

Mechanical Properties of Fiber-Filled PP and MHG Compatibilized PP/LCP Blends				
Material	%Glass or %LCP	Ten. Str. (MPa.)	Ten. Mod. (GPa.)	Flex Mod. (GPa.)
PP/GLASS	20	83	4.8-6.9	4.4
	30	97	4.8-6.9	7.0
PP/VB	20	37	3.3	n.a.
	30	50	5.3	n.a.
PP/VA	20	37	3.8	n.a.
	30	50	4.3	n.a.

1.4 Research Objectives

The prior section identified four shortcomings of compatibilized blends of PP and LCP. Of the four identified shortcomings, two of these areas will be addressed. The first three objectives will investigate how and to what extent compatibilization can improve the tensile properties of PP / LCP blends. The last two objectives will address the effect of injection molding conditions on the development of structure and properties in injection molded specimens. A particular goal will be to generate higher modulus blends from a mold with a smaller thickness; this may be at the expense of mechanical anisotropy. With this introduction, the objectives for this dissertation are as follows:

1. Determine how the amount of compatibilizer in the matrix affects the mechancial properties of the blend.
2. Determine whether the presence of compatibilizer leads to reduced interfacial tension and enhanced adhesion between the phases.
3. Determine whether compatibilization occurs as a result of physical interaction or chemical reaction.
4. Determine whether the mechanical properties of TP/LCP blends are sensitive to injection molding conditions and whether higher mechanical properties than previously reported can be obtained.
5. Determine whether the changes in the structure and mechanical properties of moldings made under various molding conditions can be related to droplet deformation and heat transfer.

1.5 References

1 G. Allegra, "Conformational Considerations of High-Modulus Polymers," Poly. Eng. Sci., 15(3), 207 (1975).

2 P.J. Barham and A. Keller, "Review: High-strength Polyethylene Fibres From Solution and Gel Spinning," J. Mater. Sci. 20, 2281 (1985).

3 S.L. Kwolek, U.S. Patent 3671542 (1972).

4 I.M. Ward, "Optical and Mechanical Anisotropy in Crystalline Polymers," Proc. Phys. Soc., 80, 1176 (1962).

5 N.G. Gaylord, "Compatibilizing Agents: Structure and Function in Polyblends," J. Macromol. Sci., Chem., A26(8), 1211 (1989).

6 A.Y. Coran and R. Patel, Rubber Chem. Technol., 56, 1045 (1983).

7 R.L. Markham, "Introduction to Compatibilization of Polymer Blends", Advances in Polymer Technology, 10(3), 231 (1990).

8 M. Xanthos, "Interfacial Agents for Multiphase Polymer Systems: Recent Advances," Polym. Eng. Sci., 28(21), 1392 (1988).

9 B.D. Favis, "Polymer Alloys and Blends: Recent Advances," Can. J. Chem. Engr., 69, 619 (1991).

10 S. Meretz, M. Kwiatkowski, G. Hinrichsen, "Production and Characterization of Fine-Dispersed Mixtures of Liquid Crystalline with Conventional Polymers," Intern. Polym. Proc., VI, 239 (1991).

11 G.I. Taylor, "The Viscosity of a Fluid conataining Small Drops of Another Fluid," Proc. Roy. Soc., A138, 41 (1932).

12 G.I. Taylor, "The Formation of Emulsions in Definable Fields of Flow," Proc. Roy. Soc. A146, 501 (1934).

13 F.D. Rumscheidt and S.G. Mason, "Particle Motion in Sheared Suspensions XII," J. Coll. Sci., 16, 238 (1961).

14 S. Tomotika, "On the Instability of a Cylindrical Thread of a Viscous Liquid Surrounded by Another Viscous Fluid," Proc. Roy. Soc., 150, 322 (1935).

15 W.J. Milliken and L.G. Leal, "A Note on the Effect of Vorticity on the Deformation and Breakup of Polymer Drops," J. Non-Newtonian Fluid Mech., 42, 231 (1992).

16 W. Dietz, J.L. White, and E.S. Clark, "Orientation Development and Relaxation in Injection Molding of Amorphous Polymers," Polym. Eng. Sci., 18(4), 273 (1978).

17 M.C. Muir, and R.S. Porter, "Processing Rheology of Liquid Crystalline Polymers: a Review," Mol. Cryst. Liq. Cryst., 169, 83 (1989).

18 W.J. Jackson and H.F. Kuhfuss, J. Polym. Sci., Polym. Chem. Ed., 14, 2043 (1976).

19 G.W. Calundann and M. Jaffe, "Anisotropic Polymers, Their Synthesis and Properties," Proceedings of the Robert A. Welch Conference on Chemical Research, XXVI. Synthetic Polymers, (1982).

20 T. Asada, S. Onogi, H. Yanase, "A Rheooptical Study of the Reformation of

Structure in Racemic Poly(γ-benzyl glutamate) Liquid Crystals," Poly. Eng. Sci., 24(5), 355 (1984).

21 T. Asada, H. Muramatsu, R. Watanabe, and S. Onogi, "Rheooptical Studies of Racemic Poly(γ-benzyl glutamate) Liquid Crystals," Macromolecules, 13, 867 (1980).

22 K.F. Wissbrun, G. Kiss, and F.N. Cogswell, "Flow Behavior of a Thermotropic Liquid Crystal Aromatic Copolyester," Chem. Eng. Comm., 53, 149 (1987).

23 D.G. Baird, "Concepts in Rheological Studies of Polymeric Liquid Crystals," in Polymeric Liquid Crystals, A. Blumstein, Ed., Plenum Press, New York (1983).

24 K.F. Wissbrun, "Observations on the Melt Rheology of Thermotropic Aromatic Polyesters," Brit. Poly. J., 12(4), 163 (1980).

25 D. Done and D.G. Baird, "The Effect of Thermal History on the Rheology and Texture of Thermotropic Liquid Crystalline Polymers," Polym. Eng. Sci., 27(11), 816 (1987).

26 D. Done and D.G. Baird, "Solidification Behavior and Recovery Kinetics of Liquid Crystalline Polymers," Polym. Eng. Sci., 30(16), 989 (1990).

27 Y.G. Lin and H.H. Winter, "Formation of a High Melting Crystal in a Thermotropic Aromatic Copolyester," Macromolecules, 21, 2439 (1988).

28 Y.G. Lin and H.H. Winter, "High-Temperature Recrystallization and Rheology of a Thermotropic Liquid Crystalline Polymer," Macromolecules, 24, 2877 (1991).

29 K.F. Wissbrun and A.C. Griffin, "Rheology of a Thermotropic Polyester in the Nematic and Isotropic States," J. Polym. Sci. Polym. Phys. Ed., 20, 1835 (1982).

30 F. Cocchini, M.R. Nobile, and D. Acierno, "Transient and Steady Rheological behavior of the Thermotropic Liquid Crystal Copolymer 73/27 HBA/HNA," J. Rheol., 35(6), 1171 (1991).

31 Y. Ide and Z. Ophir, "Orientation Development in Thermotropic Liquid Crystal Polymers," Poly. Eng. Sci., 23(5), 261 (1983).

32 T-S. Chung, "Fluid Behavior and Orientation Developments During Extrusion of Liquid Crystal Polymeric Rods," J. Polym. Sci.: C Polym. Lett., 24, 299 (1986).

33 T-S. Chung, "Production of Ultrahigh Modulus Liquid Crystal Polymer Rods," J. Polym. Sci.: Part B: Polym. Phys., 26, 1549 (1988).

34 E.G. Joseph, G.L. Wilkes, and D.G. Baird, "Effect of Flow History on the Morphology of Thermotropic Liquid Crystalline Copolyesters," Poly. Eng. Sci., 25(7), 377 (1985).

35 Y. Ide, and T-S. Chung, "Macromolecule Composites of Extruded Thermotropic Polymer Sheets," J. Macromol. Sci, Phys. Ed., B23(4-6), 497 (1985).

36 S. Kenig, "Orientability of Liquid Crystal Polymers in Elongational Flow," Poly. Eng. Sci., 27(12), 887 (1987).

37 S. Kenig, "Shear-Induced Orientation in Liquid Crystalline Polymers," Poly. Eng. Sci., 29(16), 1136 (1989).

38 S.K. Garg and S. Kenig, "Development of Orientation During Processing of

Liquid Crystalline Polymers," in High Modulus Polymers, A.E. Zachariades, R.S. Porter, Eds., Marcel Dekker, New York, 1988: pg. 71.

39 D.J. Blundell, R.A. Chivers, A.D. Curson, J.C. Love, and W.A. MacDonald, "The Relationship of Chain Linearity of Aromatic Liquid Crystal Polyesters to Molecular Orientation and Stiffness of Mouldings," Polymer, 29, 1459 (1988).

40 G.W. Farell and J.F. Fellers, "A Rotating Annular Die to Control The Biaxial Orientation in Melt Processed Thermotropic Liquid Crystalline Cellulose Derivatives," J. Polym. Eng., 6(1-4), 263 (1986).

41 A.E. Zachariades and J. Economy, "Super Strong Polymers in Planar Directions," Poly. Eng. Sci. 23(5), 266 (1983).

42 P. Zhuang, T. Kyu, and J.L. White, "Characteristics of Hydroxybenzoic Acid - Ethylene Terephthalate Copolymers and Their Blends With Polystyrene, Polycarbonate, and Polyethylene Terephthalate," Poly. Eng. Sci., 28(17), 1095 (1988).

43 A. Kohli, N. Chung, and R. A. Weiss, "The Effect of Deformation History on the Morphology and Properties of Blends of Polycarbonate and a Thermotropic Liquid Crystalline Polymer," Polym. Eng. Sci., 29(9), 573 (1989).

44 A. Valenza, F.P. La Mantia, M. Paci, and P.L. Magagnini, "Processing and Properties of Polycarbonate / Liquid Crystal Polymer Blends," Intern. Polym. Proc. VI(3), 247 (1991).

45 A. Siegmann, A. Dagan, and S. Kenig, "Polyblends Containing a Liquid Crystalline Polymer," Polymer, 26, 1325 (1985).

46 R.A. Weiss, W.H. Huh, and L. Nicolais, in High Modulus Polymers, Marcel Dekker, New York, 1988.

47 D. Dutta, H. Fruitwala, A. Kohli, and R.A. Weiss, "Polymer Blends Containing Liquid Crystals: A Review," Polym. Eng. Sci., 30(17), 1005 (1990).

48 D.J. Williams, "Applications for Thermotropic Liquid Crystal Polymer Blends," Adv. Polym. Tech., 10(3), 173 (1990).

49 V.G. Kulichikhin, and N.A. Plate, "Blend Composites Based on Liquid Crystal Thermoplasts. Review," Polym. Sci. U.S.S.R., 33(1), 1 (1991).

50 A.I. Isayev and M. Modic, "Self-Reinforced Melt Processible Polymer Composites: Extrusion, Compression, and Injection Molding," Polym. Comp., 8(3), 158 (1987).

51 M.R. Nobile, E. Amendola, and L. Nicolais, "Physical Properties of Blends of Polycarbonate and a Liquid Crystalline Copolyester," Polym. Eng. Sci., 29(4), 244 (1989).

52 O. Federico, "In Situ Composites of a Thermotropic Liquid Crystalline Polymer and Polycarbonate: Processing, Morphology and Properties," Ph.D. Dissertation, Univ. of Massachusetts, Amherst, MA. (1989).

53 K.G. Blizard, C. Federici, O. Federico, and L.L. Chapoy, "The Morphology of Extruded Blends Containing a Thermotropic Liquid Crystalline Polymer", Poly. Eng. Sci., 30(22), 1442 (1990).

54 F.P. La Mantia, M. Saiu, A. Valenza, M. Paci, and P.L. Magagnini, "Relationships Between Mechanical Properties and Structure for Blends of Nylon-6 with a Liquid Crystal Polymer," Eur. Polym. J., 26(3), 323 (1990).

55 K.G. Blizard and D.G. Baird, "The Morphology and Rheology of Polymer Blends Containing a Liquid Crystalline Copolyester," Poly. Eng. Sci., 27(9), 653 (1987).

56 M. Paci, M. Liu, P.L. Magagnini, F.P. La Mantia, and A. Valenza, "Compatibility of Blends of Poly(Butylene Terephthalate) and Liquid Crystal Polymers: A DSC Study," Thermochimica Acta, 137, 105 (1988).

57 A. Datta, J.P. De Souza, A.M. Sukhadia, and D.G. Baird, "Processing Studies of Blends of Polypropylene with Liquid Crystalline Polymers," Annual Technical Conference of the Society of Plastic Engineers (ANTEC '91), 49, 913 (1991).

58 H.J. O'Donnell, A. Datta, D.G. Baird, "The Effect of Compatibilization on the Properties of Blends of LCPs with Polypropylene," Annual Technical Conference of the Society of Plastic Engineers (ANTEC'92), 50, 2248 (1992).

59 A.M. Sukhadia, A. Datta, and D.G. Baird, "Generation of Continuous Liquid Crystalline Polymer Reinforcements in Thermoplastics by a Novel Blending Process," Annual Technical Conference of the Society of Plastic Engineers (ANTEC'91), 49, 1008 (1991).

60 C.D. Han, Multiphase Flow in Polymer Processing, Academic Press, New York (1981).

61 F.P. La Mantia, a. Valenza, M. Paci, and P.L. Magagnini, "Rheology-Morphology Relationships in Nylon 6/Liquid-Crystalline Polymer Blends," Polym. Eng. Sci., 30(1), 7 (1990).

62 F.P. La Mantia, A. Valenza, and P.L. Magagnini, "Liquid Crystal Polymer-Based Blends: Universal Grade Polymers?," J. Appl. Polym. Sci., 44, 1257 (1992).

63 G. Kiss, "In Situ composites Blends of Isotropic Polymers and Thermotropic Liquid Crystalline Polymers," Poly. Eng. Sci., 27(6), 410 (1987).

64 C.U. Ko and G.L. Wilkes, "Morphological Studies of Blends Containing Liquid Crystalline Polymers with Poly(ethylene Terephthalate)," J. Appl. Polym. Sci., 37, 3063 (1989).

2.0 Literature Review

2.1 General Features of Polymer Blends

When mixing two polymers, like mixing of two low molecular weight fluids, the mixture may result in a thermodynamically miscible or partially miscible state. However, full thermodynamic miscibility of two polymers is rarely obtained and partially miscible or immiscible systems are more commonly favored. Because mechanical properties are often superior in blends that exhibit some degree of miscibility, a quest is often to enhance miscibility or to create favorable interactions at the interface. This process is called compatibilization, and it is a developing area that will lead to improving the properties of polymer blends. Since enhanced mechanical properties are the result of changes at the interface, a knowledge of the interfacial tension and work of adhesion is important. The following section is divided into an examination of the miscibility of polymer blends, a survey of the compatibilization of immiscible blends, and a review of the important aspects of the interface.

2.1.1 Miscibility of Polymers

The most widely used thermodynamic equation for polymer solutions is the Flory - Huggins equation. This equation was derived from a lattice statistics model where the probability of locating polymer repeat units contiguously on a lattice that is otherwise filled with solvent molecules determines the entropy. In addition, the athermal solutions assumption was modified by including an enthalpic contribution that accounted for interaction of molecular segments between adjacent lattice sites. Its magnitude is adjusted with the parameter χ_{12}. For polymer blends, the form of this equation is often written as

$$\Delta G_m = RT\frac{V}{V_r}\left[\frac{\phi_1}{N_1}\ln\phi_1 + \frac{\phi_2}{N_2}\ln\phi_2 + \chi_{12}\phi_1\phi_2\right] \quad \textbf{(2-1)}$$

where V is the solution volume, V_r is the lattice cell or repeat unit volume, ϕ_i is the volume fraction for the i^{th} component, and N_i is the degree of polymerization of the i^{th} polymer component. The first two terms of this equation are negative and favor mixing. For high molecular weight polymers, however, the first two terms become exceedingly small and the balance between these entropic terms and the enthalpic term determines the miscibility of polymers. For miscibility to occur, χ_{12} must therefore approach zero or become negative. For most mixtures of homopolymers, chi is positive and polymers are not miscible [8]. Some exceptions to this rule exist and are mentioned later in this section. Since proposal of this equation, many modifications have been developed. One significant modification is the expansion of χ_{12} to treat polydisperse mixtures. Some introduction to this material can be found in reference [12].

Much of the experimental use of the Flory-Huggins equation is centered on obtaining χ_{12}. Often this is approximated from relationships with the Hilderbrand solubility parameter, δ, which is related to the cohesive energy density of a component and which may be estimated based on group contribution methods [19,20]. This relationship is written below

$$\chi_{12} = \frac{V_1^0}{RT}(\delta_1 - \delta_2)^2 \quad \textbf{(2-2)}$$

It is noted from the above, that this relationship always predicts a positive value for χ_{12}. While the solubility parameter approach leads to positive heats of mixing and hence immiscible blends,

two common examples are cited as exceptions to the rule that polymers are immiscible. The first type of blend is a system that contains specific interactions which lead to negative heats of mixing. These interactions may be of several types, e.g. dipole-dipole interactions, acid-base interactions, but H-bonding is the most commonly cited mechanism. An example of this mechanism is a blend of poly(vinyl chloride) with polycaprolactone where hydrogen bonding causes a 4-6 cm^{-1} shift in the infrared carbonyl absorption band of the polycaprolactone [8]. The second type of miscible blend is a mixture that contains a block copolymer and a homopolymer. The interaction between segments of the copolymer consists of largely repulsive energies. Miscibility occurs using this type of copolymer because a lower enthalpy results when dissimilar segments of the copolymer mix with the homopolymer and dissimilar segments separate. In this condition, interactions between copolymer and homopolymer are less unfavorable than between segments of the copolymer [8].

For rigid rod polymers, Flory recognized an inherent difference between the location that rigid rod segments could occupy on a lattice versus the location that flexible chain segments could occupy on a lattice. Accordingly, he derived theories specialized to liquid crystalline polymers [13-18]. For a ternary blend that includes a rigid rod polymer, a flexible chain polymer and solvent, Flory and coworkers concluded that miscibility was unfavorable and a phase separated mixture would be the prevalent equilibrium state [17]. Thus, it is doubtful that partial miscibility would exist for LCPs based on this analysis. However, as will be reviewed in section 2.5.2 partial miscibility can exist in blends with LCPs.

In many cases, the determination of miscibility must rely on an experimental technique. There are several techniques to determine miscibility [7,9,22]. One of the easiest and most widely used experimental techniques is the detection of the glass transition temperature. For miscible

systems only one glass transition temperature exists. This transition temperature occurs between that of the two homopolymers and often it can be related to the composition, w_i , and homopolymer glass transition temperatures, $Tg_{,i}$ through the Fox equation [21]

$$\frac{1}{T_{g,b}} = \frac{w_1}{T_{g,1}} + \frac{w_2}{T_{g,2}} \qquad \textbf{(2-3)}$$

Conversely for immiscible blends two glass transition temperatures are observed, and are the same as the transition temperatures of the homopolymers. The existence of partial miscibility, hence, exhibits some shifting of the glass transition temperature with composition. In dynamic mechanical thermal analysis in addition to the shifting of the Tg a corresponding broadening of the loss peak occurs. This broadening has been related to increased compositional variation, i.e. molecular mixing, of the blend [22].

While detection of the shifts in the glass transition temperatures is widely used, a second method relying on the rheological variations with concentration is also used. For a miscible system the logarithmic rule of mixtures generally holds

$$\ln\eta_{BL} = w_1 \ln\eta_1 + w_2 \ln\eta_2 \qquad \textbf{(2-4)}$$

and for immiscible mixtures a parallel model generally holds [27]

$$\frac{1}{\eta_{BL}} = \frac{w_1}{\eta_1} + \frac{w_2}{\eta_2} \qquad \textbf{(2-5)}$$

Testing for such behavior in a LCP 'blend' composed of differing ratios of HBA and HNA copolyesters was studied by de Meuse and Jaffe [23]. According to thermodynamic theory [24-26], blends of copolymers are miscible only when the composition ratios are similar. Using blends of i) 58/42 and 75/25% HBA/HNA and blends of ii) 30/70 and 75/25% HBA/HNA, de Meuse and Jaffe, studied the rheological properties of the blends to determine if miscibility exists.

From torque measurements in a Haake-Buchler Rheocord, they determined both the power law exponent and the viscosity. The viscosity was plotted and compared to equations (6) and (7). As might be expected, the former blend, (i), approximately fit equation (6). In addition the power law exponent at all ratios reported only varied from .44 to .48. In contrast, the rheological behavior for the second blend, (ii), fit equation (7). The power law exponent in this blend was not constant but varied with the blend ratio from .37 to .55. Thus, de Meuse and Jaffe concluded from this data, and X-ray data that will not be reviewed here, that the former system is miscible and the latter system immiscible in agreement with the trend indicated by thermodynamic theory.

In summary, polymer blends are generally found to be immiscible because of low entropic energies and small positive enthalpic contributions to the Gibbs free energy of mixing. However, partial miscibility and completely miscible systems do exists. In these cases, specific interaction may exist between the polymers.

2.1.2 Compatibilization

While most polymeric blends are immiscible, they can often show improved mechanical properties. Hence, the term compatibility generally refers to blends that exhibit useful mechanical properties. This generally indicates that some mixing occurs at the interphase which leads to adhesion between the phases. In cases where this does not occur, techniques referred to as compatibilization are employed. These techniques involve the use of a third component that either has segments with similar solubility parameters to the blended polymers (i.e. $\Delta\delta < 1.0$) or has specific interactions leading to covalent, ionic, or hydrogen bonding [28]. Often these

components are block copolymers or graft polymers. Although this does not lead to a miscible system it does lead to improved physical properties which is the goal of compatibilization. Coran and Patel [29] refer to this goal as 'technological compatibilization'. They describe this effort as follows:

> "Technological compatibilization is the result of a process or technique for improving ultimate properties by making polymers in a blend less incompatible; it is not the application of a technique which induces 'thermodynamic compatibility' which would cause the polymers to exist in a single molecularly blended homogeneous phase."

In a recent review of compatibilization of blends, Markham [30] discussed both nonreactive and reactive (or interactive) compatibilizers. The basis of nonreactive compatibilization is the miscibility of segments of a polymer in each of the homopolymers to be blended while the basis of reactive compatibilization is the creation of either covalent bonds between the blended polymers or the creation of a functionalization within one polymer which provides interactions (i.e. ionic, or H-bonding) between the blended polymers. Markham states that the objectives for compatibilizing blends are to produce a useful multiphase product where the morphology enhances the properties and the interaction provides for stress transfer between the phases. In particular, three points are expressed as indications of successful compatibilizations:

1. Reduced interfacial energy
2. Finer dispersion of the minor phase
3. Improved interfacial adhesion

Xanthos [31] in a recent review compiles an extensive listing of compatibilizers for

various thermoplastic blends. This listing covers in-situ formed copolymers, physical copolymer compatibilizers and copolymers capable of reacting with one of the major phases. Gaylord [28] adds that the compatibilizer must act as a surfactant and that effective compatibilizers must be under 100,000 molecular weight to be accessible to the interface.

In a recent review, Favis [32] points out the effect of a compatibilizer on the dispersed phase size in a PP/PC blend. For the uncompatibilized blend the dispersed phase size increases dramatically as the volume fraction is increased. When the blend is compatibilized, the dispersed phase size increases as the volume fraction is increased, but the phase size is substantially less than the phase size in the uncompatibilized blend. The phase size versus composition relationship for this system is shown in Fig. 2-1. This dramatic rise in phase size of the uncompatibilized blend is the result of increased coalescence. This coalescense is surpressed in the compatibilized blend.

Rheology can also indicate the role of a compatibilizer in a blend. Rheological studies of uncompatibilized and PP-g-acrylic acid compatibilized blends of PP/polyamide illustrate distinct differences between the blends [33]. In Fig. 2-2, the viscosity versus composition of the uncompatibilized blend shows a negative deviation from the logarithmic additivity rule while a positive deviation occurs for the compatibilized system. This rheological difference was related to the enhanced interaction between the phases of the compatibilized blend which increased the blend viscosity. This one example shows that compatibilization can have a significant influence on blend rheology.

In a direct examination of the adhesion of compatibilized blends, Barlow and Paul [34] compression molded strips of uncompatibilized and compatibilized polymers into three ply lap shear specimens. Using this standard lap shear test, they showed for several polymeric blends

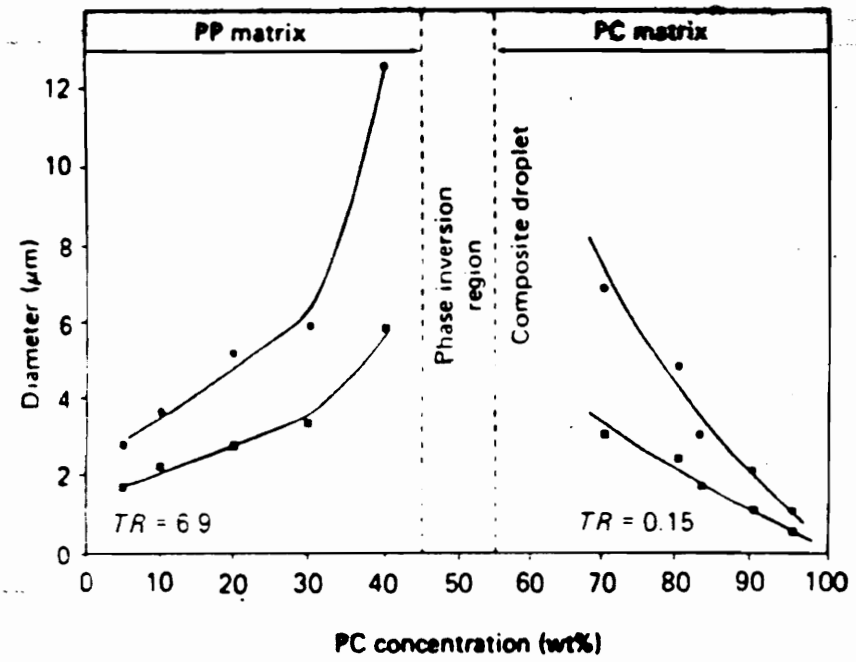

Fig. 2-1. Phase size versus composition for a PP/PC blend: ● is uncompatibilized and ■ is compatibilized blend [32].

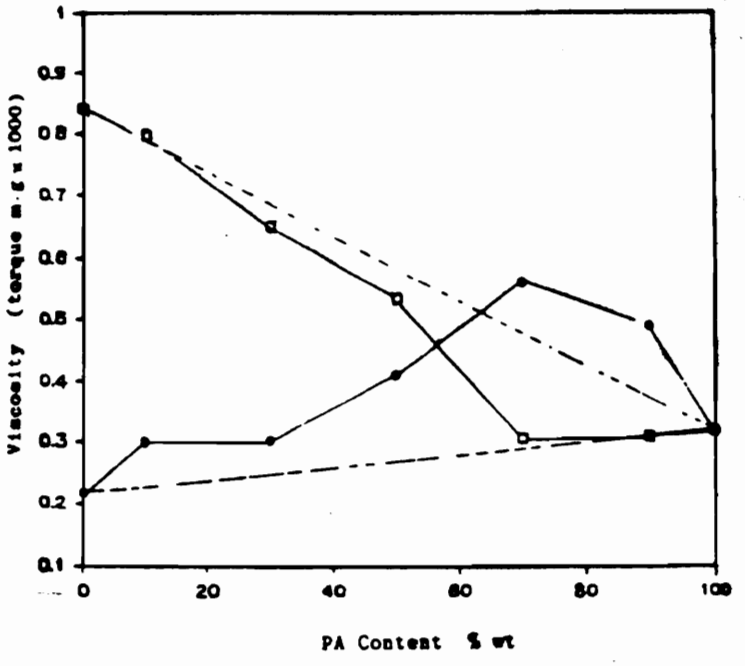

Fig. 2-2. Deviation of viscosity from the logarithmic rule for a blend of PP/PA [33].

that compatibilization directly improves adhesion.

Thus, compatibilization can increase the dispersion of blends resulting in increased interfacial surface area. Additionally, it can create positive deviations in rheological material functions as the result of better adhesion between the polymer components. This adhesion can be directly measured and related to the presence of the compatibilizer at the interface.

2.1.3 The Interface

There are two characteristics of the interface in immiscible blends: interfacial tension and interfacial thickness [8]. The first subject, interfacial tension, is an important area and an area in which experimental techniques are still being developed for viscous polymers. Young's equation is an equation describing a force balance for a liquid in contact with a solid substrate. This equation is often used to determine the surface tension of an unknown solid in contact with liquids of known surface tension. This equation is shown below.

$$\gamma_S = \gamma_{SL} + \gamma_L \cos(\theta) \qquad (2\text{-}6)$$

In the above equation, γ_S and γ_L are the solid and liquid surface tensions, respectively, and γ_{SL} is the interfacial tension. By use of a second relationship to predict the interfacial tension, γ_{SL}, Young's equation can be used to solve for the surface tension of a solid. Several equations relating the interfacial tension to the surface tension have been proposed. Often these equations take the following form

$$\gamma_{SL} = \gamma_S + \gamma_L - F(\gamma_S, \gamma_L) \qquad (2\text{-}7)$$

Wu proposed that by using polar and dispersive components of the surface tensions that the

function F takes the form of the harmonic mean of the polar and dispersive components of surface tension [40]. Wu's harmonic mean equation is shown below where superscripts d and p represent the dispersive and polar components, respectively.

$$\gamma_{SL}=\gamma_S+\gamma_L-4\frac{\gamma_S^{\,d}\gamma_L^{\,d}}{\gamma_S^{\,d}+\gamma_L^{\,d}}-4\frac{\gamma_S^{\,p}\gamma_L^{\,p}}{\gamma_S^{\,p}+\gamma_L^{\,p}} \qquad \textbf{(2-8)}$$

By combination of Young's equation with Wu's harmonic mean equation, the surface tension of solid polymers can be determined by measurement of the contact angle of two or more liquids of known polar and dispersive surface tensions. This has been a widely used technique. Another widely used technique for measuring the surface tension of solids is the Wilhemy plate method. This method uses a balance for measuring the wetting force arising from the surface tension of a liquid as it contacts a plate of test material. For polymers, it is more common to prepare the test material in fiber form rather than to prepare a plate of material.

The measurement of the surface tension of solid polymers is often performed to determine the magnitude of the work of adhesion versus the work of cohesion. For a composite material, e.g. a polymer blend, if the work of adhesion is greater than the work of cohesion than failure of the composite will occur in the matrix not at the interface. Obviously, this is an important indicator of the compatibility of polymer blends. These techniques have recently been applied by Meretz et al. [41] to aid in the selection of thermoplastic / LCP blends having strong interfacial properties.

Interfacial tension between polymers in the melt state is also important because the morphology of blends can change greatly depending upon the ratio of surface forces to shear forces. This topic is discussed in section 2.2. Several techniques exist for determining the

interfacial tension. One commonly used technique is the pendant drop technique where one polymer is suspended in a second quiescent polymer. The equilibrium shape of the suspended drop is recorded digitally and related to the interfacial tension. The drawback of this method is that the attainment of equilibrium for viscous polymers can require over 24 hours. During this time, significant degradation of the polymer can occur. Two other techniques with shorter equilibration times have recently been reported. The first is a spinning drop method reported by Elmendorp and de Vos [42]. In this method, a drop of a less dense polymer is immersed within a matrix of a more dense polymer all of which is encapsulated in a precision capillary tube. The capillary is then spun around its long axis at high speeds. When subjected to these forces, the drop quickly obtains an equilibrium shape that is used to determine the interfacial tension. Another new technique is based on retraction of a slender fiber into droplets [43,44,45]. This theory for this method is discussed in section 2.2. With the proper use of this theory, a fiber does not need to fully retract in order to calculate the interfacial tension which greatly shortens the experimental time. However, it should be noted that this method is not applicable to anisotropic fluids or fluids with a yield stress. Hence, this method is not appropriate to LCPs.

A droplet of a polymer or an immiscible solution placed in a matrix and deformed in a well defined simple flow field may also be used to determine the interfacial tension. This method was used by Taylor [51], and it was derived from hydrodynamic theory that related the drop shape and the shear stress to the interfacial tension. This technique has been used by several investigators [51,53,80]. A semi-empirical expansion of Taylor's relationship was derived by Wu [47] for the determination of the interfacial tension of compatibilized and uncompatibilized polymeric drops in polymeric matrices that were created by mixing in a twin screw extruder. This equation is shown below where $\dot{\gamma}$ is the shear rate, R is the diameter of the drop, γ_{12} is the

interfacial tension and η_d and η_m are the dispersed phase and matrix phase viscosities, respectively.

$$\eta_m \dot{\gamma} R/\gamma_{12}=4(\eta_d/\eta_m)^{.84} \quad for \quad \eta_d/\eta_m>1 \tag{2-9}$$

Xanthos et al. [195] used this relationship to estimate the interfacial tension of compatibilized blends that could not be measured by other means.

As mentioned above, the thickness of the interface is also an important interfacial property. From statistical thermodynamic theories , the interfacial thickness has been related to the interaction parameter, χ_{12}. The form of this relationship shows an inverse nature between the thickness and the interaction parameter

$$\alpha=\frac{c}{(\chi_{12})^m} \tag{2-10}$$

In the above, c and m are constants that depend upon the assumptions used in the derivation of the above equation and α is the interphase thickness [38,39]. In addition, the interphase thickness can also be related to the interfacial tension [46]. Wu used these relationship to arrive at an inverse relationship between the thickness and the interfacial tension [47]

$$\gamma_{12} \propto \alpha^{-1} \tag{2-11}$$

Wu surveyed the literature to show that this thickness can be measured by SAXS, SANS, or TEM, and he used the later in his study. Barlow and Paul [38,34] related the interphase thickness to adhesion and ductile behavior of polymer blends, e.g. impact strength and elongation at break. They concluded that it is easy to create a brittle blend from ductile polymers when the interfacial adhesion is poor. They cited fast fracture created by microcracks at the interface as

one mechanism that can account for the loss in properties.

In summary, the occurrence of miscible polymer blends is infrequent because of positive enthalpic contributions that usually overwhelm the small favorable entropic contributions. However, miscibility can occur in systems where enthalpic contributions favor mixing. These situations include systems were intermolecular interaction such as dipole-dipole or H-bonding occur. In addition, use of block copolymers that are more energetically favored when mixed with polymers than in a neat state lead to miscibility. This has lead to finding polymeric agents, i.e. compatibilizers, that improve the adhesion between phases while also lowering the interfacial tension and reducing coalescence in the melt state. Changes in the interface can be inferred from rheological measurements and also detected with methods that probe small regions of the interface.

2.2 Drop Deformation and Breakup

Obtaining well dispersed polymer mixtures is a goal in forming polymer blends, and mixing is the process that creates a dispersion. For thermoplastic polymers this mixing takes place in the viscous melt state and many reviews and books have been published on this topic [48,73]. While a review of laminar mixing of viscous fluids will not be given here, the fundamental results of the deformation and breakup of droplets in typical flows encountered in mixing will be discussed. This knowledge is important in determining the required mixing conditions that lead to a desired level of dispersion. Additionally, it is just as important to understand the dispersion process when LCPs are reinforcing resins. The LCPs must deform into an extended shapes that will not be broken before the resin solidifies. For reinforcement

purposes, this extended shape provides the highest tensile properties.

The research on droplet deformation and breakup was originally performed to understand the mechanism of emulsification of immiscible liquids. This phenomenon was typically studied using Newtonian liquids. However, the same qualitative process occurs in blending of viscoelastic polymers. Clearly, the study of viscoelastic liquids is much more difficult and only a few studies have been performed. The results to be discussed are based on both theoretical and experimental studies. The theoretical studies involve complex mathematical analysis of the equations of motion and should be consulted if more detail is desired. Two prevalent approximation techniques have been employed in these theoretical studies for the two extreme geometries assumed by droplets. For droplets with nearly spherical shape, a method called spherical harmonics as outlined by Lamb [49] have been traditionally used, and for droplets that have been deformed into slender threads a method borrowed from aerodynamics called slender body theory has been successfully used. Intermediate states of deformation are more difficult to analyze theoretically and are only now being solved numerically. Experimental studies are typically performed in devices that create either pure shear or pure straining flows to establish idealized systems. However, recent advances in both experimental and theoretical capabilities now enable droplet deformation in varying flow strengths to be generated and analyzed.

The most significant research is included below starting with the original work of G.I. Taylor. Surprisingly, this work is the basis for many subsequent studies.

2.2.1 Taylor's Study

Taylor was the first to study the deformation and breakup of viscous drops suspended in

flowing viscous fluids [50,51]. This problem was theoretically approached by solving the hydrodynamic equations for a nearly spherical drop, i.e. small ellipsoidal deformations, in a viscous flowing fluid [50]. Solutions for both the fluid and drop velocities were solved by invoking these now classical boundary conditions at the drop surface:

1. The tangential and normal velocities at the surface are continuous.
2. The tangential stress is continuous.
3. The normal force difference is equal to the force arising from surface tension.

By approximating the shape of the drop as nearly spherical, Taylor was able to relate the drop shape to the ratio of hydrodynamic to surface stresses and to the ratio of the viscosities of the dispersed, μ_d, and continuous viscosities, μ_m. The former ratio, $\eta\dot{\gamma}R/\sigma$, is referred to as either the Weber, We, or Capillary number, Ca, while the later ratio, μ_d/μ_m, is denoted by the symbol 'p' in this text. For the situation where interfacial forces dominate, i.e. $We \ll 1$ and $p=O(1)$, the following relationship between the drop shape, Weber number and viscosity ratio was obtained [51].

$$\frac{L-B}{L+B} = \frac{\eta\dot{\gamma}R}{\sigma} * \frac{19p+16}{16p+16} \quad \alpha = 45^\circ \tag{2-12}$$

In the above, L and B are the major and minor drop axis dimensions, respectively, and the term on the left hand side is often denoted by the symbol 'D'. Commonly the right hand side is denoted by E allowing the above equation to be written as D=E. It should be noted that the group containing p varies from 1 to 1.187 as the viscosity ratio, p, varies from 0 to infinity. Hence, the viscosity ratio is not a significant factor in this analysis of the deformation process under the interfacially dominated condition. What should be noted is that the drop deformation, D, can be directly related to the Weber number and this means the deformation scales directly

with the experimentally controllable shear rate, $\dot{\gamma}$. The orientation of the drop with respect to the shear plane is given by the angle α. Under conditions where the viscosity of the drop is high, $p \gg 1$, the drop behaves more like a plastic solid body. Taylor found for this condition that the above equation simplifies to the following.

$$\frac{L-B}{L+B} = \frac{5}{4} \quad \alpha = 0° \tag{2-13}$$

This theoretical analysis was then tested by Taylor in two apparatus: the parallel band mill and the four roll mill. These instruments are illustrated in Fig. 2-3.

The parallel band mill creates shear flows by rotating the bands in equal but opposite directions. Using this equipment, Taylor found close agreement with equation (14) for low Weber numbers. Three different viscosity ratio ranges were investigated, and drop shape and conditions for breakup of the drops were noted. These observations are listed below according to viscosity ratio.

For $p \ll 1$:

At a viscosity ratio of 0.0003, drops distorted and align at 45 degrees to the band. This angular orientation was common for all viscosity ratios at low Weber numbers and is related to the principle axis of strain. At the highest Weber number possible in the mill, the drop would not break but developed a slender shape with pointed tips. This droplet displayed long tails created by the release of fluid at these tips. This release mechanism is now called tip streaming.

For $p = O(1)$:

At a viscosity ratio of 0.5, the drop formed an ellipse oriented at 45 degrees to the band. As the velocity increased, the drop elongated at a Weber number of 1.4 into a thread like

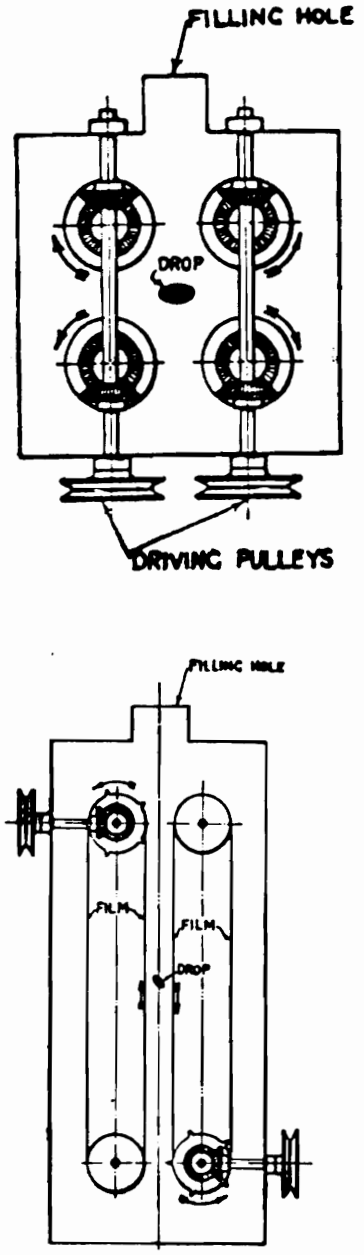

Fig. 2-3. Taylor's (a) Four Roll Mill and (b) Parallel Band Mill [51].

form which lead to breakup of the drop. For a viscosity ratio of 0.9 the drop was not ellisoidal but formed one rounded end and one pointed end. This droplet broke at a Weber number of 0.55.

For $p \gg 1$:

At a viscosity ratio of 20.0, the drop was only slightly deformed and while oriented at 45 degrees at low Weber numbers became oriented more parallel to flow as the Weber number increased. This drop did not break even at the highest rate possible in the mill. The drop shape developed an equilibrium shape with $D=0.25$ versus the prediction of 0.063 via equation (15).

To study drop deformation and breakup in straining flows, Taylor employed the four roll mill thus generating hyperbolic flow. This flow is a two dimensional planar extensional flow defined by the kinematics $u=Gx$ and $v=-Gy$ where the streamlines trace out hyperbolas. Again for small Weber numbers and over a range of viscosity ratios there was close agreement with equation (14). Deviations from this equation only occurred at higher extensional rates. Additionally, for all viscosity ratios, the drops oriented in the direction of flow (i.e. principle strain axis). Summary of these observations are given below according to the viscosity ratio.

For $p \ll 1$:

For drops with a viscosity ratio of 0.0003, the drop formed an ellipsoidal shape and for all extensional rates possible in the mill, the drop did not break but tip streaming occurred.

For $p=O(1)$:

For a drop with a viscosity ratio of 0.9 at low extensional rates the drop assumed an

ellipsoidal shape. However, for a We = .39 the drop formed an extended thread that was stable for an extended period of time in this flow field but broke into many drops shortly after cessation of flow.

For $p \gg 1$:

For drops with a viscosity ratio of 20, the drop developed an ellipsoid shape and at a low Weber number, 0.28, the drop quickly broke into two smaller drops.

Thus, for low Weber numbers all of these cases fit equation (14). However, for moderate to large Weber numbers, significant changes in the type of deformation with changes in viscosity ratio occur. Additionally, the stability of a drop varies considerably. The cases where the highest stability occurs can be summarized as follows: drops of low viscosity ratios are very stable in both shear and extensional flows; drops of viscosity ratios of O(1) are stable during hyperbolic flow; and, drops of high viscosity ratios are stable in shear flow. Conversely, drops were unstable for viscosity ratios of O(1) in shear flow and for high viscosity ratios in extensional flow.

Many new studies have been performed since 1934 but the above statements based on Taylor's observations still hold true [52]. Obviously, the above theory does not predict the onset of drop breakup and some newer developments are more suitable, but the deformation of drops at small Weber numbers is closely approximated by Taylor's theory.

2.2.2 Subsequent Studies

In one of the many subsequent studies, Rumsheidt and Mason [53] further defined and

categorized the drop deformation and breakup process for various viscosity ratios under shear flow. Fig. 2-4 illustrates three classes of drop deformation categorized by the following viscosity ratio: $p < .001$, $p \approx 1.0$, $p > 4$. For low viscosity ratios, Class A behavior is characterized by the drop oriented at 45 degrees from the flow direction and by loss of the droplet mass from the tip streaming mechanism. Class B behavior is subdivided into two subclasses: the shear rate at the critical value; and, the shear rate exceeding the critical value. For the former, a drop breaks up into two equal pieces while for the latter a thread is formed followed by breakup into many smaller drops. Finally, Class C is a category for drops that do not breakup and that orient parallel to the flow direction. In an extension of Taylor's comments, Rumscheidt and Mason also suggested that when the hydrodynamic forces are greater than the restoring interfacial forces then drop breakup would occur. This statement was put in the form of equation (14).

$$D_c = We_c * \frac{19p+16}{16p+16} = \frac{1}{2} \qquad \textbf{(2-14)}$$

where D_c and We_c are the critical deformation and Weber numbers, respectively, for the onset of breakup.

Similar results for shear flow were also found by Karam and Bellinger [58]. They investigated the breakup of droplets in a couette device using a range of liquids with various physical properties. Their results can be summarized similarly to the results of Rumscheidt and Mason. They found that drops readily breakup for viscosity ratios between 0.2 and 1 while drops do not breakup for ratios lower than 0.005 or higher than 4. These observations of the critical breakup points are typically plotted on a chart comparing We_c to p. One such plot for both shear and shearfree flows are shown in Fig. 2-5. It should be noted that droplets can be broken over wider viscosity ranges in shearfree flows versus shear flows. Thus, while equation (16) is

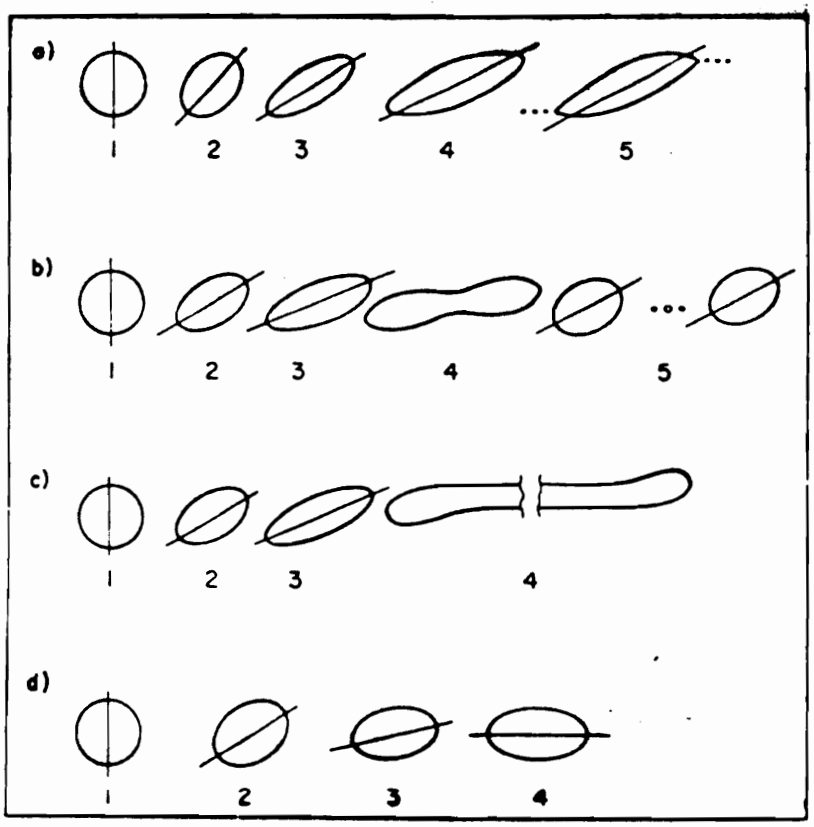

Fig. 2-4. Classes of drop deformation: a) Class A, b) Class B-1 c) Class B-2, d) Class C [53].

approximately valid for shearfree flows it holds approximately for shear flows only when the viscosity ratio is between 0.1 and 1.

A main feature of the theoretical analysis of drop deformation and breakup is that the shape of the drop must be determined. It is not known *a priori.* Starting with Taylor [51], this shape was estimated for small deformations by an ellipsoidal equation. However, Taylor's analysis can be considered a first order perturbation solution with E as the small variable. Chaffey and Brenner's [55] extended this analysis with a second order perturbation in E. On the other hand, Cox [54] consider a time dependent deformation of a drop with D as the small parameter. This work was summarized and experimentally verified by Torza et al. [56]. The results of the theory predicted a greater agreement with experiment than was obtained with Taylor's or Chaffey and Brenner's theory. It was pointed out by Tavgac [57] that the range of D is from 0 to 1 while the range of E is from 0 to infinity. Hence, in most cases D is the smaller parameter and this explains why Cox's approach yields better results. The equilibrium relationships for D and the orientation angle derived by Cox follow:

$$D=\frac{5(19p+16)}{4(1+p)\sqrt{(19p)^2+(20We^{-1})^2}}$$

$$\alpha=\frac{\pi}{4}+\frac{1}{2}\tan\left(\frac{19pWe}{20}\right) \qquad \textbf{(2-15)}$$

While this theory's only assumption is small deformation from sphericity, Torza et al. found that depending upon how the shear rate was applied, the deformation behavior could changed dramatically. By applying a gradually increasing shear rate so that the drop could reorient, it was found that drops with viscosity ratios below 3.0 deformed and broke according to class B1 in

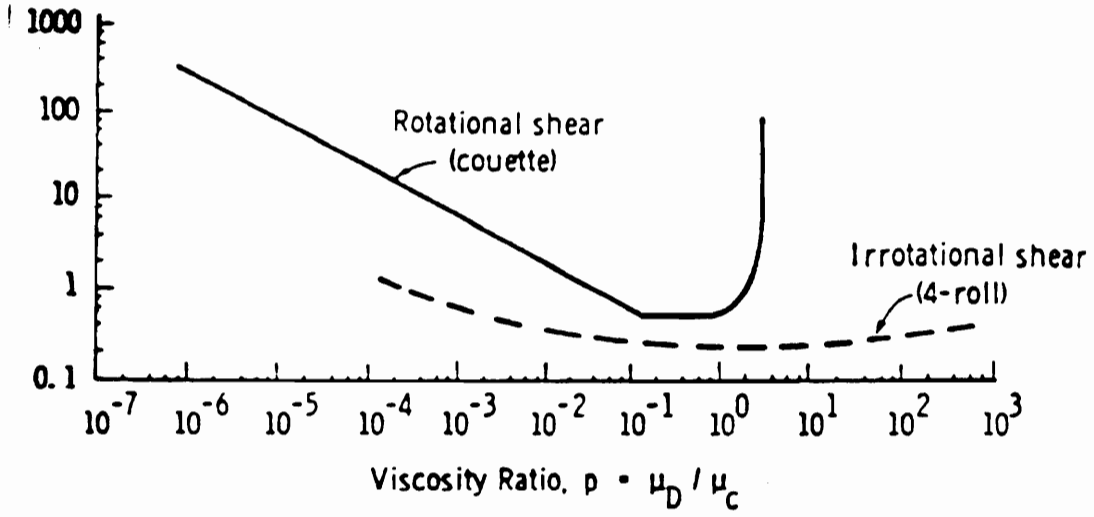

Fig. 2-5 Weber number versus viscosity ratio for shear and shearfree flows [59].

Fig. 2-4. However, for any viscosity ratio less than 3.0, if the shear rate was applied faster than the drop could respond (i.e. compared to the drop characteristic time , $\tau = p\ We/\dot{\gamma}$), the drop deformed similarly to that shown as class B2 in Fig. 2-4. In this case, the drop stretches into a thread and breaks from Rayleigh waves into many smaller drops (see section 2.2.3).

Cox also derived the analogous relationships for transient deformation in hyperbolic flow. This relationship for $We \ll 1$ and $p \neq O(1)$, however, only predicts small deformations. Barthes-Biesel and Acrivos [81] in continuing Cox's approach included higher order terms to estimate the shape. These type of expansions were placed on a more theoretical framework by Rallison [82] who proposed modeling the drop shape with expansions of spherical harmonics.

An extensive experimental study of droplet breakup was undertaken by Grace [59] and several key points were presented. First, it was noted that the dynamic surface tension rather than the equilibrium surface tension is more appropriate for use in calculating the Weber number. Typically, the equilibrium value is half of the dynamic value, and for many viscous fluids equilibrium is not reached for hours or days. Hence, in the time that the two phases mix in processing equipment, equilibrium is not reached. Second, relationships between drop deformation and the time for a drop to burst in shear flow were also presented by Grace. He noted that deformation of drops in a drawing fashion can create lengths that are 4 to over 50 times the initial drop size. The dimensionless time to burst a drawn drop, $t_b\sigma_{12}/2R\eta$, can be determined from an experimental plot shown in Fig. 2-6 for both shear and elongational flows (shown as open symbols). As the critical Weber number is exceeded, the time to burst decreases while the draw of the drop increases. In trying to verify these results, Elemans [60] repeated this work for two viscosity ratios and found that the dimensionless time does not decrease with increasing Weber number. The closed symbols in Fig. 2-6 represent Eleman's data. Eleman

proposed that Grace may have recorded the onset of tip streaming versus breakup. Regardless of this discrepancy, Grace showed that with $We > We_c$ concurrent changes such as an increase in energy consumption and a broadening of the drop size distribution occur. Hence to decrease the drop size with the minimum energy, he suggested increasing the shear rate in stages so as not to exceed the critical Weber number by an extreme measure. In a study of drop breakup in static mixers, Grace's study concluded that design of static mixers for use in droplet breakup could be scaled using prior relationships for drop breakup in shear flow. The gradual increase in the shear rate for flow through a series of static mixers with decreasingly smaller diameters was found to create the greatest degree of droplet size reduction.

An interesting theoretical and experimental study of drop deformation in shear flow was conducted by Elemans [60]. As stated by several authors [53,56], when a drop is subjected to a rapidly increasing shear rate or a shear rate that exceeds the critical Weber number a droplet deforms into a thread. Elemans calculated the change in dimensions of a sphere undergoing affine deformation in shear flow in a manner similar to that presented by Middleman [48]. The instanteous length and breath, respectively, of an affinely deformed drop are shown below.

$$\begin{aligned} L/a &= (1+\gamma^2)^{1/2} \\ B/a &= (1+\gamma^2)^{-1/4} \end{aligned} \qquad \textbf{(2-16)}$$

where 'a' is the initial drop diameter. From these equations the drop deformation, D, may be calculated. Equation (18) can be related to time through the relationship: $\gamma = \dot{\gamma}t$. Comparison of experiment with prediction shows close agreement for large Weber numbers. This data is shown in Fig. 2-7 for various supercritical values of the Weber number. From these results, it was concluded that a drop deforms affinely in shear flow when $We > 2*We_c$. This makes

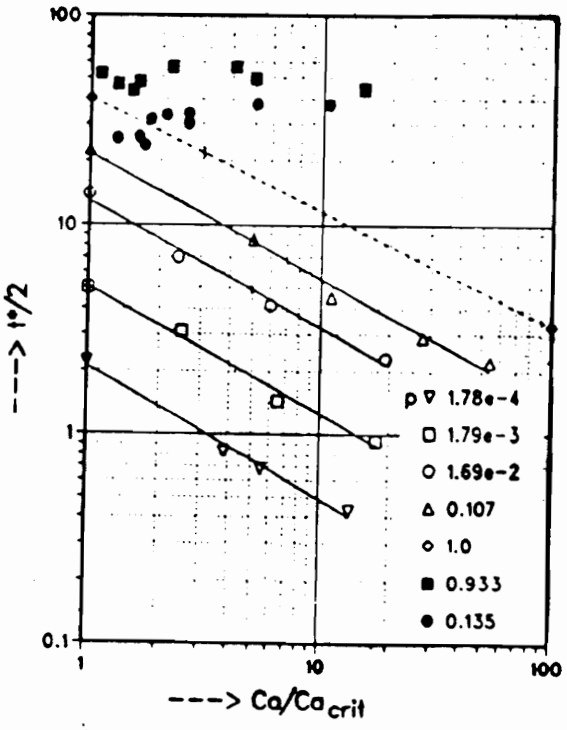

Fig. 2-6 Effect of viscosity ratio on the reduced time to burst at E_c for shear and shearfree flows [60].

intuitive sense as well that when the hydrodynamic forces are much greater that the interfacial forces then a drop deforms in proportion to its surroundings, i.e. affine deformation.

For highly deformed drops, slender body theory as proposed by Taylor [61,62] and expanded by Batchelor [63] and Buckmaster[64,65] has proved useful. This theory is a technique used in aerodynamic theory of flow around slender elements such as wings. For axisymmetric extensional flow, the slender body analysis of Acrivos and Lo [66] yields the following critical breakup relationship

$$We_c\, p^{\frac{1}{2}} = 0.148 \tag{2-17}$$

This formula was evaluated experimentally by Leal and coworker as will be discussed next.

An extensive experimental study using a computer controlled four roll mill, modeled after Taylor's apparatus, was undertaken by Bentley and Leal [79,80]. With the use of the computer controlled rolls, a drop could be maintained in the well defined central area of the mill for not only extensional flows but also for general flows (i.e. between simple shear flow and hyperbolic flows). Bentley and Leal provide an excellent summary of the major theoretical works up to the time of their experiments [80]. For small deformation of drops, Bentley and Leal have compared their experimental results with those predicted by Barthes-Biesel and Acrivos [81]. For highly deformed drops, experimental results were compared to prediction via equation (19). Because the predictions of this equation hold approximately for other straining flows, Bentley and Leal proposed an ad hoc criteria for intermediate flows. In this modification, an effective strain rate was used which incorporated the vorticity of the flow.

In their experimental work, all deformations and breakup conditions were obtained based

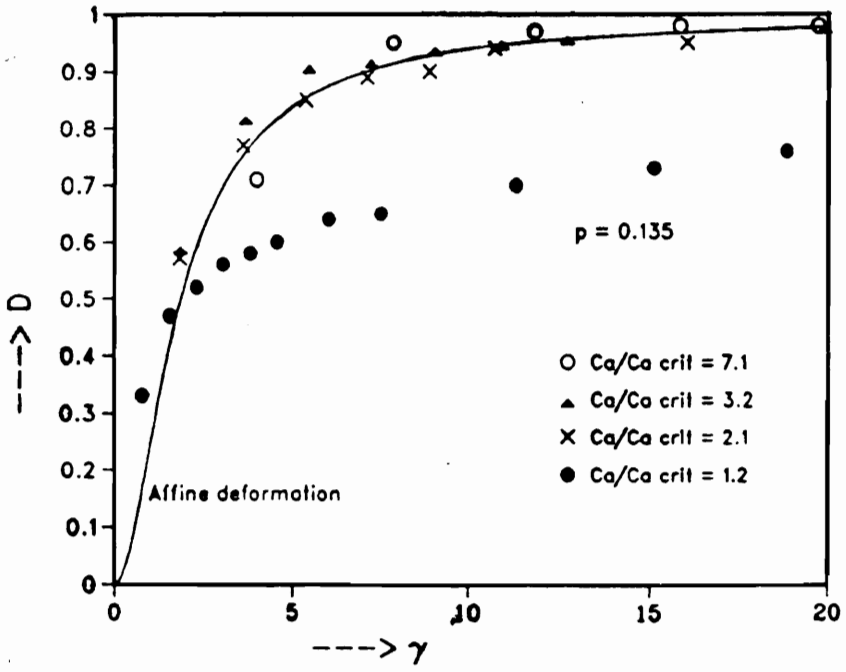

Fig. 2-7. Affine deformation at supercritical Weber numbers (Ca). The viscosity ratio is 0.135. The solid line is based on equation [60].

on slowly, i.e. 0.01 s^{-1}, incrementing the strain rate so that a quasi-equilibrium was obtained. Many of the same features as noted by Taylor were observed. Some disagreement with Graces' [59] results for high viscosity ratios in shear flow were noted. The authors suggest that the shear rate increases in Graces' work were too large thereby producing supercritical Weber numbers. This discrepancy points out the difficulty with applying equilibrium theory to processing where equilibrium is not obtained. However, for equilibrium conditions, it is shown that the small deformation theory for moderate and high viscosity ratios and the slender body theory for low viscosity ratios yields satisfactory agreement with their data.

Limited information is reported on the effects of viscoelasticity on drop deformation and breakup. Tavgac [60] studied deformation and breakup of Newtonian and viscoelastic fluids in simple shear flow. He noted that the critical Weber number increased over that of the Newtonian limit as the Deborah number increased. However, at small Deborah numbers, a critical Weber number lower than the Newtonian limit existed. He also noted that for a high viscosity drop suspended in a viscoelastic fluid, as the matrix elasticity increased the drop become easier to break. This result is in agreement with Elmendorp and Maalcke [70] who experimentally determined for various Newtonian and non-Newtonian fluids that higher matrix elasticity led to easier breakup while higher droplet elasticity led to a more stable droplet. These effects can be predicted by a modification derived by Van Oene [67] that adjusts the interfacial tension based on the difference between the first normal stress difference of the matrix and the drop. However, in contrast to Elmendorp and Maalcke, Tavgac found that for low viscosity ratios, matrix elasticity tends to stabilize a Newtonian droplet. Tavgac [60], and Milliken and Leal [86] found that low viscosity viscoelastic drops do not deform as much as their Newtonian counterparts. Several authors have noted that for high viscosity ratios, drops will form a slender thread [60,70]

that undergo rapid breakup [60] while others have noted that an extended thread is only observed in melt blends at low viscosity ratios [84]. This latter observation could be explained from the shorter life span of the more viscous thread which leads to the breakup of the morphology before the sample is quenched.

A recent study of viscoelastic systems in planar extensional flow was conducted by Milliken and Leal [85]. In this study, they found that for polymeric drops the We_c versus p is not sensitive to rheological properties of the drop. Additionally, polymeric drops preferentially tip stream rather than develop into high aspect ratio threads. In a newer study, they investigated the effects of vorticity on the breakup of both Newtonian and viscoelastic drops [86]. They noted that larger Weber numbers are required for breakup of viscoelastic drops and that the fluid elasticity within a drop inhibits drop deformation. In addition, for a viscosity ratios greater than 0.5, breakup occurs via stretch and tip streaming while only tip streaming occurs for a viscosity ratio less than 0.5.

Another area that is also not well understood is the influence of surfactants on the deformation and breakup process. Polymer surfactants or compatibilizers are increasingly being used with polymer blends, and so the technological importance of understanding this dispersion process is of increasing importance. Some studies have been attempted [76-78], but more knowledge is needed. A few findings will be mentioned here.

Rumsheidt and Mason [53] examined the effect of surfactant on the deformation and breakup of the drop. They observed that internal circulation was surpressed and that breakup was less likely to occur. This led to the hypothesis that the shear stress was not effectively transmitted through the surfactant interface. A numerical study was performed by Stone and Leal [76] for drops under axisymmetric extension. They found two competing effects must be

considered: surface convection of surfactant to the tail of the drop and dilution of surfactant at the head of the drop. The former phenomenon leads to a lowering of the interfacial tension and an increase in drop deformation at the tail while the latter phenomenon has the reverse effect on the head of the drop. Their numerical studies indicated that at low Weber numbers more deformation occurs and that at higher Weber numbers surfactant dilution arrests any further deformation. They also found that in systems where the interfacial tension changes rapidly with surface concentration of the surfactant, significant increases in We_c can occur. Although limited knowledge exists at this point, it tends to indicate that surfactants induce larger deformations and simultaneously stabilize the drop. The next section examines the stability of droplets that form into extended threads. As mentioned, retention of high aspect ratio drops is important for reinforcement of thermoplastics. Thus, it is of interest to know how capillary breakup occurs and how to avoid its effects.

2.2.3 Capillary Instability

As discussed in the previous section, transients and supercritical Weber numbers lead to the formation of threads from spherical drops. Following Taylor's observations that a stable thread in extensional flow quickly breaks up into many drops upon cessation of flow, Tomotika [69] pursued a theoretical analysis of the stability of a thread in a quiescent viscous liquid where inertia can be ignored. Starting with the Navier-Stokes equations, a stream function was derived using the same boundary conditions as were used by Taylor. This function takes the following form and simplifies to Rayleigh's prediction for viscous thread in a inviscid fluid.

$$\psi(r,z,t)=f(r)*\exp[i(nt+kz)] \qquad \textbf{(2-18)}.$$

In the above, f(r) is a function of the radius, k is inversely related to the wavelength of the breakup, and the quantity 'i*n' is real and predicts the growth rate of instability. The quantity 'i*n' is often given the symbol 'q' and is determined in the solution of a system of equations. For the general case of finite viscosity ratios the following equation is solved:

$$q=\frac{\sigma_{12}}{2*a*\mu}\Omega(k,p) \qquad \textbf{(2-19)}$$

where σ_{12} is the interfacial tension and 'a' the radius of the unperturbed thread. Thus, the rate of breakup is proportional to the interfacial tension and inversely proportional to the matrix viscosity. Also, the maximum growth rate and minimum wavelength are found via Tomotika's equations to occur for a viscosity ratio of 0.28. For a viscosity ratio of 0.91, drop size predictions based on the results from Tomotika's equations satisfactory match Taylor's experimental results. It is found that the threadline is unstable when $\lambda > 2\pi R$. Elmendorp [71] points out that for this condition, the interfacial area decreases as the distortion increase. This quantity is also directly related to the varicosity of the thread via the following equation:

$$\epsilon=\epsilon_0*\exp(q*t) \qquad \textbf{(2-20)}$$

where 'ϵ' is the perturbation to the radius at time t and ϵ_0 is the perturbation at t=0. The time dependence of the varicosity is directly obtainable from the above formula. Elmendorp [73] shows that when $\epsilon = .8a_0$ the distortion causes the thread to break. Thus, the time for breakup of a thread in a quiescent media can be directly calculated from equation (22).

In an extension of this work, Tomotika [72] also considered the stability of a thread surrounded by an extending viscous liquid. It was reported by Taylor that such threads appear to be stable for long periods of time. When breakup occurs, the drops appear to be much smaller

than if the flow had been stopped after the initial formation of the thread. This phenomenon was studied by Tomitika as a perturbation around the steady state. With this approach, nearly identical equations were determined. However, with the premise that a varicosity initially existed, i.e. $\epsilon_0 \neq 0$ at $t=0$, a maximum magnification of this varicosity (i.e. ϵ/ϵ_0) was found to be 20:1. This amplification was far less than expected to cause the breakup a thread. However, if it is assumed that the perturbations are equally likely to occur at any time after formation of the thread, then the magnification of perturbations increases rapidly as the radius 'a' of the thread is reduced. For a thread stretched to 1/8th of its original radius, the magnification of a varicosity that started at $t>0$ is $2x10^{10}$:1. Clearly, this order of distortion is responsible for breakup of the thread. In summary, any disturbance that is initially present is not responsible for breakup of the thread. Instead, disturbances that originate some time after formation and thinning of the thread are the cause for the ultimate breakup of the thread. This mechanism is responsible for the increased stability of a thread in extensional flow.

An experimental study of thread breakup in quiescent media was undertaken by Elmendorp [71]. Several different types of fluids were studied including Newtonian, viscoelastic solutions, polymer melts, and fluids exhibiting yield stresses. For Newtonian fluids and polymer melts (PS and PE), equation (22) was found to hold. However, for viscoelastic solutions, deviations from equation (22) occurred. These deviations were attributed to a strain hardening extensional viscosity that occurs with large stretching flows, i.e. as the distortion becomes large. For fluids with yield stresses, Elmendorp derived an equation relating the maximum to minimum pressure difference within a thread. The difference between maximum and minimum pressure must be greater than the yield stress for the thread to deform and for breakup to occur. For small diameter threads, the pressure difference is large, and fluids with yield stresses should

deform and break into droplets.

Chin and Han [68] analyzed both experimentally and theoretically the stability of immiscible drops of fluid in a non-steady shear flow. This flow was Poiseuille flow viewed in a clear tube which was preceeded by a converging conical channel. Long pointed ellipsoids or threads were created in this flow with the formation upon breakup of either uniform drop sizes or non-uniform sizes depending upon the initial drop size, the fluid and the flow conditions. A Weber number versus viscosity ratio plot similar to Taylor's work was obtained. Additionally, an extensive theoretical analysis of drop stability for drops obeying the Jeffrey's model was developed from the equation of motion linearized about perturbation variables. Solutions for two simplifying cases were presented: long wavelength disturbances and low Reynolds numbers. The stability criteria was evaluated numerically for both cases. For long wavelength disturbances, it was confirmed that the matrix viscosity enhances stability and interfacial tension decreases stability. Additionally, it was found that matrix elasticity enhances stability. For the low Reynolds number case, effects at all wavelengths may be examined. However, short wavelengths effects were presented. It was found that the rate of growth of instabilities was greater in viscoelastic systems than in Newtonian systems. An interesting result was noted for the size of droplets formed at different viscosity ratios. It was noted that the maximum growth rate of disturbances shifts from long wavelengths, i.e. larger drops, to short wavelengths, i.e. smaller drops, as the viscosity ratio increases. However, no theoretical analysis was presented to explain why some threads breakup into uniform versus non-uniform sizes. Also, no comparison was made at long wavelengths between the two asymptotic cases. Finally, only fluids obeying the Jeffrey's model can be interpreted from the above analysis.

In an analysis that includes a microstructural equation defining the anisotropy of a fluid,

Olbricht et al. [83] unified the stability analysis of drop breakup for any flow in which any kinematics can be specified. Starting with a vector microstructural model, where rotation, deformation, stretching, and internal viscosity are incorporated, the rate of change of the drop dimensions were derived.

$$\dot{R}=\Omega*R+G[E*R-\frac{F}{F+1}(r*E*r)R]-\frac{\alpha}{F+1}R \qquad (2\text{-}21)$$

In the above equation, R, represents a dimension of the structure such as an end to end vector or drop dimension vector, E is the rate of deformation tensor, Ω is the vorticity tensor, G is the shear rate and r is a position vector. This equation can be decomposed into a scalar length (the last two terms) and a normalized direction vector representing the rotation of the microstructure (the first two terms). When the former equation for length is solved, an eigenvalue solution is obtained. Hence, the growth of the length scale can be determined to be stable or unstable from the determination of the maximum real eigenvalue. For drop deformation, instability means that drops breakup. The advantage of this method was illustrated by Olbricht when he used extensional flow data to satisfactorily predict the critical Weber number for breakup in shear flow. It should be pointed out that the relations for the critical Weber numbers under shear and extension are quite different, and so this is quite an accomplishment.

At the risk of oversimplifying a complex subject, the phenomenon of droplet deformation and breakup may be summarized with a few statements. First, droplets in shear flow with viscosity ratios of O(1) are easily broken in shear flow. However, droplets with viscosity ratios greater than 4 do not break and droplets with viscosity ratios below 0.001 are increasingly difficult to break. Conversely, drops of all viscosity ratios can eventually be broken in shearfree flows. At low viscosity ratios, tip streaming may occur while at viscosity ratios of O(1) long

threads are created that resist breakup. At high viscosity ratios, drops are readily broken. While knowledge of how viscoelastic drops behave is still far from complete, it may be stated that viscoelastic drops are stabilized by elastic forces within the drop phase and drops are destabilized by elastic forces within the matrix. The ease of breaking a viscoelastic drop or a Newtonian drop in a viscoelastic matrix in shear flow varies depending upon the Deborah number. At low Deborah numbers, viscoelastic drops can be broken at lower Weber numbers than occurs for Newtonian drops while at high Deborah numbers drops are more difficult to break. All of the above generalization must be used with caution. These results are taken primarily from idealized systems. Factors such as yield stress or anisotropies that may be operative within LCPs are not considered in the majority of these studies. In addition, the flow fields are well defined and steady state is approached at very slow rates. It is difficult to apply these finding directly to the flow fields encountered in polymer processing operations let alone systems with LCPs. However, as will be shown in section 2.5, these processes do occur in the processing of LCP blends.

2.3 Injection Molding

Injection molding is a commonly used process for quickly shaping plastics into useful forms. It consists of a reciprocating plasticating extruder that injects a molten thermoplastic polymer or a crosslinkable liquid resin through a delivery system consisting of runners and gates into a temperature controlled mold. The process occurring within the mold is the essential area leading to the creation of structure and properties of the molded article. The cyclic process of injection molding is typically viewed as consisting of three main stages. The first stage is filling where the resin enters the mold cavity and eventually fills the cavity in a transient nonisothermal

manner. The second stage is packing so called because as the polymer cools it's specific volume decreases and more polymer is injected into the mold to maintain the shape. The third and final stage is cooling where the polymer solidifies. There has been much research devoted to understanding the filling stage, and the combined filling, packing and cooling stages. The unique features of these stages will be presented next. However, another area of interest is the microstructure of the molding and how the microstructure relates to mechanical and optical properties of the molding. Various techniques are employed to study the microstructure. Obviously, the thermomechanical history of the polymer in forming the molded part is the basis of varying morphologies and properties within the mold. Some newer studies now attempt to relate the fluid mechanics, heat transfer and the thermorheological properties of the polymer to the final microstructure. These studies use numerical techniques such as finite elements or finite differences to predict the velocities, stresses, and observable properties such as density, birefringence, or modulus. These predictions are certainly adequate for homopolymers such as PE, and studies have been reported for fiber-filled systems. However, no studies have been reported for polymer blends. The following review will concentration on the process of injection molding and its influence on microstructure. These same topics for LCPs will be discussed in section 2.4.

2.3.1 Early Studies of Injection Molding

The first stage in injection molding is the filling of the mold. Understanding of this stage has been advanced with various mathematical models incorporating different levels of complexities. The earliest models assumed an one dimensional (1-D) velocity profile where

pressure in the mold could be calculated [88]. A coupled 1-D momentum and (2-D) heat transfer analysis for filling of a rectangular cavity with a power law fluid was presented by Harry and Parrott [89]. A more extensive mold filling study including varying injection conditions for a power law fluid with comparison of prediction to experimental results was presented by Williams and Lord [90,91]. Krueger and Tadmor [100] have studied the influence of elasticity upon shear stress and pressure gradients and found negligible impact. Berger and Gogos [92], and Wu, Huang, and Gogos [94] analyzed radial filling of a disk cavity. They showed that filling times differed insignificantly between isothermal and nonisothermal conditions for quick shot times. A nonisothermal model of filling, packing, and cooling of a semi-circular disk cavity was investigated by Kamal and Kenig [95]. This analysis was later expanded to rectangular molds and included the Spencer-Gilmore equation of state [96]. A study of filling, packing, and cooling of PP with a Criminale-Ericksen-Fibey constitutive equation, and Spencer-Gilmore equation of state for the packing stage was studied by Chiu et al. [93]. They found the effect of melt temperature was significant on the frozen layer thickness but the mold temperature was not a significant influence.

Solidification in the mold has also been investigated. Gutfinger et al. [97] have analyzed solidification in both filling and cooling stages. Janeschitz-Kriegl has analyzed the heat transfer in the filling stage [98]. Richardson [99] has analyzed premature freezing of polymers during the filling of molds, and he has compared predictions to results for filling of spiral molds. The above studies have focused on shear flow in the mold. An extensional flow exists during filling of the mold, and this flow coupled with heat transfer is responsible for the development of the microstructure in the molding.

2.3.2 Development of Microstructure

Although the above studies have presented many of the aspects of the molding process, one aspect was not discussed that was presented in a widely cited paper [102]. This aspect is called fountain flow, and it occurs during the filling stage. This flow occurs between the centerline of the mold and the walls (across the thinnest dimension of the mold). Rose [101] was the first to use the term 'fountain effect' later renamed fountain flow. He described it from a frame of reference moving with the advancing front where particles would appear to decelerate as it approached the advancing front and then gain a radial velocity that caused a spilling out of the particles to the wall. Tadmor [102] analyzed the mold filling process from this same frame of reference and visualized a stagnation flow at the front. He assumed a hyperbolic or planar extensional flow field existed at the front. This was subsequently verified as a good approximation via FEM analysis [107]. Behind the front, he assumed the flow to be a fully developed nonisothermal shear flow. These flows with a frozen skin layer are illustrated in Fig. 2-8. By applying the Rouse model with the fountain flow kinematics he predicted the end to end distance for the polymer in the mold. Using this distance and the relaxation that occurs prior to freezing, Tadmor qualitatively predicted the changes in shrinkage across the thickness of a molded specimen. Thus, Tadmor demonstrated that from a knowledge of a flow field, from the use of a constitutive equation, and from the freezing of the orientation, the final macroscope property (shrinkage) could be predicted.

Visualization studies were later carried out to understand the fountain flow in more detail. Schmidt [103] used a glass walled mold affixed to an Instron capillary rheometer to study the fountain flow. By preparing rods of polymers with different color die tracers located periodically

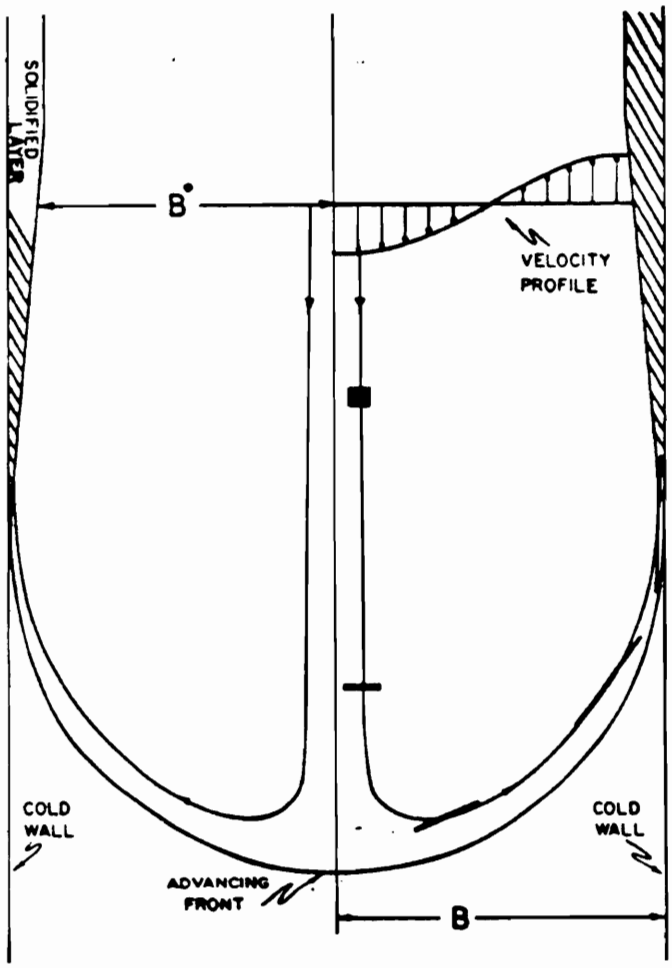

Fig. 2-8 Fountain flow, fully developed flow, and solidified layer shown in a frame of reference that moves with the front [102].

along the center of the rod, the movement of fluid particles could be observed. Using this system, Schmidt concluded that the first particles entering the mold at the centerline are deposited on the surface of the mold wall located closest to the gate. Those particles entering the mold near the end of the filling stage are located at the surface of the wall near the end of the mold. This pattern was explained as arising from the fountain effect which moves particles from the centerline to the wall. Newer visualization studies have fixed the advancing front by moving the walls to directly obtain the frame of reference used by Tadmor [112]. The only disadvantage with this newer apparatus is the effect of gravity on fluid flow. Computation of the fountain flow and tracking of material points that enter the front leads to an accurate simulation. Such a simulation revealed characteristic V patterns near the wall that are explained as originating from particles which pass through the fountain flow to positions adjacent to the wall which are subsequently translated by shear flow [105]. Near the wall, freezing retains the fluid position and orientation. This V shape has been confirmed by several authors [109,111].

Many mathematical analyses now include the fountain flow because of it's significant effect on properties. However, problems can arise in modeling the fountain flow because of singularities that occur at the three point intersection where the wall, the advancing liquid, and the retreating gas phase meet. Two techniques are typically used to accommodate this singularity and these can be directly integrated into the numerical computations. The first technique uses a slip condition [104], and the second technique uses a moving contact line [106]. The slip condition avoids the singularity by assuming slip near the contact point and no slip far from the contact point. Kamal et al. [104] have approximated Bhattacharji and Savic [113] analytical analysis of fountain flow in a tube to derive an expression for slip that is used in their numerical calculations. In the second technique, the moving contact line is located as the point at which

a particle at the k th iteration will contact the wall. This point then becomes the contact line for the k+1 iteration. To avoid conflicts with theorems prohibiting shearfree flow with a curved free surface from creating a moving contact line [114], Mavridis et al. [110] treat the contact line as stationary until the front advances sufficiently that a 180 degree contact line occurs, i.e. a flat free surface at the contact line exists.

The advantages of using the above type of computations is that this complex problem can be visualized in a few graphs. As mentioned above, the fountain flow creates high orientation in polymers, but subsequent deformation that is caused by shear flow can cause the loss of this orientation. Relaxation of the skin is generally desired for thermoplastic resins to avoid stress cracking [126,127,128]. However, for LCPs and their blends, retention of this orientation is desired. Naturally, loss of orientation can be prevented via solidification which occurs near the wall of the mold during the filling stage. Several predictions of this solidification process have been presented [97,98,118]. One widely used equation was proposed by Dietz et al. [118] and is based on transient heat transfer through a stagnant layer of polymer. The layer can be predicted from equation (24)

$$\delta = 2\left(\frac{T_s - T_w}{T_m - T_w}\right)\sqrt{\alpha t} \qquad \textbf{(2-22)}$$

where Ts, Tw and Tm are the solidification, wall and melt temperatures, respectively, and α is the thermal diffusivity.

2.3.3 Analysis of Microstructure

The microstructure of molded articles may be investigated by several techniques. These

techniques include birefringence, dichroism, X-ray diffraction, density, sonic velocity and microscopy. A review on determination of microstructure in moldings is given in reference [115].

A common feature observed in the analysis of the microstructure is a skin core feature created by two types of flows: fountain flow and shear flow. This may be seen optically by placing samples between cross polarizers. The skin exhibits complete extinction of light while a lesser degree of extinction exists as the core is approached. For acetal polymers the skin exhibits a folded-chain lamellae with "shish-kebabs" growth. In the subskin region a transcrystalline layer exists, and at the core a spherulitic structure is observed [115].

Many studies of injection molding have been conducted with PE or PS polymers, and the birefringence is a commonly used technique to determine orientation. Kamal and Tan [116] studied the birefringence variations of molded PS across the thickness direction and at various points along the length of the specimen. One typical profile is shown in Fig. 2-9. A high birefringence is found at the skin and a secondary maximum is found in a subskin layer. The region between the skin and the local minimum indicated by 'B' in the figure is believed to be the location of the instantaneous frozen layer. Point 'C' is believed to be the frozen layer developed prior to complete filling of the mold filling. The high birefringence is indicative of the high shear stresses. The decrease in birefringence as the core is approached occurs from relaxation of the melt prior to solidification in the cooling stage. With a representative viscoelastic constitutive equation the orientation and the birefringence can be predicted from the flow kinematics and/or stresses. These orientations are also important to examine in amorphous polymers to understand how residual stresses generated from flow and thermal sources influence mechanical properties [117]. The next section will describe several studies that have integrated

process modeling with microstructure predictions to better relate processing to ultimate properties.

2.3.4 Prediction of Microstructure

A formulative study relating kinematics and stresses to orientation has already been mentioned above. Since Tadmor's publication many more studies have been undertaken to relate the process to the microstructure. Current investigations are primarily numerically based techniques that use either the marker and cell (MAC) finite difference implementation or the FEM implementation. Some discussion of these methods was already mentioned. The results of these studies will be discussed here.

A widely quoted article by Dietz et al. [118] related the principle stress which includes both shear and normal stresses to the birefringence at the time the polymer vitrifies. Predictions were compared to experimentally obtained birefringence values. The thickness of the vitrified skin was calculated from the contact time and temperatures as shown above in equation (24). The orientation in the melt was determined from relaxation of the stresses after cessation of flow using the Matsui and Bogue nonlinear viscoelastic equation [119,120]. This approach has been used in other studies [121]. One such study used the MAC method to simulate the injection molding process of PE [122,123,124]. Several important aspects were included in their model such as the use of the White Metzner constitutive equation to model rheology, the Nakamura equation to model crystallization, and the energy balance which included the heat of crystallization. In the cooling stage the Matsui-Bogue nonlinear viscoelastic model was used in place of the White Metzner model since no flow occurred. The simulation enabled prediction of birefringence,

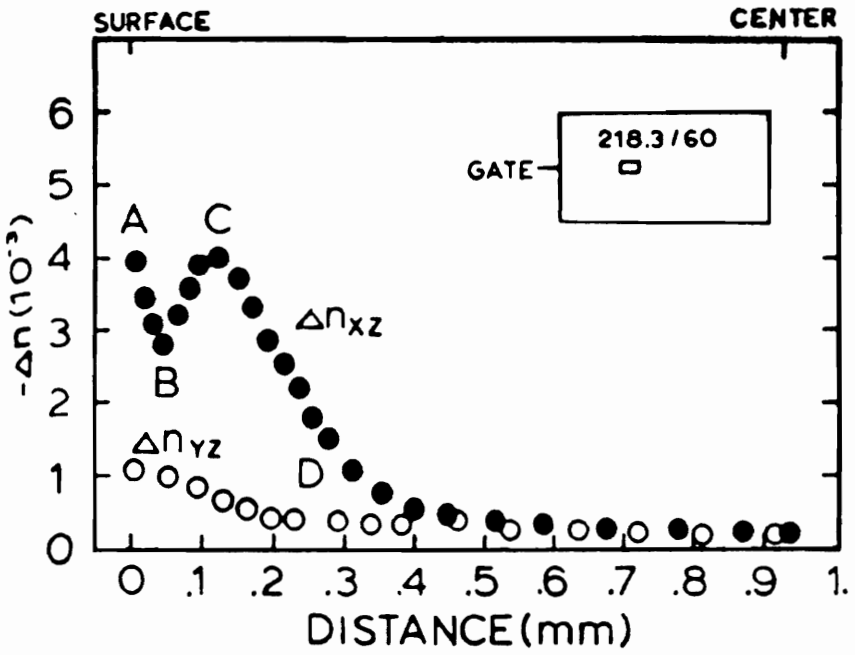

Fig. 2-9. Variation of birefringence across the thickness of injection molded PS [116].

crystallinity, and modulus. The modulus was based upon a series model of Seferis and Samuels [125]. The predicted results showed good agreement with experimentally measured values except near the wall where the grid size was not fine enough to resolve the sudden changes. A similar study with PEI and PPE was conducted by Yu, Wagner and Kalyon [126,127,128]. In this study a BKZ integral type constitutive equation and thermoelasticity equations were used to predict the residual thermal stresses. Fujiyama and Wakino [129] approached the study of injection molding of PP of various molecular weights in the framework of recoverable shear strain and its relaxation prior to solidification. They found experimentally and numerically a strong relationship between skin thickness and residual recoverable shear strain.

In summary, injection molding creates a unique structure in a specimen that affects the resulting mechanical properties. Fountain flow and instantaneous solidification creates a highly oriented skin. Solidification near the wall is also important to quench the orientation that resulted from high shear stress in this zone. These orientations may be predicted and related to mechanical and optical properties based on knowledge of the kinematics, stresses, and the temperature profile within the mold. Thermotropic liquid crystalline polymers are also subjected to these same processes. However, the presence of extensional flow has significant impact on orientation because of the rigid rod nature of LCPs. The effect of extensional flows on LCPs is analogous to the effects of extensional flow on the orientation of rigid fibers [130].

2.4 Liquid Crystalline Polymers

Liquid crystalline polymers display several distinct differences from thermoplastic resins. First, as the name implies, they display crystal like order in the liquid state. This state is called

the mesophase because properties exhibit both solid and liquid like behavior. Second, they exhibit unique rheological characterics such as high normal stresses and little die swell. They retain their orientation following shear or elongation for times several orders of magnitude longer than their random coil polymer counterparts. Lastly, because of the above, these polymers can be processed into highly oriented articles which have high strength and modulus. Their disadvantages are few but can be significant. First, at the present time these polymers are costly. Second, for thermotropic LCPs, the melting point or crystal to mesophase transition temperature is higher than most commodity plastics, and so if a blend of LCP and thermoplastics resins is desired at best a narrow thermal processing window exists. This limits the number of thermoplastics that may be blended with the LCP. Finally, because of the high orientation of the molecules, high properties are obtained in one direction, but the transverse direction suffers from much lower properties. This inherent anisotropy can limit the usefulness of the final molding.

2.4.1 Mesophases And Molecular Structure

Liquid crystalline polymers at temperatures above the crystal to mesophase transition temperature exhibit an unique appearance when observed under a polarized microscope. Contrary to the thermoplastic counterparts, LCPs display characteristic features such as threads or fans shapes when viewed between cross polarizers that occur because of the organization of molecules in this liquid state. Textures such as these are often called schlieren from the German word meaning inhomogeneous, and the field of optics dealing with inhomogeneous media is hence called schlieren optics [131]. Molecular organization is responsible for the schlieren texture, and there are three types of molecular organization commonly cited [132]. These organizations are

termed nematic, smetic, and chloresteric mesophases. The nematic structure is commonly observed for synthetic polymers and consists of a local group of highly aligned molecules called domains which are characterized by their molecular direction (or director). These mesophases appear threadlike under polarized microscope, and hence the Greek name nematic or threadlike [160]. When averaging these many domains in the quiescent state, no preferred orientation of these domains exist. The structure of a nematic domain is illustrated in Fig. 2-10. The second mesophase listed above, smetic, is characterized by a registry of molecules and hence exhibits more order than the nematic system. The smetic state may be further divided into smetic A, smetic B, or smetic C subsets. These subsets separate systems according to the alignment, tilt, or overlap of the molecules. Under the polarized microscope, the smetic mesophases often appear fan like [136]. The last category, cholesteric is a nematic-like structure. However, the molecular layers are not unidirectional as found in the nematic mesophase but form a helical pattern. This is also illustrated in Fig. 2-10. Some polymers can exhibit more than one of these forms dependent on either the temperature or concentration of the LCP, and these polymers are called polymorphic. More information on identification of these mesophases can be found in references [132,133,136].

The first polymeric liquid crystalline polymer was observed in a suspension of tobacco mosaic virus [160]. Since this time many other liquid crystalline polymers have been observed in solution, and these polymers are called lyotropic liquid crystalline polymers. The first commercially successful LCP was poly(1,4-phenylene terephthalamide) and it was used to make high performance Kevlar® aramid fibers [3]. Kevlar® is a wholly aromatic para substituted amide polymer that is infusible, and so it is processed in a solvent, sulfuric acid, and spun using a dry-jet wet spinning process. This dry-jet process permits the stretching of the fiber prior to

coagulation. Tensile strengths of 2.3 to 4.1 GPa and moduli of 45 to 102 GPa are obtained from this process [122]. While this fiber has a specific strength of five times that of steel, it is costly and involves further processing steps to convert the fiber into a usable form. A review of other processing techniques (e.g. film extrusion) that have also been attempted with lyotropic LCPs can be found in reference [175].

If liquid crystalline polymers could be processed in the melt state, i.e. a thermotrobe, the multiple processing steps and expense for manufacturing lyotropic liquid crystalline polymers could be minimized. One of the first such thermotropic liquid crystalline polymers was disclosed by Jackson and Kuhfuss [138]. The key to the creation of LCPs is the use of disrupting units [137] which are often accomplished with the insertion into the main chain of flexible aliphatic groups, e.g. ethylene, or the use of kinking units such as 2,6-naphthalene groups [141]. These disrupting units lower the crystal - nematic transition temperature. When the depression is sufficiently below the degradation temperature, a LCP may be produced. However, as a direct result of this disruption, the orientation is lowered, and the tensile modulus is not as high as it is for lyotropic LCPs. A review of this work and the effect of optimum randomization on melt temperature, relaxation times and physical properties can be found by Calundann and Jaffe [139], Chung [140], and Jackson [141]. In addition to the development of LCP copolyesters, development of poly(ester-amide) LCP has also been an active research area. Information relating the chemical composition of a poly(ester-amide) LCP to the resulting structure and properties of a spun fiber was presented by East et al. [135]. Their intent in developing this LCP was to include the amide group for enhanced fiber to rubber adhesion. Their concern was that the amide level would be limited by intractability created from intermolecular hydrogen bonding as experienced with Kevlar fibers. However, it was found that the incorporation of an aminophenol

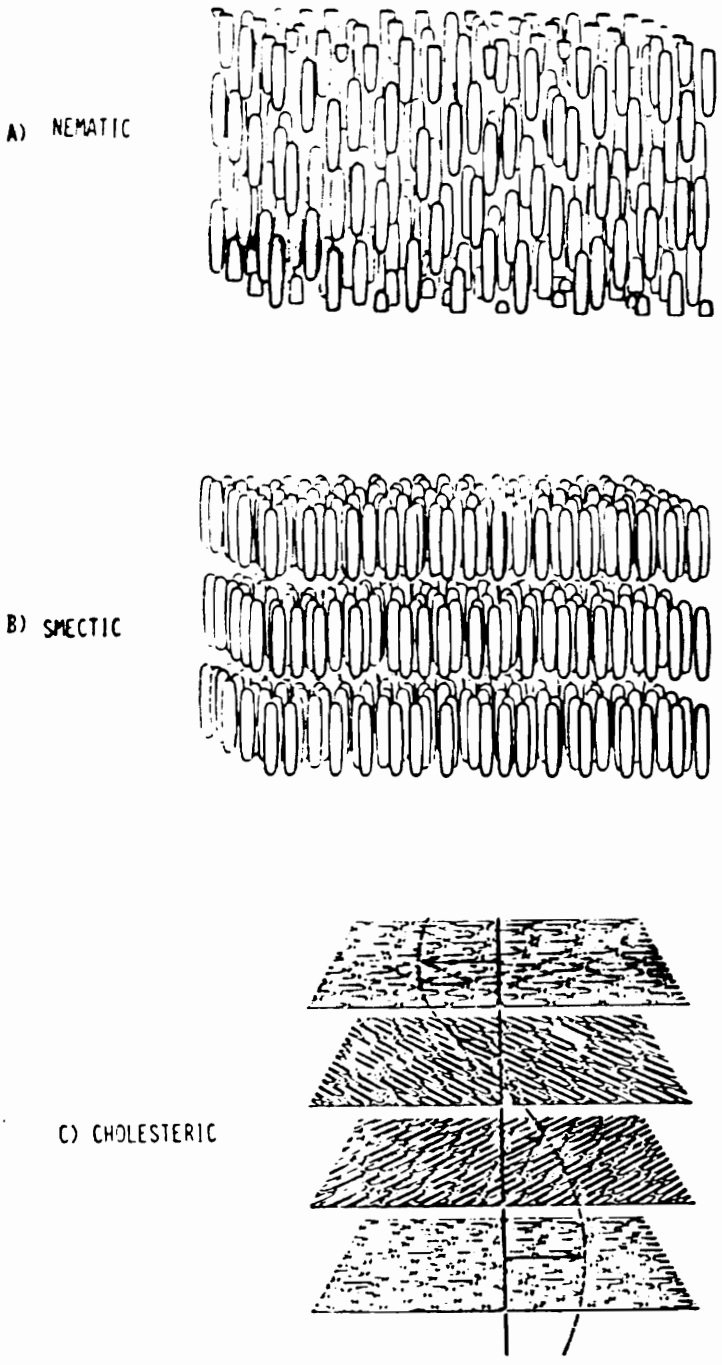

Fig. 2-10. Classification of LCP mesophases: a) nematic; b) smetic; c) cholesteric [140].

monomer actually created a randomness that permitted up to 30 mol % of this amine to be included without loss of tractability. Thus, both copolyester and poly(ester-amide) LCPs are produced commercially. The rheological properties of these polymers will be examined in the next section. As will be discussed, the rheology of LCPs exhibit some unusual phenomena.

2.4.2 Rheology

The rheology of LCPs is more complex than that of thermoplastics. As mentioned above, unusual phenomena such as high normal stresses relative to the storage modulus, large end corrections for capillary rheometry [151], and a low degree of die swell occur [151,152]. In addition, dependence of the rheology on both thermal and shear history occur. These rheological phenomena can partially be explained in a frequently cited morphological model of Asada and Onogi [142,143] for the liquid crystalline state. They postulated based on observations of the flow birefringence of nematic solutions of poly(γ-benzyl glutamate) that a structural transformation occurs as the shear rate is increased. Their model, shown in Fig. 2-11, indicates that as the shear rate increases the structure changes from an initially densely packed or 'piled' polydomain to a dispersed polydomain that is created via shear induced coalescence. At higher shear rates, an oriented monodomain state occurs. The reverse process, nucleation of domains, was also investigated by Asada [144]. A three region flow curve proposed by Onogi and Asada [143], shown in Fig. 2-12, typifies the viscosity behavior for many LCPs. Many authors claim that the existence of region I, a shear thinning zone which lacks a zero shear plateau viscosity, is regarded as proof of a yield stress [176,143,153]. This yield is believed to originate from the deformation and breakup of the domains. However, the slope of this region is rarely -1 which

corresponds to a stress that is independent of shear rate [137,152], and experiments on stress relaxation following a constant shear rate have shown that relaxation can be complete [152]. Additionally, for tests in constant stress rheometers for some LCPs, a yield stress can not be detected [159]. Thus, it is not clear that a yield stress must exist. The second region of this model is a Newtonian like behavior of nearly constant viscosity. In this region, the domains have coalesced, and molecular alignment prevails. The third region is another shear thinning zone.

Mathematical models for liquid crystals [145,146] and liquid crystalline polymers [147] have also been proposed to explain some of these phenomena from continuum and molecular viewpoints. Some comparison of these models versus experimental observation can be found in references [148-150].

A small degree of die swell and large entrance pressure drops are characteristics of LCPs. Typically, LCPs exhibit little to no swell on exiting from a capillary. This has been attributed by some authors as the result of yield stresses that reduce the recovery of elastic forces [124]. Beery et al. [236] examined the entrance pressure drop and shear viscosity for LCPs. They found that large entrance pressure losses did occur with LCPs with the entrance pressures losses reached 50% of the total pressure drop. This large pressure loss was explained as arising from the energy to orient the LCP domains. Because of these high entrance pressure losses, the ratio of elongational to shear viscosity was determined to be 1 to 2 orders of magnitude greater than that measured for Newtonian liquids.

Transient rheological behavior has also been investigated. For instance, LCPs can exhibit two types of relaxation on cessation of shear flow. The stresses decay typically within seconds while the orientation can persist for half an hour. This effect has been observed using rheooptics for hydroxypropylcellulose [176] and using rheological interrupted step tests for PHB/PET [152].

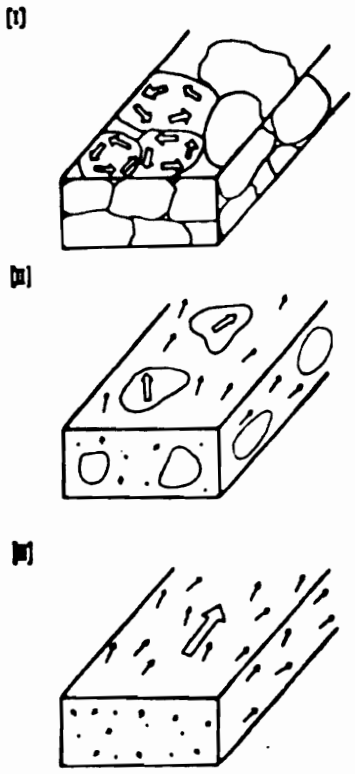

Fig. 2-11. Transformation of LCP structure as proposed by Asada and Onogi [143]: a) piled polydomain; b) disperse polydomain; c) monodomain.

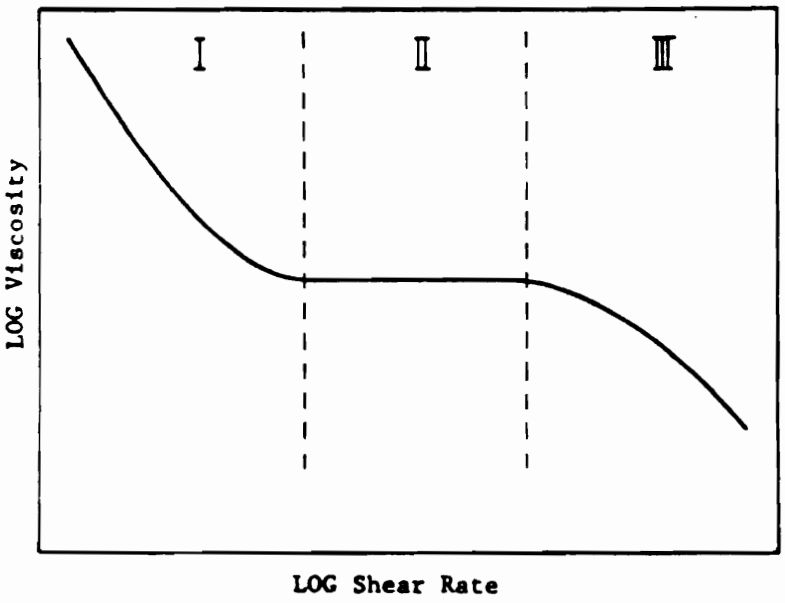

Fig. 2-12. Three region flow curve as proposed by Onogi and Asada [142].

In an unusual analysis of relaxation time, Ide and Chung [185] produced copolyester and poly(ester-amide) fibers. They subjected these fibers to temperatures at or above the melt temperature of the LCP. The specimens were simultaneously tested for tensile modulus, and the tensile modulus, M, was fitted to the following relaxation equation

$$M(t)=M(0)*\exp(-t/\tau) \tag{2-23}$$

where the relaxation time, τ, was found to vary between 10 and 40 minutes. In contrast, many of the relaxation times of thermoplastics are on the order of seconds [48]. Hence, this demonstrates in an another manner the long relaxation times of LCPs.

2.4.2.1 Dependence of Rheology on Temperature and Thermal History

For polymers, the rheology changes with temperature. However, for LCPs, the rheology depends upon the phase as well as the temperature. Starting from a high enough temperature to be well within the isotropic phase, the viscosity increases as the temperature falls as it does for thermoplastics. At the mesophase to isotropic phase transition, the viscosity suddenly falls. This drop in viscosity has been related to the formation of molecular alignment in the mesophase which lowers the viscosity. As the temperature is continually lowered, the viscosity again rises until the mesophase to crystal phase transition is reached, and the LCP crystallizes. These transitions are discussed further in references [182,183], and a recent review of LCP rheology by Weiss et al. can be found in reference [180].

In addition to temperature dependence, thermal history also affects the rheology of LCPs. A well known experiment conducted by Wissbrun [153] was one of the first studies to report the effect of thermal history upon the rheology. Using a capillary rheometer, Wissbrun compared

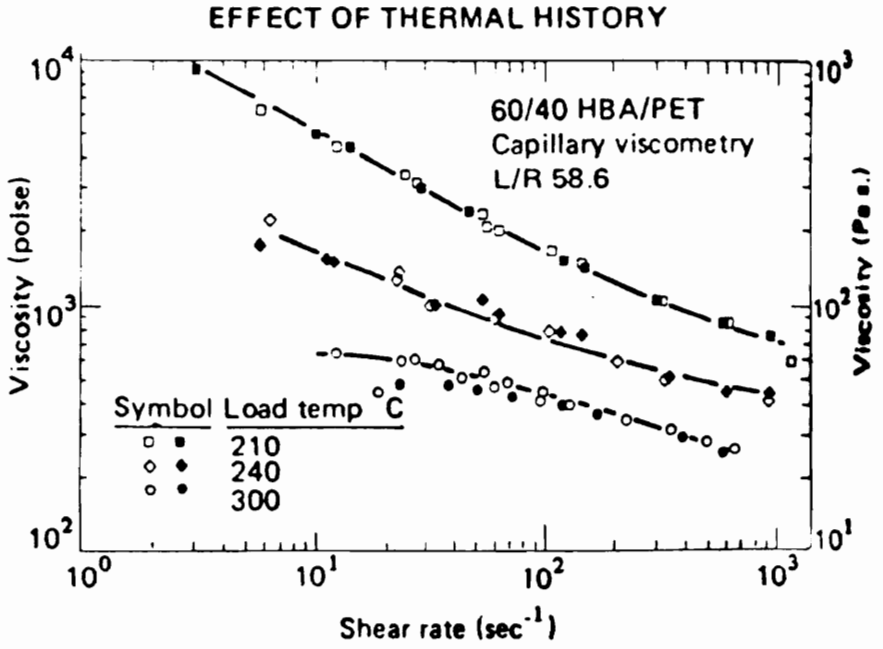

Fig. 2-13. Effect of thermal history on the shear viscosity of a LCP [153].

the viscosity of a LCP subjected to three different thermal paths. The first path consisted of holding and subsequently testing a LCP at 210° C. The second and third paths consisted of holding the LCP at 240 and 300° C, respectively, and then decreasing the temperature to 210° C followed by measurement of the viscosity once thermal equilibrium was achieved. The results of these tests are displayed in Fig. 2-13. A dramatic influence of the temperature history on the viscosity tested at 210° C is shown. These results differ considerably from thermoplastic polymers which do not depend upon the thermal history but only depend upon the equilibrium test temperature. A similar test of the dynamic viscosity also showed a dramatic effect. By raising the temperature from 210° C to 240° C for one minute followed by decreasing the temperature to 210° C, a substantial viscosity drop occurred that required six minutes for the viscosity to returned to an equilibrium value.

Other thermal history tests on LCPs were conducted by Done and Baird [154,155]. For PET/HBA80 sheared in parallel plate fixtures, they showed that the orientation of samples sheared to the same degree is less in the samples preheated well above the melting point than in samples heated near the melting point. Lin and Winter [156,157] studied this situation for Vectra A900. Annealing this LCP at 290°C, above the melting temperature, they found from X-ray analysis that an additional ring formed at a spacing of d=3.8Å. Subsequent thermal analysis indicated that a second endothermic peak formed between 305 and 315°C. Concurrent with formation of this second endotherm was a proportionate increase in the complex modulus. However, preheating at 320°C substantially reduced crystallization when the sample was subsequently cooled to 290° C. The results of these two studies both indicate that preheating is important to obtain low viscosity and to permit significant supercooling while retaining molecular orientation for extended times. However, excessive preheating melts any residual crystals and

greatly shortens the relaxation time for molecular order thereby resulting in lower orientation and mechanical properties.

An additional study of the change in texture and mechanical properties of LCPs was undertaken by Zachariades and Logan [167] for a PET/PHB80 LCP produced by Tennessee Eastman. Examination of this polymer below the melting point revealed a two phase structure with PHB rich domains. Upon shearing, these PHB domains remained undeformed. Upon heating above the melt temperature, the PHB domains merge into the surrounding mesophase and upon subsequent shearing band patterns, 5 to 10 microns apart, formed perpendicular to the shear direction. Fibers prepared above the melting point of the PHB domains demonstrated 4 to 5 times the modulus of fibers produced below the PHB melting point. Thus, for phase separated LCPs, melting of crystals is a prerequisite for obtaining high mechanical properties.

2.4.2.2 Dependence of Rheology on Shear History

The rheology of LCPs depends not only on temperature and thermal history, but it also depends upon shearing history. This includes both the magnitude of shear and the magnitude of the shear rate. Some classic experiments will be reviewed in this section. The first such experiment was conducted by Wissbrun [153] who measured the complex viscosity of a LCP. Wissbrun found upon sweeping the frequency from low to high frequency immediately followed by sweeping the frequency from high to low values that hysteresis existed. Additional tests were performed by subjecting samples to high shear rates followed by a rest time and subsequent measurement at low shear rates. The results indicated that the LCP behaved in a thixotropic manner where the viscosity decreased for the sample subjected to the smallest rest time but the

viscosity rose exponentially to values found without preshearing for those samples tested after long rest times. These results strongly suggest that a structure exists which takes a large shear rate or long time to destroy and that can reestablish or can be reversibly formed with time.

Tests similar to the above were also performed by Wissbrun and Griffin [158]. In these tests, the effects of steady shear history on subsequently measured dynamic viscosity were examined. The results of these tests are shown in Fig. 2-14. It is clearly seen that for the two frequencies displayed that the magnitude of total shear affects the viscosity. It can also be seen that the dynamic viscosity measured at the lowest shear rate is more sensitive to the shear history than the dynamic viscosity at higher shear rates. Wissbrun and Griffin viewed these shear history phenomena in regard to the Leslie-Ericksen theory. While they could not rule out that this theory applied, they suggested that the domain model proposed by Onogi and Asada was a more credible cause of these phenomena since the rheological behavior conformed closer to that of a dispersion.

In a recent paper, Cocchini, Nobile and Acierno [159] examined the rheology of HBA/HNA27 copolyester LCP in a rotational rheometer. They found that precise loading and preshearing procedures were needed to create a relaxed reproducible structure. They first noted that after loading a sample between cone and plate fixtures that several hours were required for the normal stress to relax. Failure to permit the normal forces to relax can lead to misinterpreting normal stresses differences. They suggested that this may be the source for some reports of negative normal stress differences. However, applying a total strain greater than 100 resulted in the normal stress relaxing to zero in a quicker time than required for samples that were not presheared. As pointed out by Viola and Baird [148] in interrupted step rate tests, the transient test depends upon prior strain history. Thus, Cocchini et al. adopted a rest time of at least 400 s after applying a strain of 100 before conducting a rheological test. These studies

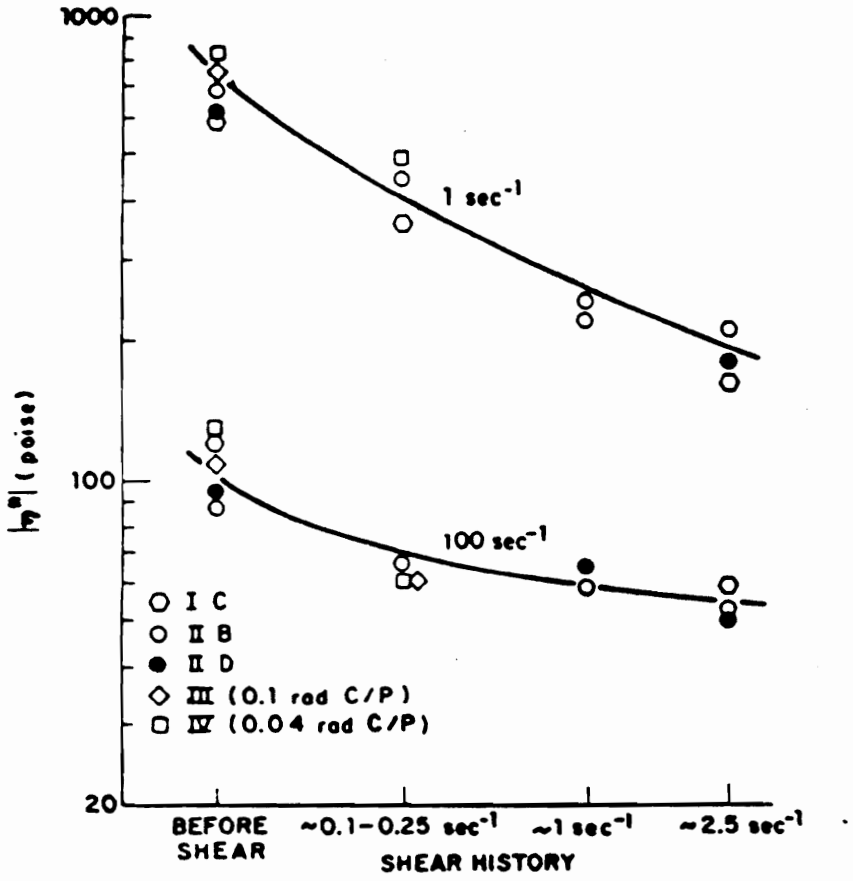

Fig. 2-14 Effect of preshear on the dynamic viscosity for a LCP [158].

indicate that the rheological data for LCPs must consider strain history, and the results should be reported with information pertaining to the prior shear history of the sample.

2.4.3 Morphology

Features such as incomplete extinction of polarized light in highly oriented regions, banding textures from articles produced in high shear rate processes, and hierarchial structure are several noted peculiarities of LCPs. The morphology of LCPs can be observed at different levels. Structures greater than one micron can be viewed with the optical microscope while submicron structures can be viewed with the electron microscope. Molecule orientation may be examined with the use of X-ray diffraction, infrared dichroism or birefringence techniques. A review of microscopy techniques including birefrigence used to characterized the morphology of LCPs can be found in reference [160] by Sawyer and Jaffe, and an extensive discussion for thermotropic copolyesters can be found in reference [161].

An unusual feature of LCPs is the incomplete extinction of light when a sample is placed between crossed polarized light and aligned with the machine direction parallel to the polarizer. Sawyer and Jaffe [160] attribute this phenomenon to slightly different orientations of the directors between the many nematic domains in the skin. When the machine direction is oriented 45° to the polarizer, a banded texture is observed in the core. For Vectra polymers, this banding has a periodicity of 500 nm. The origin of this texture has been studied by Windle and coworkers [162,163] and is explained as a periodic variation in the alignment of the director. These researchers have extended their finding and now predict the optical diffraction pattern occurring from these director variations [164]. A similar phenomenon called banded patterns, as opposed

to banded textures, was examined by Takeuchi et al. [165]. They investigated the formation of banded patterns in shear flow following capillary extrusion at 6 to 6080 s^{-1}. The banded patterns were found to occur at shear rates greater than 600 sec^{-1}, and the patterns could be related to the mechanical properties and the fracture mechanisms. They found that samples tested with banded patterns fractured into conical pieces along the bands as opposed to flat fracture surfaces for samples prepared at low shear rates. In addition, there is a discontinuity in fracture surfaces between the skin and core suggesting that each layer fractured independently. This indicated that the integrity between the skin and core was poor when banded patterns were formed. They explained the origin of this banded pattern as resulting from residual stresses in the core which preceded the formation of microdefects as has been observed with PET [166].

An overall structure for fiber and molded articles was presented by Sawyer and Jaffe [160,161] based on SEM observation of fracture surfaces. This structure is illustrated in Fig. 2-15 for fibers, extrudates and moldings. These illustrations show a fibrillar structuring consisting of three levels: macro fibril, fibril, and micro fibril. The size of these structures are indicated in the figure. In addition to the fibrillar morphology, a macroscopic morphology is superimposed on this structure. Here an outer skin, inner skin, and core regions exist. Within these regions the fibrillar morphology is also illustrated. Through X-ray techniques, Thapar and Bevis [168] and Baer et al. [169] have examined molded articles in more detail. They have shown that orientation within a molded part depends upon the flow patterns within the mold. As the melt moves out from the center toward the wall a tilting of the molecular alignment is displayed in the X-ray pattern. At the center, the molecules are oriented perpendicular to the flow direction, and the molecular alignment gradually turns to become parallel to the skin as the wall is approached. These X-ray results match the patterns displayed in SEM photomicrographs

of etched samples. More details on X-ray analysis of LCPs can be found in references [170-172], and the use of infrared dichroism to obtain order parameters of moldings and fibers can be found in references [173,174].

Use of ESCA has also been performed to show the presence of a blocky nature of PET/PHB60 in injection molded parts. In particular Joseph et al. [181] found from microscopy of etched fracture surfaces and from ESCA that PHB rich copolymer migrated to the surface. It was speculated that this occurred because the lower viscosity rigid PHB segments migrated to the surface where the shear stress was greatest. Many of these techniques for examination of neat LCPs have not been applied to the examination of LCP blends. Research into these areas may reveal new knowledge between processing and structure / property relationships for LCP reinforced thermoplastic blends. The next section will examine the role of processing and its affect upon structure and properties.

2.4.4 Processing

Processing has a distinct effect on the mechanical properties of LCPs. Processes such as fiber spinning, strand extrusion, sheet extrusion, and injection molding each create unique properties. These properties are created for the most part as a result of the flow kinematics. As will be discussed, elongational flows produce a greater orientation than shear flows, and this leads to significant differences in mechanical properties. However, thermal history is also an important factor, and the ability for a LCP to retain its orientation until solidification occurs is another key reason for the high properties of LCPs. The effect of flow kinematics will be the first area examined.

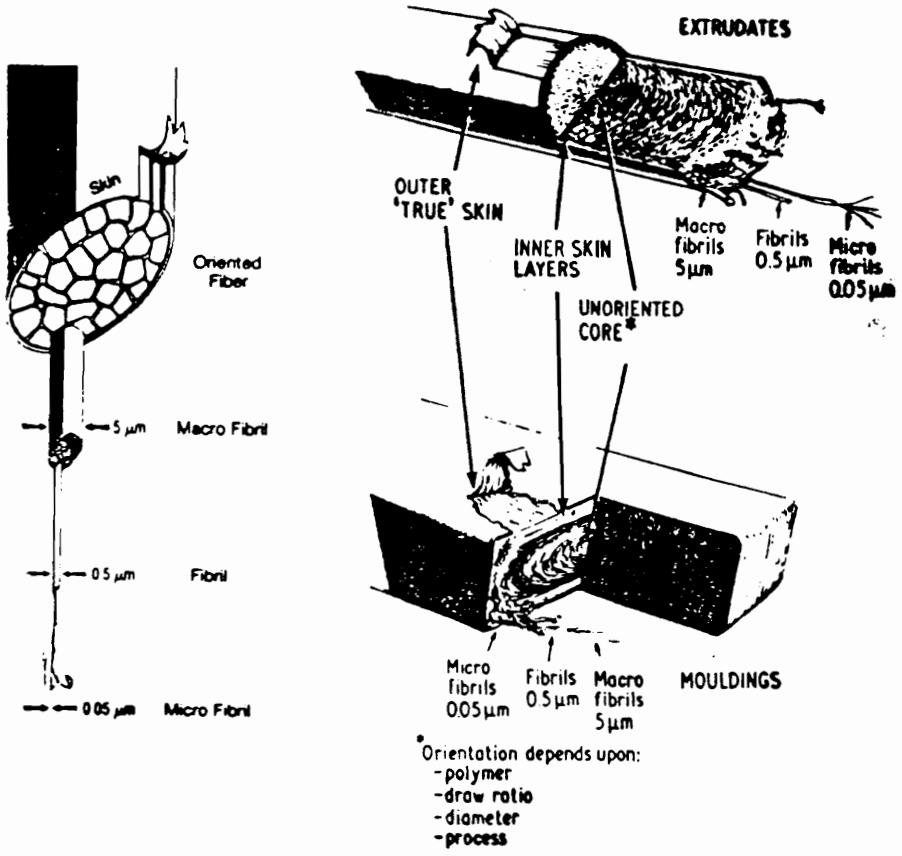

Fig. 2-15. Morphological description of LCP fiber, extrudate and molding [160].

Ide and Ophir [177] studied the effects of draw ratio on the orientation and mechanical properties of a LCP extruded through a capillary die. This was one of the first clear investigations of the effect of elongational flow on LCP properties. Their study revealed several findings. First, a skin-core morphology was created from the flow rearrangement that takes place upon exit from the die where the skin must stretch and the core must compress to generate a uniform velocity in the strand. Second, from measurement of the modulus and the orientation of strands elongated with draw ratios from 1, i.e. not elongated, to over 50, they concluded that elongational flow greatly increase the molecular orientation, tensile modulus and tensile strength. In these experiments, the modulus increased from 5 to more than 40 GPa and the strength increased from 100 to 700 MPa. Extrusion of strands with increasing shear rates decreased the modulus from 5 to 3 GPa and slightly decreased the strength. They concluded that orientation occurs in elongational not shear flow. This orientation does not depend on the stress as found by varying the stress at a constant draw ratio, and so this indicated that LCPs are an exception to the stress optic rule which holds for thermoplastic polymers.

Fiber spinning studies of PET/PHB60 were conducted by Lewis and Fellers [175] to investigate the extrusion of LCPs in an analogous manner to the dry-jet wet spinning method used in the manufacture of lyotropic LCPs. In the dry-jet wet spinning process, the dry-jet allows elongation of the fiber prior to coagulation. In a like manner, Lewis and Fellers wanted to determine if an isothermal gap would cause more orientation and higher mechanical properties than in a non-isothermal gap. They found that neither shear rate or draw ratio created a significant change in orientation or properties although lower properties were measured at higher shear rates in agreement with Ide and Ophir [177]. It was speculated that the bulk orientation decreased as the result of psuedoplastic behavior (e.g. plug flow velocity profile) which lead to

a skin-core morphology. However, the greatest impact on properties was the extrusion temperature, and the isothermal gap process producing the highest properties.

Chung [178] studied the extrusion of strands of HNA based LCPs that were extruded through a conical die and drawn to various degrees. The resulting relationship between initial modulus and Hermans orientation function is shown in Fig. 2-16. This figure shows for strands with a high degree of orientation that small increases in the orientation creates large increases in the modulus. In a further study, Chung [179] determined that the modulus of thick strands was lower than the modulus of thin strands. Postulating that heat transfer was involved, Chung evaluated the performance of a die which used a cooled inner cone to simultaneously create a converging flow and to lower the temperature of the extrudate core. These enhancements lead to higher orientation and modulus than found using the same conditions in the standard conical die. Thus, Chung's work illustrated the importance of using elongational flow with rapid solidification to obtain high properties in LCPs.

To quantify these relationships between processing, orientation and mechanical properties Kenig proposed a model for LCPs [186,187]. Starting with the premise that the LCP domains are the orientable species, Kenig modeled these domains as rigid rods suspended in an elongational flow. This framework was based on prior studies of the motion of an ellipsoid in a fluid [188]. The orientation of the domains was related to the draw ratio, DR, initial orientation, C_1, and a orientability material constant, λ, but it was not related to the elongation rate,

$$\tan\phi = C_1 DR^{-\lambda} \qquad \textbf{(2-24)}$$

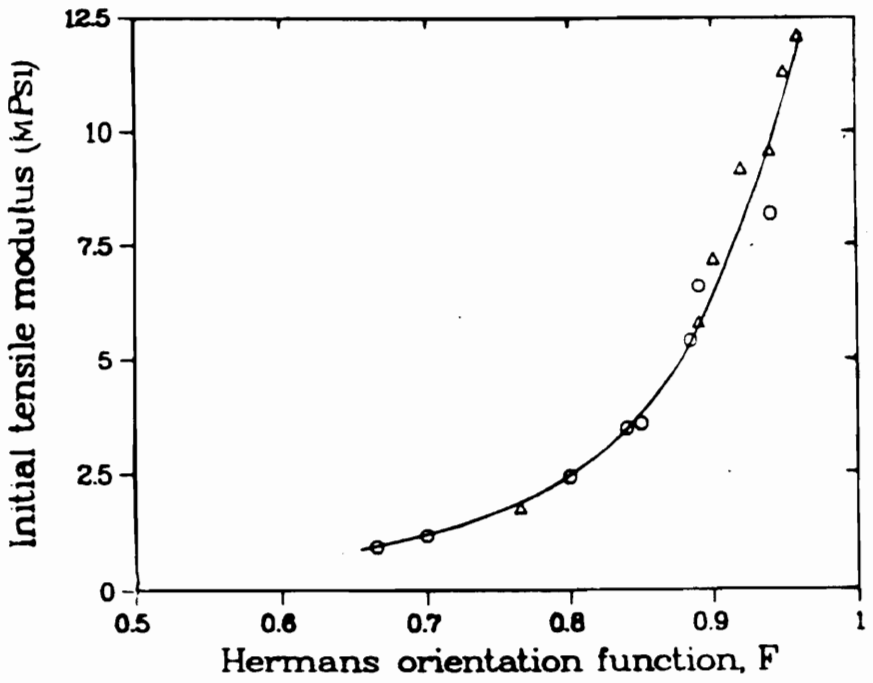

Fig. 2-16 Initial modulus versus Herman's orientation parameter for extrusion of LCP through a conical die: ○ standard die; △ new die [178].

Kenig also theoretically related the orientability constant to the aspect ratio of the LCP domains and suggested that domains with higher aspect ratios yield fibers with higher orientability. The same approach for simple shear flow yielded a relationship between orientation angle, ϕ, and total shear strain, γ, [187]

$$\tan\phi = \frac{1+B}{(1-B^2)^{\frac{1}{2}}} \tan\left[\frac{(1-B^2)^{\frac{1}{2}}}{2}\gamma\right] \qquad \textbf{(2-25)}$$

where for the Poisuelle flow the total strain is equal to the product of strain rate and time which yields a strain that is proportional to the L/D ratio of the capillary die. Experimentally, Kenig studied the orientation in combined Poisuelle and extensional flow for two capillary lengths. In all cases, the orientation and modulus improved with higher L/D ratios. However, elongational flow was found to be vastly more effective at orienting the LCP domains.

LCPs are often used in injection molding. In one of the first papers disclosing the creation of a LCP, Jackson an Kuhfuss [138] related the mechanical properties of injection molded specimens to the mold thickness. This relationship is shown in Fig. 2-17. As illustrated in this figure, there is a large increase in the machine direction flexural modulus as the mold thickness decreases with a corresponding, albeit, small decrease in transverse properties. Thus, a highly anisotropic article results from thin molds. Conversely, a nearly isotropic article results from thick molds. These results are unique to LCPs and the cause for these relationships was not explained in this paper.

Another unique feature of molded LCPs is the orientation profile through the thickness of the mold. Blundell et al. [191] using several LCPs with varying degrees of molecular stiffness

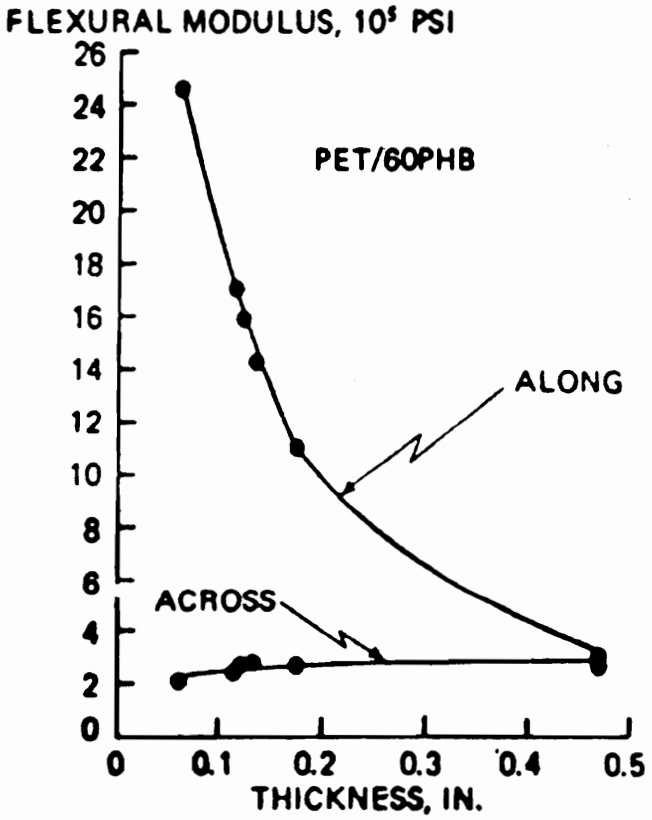

Fig. 2-17. Flexural modulus versus the mold thickness [138].

or linearity determined the orientation profile through the thickness of the mold via microbeam X-ray diffraction. The LCPs used in their study contained varying degrees of HBA, and this rigid unit was responsible for substantial changes in the orientation profile. In Fig. 2-18, the X-ray intensities at $2\theta=20°$ versus the location in the mold for LCPs with 36, 27, and 15% HBA respectively. The optical axis as determined with an optical microscope is illustrated at the bottom of the figure. Clearly the inclusion of higher amounts of rigid units leads to more variations in the orientation. These authors do not explain why this variation develops but other authors relate it to the type of flow experienced in the mold [189]. The LCP with only 15% HBA shows a profile more like that of a thermoplastic polymer. These authors have clearly demonstrated that when dealing with LCPs, the rigidity of the polymer leads to more complex orientation profiles.

An advancement in the understanding and modeling of orientation of LCPs in molds was presented by Garg and Kenig based on the analysis of elongational and shear flow reviewed above [189]. As pointed out by Garg and Kenig, filling of a rectangular mold can create four distinct flow fields: radial, converging, fountain, and shear flows. The first flow field leads to transverse orientation of rigid rods while next two flow fields lead to machine direction orientation of rigid rods. The orientation of a fiber in fountain flow was solved with an equation for the velocity in the fountain flow [102]. The orientation was related to the initial orientation, material parameter, and coordinates in a similar manner to that found for orientation in shear flow. Garg and Kenig show how the results of these predictions can be investigated experimentally with mechanical property measurements. Because of the highly nonisothermal nature of injection molding, it should be noted that the shear rates in filling operations need to be analyzed carefully because maximum shear rates can be obtained at locations other than the mold wall [95,190]. This can

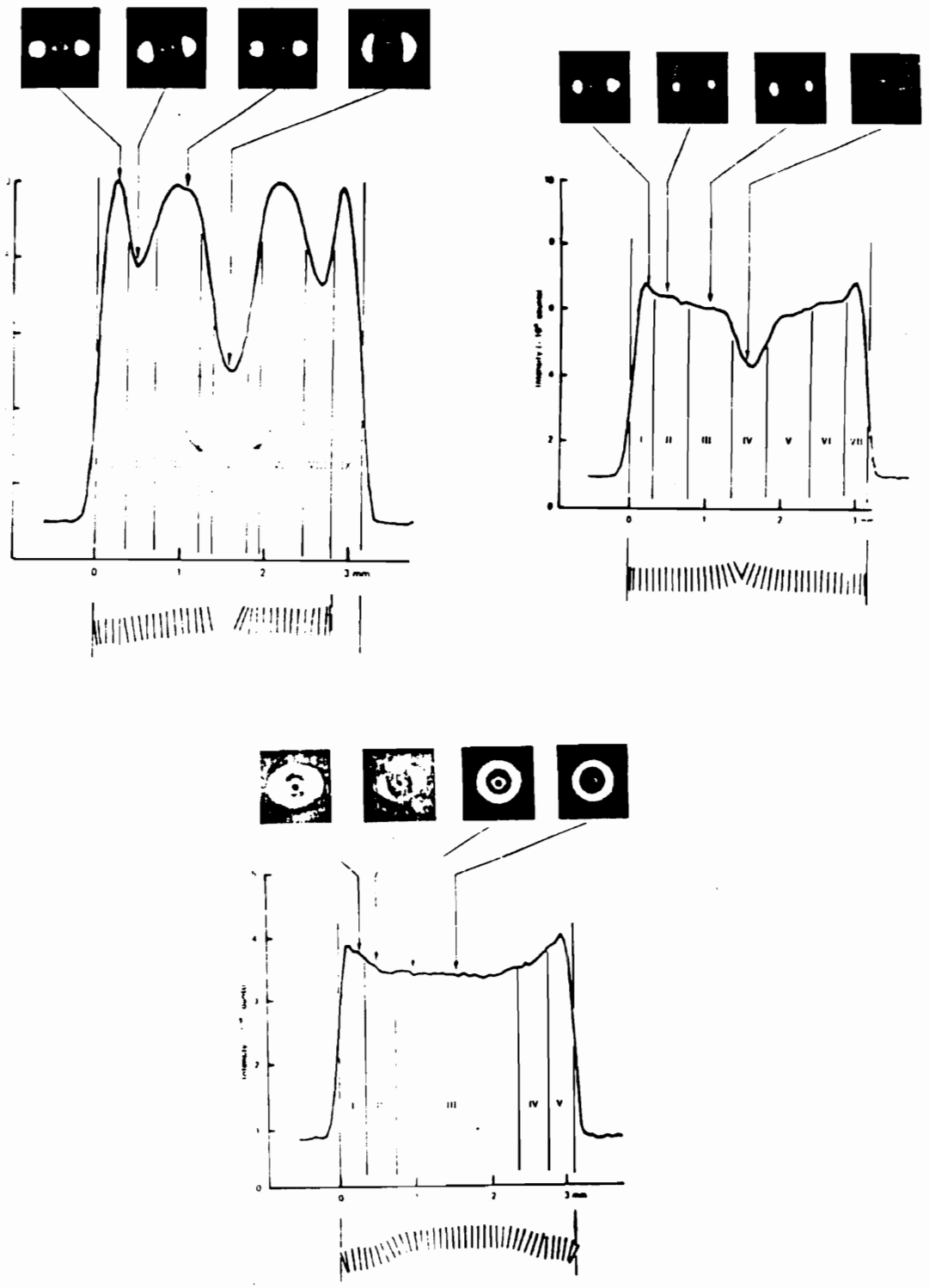

Fig. 2-18 Orientation profile through the thickness of LCP moldings containing a) 36%, b) 27%, c) 15% HBA [191].

lead to different degrees of extensional, shear, and plug flow across the mold thickness, and this may be reflected in orientation profiles of rigid rod polymers as noted by Blundell [191].

2.4.5 Mechanical Properties

To understand how processing affects the mechanical properties of LCPs several studies are discussed. These studies have a common vantage of viewing the structure as a composite either in the thickness direction or within the plane of the specimen. The first study examines modeling of in-plane anisotropies.

An investigation by Ide and Chung [185] of sheets of extruded LCP which were based on HBA/HNA revealed the close fit of this system to traditional unidirectional continuous fiber reinforced composite structures. In Fig. 2-19, the change in tensile strength and modulus of anisotropic LCP sheets are shown as the testing angle is rotated from the machine direction to the transverse direction. The composite theory equations for predicted properties are shown below

$$\frac{1}{\sigma(\theta)^2} = \frac{\cos(\theta)^4}{X^2} + \frac{\sin(\theta)^4}{Y^4} + \left(\frac{1}{S^2} + \frac{1}{X^2}\right) * \sin(\theta)^2 * \cos(\theta)^2$$

$$E(\theta) = \frac{E_1 * E_2}{E_1 - (E_1 - E_2) * \cos(\theta)^4} \qquad \textbf{(2-26)}$$

where X and Y are the tensile strength in the flow and transverse directions, respectively, and S is the shear strength. In the second equation, E1 and E2 are the tensile moduli in the flow and transverse directions, respectively. They noted that the in-plane shear strength is typically low for LCPs and the origin of these low values in speculated to be the result of low intermolecular cohesion.

In a study which modeled the domains as a two phase structure, Dibenedetto et al. [184] related the nematic morphology of drawn PET/PHB60 LCP fiber to the domain aspect ratio. The effect of the drawing process was claimed to change the equilibrium nematic phase morphology. The morphology of undrawn fiber consisted of randomly oriented spherical domains of high order surrounded by less ordered boundary regions. By drawing, this morphology approached parallel cylindrical domains. The aspect ratio of these domains were calculated from the draw ratio. By using a two phase model (i.e. ordered domains and unordered boundaries), both the longitudinal and transverse modulus were obtained from the Halpin-Tsai equation which was modified for fiber angular dependence.

An interesting study that treated injection molded tensile bars of LCPs as a laminated composite was performed by Blundell et al. [191]. Using several LCPs with varying degrees of molecular stiffness or linearity the authors determined the orientation profile via microbeam X-ray diffraction. Assuming the molding was composed of many lamina cut across the thickness direction, Blundell applied the orientation distribution to the aggregate model [192] for highly oriented units. The fundamental properties of these units included an axial modulus of 100 GPa and a transverse modulus of 2 GPa. The aggregate model enabled a lamina property to be calculated from the distribution of orientations at a given depth into the tensile bar, and these properties were used to determine laminate, i.e. the tensile bar, properties using standard composite theory.

Garg and Kenig [189] investigated the mechanical properties of sections of LCPs made in a long rectangular mold. These sections isolated either radial, converging, or planar flow regions. As reviewed above, radial flow should orient rigid rods transverse to the flow direction, while converging and planar flow should orient rigid rods parallel to the flow direction. Testing

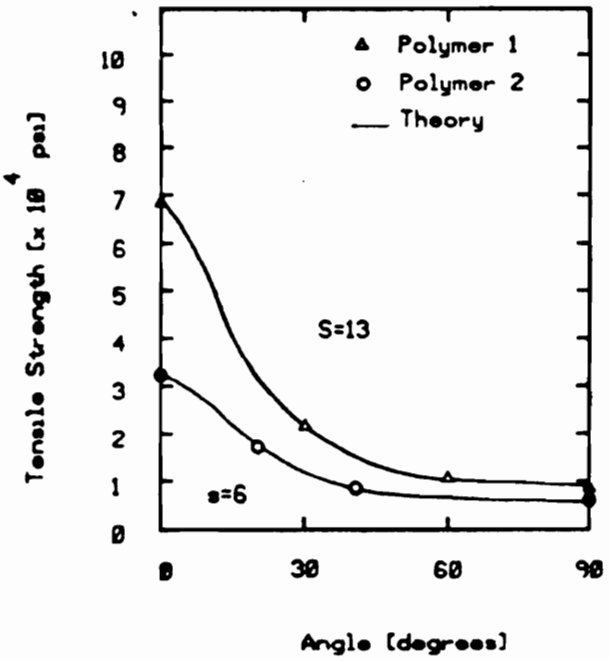

Fig. 2-19. Variation in tensile strength with angle of testing for HBA/HNA LCP [185].

of the tensile modulus at various angles from the machine direction revealed the orientation of the LCP. By testing two LCPs which possessed different orientation material parameters, λ, Garg and Kenig confirmed the expected dependence of orientation on the flow field. These results are shown in Fig. 2-20. Polymer A (Fig. 2-20a) has a lower orientability than polymer B (Fig. 2-20b), and the changes in profiles are less pronounced. This is analogous to Blundell's observations which were discussed in the previous section. Additionally, the radial flow section, region 1, shows less anisotropy for polymer A than polymer B. However, because of the higher orientability of polymer B, this polymer reaches a peak in the modulus in the transverse direction. Regions 2 and 3 for converging and planar flows, respectively, show profiles reminiscent of uniaxial fiber reinforced composites.

An important parameter for retaining the orientation created in the fountain flow is the freezing of the polymer near the walls. The thickness of this frozen layer can be estimated via an equation derived by Dietz et al. [118] and shown below

$$d=2\left(\frac{T_s-T_w}{T_m-T_W}\right)(\alpha t)^{1/2} \qquad \textbf{(2-27)}$$

where d is the frozen layer thickness, Tm is the melt temperature, Tw is the wall temperature, Ts is the solidification temperature, α is the thermal diffusivity, and t is time the polymer is in contact with the wall during the filling stage. From experimental measurements, Garg and Kenig found the term αt to be nearly constant. This naturally led to plotting the frozen layer thickness measured from optical microscopy versus the temperature group in the above equation. This plot was linear which showed good agreement with the prediction. As might be expected, the flexural modulus increased with increases in the frozen layer thickness. This relationship is

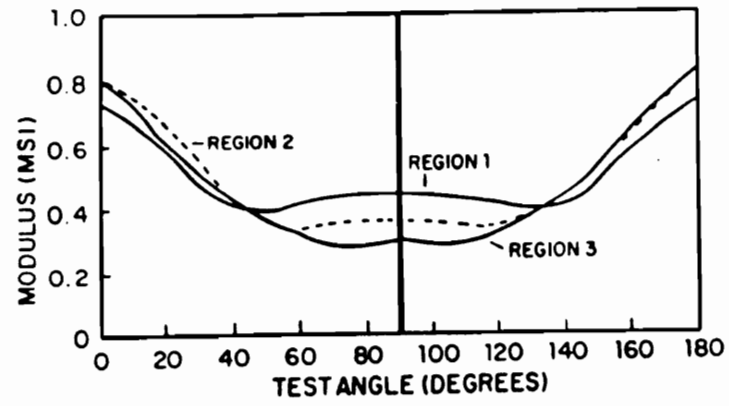

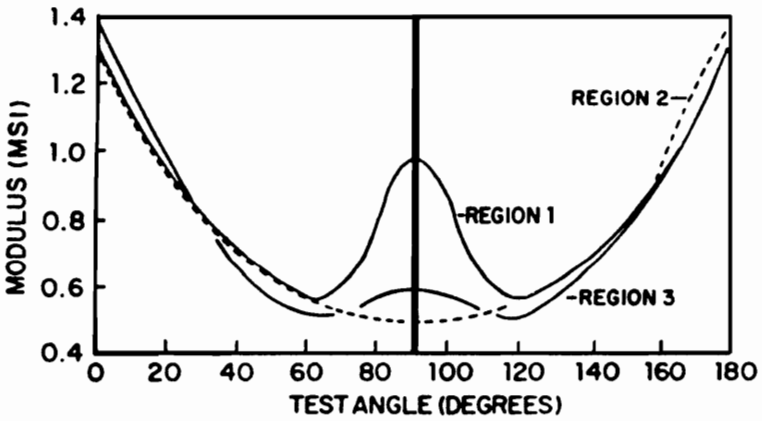

Fig. 2-20 Properties from polymers with different orientation material parameters in (1) radial, (2) converging, and (3) planar flows [189].

shown in Fig. 2-21. Finally, the because of changes in the size of extensional, shear, and plug flow regions with changes in the mold temperature, the tensile modulus does not follow the same relationship as the flexural modulus. Instead the tensile modulus is greatest were the shear flow zone is the greatest and the plug flow zone is the smallest. These regions where determined by color changes within the thickness of the mold that are observed in polished and etched samples.

A interesting device for controlling anisotropy of a LCP, hydroxypropyl cellulose (HPC), was investigated by Farrell and Fellers [193]. This device was a rotating annular die which was used for blowing film. Rotational speeds of both the outer cylinder and the inner mandrel could be varied independently. By variation of the axial shear stress to the tangential shear stress, anisotropy could be modified so that the modulus was made more uniform in all directions.

In a similar manner, the effect of the flow field on the mechanical anisotropy of injection molded parts was investigated by Zachariades and Economy [194]. A special mold which consisted of a center gated configuration with a rotating and compressing wall created triaxial flow. This flow created triaxial orientation which resulted in high strength and impact resistant parts for both thermoplastic and thermotropic polymers. These last two studies reveal that processing equipment must be designed so that flows create an orientation which leads to transversely isotropic properties.

2.5 LCP Blends: In Situ Composites

The blending of LCPs with thermoplastic resins can lead to mechanical properties which are significantly greater than the mechanical properties of neat thermoplastic resins. Hence, these blends are receiving more research effort from both the industrial and academic communities.

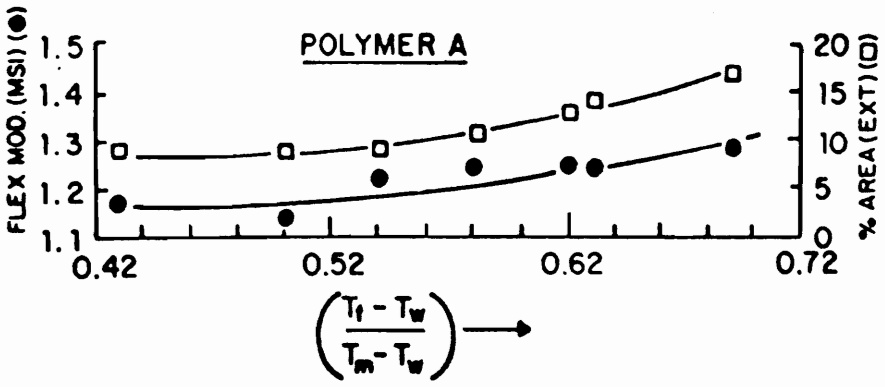

Fig. 2-21 Flexural modulus versus the frozen layer thickness [189].

Several reviews are available describing the rheology, morphology, processing and technological opportunities for LCP blends [207-210]. These blends possess several characteristics that make them unique and potentially useful. One aspect noted earlier was that the addition of small amounts of LCPs to thermoplastic matrices can drastically reduce the viscosity. Another aspect is that the dispersed LCP droplets can readily form fibrils in elongational and high shear rate flow fields. These elongated fibrils are responsible for reinforcement of the thermoplastic matrix. Another aspect of these blends is that they have good dimensional stability and a coefficient of thermal expansion (CTE) that can be tailored to a desired value based on the quantity of LCP in the blend [209]. However, LCP blends have some disadvantages which include anisotropy and brittleness. The former condition can be modified via judicious process design, and the latter condition may be ameliorated via improved adhesion between the phases.

2.5.1 Rheology and Morphology

The first rheological data to be examined is the viscosity of neat thermoplastics and LCPs. As mentioned in an earlier section, a viscosity ratio close to one is desired for the greatest ease in causing the breakup of droplets. One ideal matrix from this standpoint is PET with the LCP, PET/HBA. As shown in Fig. 2-22, PET exhibits a Newtonian like viscosity over a wide shear rate range. Also plotted on this chart is the viscosity of PET/HBA for three different copolymer ratios (30, 60, 80% HBA) at 270° C that was determined in a capillary rheometer [198]. From this plot, it is easy to see that the viscosity of PET/HBA30 crosses over the viscosity of PET near 25 s^{-1}. This crossover point indicates that a viscosity ratio near unity will occur in many processing operations. However, the use of this LCP while advantageous from

a processing point of view is not useful for reinforcing thermoplastics because of its lower physical properties. For a blend of PC and PET/HBA60, a crossover point occurs near a shear rate of 0.2 s^{-1} [212]. This crossover point is too low for most practical processing operations, and so the viscosity ratio at processing conditions will be less than unity as occurs for most LCP blends.

Upon examination of the blend viscosities a common finding is that the viscosity of the blends is intermediate between that of the thermoplastic and the LCP. This occurs for PC - PET/HBA60 and PET - PET/HBA60 [198]. However, this is not always the case. For PS with PET/HBA60, the viscosity of the blends is lower than that of either neat polymer [198]. This has also been shown to be the case for nylon 6 and Vectra B950 blends [232]. In blends of PBT with 20% or less Vectra B950, the viscosity is below that of either neat polymer. However, above 20% the viscosity of the blend rises and is between that of the neat polymers [199]. Thus, these relationships are not predictable *a priori* and more research is needed to relate these phenomena with fundamental mechanisms.

An interesting idea of a 'Universal Grade' polymer was suggested by La Mantia [239]. Because of the decrease in viscosity of blends versus the neat matrix, La Mantia et al. suggested producing only one grade of polymer and subsequently adjusting the melt flow index by varying the amounts of LCP. This was tested with PC, nylon 6, and PP matrices with two LCPs. The tensile modulus showed increases in all cases over the neat matrices while the impact properties showed equivalent or slightly decreased strength. Thus, this idea may be technically feasible but it must be left to economics whether it will be advantageous to purse this course.

A peculiar extrusion phenomenon was noted by Valenza et al. [202] as low concentrations of Vectra B950 were added to a PC matrix which was fed to an extruder. The torque (or power)

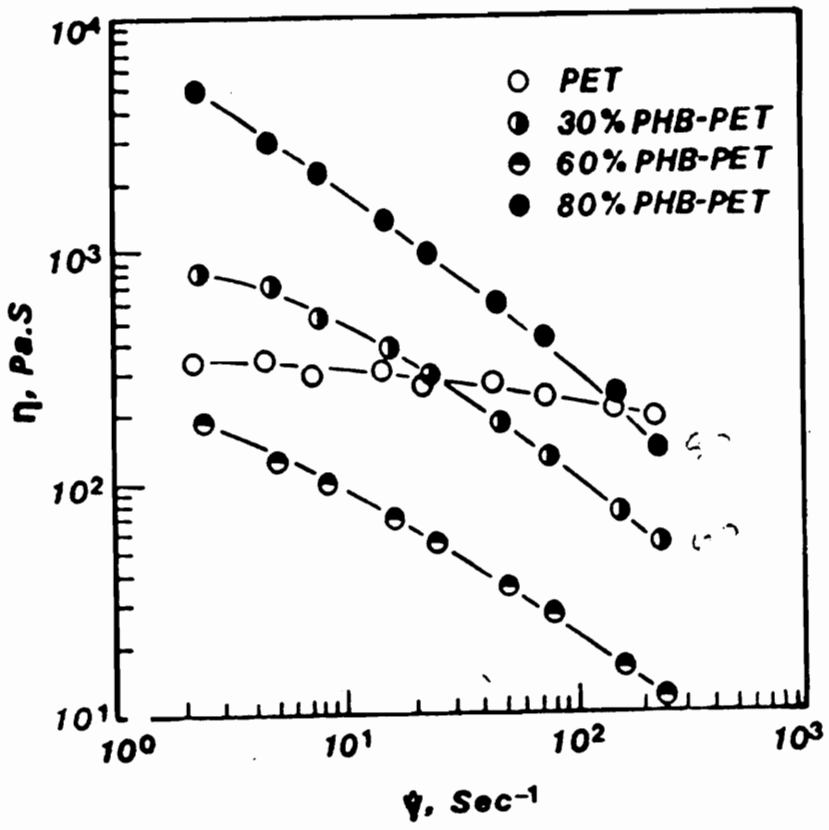

Fig. 2-22. Viscosity versus shear rate for PET and copolymers of PET/HBA with various comonomer ratios [198].

to extrude the blend and the flow rate decreased as the Vectra B950 content increased. It was expected that the torque would decrease because LCPs are known as processing aids, but a decrease in the flow rate was not expected. This decreased flow rate was explained by an apparent decrease in the friction factor within the solid transport zone. The structure of extruded ribbons also showed an interesting feature. When LCP was the dispersed phase, elongated drops were observed while spherical droplets were observed when PC was the dispersed phase. These structures were explained based on Taylor's [51] work where it was noted that a droplet with low viscosity relative to the matrix viscosity will extend when stressed while a droplet with high viscosity relative to the matrix viscosity will remain spherical as would a solid plastic sphere. Another interesting feature was the excess LCP at the skin of the ribbon. This excess LCP at the surface was assumed to be the result of migration as is commonly noted for lower viscosity fluid.

While the above studies focus more on shear results, several investigators have related capillary viscometer data to the shear and elongation viscosities of the blends [236,237]. Beery et al. [236] examined the effect of entrance angle on entrance pressure drop and shear viscosity for blends of PC with LCPs and found little influence of this angle on the pressure or shear viscosity. They did note that large entrance pressure losses occurred with LCP or LCP blends, and the entrance pressure losses reached 50% of the total pressure drop. These large entrance pressure losses were explained as arising from the energy to orient the LCP domains. The ratio of elongational to shear viscosity which was calculated from this data was found to be 1 to 3 orders of magnitude greater than the Trouton ratio (equal to three for Newtonian liquids). For the LCP and LCP blends, the elongational viscosity versus shear rate was well characterized with a power law model illustrating elongational thinning viscosity.

The morphology of the dispersed phase is affected by the shear rates, the type of flow field, and the concentration of the dispersed phase. The shape of the dispersed phase is important because in the solid state the aspect ratio of a reinforcing phase is typically related to the mechanical properties. In addition, the orientation within the dispersed phase will also be a significant variable in obtaining high mechanical properties in the solid state. Droplets, fibrils, and ribbons can all be formed within a matrix with ensuing differences in the rheological properties [219] and physical properties.

Blizard and Baird [220] investigated the rheology and morphology of PET/HBA60 in PC and nylon 6,6 matrices. For extrusion through small L/D dies, fine fibrils were formed for blends with 30% LCP while only droplets were observed for blends with 10% LCP. The formation of droplets and not fibrils at 10% LCP was explained by the small size of the droplets which had correspondingly high surface forces that restrained deformation. At 30% LCP, coalescence occurred which raised the average dispersed size and enabled the shear stress to overcome the interfacial stress. This phenomenon has also been observed by others [206] while Beery et al. [227] reported for nylon 6 that fibrils do not develop. Blizard and Baird observed for extrusion through large L/D dies that no fibrils were formed, and they suggested that continual extensional forces were required to generate and maintain fibrils.

It is interesting to note the dependence of the morphology upon the processing temperature. Nobile et al. [212] found when drawing a PC matrix with 10% PET/HBA that only droplets of LCP were formed at 260°C while fibers were formed in this blend at 220° C. This difference in morphology was explained by poor stress transfer at higher temperatures. It is plausible that the lower shear viscosity of the matrix at 260°C was not above the critical Weber number required for deformation in elongation flows. This phenomenon was also noted by

Federico [213].

La Mantia et al. [229] investigated the rheology of PBT and Vectra B950 below the crystal to nematic transition temperature of Vectra B950. At this temperature, PBT exhibits a Newtonian behavior while the Vectra B950 is shear thinning. For the blends, they observed an apparent yield stress at low shear rates as the fraction of LCP increased above 20 %. A minimum in the viscosity versus composition relationship was also noted for Vectra B950 at concentrations less than 20% LCP, and this phenomenon was postulated as resulting from interphase slippage between the immiscible phases. Additional work published by La Mantia [230] indicated that for blends of Vectra B950 with nylon 6 where the temperature is again below the crystal to nematic temperature of Vectra B950 a maximum viscosity occurred at 1% LCP and a minimum viscosity occurred at 10% LCP. Blizard and Baird [220] found a similar minimum at 50% LCP for blends with nylon 6,6. However the composition range did not include levels below 10%, so comparison with the maximum viscosity noted above could not be made. Typically, a lowering of the viscosity is explained as resulting from either incompatible polymers where slip between the phases occurs or from elongated fibrils that lubricate the melt and reduce the pressure drop in the entrance region [231]. From examination of the LCP phase emerging from small L/D ratio dies, the viscosity minimum existed at all shear rates while the fibrils existed only at high shear rates [232]. Obviously, the viscosity minimum was not created by elongated fibrils. La Mantia et al. explained this phenomenon as resulting from the LCP preferentially moving to the wall where the LCP provided a lubricating effect. At 1% LCP, insufficient quantities of LCP existed to provide this lubricating mechanism, and a viscosity maximum occurs as would be expected from suspension theory.

In a study of the morphology of a copolyester LCP blended with several matrices, Beery

et.al. [196] observed the formation of LCP fibers within a PC matrix. At a higher concentration of LCP, these fibers coalesced to form a network. However, fibers were not stable in a nylon matrix and drops were the dominant structure. In subsequent studies, Beery et al. [197] evaluated the rheology and structure of a HBA/HNA LCP in three thermoplastic matrices: PC, PBT, nylon 6 (N6). The blends were examined after extrusion through a capillary rheometer. Extrudates were prepared at both high and low shear rates. A skin-core structure was observed that was related to exit rearrangement flows. The skin possessed a more fibrillar texture because of the greater extension on leaving the capillary. The core exhibited a more spherical LCP phase. At higher shear rates and for matrices in which the LCP viscosity was lower than the matrix viscosity, highly elongated droplets were observed. However, for blends in which the LCP was of higher viscosity than the matrix spherical droplets were observed at the core even at high shear rates. This morphology indicated that the viscosity ratio was too high.

The morphology of LCP blends can also be revealed in more detail by separating the LCP from the thermoplastic resin. Some investigators have dissolved away the resin, centrifuged the LCP extract, and sieved the dispersed phase to determine a particle size distribution [213,214]. Another technique is to sandwich a section of a mold or fiber between filter paper followed by extraction of the matrix. This method leaves the position of the dispersed phase intact [213].

2.5.2 Miscibility and Compatibility

The miscibility of LCP blends is an indicator of the compatibility between the component phases. Examination of this aspect of blends can aid in understanding the role of miscibility on

mechanical properties. The majority of investigations to be discussed have used thermal transitions to determine if the polymers are miscible. Several studies have used spectroscopic methods to determine if chemical reaction or interaction between the components occurred which led to more compatible blends.

Isayev and Modic [211] blended PC with two copolyester LCPs based on HBA and HNA. They were interested in enhancing the mechanical properties of PC reinforcement by the LCP. By examining the thermal transitions of the blends, they found that the Tg of PC changed slightly with LCP composition. Slight changes of the Tg of PC with the addition of LCPs was also found by other authors [234,212]. It was found that properties of the PC/LCP blend with less than 10% LCP exceeded the law of mixtures for blends, and they proposed that these high properties were caused by potential transesterfication between PC and copolyester.

A study by Zhaung et al. [198] of a PET/HBA LCP blended with PS, PC, and PET, showed that PS was immiscible, PC was partially miscible, and PET was miscible with PET/HBA. These miscibility differences manifested themselves in thermal, rheological and mechanical property differences. For immiscible PS two Tgs were observed over the entire composition range, a minimum in viscosity was exhibited, and tensile strength was low at all compositions. For partially miscible PC, only one Tg existed over a large composition range and strength was intermediate to the two neat polymers over the entire composition range. Nobile et al. [212] showed via infrared spectroscopy on the extracted PC that no reaction with the ester groups of the LCP occurred, and hence chemical reaction was not responsible for the partial miscibility. For miscible PET, Zhuang et al. [198] showed one Tg existed over the entire composition range. Other investigators determined that PET crystallized in the presence of PET/HBA incorporated some PET/HBA into the PET crystals [204]. For both PC and PET

blends, the viscosity changed monotonically with composition, and an increase in tensile modulus and strength with small percentages of LCP occurred. The dispersed phase size was nearly an order of magnitude smaller for the partially miscible PC blends than the immiscible PS blends. The modulus and tensile strength for these three blends are shown in Fig. 2-23. Although there are no large differences among the modulus of these blends, there is a dramatically lower strength of the immiscible PS blends over the entire composition range. Thus, in these examples, partially or fully miscible systems have higher tensile properties than immiscible systems. It should be remembered, however, that miscibility depends greatly on the chemical makeup of the matrix and LCP. For instance, while PS and PET/HBA are immiscible, investigators have shown that partial miscibility exists between PS and other LCPs [200].

Valenza et al. [202] investigated the blend of PC and Vectra B950. They found that the modulus approached the rule of mixtures for this system while the tensile strength rose quasi-linearly only at LCP contents greater than 20%. This behavior was attributed to blend incompatibility, poor interfacial adhesion, and a low concentration of LCP that did not lead to the orientation of the LCP phase. Additionally, the impact strength of the blend was slightly lower than the impact strength of the PC matrix. While the adhesion was evidently poor, thermal analysis indicated partial miscibility existed. Other authors investigating blends of PC, PBT, nylon 6, and amorphous nylon with naphthalene based LCP have also attributed both LCP orientation and interfacial adhesion as determinates in ultimate tensile strength [227].

The miscibility of poly(butylene terephthalate) (PBT) and PET/HBA60 was investigated spectroscopically by Kimura and Porter [228]. Samples prepared in solution were analyzed via NMR. The NMR analysis confirmed that a reaction did not occur, and so physical interaction was cited as the cause of miscibility. However, the PET glass transition of the PET segments

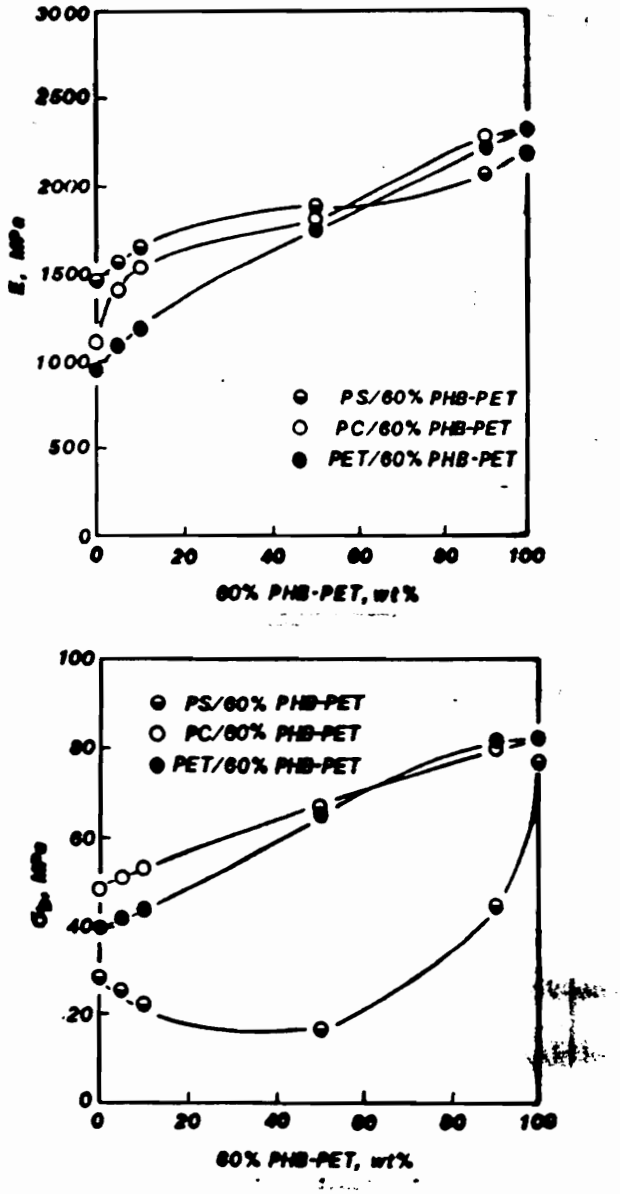

Fig. 2-23. Tensile modulus and tensile strength of PC and PS blends with PET/HBA60 LCP [198].

in PET/HBA60 shifted as the PBT concentration was increased which indicated that partial miscibility existed between the PBT and PET segments. The crystallization behavior exhibited a constant melting temperature for PBT with a constant specific enthalpy of fusion based on the weight of PBT present in the blend. This behavior indicated that PBT crystallizes via the exclusion of the LCP. Thus, the PBT mixes with PET, but the PET does not mix with the PBT phase.

Kodama [221] investigated the compatibility of a phenoxy resin and LC3000, i.e. PET/HBA60. Blends were prepared in solution with mixed solvent p-chlorophenol / o-dichlorobenzene followed by solvent removal and compression molding. Samples were molded at 260°C for 7, 30, 60, and 120 minutes and were analyzed via several techniques. Extraction of the soluble phase, the phenoxy resin, showed decreased amounts of material recovered and changed dynamic mechanical properties as the molding time increased. Finally, changes in the infrared spectrum of the extract showed increasing absorption at wavenumbers related to the HBA phenyl out-of-plane hydrogens, and the carbonyl vibrations. Thus, the above techniques showed that compatibilization of this blend occurred via chemical reaction.

Investigation of the compatibility between PBT and two LCPs (Vectra B950 and poly(biphenyl-4,4'-ylene sebacate), called PB8) was studied via thermal analysis by Paci et al. [223]. For PBT/Vectra B950 blends, no change in the thermal transitions were noted. However, for PBT/PB8 blends, both the glass transition and melting temperatures of PBT and PB8 shifted with changes in composition which indicated that partial miscibility existed. Annealing PBT/PB8 for increasingly longer periods of time prior to DSC analysis showed progressive loss of the smetic-isotropic endotherm. This loss of thermal transition was believed to be related to chemical changes that occurred between PBT and PB8. Finally, the dispersion of PB8 within PBT showed

nearly an order of magnitude smaller droplet size than blends of Vectra B950 and PBT. The above results indicated that compatibilization occurred in the PBT/PB8 system while little or no compatibilization occurred in the PBT/Vectra B950 system.

Blends of LCP with LCP have also been reported. A recent investigation by Dibenedetto and coworkers [222] has shown that compatibilization via chemical reaction between wholly aromatic copolyester K161 from Bayer A.G. (polymerized from five aromatic monomers) and X7G (PET/HBA60) from Tennessee Eastman occurred. Dynamic mechanical thermal analysis of the X7G extracted after mixing for increasingly longer times in a Brabender mixer revealed progressive shifts in the Tg. Proton NMR of the extract revealed changes in the relative amount of terephthalic acid (TA) and HBA moieties, and an overall increase in the amount of aromatic groups relative to the as received X7G was also revealed. Carbon-13 NMR of the X7G extract was subsequently used to confirm that aromatic moieties other than HBA and TA were present in the soluble fraction. Observation of the interface via TEM revealed a 50 nm gradient between the two LCP phases indicating that compatibilization through molecular mixing at the interface did occur. It is believed that blends of X7G which have been shown to be compatible with thermoplastic resins might provide a bonding mechanism for other LCPs in the creation of ternary thermoplastic/LCP system.

The above studies have indicated that compatibility depends entirely on the chemistry of the two polymers that are blended. However, an immiscible system with poor interfacial adhesion has been altered through the use of compatibilizing agent. This blend consists of PP with Vectra B950, Vectra A900, or LC3000 LCPs [224,225]. In these blends, the compatibilizer is a maleic anhydride grafted PP which is suggested to undergo a reaction with the LCPs. Significant improvements of tensile strength and modulus have been reported with little to any

fiber pullout [225]. The morphology of these blends reveals a smaller and more uniform particle size as would be expected for a thermoplastic compatibilized blend.

2.5.3 Processing and Properties

By spinning a LCP in a PS matrix, Basset and Yee [240] showed that fibrils of LCP could be created in a PS fiber. These fibers could be arranged in a uniaxial direction and consolidated into a fiber reinforced thermoplastic composite. The spinning process enabled attainment of aspect ratios well over 100, and the elongation of the dispersed phase was only limited by the ability of the LCP to supercool to the drawing temperatures. Inspection of the fracture surface of the fiber showed that fibrils formed with little draw exhibited twisting and splitting which indicated that mechanical coupling between tensile and torsion modes occurred. Samples prepared from a high draw ratio process did not exhibit this twisting and splitting. The authors concluded that this coupling is related to molecular alignment and those fibrils with low alignment exhibited the highest degree of coupling.

Mithal et al. [243] studied fiber spinning of PET with VA. They found that at low percentages of LCP the tensile strength dropped below that of PET. This effect was related to orientation suppression as reported by Brody [244] where the presence of small quantities of LCP lowered the orientation of PET. This orientation suppression occurred because of the flow field around the droplets was perturbed by the droplet and deformation occurred in a nonaffine manner. Mithal found, however, that as the percentage of LCP increased, both tensile strength and modulus followed the rule of mixtures. Heat treatment of these fiber blends showed opposing results that depended upon the composition. For high percentages of LCP, annealing

increased both the strength and the modulus as commonly occurs for LCPs [245]. For low percentages of LCPs, the strength decreased with heat treatment as the PET phase relaxed.

Crevecoeur [237] also investigated LCP blends. In a study of PPE/PS/Vectra A950 blends, strands were drawn to draw ratios of approximately 30 at elongation rates that varied over two orders of magnitude. He determined that after a sufficiently large elongation rate, the orientation of the blend was not influenced by the elongation rate. This elongational rate independence was related to achieving affine deformation ($We > 2We_c$).

In a study relating the morphology and orientation to the tensile properties of K161, a LCP from Bayer, in an Ultem matrix , Carfagna, et al. [233] concluded that some LCP undergoes tip streaming at the low viscosity ratios used in processing. This tip streaming material no longer contributes to mechanical reinforcement because of it's random orientation and low aspect ratio. However, when the LCP volume fraction was adjusted by this low aspect ratio fraction, and the orientation of the LCP phase measured, then the aspect ratio of the fibrous LCP was calculated via the Halpin-Tsai equation. Agreed of the calculated aspect ratio with the aspect ratio obtained from optical microscopy measurements was good. However, the authors found that for this system, the orientation of K161 in Ultem strands drawn to 50X were nearly equivalent to undrawn K161 strands. The mismatch in the Tg of these polymers resulted in the LCP freezing in the spinline prior to significant extension.

Blizzard et al. [214] studied extrusion and drawing of several LCPs in PC and PEI matrices. It was found that the LCPs could be drawn as long as the temperature was high enough to ensure that the viscosity ratio was equal or below unity. Comparison of the LCP rheological cooling behavior and the morphology creating during drawing indicated that high aspect ratio fibers were only created when the LCP supercool to temperatures at or below the drawing

temperature. For those LCPs where limited ability to supercooling existed, little fiber formation occurred. They also noted that as the LCP concentration increased so did the fibril diameters which suggested that coalescent occurred.

Seppala et al. [203] studied the mechanical properties of blends of Vectra A950 with PET, PP, and PPS. Blends were prepared by extrusion in a corotating twin screw extruder. The modulus versus composition approached the law of mixtures for PP and PPS while for PET the modulus did not increase until the composition exceeded 10% LCP. It was noted that at 5% LCP, only spherical inclusions were obtained in the PET and PP matrices.

LaMantia et al. [215] blended 5 to 20% Vectra B950 with nylon-6 to form fiber. They reported that the draw ratio greatly increased the modulus especially at higher LCP content. Two L/D ratio dies were used in producing fibers. For a small L/D ratio die, the LCP phase became elongated, but for a L/D ratio of 40, this elongated morphology was lost before reaching the exit of a capillary. Further drawing was required to produce a fibrillar morphology. Properties of these blends were related to parallel, series, and Halpin-Tsai composite mechanical models. Both the parallel and Halpin-Tsai models overpredicted the properties, but closer agreement was found with the latter model. Weak interfacial adhesion and incomplete fibrillation were speculated as causes for disagreement with the Halpin-Tsai model.

In addition to LCP / thermoplastic blends, some interest is growing toward blending LCP with LCP. Isayev [125] blended two LCPs, Vectra A900 and Ultrax KR-4002 which was manufactured by BASF. This blend exhibited an increased tensile strength over the entire composition range, and both the modulus and impact strength exceeded that of either neat LCPs over a limited compositional region. These enhanced mechanical properties would not have been predicted *a priori*.

In a study of the effect of mixing on the mechanical properties of thermoplastic/LCP blends, Kiss [241] found that mechanical properties are independent of the blending methods. He concluded that compounding does not increase the mechanical properties of injection molding in situ composites. However, several exceptions exists.

Nobile et al. [212] investigated the role of mixing on the morphology and properties of PC and PET/HBA60 blends. Blending of these polymers was performed in an internal mixer and in an extruder with a static mixer attachment. While no difference in the rheological properties were noted, it was found that the extruder/static mixer yielded a better dispersion of PET/HBA60 in PC and yielded higher properties. Studies of the effect of shear rate on the mechanical properties determined that higher extrudate properties were measured for blends processed at the highest shear rate while conversely injection molded properties were greater for blends processed at the lower shear rate. It was also found that greater extrudate properties were obtained from dies with shorter L/D ratios as has been reported for neat LCPs [177,139]. Mechanical properties of spun fibers were also investigated. It was determined that temperature had a dramatic effect on morphology and properties. At 260°C while significant modulus increases occurred upon drawing neat LCP, little to any difference between the moduli of blend and PC was measured. The morphology revealed that LCP existed as droplets at all draw ratios. Hence, the LCP was not elongating and developing a high modulus which could reinforce the matrix. However, at 220° C there was a significant modulus enhancement over that of PC. In this case, the LCP was fibrillar, and this change in morphology indicated that higher stresses deformed the LCP and/or lead to rapid solidification of the morphology.

Isayev and Modic [211] blended PC with two copolyester LCPs based on HBA and HNA. Their purpose was two-fold. First, they were interested in enhancing the mechanical properties

of PC via reinforcement by the LCP. Second, they desired to reduce the anisotropy typically found in LCPs. A comparison was made between the mechanical properties of blends that were premixed to the blends that were not premixing. Premixing was performed via a extruder/static process. A significant enhancement of mechanical properties of the premixed material over material with no premixing occurred. Mechanical properties were also increased by varying the injection speed. At higher speeds, higher properties resulted while at lower speeds, lower properties were measured. Finally, mechanical properties from specimens measured in the machine direction were compared to the rule of mixtures where both the injection molded and fiber properties were used. At low concentration, properties generally fell between the limits set by the two neat LCP moduli. Transverse properties were compared for a series model and it was found that properties exceeded this law. Positive deviation was explained by increased adhesion that was caused by transesterfication between PC and the copolyester LCP. Comparison of transverse to machine direction properties revealed that by blending an isotropic polymer with anisotropic LCP that anisotropy does decrease.

Ko and Wilkes [242] prepared sheets of PET and PET/HBA60 blends in an extruder that used a gear pump to control the throughput independently of extruder screw speed. They investigated the effect of screw speed on the morphology and properties of these films. Their results clearly demonstrated that as the screw speed increased the dispersed LCP phase changed from a droplet morphology to a fibrillar morphology. Correspondingly, the machine direction modulus increased over 4 fold as the screw speed increased albeit no increase in transverse modulus occurred and thus anisotropy increased.

Sukhadia et al. [226] prepared strands and films of PP or PET with several LCPs using a unique mixing method. This method consisted of using separate extruders for the LCP and the

thermoplastic matrix. This method permits plastication of these polymers at their respective standard processing temperatures. Outflow from these extruders is joined into a common static mixing where continuous fibers of the LCP within the thermoplastic matrix were formed. Sukhadia found that strands prepared in this manner could be drawn to a draw ratio 50 with significant improvement in tensile modulus that surpassed properties of these materials prepared in a single screw extruder. Thus, unique mixing/processing methods can lead to significant differences in the morphology and properties of LCP blends.

In summary, LCP blends may be processed in the same manner as thermoplastic resins, but they offer some unique advantages over thermoplastic resins. These advantages include greatly reduced blend viscosities, and the ability to form a fibrous LCP phase within the matrix that enhances the modulus and the strength. Extensional flows such as flow through short capillaries or drawing of strands and fibers are excellent means to create this morphology. In addition, higher shear rates can also lead to fibrous morphologies. However, even with these favorable conditions, there is a concentration dependence that affects the resulting morphology. Generally, fibrous forms can be achieved with blends containing 20% or more LCP while drops are formed for blends with less than 20% LCP. Obtaining a fibrous morphology does depend upon the extrusion temperature. The solidification point of the LCP must be below the drawing temperature to enhance the properties. The strength of these blends can be greatly influenced by the miscibility between the phases. In one case where miscibility clearly is lacking, compatibility can be achieved via a polymeric compatibilizer. Finally, processing methods must be developed to reduce the anisotropy without significantly lowering the mechanical properties.

2.6 References

1 G. Allegra, "Conformational Considerations of High-Modulus Polymers," Poly. Eng. Sci., 15(3), 207 (1975).

2 P.J. Barham and A. Keller, "Review: High-strength Polyethylene Fibres From Solution and Gel Spinning," J. Mater. Sci. 20, 2281 (1985).

3 S.L. Kwolek, U.S. Patent 3671542 (1972).

4 I.M. Ward, "Optical and Mechanical Anisotropy in Crystalline Polymers," Proc. Phys. Soc., 80, 1176 (1962).

5 Product Data from Himont, Inc., Wilmington, DE.

6 Modern Plastic Encyclopedia, McGraw Hill, New York, 1991.

7 O. Olabisi, L.M. Roberson, and T.M. Shaw, Polymer-Polymer Miscibility, Academic Press, New York (1979).

8 D.J. Walsh, in Comprehensive Polymer Science, Vol 2, G. Allen and J.C. Bevington, Eds., Pergamon Press, New York, 1989: pg. 135

9 W.J. MacKnight and F.E. Karasz, in Comprehensive Polymer Science, Vol 72, G. Allen and J.C. Bevington, Eds., Pergamon Press; New York, 1989: pg. 111.

10 H.L. Snyder, P. Meakin, and S. Reich, "Dynamical Aspects of Phase Separation in Polymer Blends," Macromol. 16, 757 (1983).

11 R. Hashimoto, J. Kumaki, and H. Kawai, "Time-Resolved Light Scattering Studies of Kinetics of Phase Separation and Phase Dissolution of Polymer Blends: I. Kinetics," Macromol., 16, 641 (1983).

12 M. Kurata, Thermodynamics of Polymer Solutions, Harwood Academic, New York, 1982.

13 P.J. Flory and A. Abe, Macromolecules, 11(6), 1119 (1978).

14 A. Abe and P.J. Flory, Macromolecules, 11(6), 1122 (1978).

15 P.J. Flory and R.S. Frost, Macromolecules, 11(6), 1126 (1978).

16 R.S. Frost and P.J. Flory, Macromolecules, 11(6), 1134 (1978).

17 P.J. Flory, Macromolecules, 11(6), 1138 (1978).

18 P.J. Flory, Macromolecules, 11(6), 1141 (1978).

19 J.H. Hilderbrand and R.L. Scott, Regular Solutions, Prentice Hall, Englewood Cliffs, N.J., 1962.

20 P.J. Hoftyzer and D.W. van Krevelen, Properties of Polymers, 2nd. ed., Elesevier, New York, 1976: pp. 152-155.

21 T.G. Fox, Bull. Am. Phys. Soc. [2]2, 123 (1956).

22 W.J. MacKnight and F.E. Karasz, "Solid State Transition Behavior of Blends," in Polymer Blends, D.R. Paul and S. Newman, Eds., Academic Press, New York, 1978: Vol. 1, pg. 224.

23 M.T. de Meuse, and M. Jaffe, "Model System For Liquid Crystal Polymer Blends," Mol. Cryst. Liq. Cryst. Inc. Nonlin. Opt., 157, 535 (1988).

24 G. ten Brinke, F.E. Karasz, and W.J. MacKnight, Macromolecules, 16, 1827 (1983).

25 R.P. Kambour, J.T. Bendler, and R.C. Bopp, Macromolecules, 16, 753 (1983).
26 D.R. Paul and J.W. Barlow, Polymer, 25, 487 (1984).
27 L.A. Utracki and M.R. Kamal, "Melt Rheology of Polymer Blends," Polym. Eng. Sci., 22(2), 96 (1982).
28 N.G. Gaylord, "Compatibilizing Agents: Structure and Function in Polyblends," J. Macromol. Sci., Chem., A26(8), 1211 (1989).
29 A.Y. Coran and R. Patel, Rubber Chem. Technol., 56, 1045 (1983).
30 R.L. Markham, "Introduction to Compatibilization of Polymer Blends", Advances in Polymer Technology, 10(3), 231 (1990).
31 M. Xanthos, "Interfacial Agents for Multiphase Polymer Systems: Recent Advances," Polym. Eng. Sci., 28(21), 1392 (1988).
32 B.D. Favis, "Polymer Alloys and Blends: Recent Advances," Can. J. Chem. Engr., 69, 619 (1991).
33 Z. Liang and H. L. Williams, "Dynamic Mechanical Properties of Polypropylene-Polyamide Blends: Effect of Compatibilization," J. Appl. Polym. Sci., 44, 669 (1992).
34 J.W. Barlow and D.R. Paul, "Mechanical Compatibilization of Immiscible Blends," Polymer Eng. and Sci., 24(8), 525 (1984).
35 R. Kosfeld, K. Schaefer, E.A. Hemmer, M. Hess, A. Theisen, and T.H. Uhlenbroich, "Blends From EPDM, PP, and Inorganic Filler," in Controlled Interphases in Composite Materials, H. Ishida, Ed., Elsevier, 1990.
36 A. Galeski, "Toughening of Crystalline Polyolefins Containing Particulate Fillers By Interface Modifications," in Controlled Interphases in Composite Materials, H. Ishida, Ed., Elsevier, 1990.
37 Y.S. Lipatov, "Interfaces in Polymer-Polymer Composites," in Controlled Interphases in Composite Materials, H. Ishida, Ed., Elsevier, 1990.
38 J. W. Barlow and D.R. Paul, "The Importance of Enthalpic Interactions in Polymeric Systems," Polym. Eng. Sci., 27(20), 1482 (1987).
39 J. Noolandi, "Recent Advances in the Theory of Polymeric Alloys," Polym. Eng. Sci., 24(2), 71 (1984).
40 S. Wu, "Calculation of Interfacial Tension in Polymer Systems," J. Polym. Sci.: Part C, 34, 19 (1971).
41 S. Meretz, M. Kwiatkowski, G. Hinrichsen, "Production and Characterization of Fine-Dispersed Mixtures of Liquid Crystalline with Conventional Polymers," Intern. Polym. Proc., VI, 239 (1991).
42 J.J. Elmendorp and G. de Vos, "Measurement of Interfacial Tensions of Molten Polymer Systems by Means of the Spinning Drop Method," Polym. Eng. Sci., 26(6), 415 (1986).
43 A. Cohen, and C.J. Carriere, "Analysis of a Retraction Mechanism for Imbedded Polymeric Fibers," Rheol. Acta., 28, 223 (1989).
44 C.J. Carriere, A. Cohen, and C.B. Arends, "Estimation of Interfacial Tension Using Shape Evolution of Short Fibers," J. Rheol., 33(5), 681 (1989).
45 C.J. Carriere and A. Cohen, "Evaluation of the Interfacial Tension Between High Molecular Weight Polycaronate and PMMA resins with the Imbedded Fiber Retraction Technique," J. Rheol., 35(2), 205 (1991).

46 E. Helfand and A.M. Sapse, J. Chem. Phys., 62, 1327 (1975).
47 S. Wu, "Formation of Dispersed Phase in Incompatible Polymer Blends: Interfacial and Rheological Effects," Polym. Eng. Sci., 27(5), 335 (1987).
48 S. Middleman, Fundamentals of Polymer Processing, McGraw Hill, New York, 1977.
49 H. Lamb, Hydrodynamics, Dover, New York, 6th Ed., 1932.
50 G.I. Taylor, "The Viscosity of a Fluid Containing Small Drops of Another Fluid," Proc. Roy. Soc., A138, 41 (1932).
51 G.I. Taylor, "The Formation of Emulsions in Definable Fields of Flow," Proc. Roy. Soc. A146, 501 (1934).
52 J.M. Rallison, "The Deformation of Small Viscous Drops and Bubbles in Shear Flows," Ann. Rev. Fluid Mech., 16, 45 (1984).
53 F.D. Rumscheidt and S.G. Mason, "Particle Motion in Sheared Suspensions XII," J. Coll. Sci., 16, 238 (1961).
54 R.G. Cox, "The Deformation of a Drop in a General Time-Dependent Fluid Flow," J. Fluid Mech., 37(3), 601 (1969).
55 C.E. Chaffey and H. Brenner, J. Colloid Interface Sci., 24, 258 (1967).
56 S. Torza, R.G. Cox, and S.G. Mason, "Particle Motion in Sheared Suspensions XXVII," J. Coll. Sci., 38(2), 395 (1970).
57 T. Tavgac, "Drop Deformation and Breakup in Simple Shear Fields," Ph.D. Dissertation, Univ. of Houston, Houston, TX., 1972.
58 H.J. Karam and J.C. Bellinger, "Deformation and Breakup of Liquid Droplets in a Simple Shear Flow," I&EC Fund., 7(4), 576 (1968).
59 H.P. Grace, "Dispersion Phenomena in High Viscosity Immiscible Fluid Systems and Application of Static Mixers as Dispersion Devices in Such Systems," Chem. Eng. Commun., 14, 225 (1982).
60 P.H.M. Elemans, "Modelling of the Processing of Incompatible Polymer Blends," Ph.D. Dissertation, Univ. of Eindhoven, Eindhoven, Netherlands, 1989.
61 G.I. Taylor, "Conical Free Surfaces and Fluid Interfaces," Applied Mech.: Proceedings of the Eleventh International Congress of Applied Mechanics, Munich, 1964.
62 G.I. Taylor, "Motion of Axisymmetric Bodies in Viscous Fluids, " Motion of Axisymmetric Bodies in Viscous Fluids," in Problems of Hydrodynamics and Continuum Mechanics, SIAM, 1969, pg. 718.
63 G.K. Batchelor, "Slender-Body Theory for Particles of Arbitrary Cross-Section in Stokes Flow," J. Fluid Mech., 44(3), 419 (1970).
64 J.D. Buckmaster, "Pointed Bubbles in Slow Viscous Flow," J. Fluid Mech., 55(3), 385 (1972).
65 J. Buckmaster, "The Bursting of Pointed Drops in Slow Viscous Flow," J. Applied Mech., E40, 18 (1973).
66 A. Acrivos and T.S. Lo, "Deformation and Breakup of a Single Slender Drop in an Extensional Flow," J. Fluid Mech., 86(4), 641 (1978).
67 H. Van Oene, "Modes of Dispersion of Viscoelastic Fluids in Flow," J. Coll. Interf. Sci., 40(3), 448 (1972).

68 H.B. Chin, and C.D. Han, J. of Rheol., 24(1), 1 (1980).
69 S. Tomotika, "On the Instability of a Cylindrical Thread of a Viscous Liquid Surrounded by Another Viscous Fluid," Proc. Roy. Soc., 150, 322 (1935).
70 J.J. Elmendorp, and R.J. Maalcke, "A Study of Polymer Blending Microrheology: Part 1," Poly. Eng. Sci., 25, 1041 (1985).
71 J.J. Elmendorp, "A Study of Polymer Blending Microrheology," Poly. Eng. Sci., 26(6), 418 (1986).
72 S. Tomotika, "Breaking up of a Drop of Viscous Liquid Immersed in Another Fluid Which is Extending at a Uniform Rate," Proc. Roy. Soc., A, 153, 302 (1936).
73 J.J. Elmendorp, "Dispersive Mixing in Liquid Systems," in Mixing in Polymer Processing, C. Ramwendaul, Ed., Marcel Dekker, New York, 1991.
74 H.B. Chin, and C.D. Han, J. of Rheol, 24(1), 1 (1980).
75 G. Crevecoeur, "In-Situ Composites: Blends of Thermotropic Liquid Crystalline Polymer in a Thermoplastic Matrix," Ph.D. Dissertation, Katholieke Universiteit, Leuven (1991).
76 H.A. Stone and L.G. Leal, "The Effects of Surfactant on Drop Deformation and Breakup," J. Fluid Mech., 220, 161 (1990).
77 R.W. Flumerfelt, "Effects of Dynamic Interfacial Properties on Drop Deformation and Orientation in Shear and Extensional Flow Fields," J. Coll. Intern. Sci., 76(2), 330 (1980).
78 R.W. Flumerfelt, "Experimental Studies of Drop Dynamics in Shear Fields: Role of Dynamic Interfacial Effects," J. Coll. Inter. Sci., 76(2), 350 (1980).
79 B.J. Bentley and L.G. Leal, "A Computer-Controlled Four-Roll Mill For Investigation of Particle and Drop Dynamics," J. Fluid. Mech., 167, 219 (1986).
80 B.J. Bentley and L.G. Leal, "An Experimental Investigation of Drop Deformation and Breakup in Steady, Two Dimensional Flows," J. Fluid. Mech., 167, 241 (1986).
81 D. Barthes-Biesel, and A. Acrivos, "Deformation and Burst of a Liquid Droplet Freely Suspended in a Linear Shear Field," J. Fluid. Mech., 61, 1 (1973).
82 J.M. Rallison, "A Note On The Time-Dependent Deformation of a Viscous Drop Which is Almost Spherical," J. Fluid Mech., 98, 625 (1980).
83 W.L. Olbricht, J.M. Rallison, and L.G. Leal, "Strong Flow Criteria Based On Microstructure Deformation," J. Non-Newtonian Fluid Mech., 10, 291 (1982).
84 V.E. Dreval, G.V. Vinogradov, E.P. Plotnikova, M.P. Zabugina, N.P. Krasnikova, E.V. Kotova, and Z. Plezbauer, "Deformation of Melts of Mixtures of Incompatible Polymers in a Uniform Shear Field and the Process of Their Fibrillation," Rheol. Acta, 22, 102 (1983).
85 W.J. Milliken and L.G. Leal, "Deformation and Breakup of Viscoelastic Drops in Planar Extensional Flow Fields," J. Non-Newtonian Fluid Mech., 40, 355 (1991).
86 W.J. Milliken and L.G. Leal, "A Note on the Effect of Vorticity on the Deformation and Breakup of Polymer Drops," J. Non-Newtonian Fluid Mech., 42, 231 (1992).
87 S.K. Garg and S. Kenig, "Development of Orientation During Processing of

Liquid Crystalline Polymers, " in High Modulus Polymers, A.E. Zacharaides and R.S. Porter, Eds., Marcel Dekker, New York (1988).

88 R.L. Ballman, L. Shusman, and H.L. Toor, "Injection Molding. Flow of a Mothen Polymer into a Cold Cavity," Ind. and Eng. Chem., 51, 847 (1959).

89 D.H. Harry and R.G. Parrott, "Numerical Simulation of Injection Mold Filling," Polym. Eng. Sci., 10, 209 (1970).

90 G. Williams, and H.A. Lord, "Mold Filling Studies for the Injection Molding of Thermoplastic Materials. Part I," Polym. Eng., 15(8), 553 (1975).

91 G. Williams, and H.A. Lord, "Mold Filling Studies for the Injection Molding of Thermoplastic Materials. Part II," Polym. Eng., 15(8), 569 (1975).

92 J.L. Berger and C.G. Gogos, "A Numerical Simulation of the Cavity Filling process with PVC in Injection Molding," Polym. Eng. Sci., 12, 102 (1973).

93 W-Y. Chiu, L-W Chen, C. Wang, and D-C. Wang, "Analysis of Filling, Packing, and Cooling Stages in Injection Molding of Disk Cavities," J. Appl. Polym. Sci., 43, 39 (1991).

94 P.C. Wu, C.F. Huang, and C.G. Gogos, Polym. Eng. Sci., 14, 223 (1974)

95 M.R. Kamal and S. Kenig, "The Injection Molding of Thermoplasics. Part I: Theoretical Model," Polym. Eng. Sci., 12(4), 294 (1972).

96 M.R. Kamal, Y Kuo, and P.H. Doan, "The Injection Molding Behavior of Thermoplastics in Thin Rectangular Cavities," Polym. Eng. Sci., 15(12), 863 (1975).

97 C. Gutfinger, E. Broyer, and Z. Tadmor, "Melt Solidification in Polymer Processing," Polym. Eng. Sci., 15(7), 515 (1975).

98 H. Janeschitz-Kriegl, "Injection Moulding of Plastics II. Analytical Solution of Heat Transfer Problem," Rheol. Acta, 18, 693 (1979).

99 S.M. Richarson, "Injection Moulding of Thermoplastics. II. Freezing Off in Cavities," Rheol. Acta, 24, 509 (1985).

100 W.L. Krueger and Z. Tadmor, "Injection Molding into a Rectangular Cavity with Inserts," Polym. Eng. Sci., 20, 426 (1980).

101 W. Rose, "Fluid-Fluid Interfaces in Steady Motion," Nature, 191, 242 (1961).

102 Z. Tadmor, "Molecular Orientation in Injection Molding," J. Appl. Polym. Sci., 18, 1753 (1974).

103 L.R. Schmidt, "A Special Mold and Tracer Technique for Studying Shear and Extensional Flows in a Mold Cavity During Injection Molding," Polym. Eng. Sci., 14(11), 797 (1974).

104 M.R. Kamal, S.K. Goyal, and E. Chu, "Simulation of Injection Mold Filling of Viscoelastic Polymer with Fountain Flow," AIChEJ, 34(1), 94 (1988).

105 C.G. Gogos and C-F. Huang, "The Process of Cavity Filling Including the Fountain Flow in Injection Molding," Polym. Eng. Sci., 26(20), 145 (1986).

106 R.A. Behrens, M.J. Crochet, C.D. Denson, and A.B. Metzner, "Transient Free-Surface Flows: Motion of a Fluid Advancing in a Tube," AIChEJ, 33(7), 1178 (1987).

107 R.A. Behrens, "Transient Domain Free Surface Flows and Their Applications to Mold Filling," Ph.D. Dissertation, Univ. Delaware, Newark, DE., 1983.

108 H. Mavridis, A.N. Hrymak, and J. Vlachopoulos, "Finite Element Simulation

of Fountain Flow in Injection Molding," Polym. Eng. Sci., 26(7), 449 (1986).
109 H. Mavridis, A.N. Hrymak, and J. Vlachopoulos, "Deformation and Orientation of fluid Elements Behind an Advancing Flow Front," J. Rheol., 30(3), 555 (1986).
110 H. Mavridis, A.N. Hrymak, and J. Vlachopoulos, "Transient Free-Surface Flows in Injection Mold Filling," AIChEJ, 34(3), 403 (1988).
111 A.N. Beris, "Fluid Elements Deformation Behind an Advancing Flow Front," J. Rheol., 31(2), 121 (1987).
112 D.J. Coyle, J.W. Blake, and C.W. Macosko, "The Kinematics of Fountain Flow in Mold-Filling," AIChEJ, 33(7), 1168 (1987).
113 S. Bhattacharji and P. Savic, Proc. Heat Transfer Fluid Mech. Inst., 248 (1965).
114 L.D. Landau and E.M. Lifshitz, in Course of Theoretical Physics, Vol 6, Pergamon Press, Oxford, 1959: pg. 233.
115 M.R. Kamal and F.H. Moy, "Microstructure in Polymer Processing. A Case Study: Injection Molding," Polymer Eng. Reviews, 2(4), 381 (1983).
116 M.R. Kamal and V. Tan, "Orientation in Injection Molded Polystyrene," Polym. Eng. Sci., 19(8), 558 (1979).
117 A. Siegmann, S. Kenig, and A. Buchman, "Residual Stresses in Injection Molded Amorphous Polymers," Polym. Eng. Sci., 27(14), 1069 (1987).
118 W. Dietz, J.L. White, and E.S. Clark, "Orientation Development and Relaxation in Injection Molding of Amorphous Polymers," Polym. Eng. Sci., 18(4), 273 (1978).
119 M. Matsui and D.C. Bogue, Polym. Eng. Sci., 16, 735 (1976).
120 M. Matsui and D.C. Bogue, Trans. Soc. Rheol., 27, 133 (1977).
121 A.I. Isayev and C.A. Hieber, Rheol. Acta, 19, 168 (1980).
122 P.G. Lafleur, "Computer Simulation of the Injection Molding of Viscoelastic Crystalline Thermoplastics," Ph.D. Dissertation, McGill Univ., Montreal, Canada, 1983.
123 P.G. Lafleur, and M.R. Kamal, "A Structure Oriented Computer Simulation of the Injection Molding of Viscoelastic Crystalline Polymers Part I: Model with Fountain Flow, Packing, Solidification," Polym. Eng. Sci., 26(1), 92 (1986).
124 M.R. Kamal and P.G. Lafleur, "A Structure Oriented Computer Simulation of the Injection Molding of Viscoelastic Crystalline Polymers Part II: Model Predictions and Experimental Results," Polym. Eng. Sci., 26(1), 103 (1986).
125 J.C. Seferis and R.J. Samuels, Polym. Eng. Sci., 19, 977 (1979).
126 A.H. Wagner, J.S. Yu, and D.M. Kalyon, "Microstructure and Ultimate Properties of Injection Molded Amorphous Engineering Plastics: Poly(ether imide) and Poly(2,6-dimethyl-1,4-phenylene ether)," Polym. Eng. Sci., 29(18), 1298 (1989).
127 A.H. Wagner, J.S. Yu, and D.M. Kalyon, "Injection Molding of Engineering Plastics," Adv. Polym. Tech., 9(1), 17 (1989).
128 A.H. Wagner, J.S. Yu, and D.M. Kalyon, "Simulation of Microstructure Development in Injection Molding of Engineering Plastics," J. Appl. Polym. Sci., 44, 477 (1992).
129 M. Fujiyama and T. Wakino, "Distribution of Higher Order Structures in

Injection Molded Polypropylenes," J. Appl. Polym. Sci., 43, 57 (1991).
130 Z. Ophir and Y. Ide, "Injection Molding of Thermotropic Liquid Crystal Polymers," Polym. Eng. Sci., 23(14), 792 (1983).
131 J.R. Meyer-Arendt, Introduction to Classical and Modern Optics, Prentice Hall, New Jersey, 1972, pg. 315.
132 A.C. Griffin, S.R. Vaidya, and M.L. Steele, in Polymeric Liquid Crystals, A. Blumstein, Ed., Plenum Press, New York, 1983: pg. 1
133 C. Noel, "Identification of Mesophases Exhibited by Thermotropic Liquid Crystlline Polymers," in Polymeric Liquid Crystals, A. Blumstein, Ed., Plenum Press, New York, 1983.
134 J.L. White, "Historical Survey of Polymer Liquid Crystals," J. Appl. Poly. Sci. Symp., 41, 3 (1985).
135 A.J. East, L.F. Charbonneau, and G.W. Calundann, "Thermotropic Poly(ester-amides) Based On Naphthalene Monomers," Mol. Cryst. Liq. Cryst., 157, 615 (1988).
136 W.R. Krigbaum, "Identification of the Type of Mesophases For Thermotropic Polymers," J. Appl. Poly. Sci. Symp., 41, 105 (1985).
137 M.C. Muir, and R.S. Porter, "Processing Rheology of Liquid Crystalline Polymers: a Review," Mol. Cryst. Liq. Cryst., 169, 83 (1989).
138 W.J. Jackson and H.F. Kuhfuss, J. Polym. Sci., Polym. Chem. Ed., 14, 2043 (1976).
139 G.W. Calundann and M. Jaffe, "Anisotropic Polymers, Their Synthesis and Properties," Proceedings of the Robert A. Welch Conference on Chemical Research, XXVI. Synthetic Polymers, (1982).
140 T-S. Chung, "The Recent Developments of Thermotropic Liquid Crystalline Polymers," Polym. Eng. Sci., 26(13), 901 (1986).
141 W.J. Jackson, "Liquid Crystal Polymers. IV. Liquid Crystalline Aromatic Polyesters," The British Journal, 12(4), 154 (1980).
142 S. Ogoni and T. Asada, "Rheology and Rheo-optics of Polymer Liquid Crystals," Rheology, Vol. I, Astarita, Murrucci, and Nicolais, Eds., Plenum Press, New York, 1980.
143 T. Asada, H. Muramatsu, R. Watanabe, and S. Onogi, "Rheooptical Studies of Racemic Poly(γ-benzyl glutamate) Liquid Crystals," Macromolecules, 13, 867 (1980).
144 T. Asada, S. Onogi, H. Yanase, "A Rheooptical Study of the Reformation of Structure in Racemic Poly(γ-benzyl glutamate) Liquid Crystals," Poly. Eng. Sci., 24(5), 355 (1984).
145 J.L. Ericksen, Kolloid Zeitschrift, 173(2), 117 (1960).
146 F.M. Leslie, Arch. Rat. Mech. Anal., 28, 265 (1968).
147 M. Doi, J. Polym. Sci., Polym Phys, Ed., 19, 229 (1981).
148 G.G. Viola and D.G. Baird, "Studies on the Transient Shear Flow Behavior of Liquid Crystalline Polymers," J. Rheol., 30(3), 601 (1986).
149 G.M. Prilutski, "The Rheology of Polymeric Liquid Crystals," Ph.D. Dissertation, Univ. of Delaware, 1984.
150 T.S. Wilson, Ph.D. Dissertation, Virginia Tech., Blacksburg, VA., 1991.

151 K.F. Wissbrun, G. Kiss, and F.N. Cogswell, "Flow Behavior of a Thermotropic Liquid Crystal Aromatic Copolyester," Chem. Eng. Comm., 53, 149 (1987).
152 D.G. Baird, "Concepts in Rheological Studies of Polymeric Liquid Crystals," in Polymeric Liquid Crystals, A. Blumstein, Ed., Plenum Press, New York, (1983).
153 K.F. Wissbrun, "Observations on the Melt Rheology of Thermotropic Aromatic Polyesters," Brit. Poly. J., 12(4), 163 (1980).
154 D. Done and D.G. Baird, "The Effect of Thermal History on the Rheology and Texture of Thermotropic Liquid Crystalline Polymers," Polym. Eng. Sci., 27(11), 816 (1987).
155 D. Done and D.G. Baird, "Solidification Behavior and Recovery Kinetics of Liquid Crystalline Polymers," Polym. Eng. Sci., 30(16), 989 (1990).
156 Y.G. Lin and H.H. Winter, "Formation of a High Melting Crystal in a Thermotropic Aromatic Copolyester," Macromolecules, 21, 2439 (1988).
157 Y.G. Lin and H.H. Winter, "High-Temperature Recrystallization and Rheology of a Thermotropic Liquid Crystalline Polymer," Macromolecules, 24, 2877 (1991).
158 K.F. Wissbrun and A.C. Griffin, "Rheology of a Thermotropic Polyester in the Nematic and Isotropic States," J. Polym. Sci. Polym. Phys. Ed., 20, 1835 (1982).
159 F. Cocchini, M.R. Nobile, and D. Acierno, "Transient and Steady Rheological behavior of the Thermotropic Liquid Crystal Copolymer 73/27 HBA/HNA," J. Rheol., 35(6), 1171 (1991).
160 L.C. Sawyer and M. Jaffe, "Structure-Properties Relationships in Liquid Crystalline Polymers," in High Performance Polymers, E. Baer and A. Moet, Eds., Hanser, New York, 1991: p.55.
161 L.C. Sawyer and M. Jaffe, "The Structure of Thermotropic Copolyesters," J. Mat. Sci., 21, 1897 (1986).
162 C. Viney, A.M. Donald, A.H. Windle, J. Mater. Sci., 18, 1136 (1983).
163 A.M. Donald, A.H. Windle, J. Mater. Sci., 18, 1143 (1983).
164 C. Viney, A.H. Windle, "On Predicting the Optical Diffraction Pattern From Thermotropic Specimens Having a Banded Texture," Polymer, 27, 1325 (1986).
165 Y. Takeuchi, Y. Shuto, and F. Yamamoto, "Band Pattern Development in Shear-Oriented Thermotropic Copolyester Extrudates," Polymer, 29, 605 (1988).
166 N. Nakano, M. Kishino, and A. Konda, J. Soc. Fiber Sci. Technol., Jpn., 26, 191 (1970).
167 A.E. Zachariades and J.A. Logan, "The Preparation of Oriented Morphologies of the Thermotropic Aromatic Copolyester of Poly(ethylene terephthalate) and 80 Mole Percent p-Acetoxybenzoic Acid," Polym. Eng. Sci., 23(15), 797 (1983).
168 H. Thapar and M. Bevis, "The Micromorphology of An Injection Moulded Thermotropic Liquid Crystal Polymer," J. Mat. Sci. Lett., 2, 733 (1983).
169 E. Baer, A. Hiltner, T. Weng, L.C. Sawyer, and M. Jaffe, "Hierarchial Structures In Thermotropic Liquid Crystal Polymers," Polym. Mater. Sci. Eng., 52, 88 (1985).
170 R.A. Chivers, J. Blackwell, G.A. Gutierrez, J. B. Stamatoff, and H. Yoon "X-

Ray Studies of The Structure of HBA/HNA Copolyesters," Polym. Preprints, 24, 288 (1983).
171 J. Blackwell, G.A. Gutierrez, R.A. Chivers, "X-ray Diffraction by Liquid Crystalline Copolymers Prepared from 4-Hydroxybenzoic Acid and 2-Hydroxy-6-Naphthoic Acid: A One-Dimensional Paracrystalline Model," J. Polym. Sci. Polym. Phys. Ed., 22, 1343 (1984).
172 M.T. De Meuse and M. Jaffe, "Model System for Liquid Crystal Polymer Blends," Mol. Cryst. Liq. Cryst., 157, 535 (1988).
173 A. Pirnia and C.S.P. Sung, "Molecular Orientation Profiles in an Injection Molded Liquid Crystalline Copolyester Characterized by Fourier Transform Infrared Attenuated Total Reflection Dichroism," Macromol., 21, 2699 (1988).
174 A. Kaito, M. Kyotani, and K. Nakayama, "Orientation Profiles in the Strand of Thermotropic Liquid Crystalline Polymer Studied by Polarized Fourier Transform Infrared Microspectroscopy," Macromol., 24, 3244 (1991).
175 D.N. Lewis and J.F. Fellers, "Processing of Polymer Liquid Crystals," in High Modulus Polymers, A. Zachariades and R.S. Porter, Eds., Marcel Dekker, New York, 1988: pg. 1.
176 K. Shimamura, J.L. White, J.F. Fellers, "Hydroxypropyl-cellulose, a Thermotropic Liquid Crystal: Characteristics and Structure Development in Continuous Extrusion and Melt Spinning," J. Appl. Poly. Sci, 26, 2165 (1981).
177 Y. Ide and Z. Ophir, "Orientation Development in Thermotropic Liquid Crystal Polymers," Poly. Eng. Sci., 23(5), 261 (1983).
178 T-S. Chung, "Fluid Behavior and Orientation Developments During Extrusion of Liquid Crystal Polymeric Rods," J. Polym. Sci.: C Polym. Lett., 24, 299 (1986).
179 T-S. Chung, "Production of Ultrahigh Modulus Liquid Crystal Polymer Rods," J. Polym. Sci.: Part B: Polym. Phys., 26, 1549 (1988).
180 R.A. Weiss, W. Huh, and Luigi Nicolais, in High Modulus Polymers, A.E. Zachariades, and R.S. Porter, Eds. Marcel Dekker, New York, 1988: pg. 145
181 E.G. Joseph, G.L. Wilkes, and D.G. Baird, "Effect of Flow History on the Morphology of Thermotropic Liquid Crystalline Copolyesters," Poly. Eng. Sci., 25(7), 377 (1985).
182 R.S. Porter and J.F. Johnson, "The Rheology of Liquid Crystals," in Rheology, Vol. 4, Academic Press, New York, 1969.
183 R.S. Porter and J.F. Johnson, J. Appl. Phys., 34, 51 (1963).
184 Dibenedetto, A.T., L. Nicolais, E. Amendola, C. Carfagna, and M.R. Nobile, "The Effect of Hot Drawing on the Properties of Thermotropic Polymer Fibers," Poly. Eng. Sci. 29(3), 153 (1989).
185 Y. Ide, and T-S. Chung, "Macromolecule Composites of Extruded Thermotropic Polymer Sheets," J. Macromol. Sci, Phys. Ed., B23(4-6), 497 (1985).
186 S. Kenig, "Orientability of Liquid Crystal Polymers in Elongational Flow," Poly. Eng. Sci., 27(12), 887 (1987).
187 S. Kenig, "Shear-Induced Orientation in Liquid Crystalline Polymers," Poly. Eng. Sci., 29(16), 1136 (1989).
188 G.B. Jeffrey, Proc. R. Soc., A102, 161 (1922).

189 S.K. Garg and S. Kenig, "Development of Orientation During Processing of Liquid Crystalline Polymers," in High Modulus Polymers, A.E. Zachariades, R.S. Porter, Eds., Marcel Dekker, New York, 1988: pg. 71.

190 J.L. White, Polym. Eng. Sci., 15, 44 (1975).

191 D.J. Blundell, R.A. Chivers, A.D. Curson, J.C. Love, and W.A. MacDonald, "The Relationship of Chain Linearity of Aromatic Liquid Crystal Polyesters to Molecular Orientation and Stiffness of Moldings," Polymer, 29, 1459 (1988).

192 D.W. Hadley and I.M. Ward, in Structure and Properties of Oriented Polymers, Wiley and Sons, New York, 1974.

193 G.W. Farell and J.F. Fellers, "A Rotating Annular Die to Control The Biaxial Orientation in Melt Processed Thermotropic Liquid Crystalline Cellulose Derivatives," J. Polym. Eng., 6(1-4), 263 (1986).

194 A.E. Zachariades and J. Economy, "Super Strong Polymers in Planar Directions," Poly. Eng. Sci. 23(5), 266 (1983).

195 M. Xanthos, M.W. Young, and J.A. Biesenberger, "Polypropylene / Polyethylene Terephthalate Blends Compatibilized Through Functionalization," Polym. Eng. Sci., 30(6), 355 (1990).

196 D. Beery, A. Siegmann, S. Kenig, "Structured Polymer Blends Containing Liquid Crystalline Polymers," J. Mater. Sci. Letters, 7, 1071 (1988).

197 D. Beery, S. Kenig, And A. Siegmann, "Structure Development During Flow of Polyblends Containing Liquid Crystalline Polymers," Poly. Eng. Sci., 31(6), 451 (1991).

198 P. Zhuang, T. Kyu, and J.L. White, "Characteristics of Hydroxybenzoic Acid - Ethylene Terephthalate Copolymers and Their Blends With Polystyrene, Polycarbonate, and Polyethylene Terephthalate," Poly. Eng. Sci., 28(17), 1095 (1988).

199 F.P. La Mantia, A. Valenza, M. Paci, P.L. Magagnini, "Shear Viscosity of Polybutyleneterephthalate / Liquid Crystal Polymer Blends," Rheological Acta, 28, 417 (1989).

200 R.A. Weiss, W. Huh, and L. Nicolais, "Novel Reinforced Polymers Based on Blends of Polystyrene and a Thermotropic Liquid Crystalline Polymer," Poly. Eng. Sci., 27(9), 684 (1987).

201 A. Kohli, N. Chung, and R. A. Weiss, "The Effect of Deformation History on the Morphology and Properties of Blends of Polycarbonate and a Thermotropic Liquid Crystalline Polymer," Polym. Eng. Sci., 29(9), 573 (1989).

202 A. Valenza, F.P. La Mantia, M. Paci, and P.L. Magagnini, "Processing and Properties of Polycarbonate / Liquid Crystal Polymer Blends," Intern. Polym. Proc. VI(3), 247 (1991).

203 J. Seppala, M. Heino, and C. Kapanen, "Injection-Molded Blends of a Thermotropic Liquid Crystalline Polymer with Polyethylene Terephthalate, Polypropylene, and Polyphenylene Sulfide," J. Appl. Polym. Sci., 44, 1051 (1992).

204 S.K. Bhattacharya, A. Tendolkar, and A. Misra, "Blends of a Liquid Crystalline Polyester with Polyethylene Terephthalate," Mol. Cryst. Liq. Cryst., 153, 501 (1987).

205 Y. Cavaille, C. Jourdan, and J. Perez, "Dynamic Mechanical Spectrometry For The Study of Multiphase Polymer Materials," Makromol. Chem., Macromol. Symp., 16, 341 (1988).
206 A. Siegmann, A. Dagan, and S. Kenig, "Polyblends Containing a Liquid Crystalline Polymer," Polymer, 26, 1325 (1985).
207 R.A. Weiss, W.H. Huh, and L. Nicolais, in High Modulus Polymers, Marcel Dekker, New York, 1988.
208 D. Dutta, H. Fruitwala, A. Kohli, and R.A. Weiss, "Polymer Blends Containing Liquid Crystals: A Review," Polym. Eng. Sci., 30(17), 1005 (1990).
209 D.J. Williams, "Applications for Thermotropic Liquid Crystal Polymer Blends," Adv. Polym. Tech., 10(3), 173 (1990).
210 V.G. Kulichikhin, and N.A. Plate, "Blend Composites Based on Liquid Crystal Thermoplasts. Review," Polym. Sci. U.S.S.R., 33(1), 1 (1991).
211 A.I. Isayev and M. Modic, "Self-Reinforced Melt Processible Polymer Composites: Extrusion, Compression, and Injection Molding," Polym. Comp., 8(3), 158 (1987).
212 M.R. Nobile, E. Amendola, and L. Nicolais, "Physical Properties of Blends of Polycarbonate and a Liquid Crystalline Copolyester," Polym. Eng. Sci., 29(4), 244 (1989).
213 O. Federico, "In-Situ Composites of a Thermotropic Liquid Crystalline Polymer and Polycarbonate: Processing, Morphology and Properties," Ph.D. Dissertation, Univ. of Massachusetts, Amherst, MA. (1989).
214 K.G. Blizard, C. Federici, O. Federico, and L.L. Chapoy, "The Morphology of Extruded Blends Containing a Thermotropic Liquid Crystalline Polymer", Poly. Eng. Sci., 30(22), 1442 (1990).
215 F.P. La Mantia, M. Saiu, A. Valenza, M. Paci, and P.L. Magagnini, "Relationships Between Mechanical Properties and Structure for Blends of Nylon-6 with a Liquid Crystal Polymer," Eur. Polym. J., 26(3), 323 (1990).
216 J.C. Halpin, and J.L. Kardos, J. Appl. Phys., 43(5), 2235 (1972).
217 W. Brostow, T.S. Dziemaianowicz, J. Romanski, and W. Werber, "Transmission of Mechanical Energy Through Polymeric Liquid Crystals and Their Blends," Poly. Eng. Sci., 28(12), 785 (1988).
218 K. G. Blizard, C. Ferderici, O. Federico, and L.L. Chapoy, "The Morphology of Extruded Blends Containing a Thermotropic Liquid Crystalline Polymer," Poly. Eng. Sci. 30(22), 1442 (1990).
219 H. Van Oene, in Polymer Blends, D.R. Paul and S. Newman, Eds., 1, Academic Press, New York, 1978. p295.
220 K.G. Blizard and D.G. Baird, "The Morphology and Rheology of Polymer Blends Containing a Liquid Crystalline Copolyester," Poly. Eng. Sci., 27(9), 653 (1987).
221 M. Kodama, "Effects of Thermal Modification on the Structural Properties of Thermotropic Liquid Crystalline Copolyester and Phenoxy Resin Blends," Polym. Eng. Sci., 32(4), 267 (1992).
222 W-C. Lee and A.T. DiBenedetto, "Processing of Thermotropic Liquid Crystalline Polymers and Their Blends - Analysis of an In-Situ LCP Composite

System," Polym. Eng. Sci., 32(6), 400 (1992).
223 M. Paci, M. Liu, P.L. Magagnini, F.P. La Mantia, and A. Valenza, "Compatibility of Blends of Poly(Butylene Terephthalate) and Liquid Crystal Polymers: A DSC Study," Thermochimica Acta, 137, 105 (1988).
224 A. Datta, J.P. De Souza, A.M. Sukhadia, and D.G. Baird, "Processing Studies of Blends of Polypropylene with Liquid Crystalline Polymers," Annual Technical Conference of the Society of Plastic Engineers (ANTEC '91), 49, 913 (1991).
225 H.J. O'Donnell, A. Datta, D.G. Baird, "The Effect of Compatibilization on the Properties of Blends of LCPs with Polypropylene," Annual Technical Conference of the Society of Plastic Engineers (ANTEC'92), 50, 2248 (1992).
226 A.M. Sukhadia, A. Datta, and D.G. Baird, "Generation of Continuous Liquid Crystalline Polymer Reinforcements in Thermoplastics by a Novel Blending Process," Annual Technical Conference of the Society of Plastic Engineers (ANTEC'91), 49, 1008 (1991).
227 D. Beery, S. Kenig, and A. Siegmann, "Structure and Proprties of Molded Polyblends Containing Liquid Crystalline Polymers," Poly. Eng. Sci., 31(6), 459 (1991).
228 M. Kimura and R. S. Porter, "Compatibility of Poly(butylene terphthalate) with a Liquid Crystalline Copolyester," J. Poly. Sci., Poly. Phys. Ed., 22, 1647 (1984).
229 F.P. La Mantia, A. Valenza, M. Paci, and P.L. Magagnini, "Shear Viscosity of Polybutyleneterephthalate / Liquid Crystal Polymer Blends," Rheol. Acta., 28, 417 (1989).
230 F.P. La Mantia, "Liquid Crystal Polymers as Processing Aids and Reinforcing Agents. A Study of Nylon 6 / LCP Blends," J. Appl. Poly. Sci., 38, 583 (1989).
231 C.D. Han, Multiphase Flow in Polymer Processing, Academic Press, New York (1981).
232 F.P. La Mantia, a. Valenza, M. Paci, and P.L. Magagnini, "Rheology-Morphology Relationships in Nylon 6/Liquid-Crystalline Polymer Blends," Polym. Eng. Sci., 30(1), 7 (1990).
233 C. Carfagna, E. Amendola, L. Nicolais, D. Acierno, O. Francescangeli, B. Yang, "Blends of a Polyetherimide and a Liquid Crystalline Polymer: Fiber Orientation and Mechanical Properties," J. Appl. Polym. Sci., 43, 839 (1991).
234 S.H. Jung and S.C. Kim, "Morphology and Mechanical Properties of Poly(ethylene terephthalate)-Poly(hydroxybenzoic acid) and Polycarbonate Blends," Polymer Journal, 20(1), 73 (1988).
235 A.I. Isayev, "Self-Reinforced Composites of Thermotropic Liquid Crystalline Polymers," SPE ANTEC Tech. Paper, 908 (1991).
236 D. Berry, S. Kenig, and A. Siegmann, "Shear and Elongational Viscosities of a Thermotropic Liquid Crystalline Polymer and Its Blend With Polycarbonate," Polym. Eng. Sci., 32(1), 14 (1992).
237 G. Crevecoeur, "In-Situ Composites, Blends of Thermotropic Liquid Crystalline Polymers in a Thermoplastic Matrix," Ph.D. Dissertation, Katholieke Universiteit Leuven, Holland (1991).
238 S.M. Hong, B. C. Kim, K.U. Kim, and J Chung, "Rheology and Physical of

Polysulfone In-Situ Reinforced with a Thermotropic Liquid-Crystalline Polyester," Polymer J., 23 (11), 1347 (1991).

239 F.P. La Mantia, A. Valenza, and P.L. Magagnini, "Liquid Crystal Polymer-Based Blends: Universal Grade Polymers?," J. Appl. Polym. Sci., 44, 1257 (1992).

240 B.R. Bassett and A.F. Yee, "A Method of Forming Composite Structures Using In Situ-Formed Liquid Crystal Polymer Fibers in a Thermoplastic Matrix," Poly. Eng. Sci., 11(1), 10 (1990).

241 G. Kiss, "In-Situ Composites Blends of Isotropic Polymers and Thermotropic Liquid Crystalline Polymers," Poly. Eng. Sci., 27(6), 410 (1987).

242 C.U. Ko and G.L. Wilkes, "Morphological Studies of Blends Containing Liquid Crystalline Polymers with Poly(ethylene terephthalate)," J. Appl. Polym. Sci., 37, 3063 (1989).

243 A.K. Mithal, A. Tayebi, and C.H. Lin, "In-Situ Composite Fibers: Blends of Liquid Crystalline Polymer and Poly(ethylene terephthalate)," Poly. Eng. Sci., 31(21), 1533 (1991).

244 H. Brody, "Orientation Suppression in Fibers Spun From Polymer Melt Blends," J. Appl. Polym. Sci., 31, 2753 (1986).

245 D.C. Prevorsek, in Polymer Liquid Crystals, A. Ciferri, W.R. Krigbaum, R.B. Meyer, Eds., Academic Press, New York, 1982: Chapter 12.

246 A. Apicella, P. Iannelli, L. Nicodemo. L. Nicolais, A. Roviello, and A. Sirigu, "Dimensional Stability of Polystyrene / Polymeric Liquid Crystal Blends," Polym. Eng. Sci., 26(9), 600 (1986).

247 Z. Tadmor and I. Klein, Engineering Principles of Plasticating Extrusion, Krieger Publishing, New York, 1978.

248 D. Bigg and S. Middleman, "Mixing in a Screw Extruder. A Model for Resident Time Distribution and Strain," Ind. Eng. Chem., Fundm., 13(1), 66 (1974).

249 A.M. Sukhadia, "The In-Situ Generation of Liquid Crystalline Polymer Reinforcements in Thermoplastics," Ph.D. Dissertation, Virginia Tech, Blacksburg, 1991.

3.0 In Situ Reinforcement of Polypropylene with LCP: Effect of Maleic Anhydride Grafted Polypropylene [1]

3.1 Introduction

A frequent goal of polymeric material research is the improvement of physical properties. An approach that is widely used is the combination of two polymers in hope of obtaining favorable properties in the blend. If successful, this route can lead to the creation of attractive new composite materials. One relatively new type of blend is that of thermotropic liquid crystalline polymers, LCPs, and thermoplastic matrices, TP. Neat LCPs exhibit very high mechanical properties as a result of their stiff molecular backbones [1], their relative ease to orient, and their ability to retain this orientation for up to several minutes in the melt state [13,14]. Commercially available LCP resins processed by means of injection molding have moduli in the range from 4 to 20 GPa and strengths from 139 to 213 MPa [2]. In comparison, injection molded thermoplastic resins have much lower properties with moduli typically in the range of 1 to 4 GPa and strengths from 20 to 60 MPa [3]. If the LCP is used as a fiber-like reinforcement in the TP matrix then LCPs have the potential for greatly reinforcing thermoplastic matrices. This fiber-like morphology can be generated during processing of the blend, and so the term in situ composite is used to describe the reinforced blend.

Several key factors affect the ability of LCPs to reinforce thermoplastics. The first factor is the influence of the flow field on orientation and mechanical properties of neat LCPs. An uniaxial extensional flow field is very effective in bringing about molecular orientation within neat LCPs [15-20]. Ide and Ophir [16] demonstrated this point by varying the draw ratio and

---

[1] This chapter is being submitted to Polymer

shear rate during capillary extrusion of a LCP. Both the orientation and moduli of these samples were significantly improved by drawing the extrudate. Conversely, increasing the shear rate within the die decreased the moduli.

While the type of flow field is important in creating orientation in neat LCPs, it also plays an important role when the LCP is the dispersed phase of a polymer blend. In polymer blends, the deformation of the LCP phase occurs most readily in an extensional flow field such as uniaxial flow to form fibrils with high aspect ratios; these fibrils can create effective reinforcement of the matrix leading to high mechanical properties [22-25,34]. However, once the fibrils are formed they must be solidified before interfacial instabilities occur which would lead to breakup of the fibers into droplets [10,11] or before undergoing relaxation that would cause a significant loss in their molecular orientation [13,14].

The concentration of a LCP within a matrix has also been shown to be a critical factor in achieving deformation of the LCP phase [23-25]. Blizard and Baird [25] demonstrated this point with blends of a LCP based on polyethylene terephthalate / p-hydroxybenzoic acid (PET/PHB) with polycarbonate (PC) and nylon 6,6 matrices. Blends with 10 wt% LCP extruded through a capillary die with a small L/D ratio (7) were found to have a droplet morphology. However, fibrils were obtained when the concentration reached 30% LCP. An increased dispersed phase size created by an increased rate of coalescence at the higher LCP concentration was believed responsible for the formation of fibers at 30 wt% LCP. In a larger L/D ratio die (27) a droplet morphology was found at both concentrations. The change from a smaller to greater L/D ratio die is accompanied by an increased resident time in the die. While fibers may have been formed at the entrance to the die, the increased time under shear flow in the longer die allows interfacial forces to break the fibers into droplets. From this study, it can be stated

that the existence of extensional flows and higher concentrations are important factors that can lead to the creation of a reinforcing morphology.

Even when extensional flows and higher concentrations exist, this may not be sufficient for obtaining reinforcing morphology. The temperature range required for processing each material must suitably overlap. Typically, LCPs are processed above 300°C while thermoplastics are processed below this temperature. Despite the temperature difference between LCP and TP matrices, a fibrous morphology with enhanced mechanical properties can often be created from many TP/LCP blends. However, some exceptions do exist [33,26,24]. For instance, in drawing of extruded strands of K161, a LCP from Bayer Co., in an polyetherimide (PEI) matrix, Carfagna et al. [33] found little improvement in the mechanical properties as the draw ratio was increased. The limited effect of draw ratio on the mechanical properties was related to the large differences between the glass transition temperatures of the two materials [33]. Blizard et al. [26] found similar results for the drawing of blends of LCPs in PC and PEI matrices.

While high temperatures are generally required to process TP/LCP blends, temperatures much higher than the melting point of the LCP may lead to a reduction in the mechanical properties. Nobile et al. [24] found that the morphology and the mechanical properties of drawn strands of 10 wt% PET/PHB in a PC matrix were sensitive to temperature. At 260°C, a droplet morphology was observed and lower properties were measured in contrast to a fibrillar morphology and higher properties when extrusion was performed at 220°C. The improved properties at a lower processing temperature may be the result of at least two factors. The first factor is that higher hydrodynamic stresses at the lower temperature lead to a higher Weber number which would deform smaller LCP droplets. The second factor is that the lower temperature may result in improved retention of molecular orientation or may permit

solidification of the elongated LCP structures before interfacial tension could cause breakup or retraction of the elongated structures.

While the above factors significantly affect the ability of LCPs to reinforce TPs, the combination of a particular TP/LCP pair can also have a marked influence on the resulting properties. Often partially miscible systems exhibit the highest strengths while totally immiscible systems display strengths that are weaker than the matrix [21]. In an attempt to predict suitable polymer pairs, Meretz [35] proposed selecting pairs based on the interfacial tension and polarity differences as calculated from contact angle measurements on neat solid samples. Unfortunately, the mechanical properties for only one pair was investigated thus leaving open the question as to how accurate this method is in predicting properties for a wide range of polymer pairs.

While polymer pairs that lead to enhance mechanical properties are desired, two less suitable polymers might be made more integral by the use of a third interfacially active component. The process of bringing about enhanced mechanical properties by the addition of a minor third component is termed compatibilization [4,5]. Compatibilization is often used in a thermoplastic blend where a polymer that lacks toughness is modified by adding a rubbery phase to enhance the toughness and the impact strength of the matrix. Without the compatibilizer, the blend would exhibit poor adhesion and large phase sizes with resulting poor mechanical properties. The compatibilizer may be a copolymer with similar blocks to each of the polymers, blocks capable of creating specific interactions with the polymers, or a functionalization of one of the polymers that is capable of undergoing a graft reaction with the other dissimilar polymer. A review of compatibilizer types and reports of successful uses of compatibilizers may be found in references [4-6]. A common point in these reviews is that successful compatibilization can be characterized with three features: reduced interfacial tension,

finer dispersions, and increased adhesion. In addition, successful compatibilization results in mechanical property improvements. In particular, the impact strength and toughness of TP blends are markedly improved.

While the use of compatibilizers with TP blends is widespread, in only one case has there been a report of compatibilized TP/LCP blends: the blend of polypropylene (PP) with various LCPs [27-30]. Because of the incompatible nature of PP with the LCPs, a third polymer, maleic anhydride grafted PP(MAP), was added to improve the adhesion between the phases and enhance the mechanical properties of the blend. Since this time, others have investigated the same blends [32]. However, as noted above, the LCP phase must deform into an elongated fibrillar morphology to reinforce a matrix while, contrarily, in thermoplastic blends a compatibilizer creates a droplet morphology which would not reinforce tensile properties. Obviously, the use of a compatibilizer in TP/LCP blends must generate the former morphology to be of value. It was found [27-30] that compatibilized PP/LCP blends created a more fibrillar dispersed structure that resulted in enhanced tensile strength and modulus of the blends over the entire PP/LCP composition range. Additionally, a greatly reduced degree of fiber pullout occurred indicating that adhesion did, indeed, improve [27].

There are still several questions remaining as to the effect of MAP on the mechanical properties of PP/LCP blends. The first question pertains to the effect of the amount of MAP on the mechanical properties of the blends. In particular, do the properties reach a plateau as the concentration of MAP increases? Second, will the use of increasing amounts of MAP lead to a morphological change from a fibrillar to a droplet morphology? Such a morphological change would lead to a change in the aspect ratio and, consequently, to a decline in the modulus as predicted for fiber reinforced composites [40]. Third, can the changes at the interface be

measured or indirectly obtained, and if so does the compatibilizer lower the interfacial tension and enhance adhesion? Finally, does MAP compatibilize these blends through a physical interaction or via a chemical reaction? Knowledge of the type of interaction may be helpful in a search for other possibly even more effective compatibilizers.

To pursue the answers to these questions, the effect of increasing concentration of MAP on the mechanical properties of PP/LCP blends with a fixed LCP percentage, 30 wt%, is investigated. The objective of this work is three fold. The first objective is to determine how the concentration of MAP affects the mechanical properties of the blend. The second objective is to determine if the presence of MAP leads to reduced interfacial tension and enhanced adhesion between the phases. The final objective is to determine if the compatibilization effect of MAP is the result of physical interaction or chemical reaction.

3.2 Experimental

3.2.1 Materials

Five polymers were used in this work. The polypropylene, Profax 6823, was a fractional melt flow index (MFI) polymer purchased from Himont, Inc. The compatibilizer was a development grade maleic anhydride grafted polypropylene, MAP, supplied by BP Chemicals, Inc. with a MFI of 50. This material was titrated as outlined elsewhere [28] and found to have 0.75 wt % maleic anhydride. Three LCPs were used in this study of which two were a copolyester while another was a poly(ester-amide). The first LCP was Vectra® A950 purchased from Hoescht Celanesse, and hereafter it is referred to as VA. This polymer was reportedly synthesized from the following monomers: 73% hydroxybenzoic acid and 27% hydroxynaphthoic

acid. The second LCP was Vectra® B950 purchased from Hoescht Celanesse and it is referred to as VB. This polymer was reportedly synthesized from 60% hydroxynaphthoic acid, 20% terephthlalic acid, and 20% aminophenol. The latter ingredient creates the amide moiety within the LCP which was incorporated to increase hydrogen bonding with other polymers [12]. The third LCP is LC3000 supplied by Unitika of Japan. This polymer was based on 40% poly(ethylene terephthalate) copolymerized with 60% hydroxybenzoic acid.

3.2.2 Sample Preparation

All blends containing MAP were first prepared by extruding PP with MAP in an one inch, 24 L/D, Killian extruder at 40 rpm and 250°C. This material is the matrix, and it will be designated as PP(MAP) throughout this paper. All injection molded specimens were prepared on an Arburg Allrounder, model 221-55-250, injection molder. Both tensile bars and plaques were produced. The tensile bars were 63.5 by 9.5 by 1.5 mm and the width at the neck was 3.2 mm. The plaques were 76 by 76 by 1.5 mm. This latter mold was machined with a film gate to provide two dimensional rectilinear flow throughout the cavity.

The blends were prepared by tumbling dried pellets of PP(MAP) with dried pellets of the appropriate LCP immediately before use in the injection molder. Both VA and VB blends were molded with the three barrel zone temperatures set to 160, 295, and 295°C, the nozzle temperature set to 280°C, and the mold temperature set to 40°C. Blends of LC3000 were molded The blend compositions are designated in a special manner. An example will best illustrate this designation. If a PP(MAP) matrix containing 10 wt% MAP is blended with a LCP so that 30 wt% LCP results then this blend will be labeled as PP(MAP)/LCP 70(10)/30. The first number, 70, indicates the weight percent of PP(MAP) within the blend while the second

number, 10, indicates the weight percent of MAP within the PP(MAP) phase. The last number indicates the weight percent LCP in the blend. This designation method was convenient to use since PP(MAP) matrices were prepared prior to blending with LCP.

3.2.3 Mechanical Testing

All samples were tested in the tensile mode on a Instron mechanical tester, model 4204, using a crosshead speed of 1.27 mm/min. An extensiometer, Instron model 2630-25, was used for all tests except for determination of the strength and elongation of neat PP or PP(MAP). Strips of 10 by 76 mm were cut from the plaques and were sanded to minimize cutting marks. A minimum of five samples were tested and the average and standard deviation were calculated.

3.2.4 Scanning Electron Microscopy

Fracture surfaces of these materials were prepared by cryogenic fracture in liquid nitrogen followed by coating with gold in a SPI sputter coater. Fracture samples were viewed on a Cambridge stereoscan S200 scanning electron microscope (SEM) using an accelerating voltage of 15 KeV. Samples for examination were taken from sprues, tensile bars, and plaques. The sprues were fractured approximately 12 mm from the gate and along the machine direction so that the profile in the flow direction could be observed. Because of the narrow size in the neck section, the tensile bars were fractured only in the transverse direction. This angle provides a view of the dispersed phase in the machine direction. The plaques were fractured in the machine direction and like the sprue samples provide a view of the flow direction. These plaque samples were subsequently etched in hypochloric acid as described by Olley et al. [37] for 15 minutes to better reveal the LCP morphology.

3.2.5 Contact Angle Measurements

Contact angles of water, formamide, and ethylene glycol on solid polymers were measured with a goniometer fitted with a video camera and monitor. These three liquids were chosen because of differences in their polar to dispersive components [38]. The solid polymer samples were prepared from injection molded plaques. These samples were cut from the plaques and rinsed with acetone prior to the measurement of contact angles. The contact angles of at least five drops per liquid were measured and averaged to determine the contact angle. These angles were determined with a standard deviation of approximately 2.8 degrees.

3.2.6 Maleic Anhydride Interaction

This section will describe the experimental methods used to determine if MAP reacts with the LCP. In brief, PP(MAP) was extruded with and without LCPs to create test and control samples. Subsequently, the PP(MAP) was isolated from the LCP and the relative change in the concentration of MAP between test and control was determined by means of FTIR spectroscopy.

In this investigation, a matrix rich in MAP (70 wt%) was used. One batch of this material was prepared by extrusion in a single screw extruder at 250°C and 40 rpm, and it is referred to as the precursor. A neat sample of MAP would have been preferred, but there is insufficient melt strength for bringing strands of MAP to the pelletizer and hence some PP was included. The precursor was then dried overnight in a vacuum oven at 100°C while the LCP was dried overnight in a convection oven at 115°C. Control samples were prepared by extruding the precursor at approximately the same residence times and processing temperatures that would be used for preparation of the test samples. The test samples, or blends, were prepared by extrusion of the dried precursor with the LCP in a Killion single screw extruder followed by pelletization.

Blends of 30 wt% VA and VB were extruded with barrel zone temperatures of 125, 295, and 295°C, a die temperature of 200°C, and a screw speed of 60 rpm. Blends of 30 wt% LC3000 were extruded with barrel zone temperatures of 125, 240, and 250°C, a die temperature of 200°C, and a screw speed of 50 rpm.

Isolation of PP(MAP) from the control samples was accomplished by placing ten grams of the PP(MAP)/LCP blends in a flask with 250 ml xylene. This suspension was agitated with a mechanical propeller under reflux for three hours. Concurrently, a Buechner funnel was heated for several hours to 130°C in a convection oven. The PP(MAP)/LCP suspension was quickly filtered through the hot funnel leaving primarily LCP as the extract and PP(MAP) as the filtrate. However, because the mixing process that occurs in the extruders can create fine submicron particles, filtrate samples from blends with VB and LC3000 possessed some LCP particles which could not be isolated from the PP(MAP) phase. The filtrate from blends with VA possessed few if any of these particles. After filtration, approximately 30 ml of ethanol were added to the filtrate to precipitate the PP(MAP). This material was subsequently filtered and dried in a vacuum oven for three days at 100°C to isolate PP(MAP) from the solvents.

Samples of the isolated PP(MAP) were pressed to films of approximately 40 micron thickness at 200°C and dried in the vacuum oven at 100°C for three days prior to obtaining a FTIR spectrum. These spectra were obtained in a Nicolet FTIR which was enclosed in a temporary dry box to minimize the effects of moisture on the instrument. To average errors involved with measurement of the film thickness, two spectra of each sample were taken at different locations on the film.

3.4 Results and Discussion

The results of this work are organized along the following lines. First the mechanical properties of these blends are presented as the concentration of MAP increases. Second, the morphology of these samples are observed in attempts to relate the properties to the morphology. Third, the interfacial tension and work of adhesion are determined. This will establish if MAP also reduces interfacial tension and increases the work of adhesion as commonly occurs for compatibiized TP blends. Finally, the type of interaction between MAP and LCP will be presented. It is hoped that knowledge of the type of interaction will lead to development of improved compatibilizers.

3.4.1 Mechanical Properties

The tensile strength of PP(MAP) with 30 wt% LCP is shown in Fig. 3-1 for tensile bars as the percentage of MAP within the PP(MAP) matrix rises to 50 wt%. The VA blend shows the least rise, from 44.5 to 55.1 MPa, and this blend tends to display a plateau in the strength. The VB blend displays a large monotonic increase in strength without signs of reaching a plateau as the percentage of MAP increases to 50%. The strength of this blend is increased from 32.4 to 57.8 MPa, a 78% increase, as the percentage of MAP is increased from 0 to 50 wt%. Lastly, the strength of LC3000 rises from 21.3 to 37.2 MPa as the percentage of MAP increases from 0 to 50 wt%. It appears as in the case of VA blends that the tensile strength of the LC3000 blends may be reaching a plateau. However, higher concentrations of MAP would be required to accurately determine if a plateau exists.

The tensile modulus for these blends shows a less pronouced variation as the percentage

of MAP increases, as shown in Fig. 3-2. For VA blends, there is an increase in the modulus from 4.1 to 4.7 GPa as MAP is added to the matrix. However, the modulus decreases below that of the uncompatibilized blend at 50 wt% MAP. Blends with VB show a more pronouced increase in the modulus with the addition of MAP. The modulus increased from 4.8 to a plateau of 5.7, a 19% percent rise, at MAP concentrations higher than 5 wt%. For LC3000, there is only a slight increase in the modulus with the addition of MAP.

The elongation at yield is also affected by the addition of MAP as shown in Fig. 3-3. For VA blends, the elongation does not markedly change until 50 wt% MAP is added. It should be noted that this corresponds to the point where the modulus dropped. At 50 wt% MAP, the elongation is only 2.30%, half of the neat VA elongation which is 4.35%. For VB blends, the elongation increases only at 30 and 50 wt% MAP. However, at 50 wt% MAP the elongation, 1.42%, approaches the elongation of neat VB which is 1.64%. The elongation of LC3000 blends displays a continual rise as the content of MAP increases. The highest elongation which occurs at 50 wt% MAP is 2.21% just slightly greater than the elongation of neat LC3000 which is 1.96%. The elongation of the blend being greater than the elongation of the neat LC3000 may be the result of higher elongation in a less oriented LC3000 phase in the blend. The approach of the elongation of the blends to the elongation of the neat LCPs may indicate that the specimen is acting as an integral specimen instead of acting as a two phase structure that can separate and fail prematurely.

The stress-strain curves of PP(MAP)/LCP tensile bars for three percentages of MAP are shown in Fig. 3-4. The stress-strain behavior illustrates not only the changes in mechanical properties as a function of the percentage of MAP, but the curves also indicate changes in adhesion. In Fig. 3-4a, the increased strength as the percentage of MAP increases and the

decreased modulus at 50 wt% MAP are clearly observed. For VB blends, the large increases in the strength and modulus with the addition of MAP are shown in Fig. 3-4b. The large increase in strength and elongation of LC3000 blends with the addition of MAP are shown in Fig. 3-4c. The additional information displayed in Fig. 3-4 is the mode of failure. It can be observed in Fig. 3-4 for blends of VA and VB that the type of failure changes as the percentage of MAP increases. For both VA and VB blends, a transition from a ductile to a brittle failure occurs for samples with 50 wt% MAP. It is believed that the addition of MAP creates an integral specimen. For this integral specimen, once the tensile stress causes failure of the LCP phase, which fails in a brittle mode, and the stress exceeds the strength of PP, failure of the blend leads to brittle fracture. This ductile to brittle transition and the mechanical property enhancements discussed above strongly suggest that adhesion between the phases is markedly improved. This transition does not occur with the LC3000 blend, but the lack of a ductile to brittle transition does not necessarily indicate that the compatibilizer is not as effective with this LCP. Instead, it is possible that the stresses never significantly exceed the tensile strength of the PP phase, and so the PP still deforms in a ductile manner. Thus, in addition to improved mechanical properties, the incorporation of MAP into these blends can create a ductile to brittle transition indicating that adhesion is markedly improved.

In the past, mechanical property differences between tensile bars and plaques were noted [27,29]. Examination of the mechanical properties of plaques can reveal information that differs from that of tensile bars. One difference is believed to be the result of the flow field present when the sample is molded. Because of the converging region near the neck of the tensile bar, elongational flow exists which has been related to the creation of high mechanical properties in neat LCPs [16,19]. However, the flow field in a plaque is predominately that of a shear field

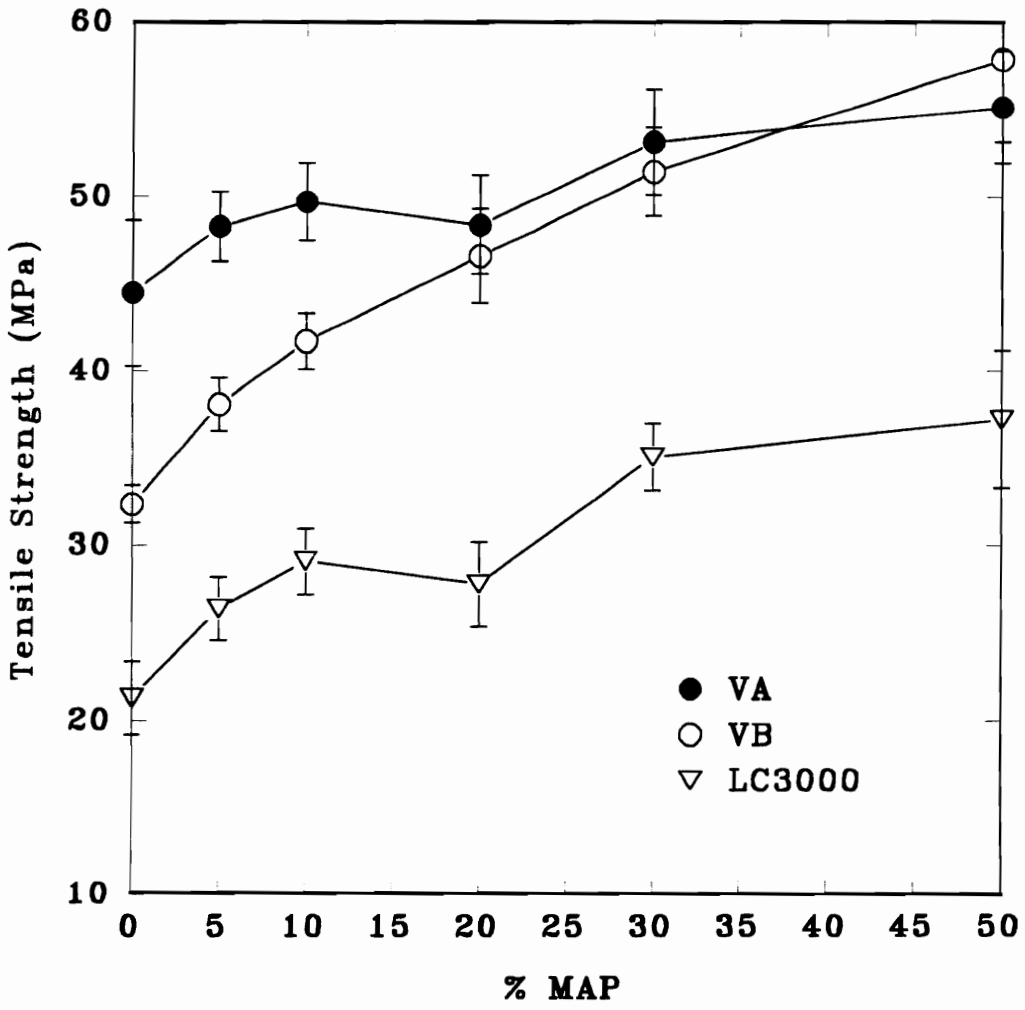

Fig. 3-1 Tensile strength of 70 wt% PP(MAP) with 30 wt% LCP as the percentage of MAP in PP(MAP) increases from 0 to 50 wt%.

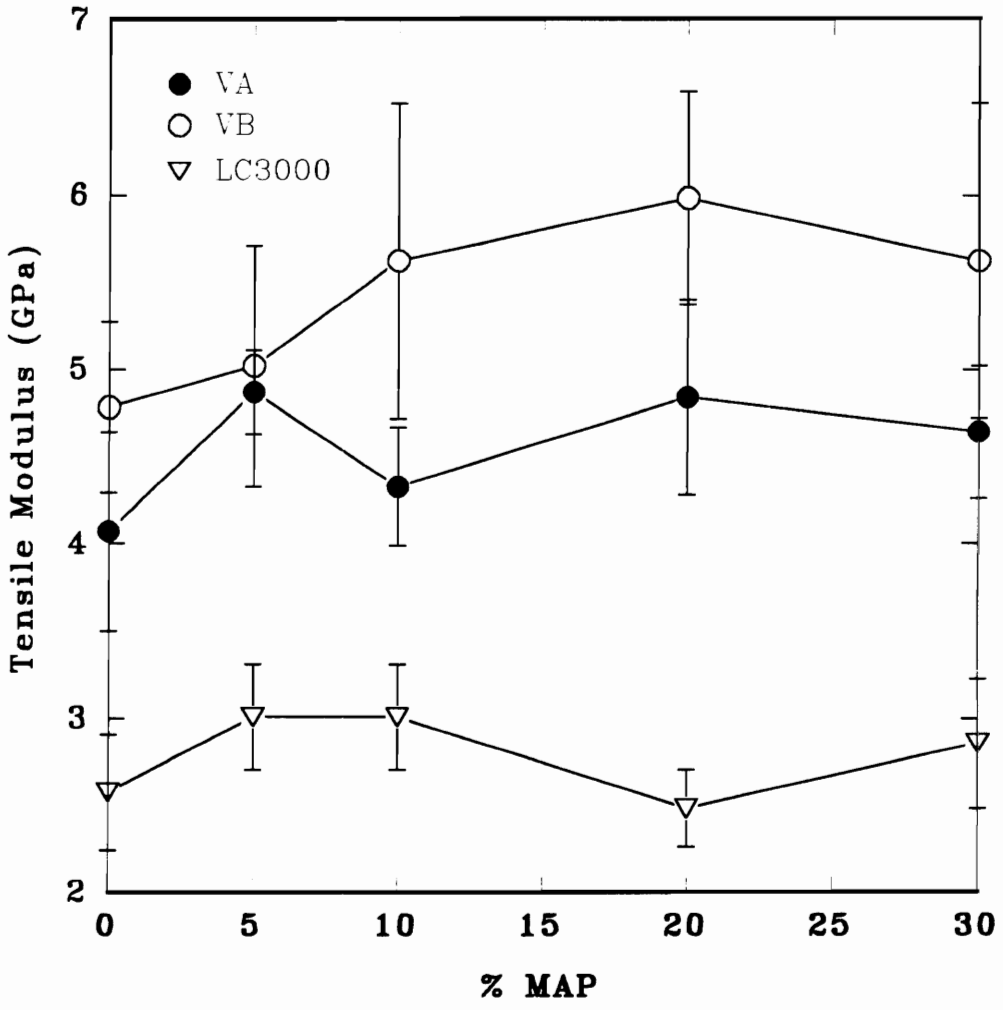

Fig. 3-2 Tensile modulus of 70 wt% PP(MAP) with 30 wt% LCP as the percentage of MAP in PP(MAP) increases from 0 to 50 wt%.

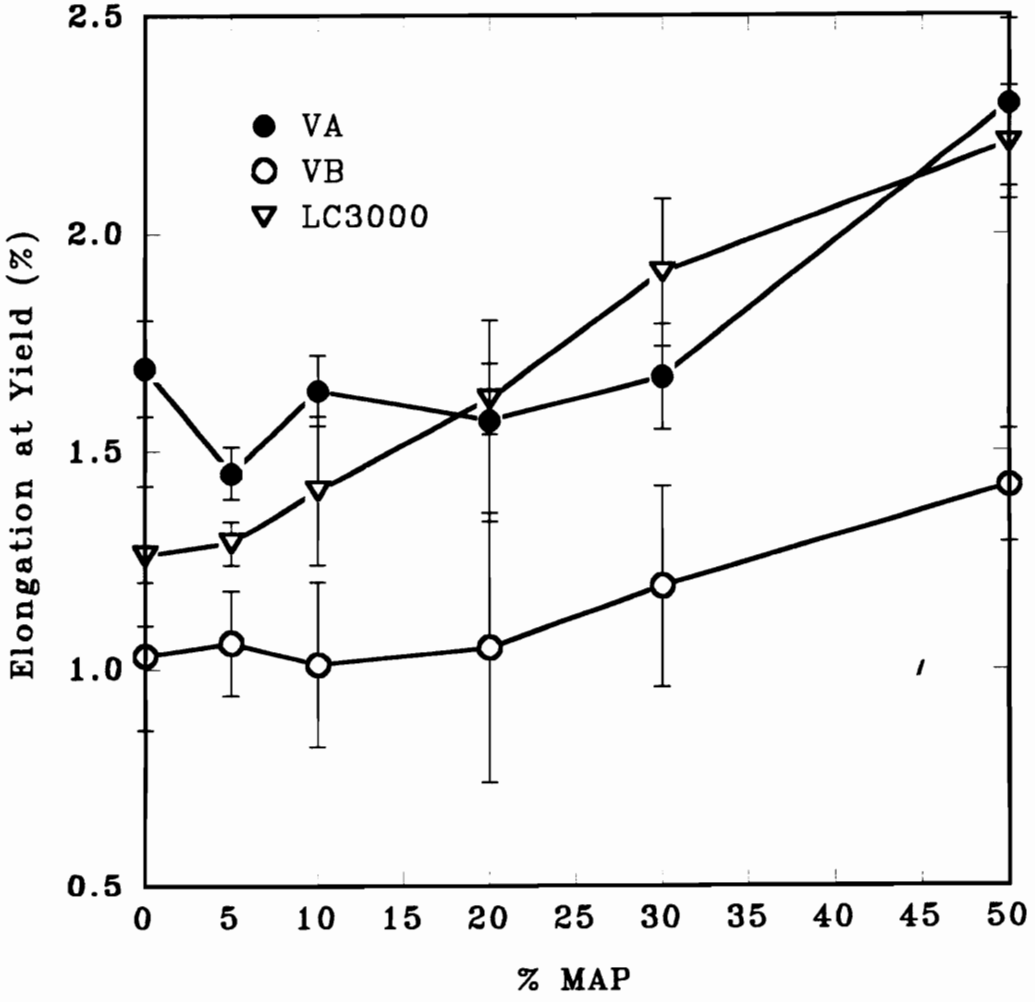

Fig. 3-3 Elongation at yield of 70 wt% PP(MAP) with 30 wt% LCP as the percentage of MAP in PP(MAP) increases from 0 to 50 wt%.

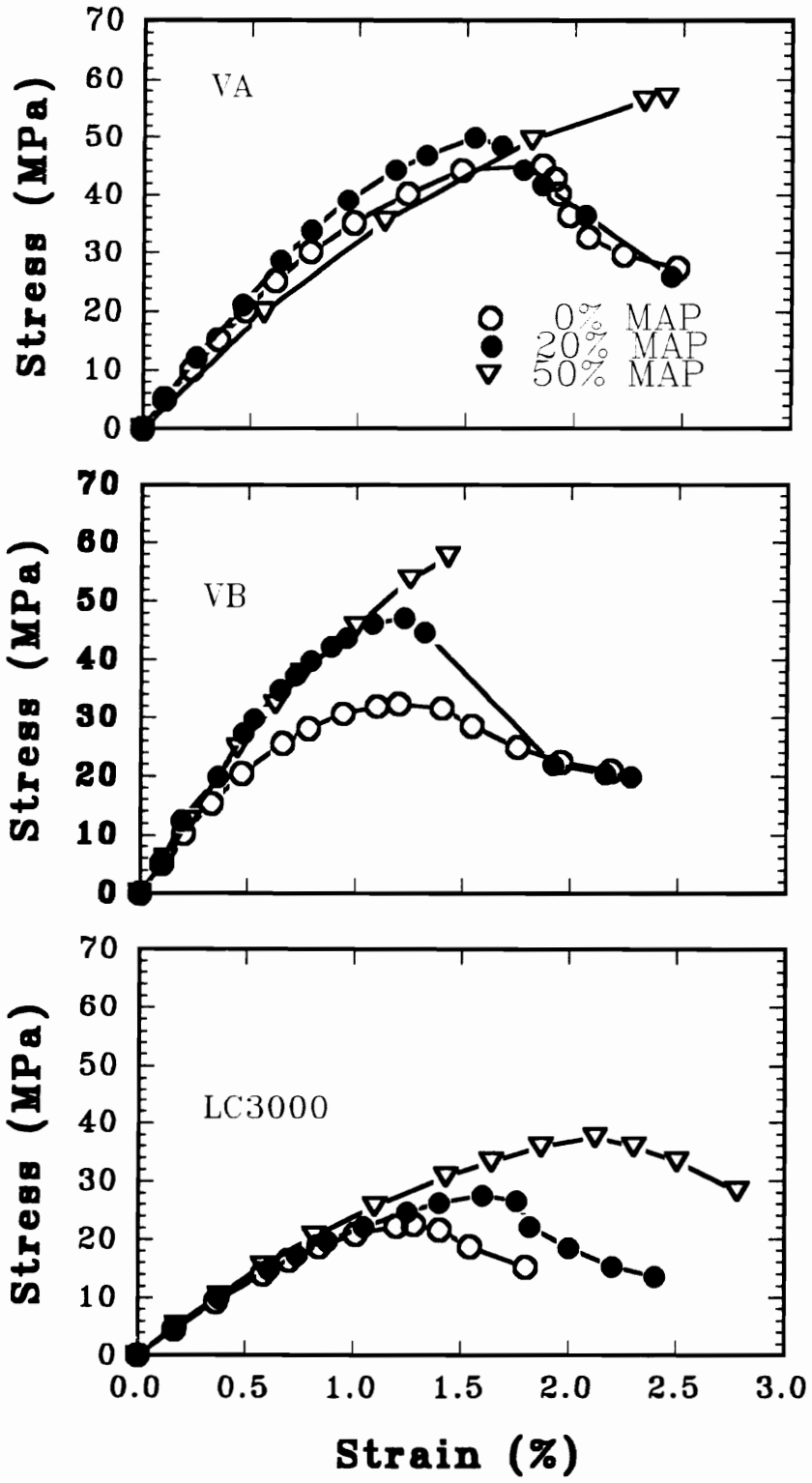

Fig. 3-4 Stress-strain curves for 70 wt% PP(MAP) with 30 wt% LCP as a function of the percentage of MAP.

which creates less orientation and reinforcement than would occur in extensional flow. The plaque is, however, reinforced by LCP that is deformed by flow in the advancing front. The flow in the advancing front is approximately a hyperbolic extensional flow field [45], and this flow field is responsible for the creation of a highly oriented skin region. Another primary difference between tensile bars and plaques is the ability to test the specimen in machine and transverse directions. The tensile bar may only be tested in the machine direction while the plaque may be tested in both the machine and transverse direction. Investigation of plaque properties can provide information about the anisotropy of the specimen. For compatibilized samples, testing the mechanical properties in the transverse direction as the concentration of MAP increases indicates whether adhesion is improving. Testing in the transverse direction loads the sample in a series manner where the stress must pass from the matrix to the LCP. This type of loading stresses the interface and therefore tests the strength of the interface more directly than testing in the machine direction.

The machine and transverse direction tensile properties of plaques of VA, VB, and LC3000 blends as a function of the percentage of MAP are presented in Tables 3-1 though 3-3. For VA blends tested in the machine direction, there is a monotonic increase in the strength from 28.3 to 38.3 MPa with increasing amounts of MAP. However, no significant change occurs in the modulus and only a slight increase occurs in the elongation. The modulus of this VA blend is slightly below the modulus calculated from the rule of mixtures, 3.1 GPa. For transverse direction properties, the strength increases monotonically from 12 to 16.7 MPa while little or no change occurs in the modulus or elongation. It should be noted that the strength of PP plaques is 26.2 GPa, and the transverse direction strength is considerably below that of the matrix. This is typical for unidirectionally fiber-reinforced plastics [41], and the low strength is related to poor

adhesion between the phases. The transverse direction modulus is equivalent to the modulus calculated from the series model, 1.2 GPa.

For VB blends, the machine direction strength also increases monotonically from 23.1 to 40.3 MPa. In contrast to VA blends, the modulus of VB blends increases substantially, from 3.69 to 4.94 MPa. This increase in modulus is a significant rise, and it equals 80% of the modulus calculated fron the rule of mixtures, 6.1 GPa. The strength in the transverse direction for VB blends increases from 11.8 to 17.8 MPa while the modulus and elongation remain unchanged. The transverse direction modulus is approximately equal to the modulus calculated fron the series model, 1.4 GPa.

For LC3000 blends, the strength in the machine direction increases from 14.4 to 26.2 MPa and the modulus increases slightly from 1.81 to 2.18 GPa. This modulus is 69% of the modulus calculated by the rule of mixtures, 3.2 GPa. This modulus can be increased by suitable choice of the injection molding conditions [31]. In the transverse direction, the strength more than doubles as it increases from 7.6 to 16.1 MPa. Concurrently, the transverse direction elongation increases from 0.73 to 1.71 %. Thus, MAP enhances the strength in both machine and transverse direction while only the VB blends show a strong increase in modulus with increasing MAP content. It is speculated that this increase in modulus is related to stronger hydrogen bonding between MAP and VB [12]. The improvements in the transverse direction strength of plaques with increasing MAP content in all three blends clearly indicates that MAP enhances the adhesion.

Table 3-1 Tensile properties of PP/VA 70/30 plaques as effected by MAP content.

% MAP	Strength (MPa)	Modulus (GPa)	Elongation at Yield (%)
Machine Direction			
0	28.3 (0.9)	2.96 (0.27)	1.51 (0.36)
5	31.6 (1.3)	3.07 (0.17)	1.57 (0.25)
10	31.9 (1.7)	2.90 (0.34)	1.70 (0.33)
20	35.8 (1.2)	2.78 (0.20)	1.74 (0.20)
30	38.3 (0.9)	3.02 (0.17)	1.69 (0.09
Transverse Direction			
0	12.0 (0.9)	1.41 (0.09)	2.57 (0.35)
5	12.8 (1.0)	1.26 (0.12)	2.54 (0.53)
10	13.9 (0.8)	1.43 (0.07)	2.63
20	15.6 (0.8)	1.18 (0.09)	2.90 (0.42)
30	16.7 (1.0)	1.57 (0.32)	2.37 (0.26)

Table 3-2 Tensile properties of PP/VB 70/30 plaques as effected by MAP content.

% MAP	Strength (MPa)	Modulus (GPa)	Elongation at Yield (%)
Machine Direction			
0	23.1 (2.5)	3.69 (0.50)	1.04 (0.29)
5	25.3 (2.0)	3.99 (0.55)	0.96 (0.16)
10	28.3 (1.9)	4.15 (0.16)	1.04 (0.18)
20	36.7 (2.7)	4.20 (0.12)	1.14 (0.14)
30	40.3 (2.4)	4.94 (0.24)	0.97 (0.07)
Transverse Direction			
0	11.8 (0.6)	1.54 (0.19)	1.54 (0.38)
5	12.3 (1.1)	1.60 (0.25)	1.95 (0.24)
10	14.6 (1.3)	1.58 (0.24)	2.01 (0.42)
20	16.9 (1.2)	1.61 (0.20)	1.50 (0.68)
30	17.8 (1.5)	1.71 (0.18)	1.44 (0.14)

Table 3-3 Tensile properties of PP/LC3000 70/30 as effected by MAP content.

% MAP	Strength (MPa)	Modulus (GPa)	Elongation at Yield (%)
Machine Direction			
0	14.4 (0.5)	1.81 (0.24)	1.15 (0.14)
5	18.6 (0.8)	2.07 (0.17)	1.27 (0.23)
10	23.5 (0.5)	2.30 (0.23)	1.64 (0.16)
20	20.2 (1.8)	2.33 (0.12)	1.53 (0.63)
30	26.2 (1.1)	2.18 (0.18)	1.94 (0.16)
Transverse Direction			
0	7.6 (1.0)	1.28 (0.13)	0.73 (0.13)
5	10.0 (0.2)	1.25 (0.07)	0.97 (0.05)
10	13.3 (0.9)	1.34 (0.07)	1.23 (0.16)
20	11.8 (0.4)	1.18 (0.16)	1.23 (0.10)
30	16.1 (0.9)	1.29 (0.06)	1.71 (0.18)

3.4.2. Morphology

It is anticipated that examination of the morphology of these blends will uncover relationships between the mechanical properties and the structure. In the processing / morphology studies mentioned in the introduction, two limiting morphologies were observed: droplets and fibrils. At a fixed LCP concentration and with an increasing MAP concentration, it is of interest to determine if MAP changes the dispersed phase size or shape. Accordingly, the morphology will be investigated by examination of fracture surfaces from sprue, tensile bar, and plaque samples.

The fracture surfaces of the sprue for VA blends are shown in Fig. 3-5a through 3-5d for 5, 10, 20, and 50 wt% MAP, respectively. These views were centered near the core of the sprue where temperatures declined more slowly upon cooling and where more time for breakup of fibers into droplets existed before solidification occured. In Fig. 3-5a, the fracture surface of the VA blend with 5 wt% MAP is shown; a network like system and small micron size droplets exists simultaneously. It appears that some breakup via capillary instability may have been occuring when the material froze. At 10 wt% MAP, the network has nearly vanished being replaced by long fibrils of approximately ten microns. At 20 and 50 wt% MAP, the size reduction and dispersion of the LCP phase appears complete with the formation of a droplet morphology. It must be pointed out that since the sprue was not quickly quenched, it is not possible to state if this latter morphology is the direct result of a finer dispersion created before cessation of flow or if it is the result of a reduction in the phase size to the point where interfacial instabilities cause the breakup of the LCP during the cooling in the core of the sprue. In either case, however, the inclusion of MAP clearly causes a reduction in the phase size. Similar morphological changes are also observed for VB blends over this same composition range. For

LC3000 blends, while size reduction and increased dispersion occur with increasing concentration of MAP, as shown in Fig. 3-6, numerous large sections of LC3000 exist at 10 and 20 wt% MAP. These large sections are finally dispersed at 50 wt% MAP. It has been found that a change in the viscosity ratio leads to a finer dispersion of LC3000 in PP [31].

Examination of the fracture surfaces in tensile bars illustrates the effect of MAP on the morphology in the neck region of the bar where an extensional flow may exist. Figs. 3-7a through 3-7c shows the fracture surfaces for VA blends with 0, 20, and 50 wt% MAP, respectively. At 0 wt%, a course LCP structure exists with a large distribution of sizes including ribbons and fibers. At 20 wt% MAP, the LCP phase becomes more uniform with a fibrous appearance. The blend morphology becomes much finer and exhibits much smaller sizes at 50 wt% MAP. This was the concentration where the modulus decreased. It might be speculated that the aspect ratio of the LCP phase decreased with increasing MAP concentration. However, this information is not attainable from this SEM, and the dogbone neck region was too small to permit fracture in a direction that would yield a view of the aspect ratio. Additionally the same trends in morphological appearance exist with VB blends. These blends are shown in Figs. 3-8a through 3-8c for 0, 20, and 50 wt% MAP, respectively. The same changes that occurred for VA blends also occur in the VB blends. At 0 wt% MAP, a course ribbon like morphology exists. A fibrous morphology occurs at 20 wt% MAP, and a fine dispersion with small LCP size occurs at 50 wt% MAP. Note that at 50 wt% MAP, the modulus of the VB blend does not decrease, and the morphology looks similar to the morphology of the VA blend which exhibited the decreased modulus. As mentioned before, it is not possible to determine the aspect ratio of these structures from SEM photomicrographs. It is probable that the aspect ratio of structures within the VA blend is reduced because of the additional MAP while the aspect ratio of structures within

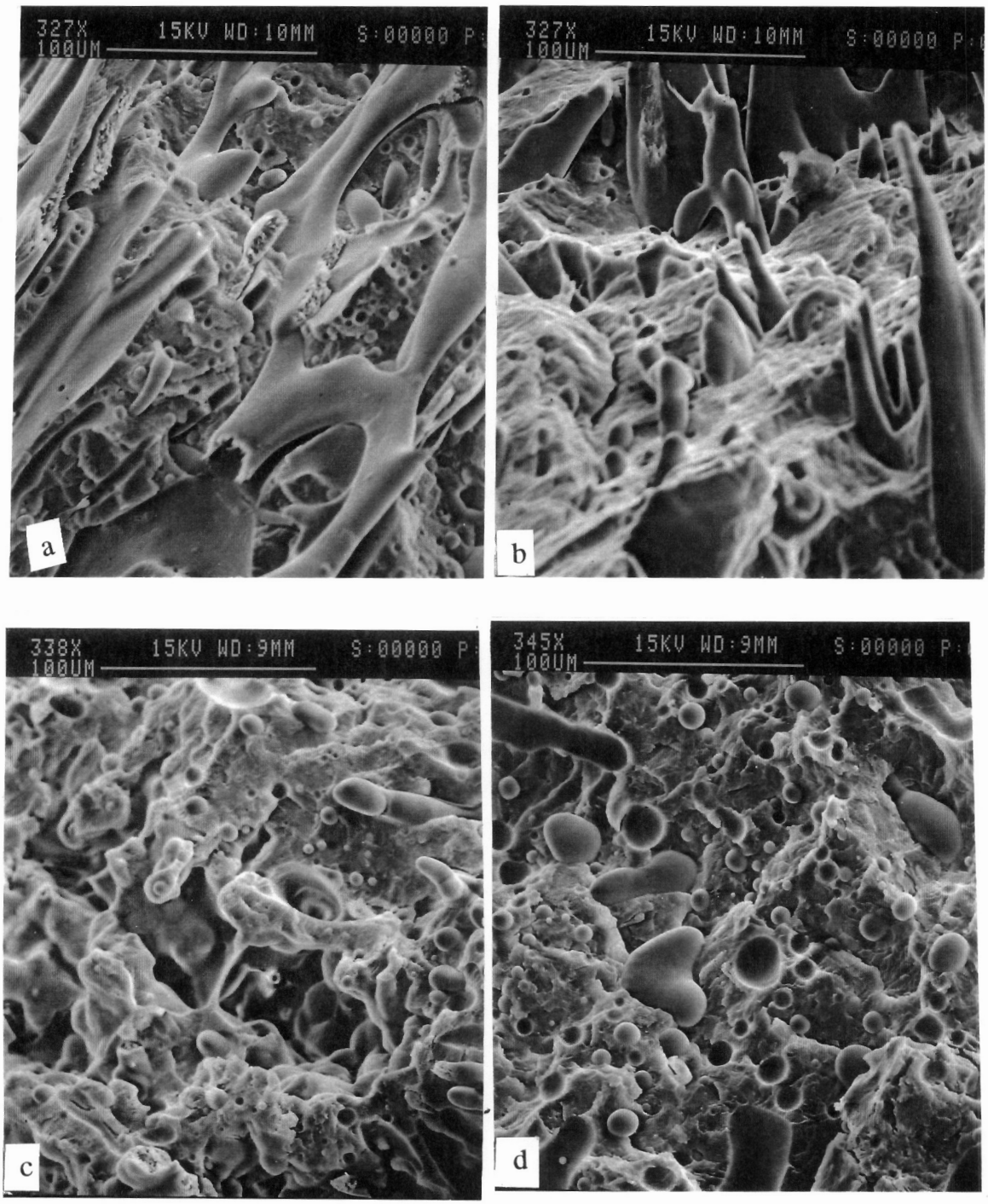

Fig. 3-5 SEM micrographs of the core of a PP(MAP)/VA 70/30 sprue: (a) 5 wt% MAP; (b) 10 wt% MAP; (c) 20 wt% MAP; (c) 50 wt% MAP.

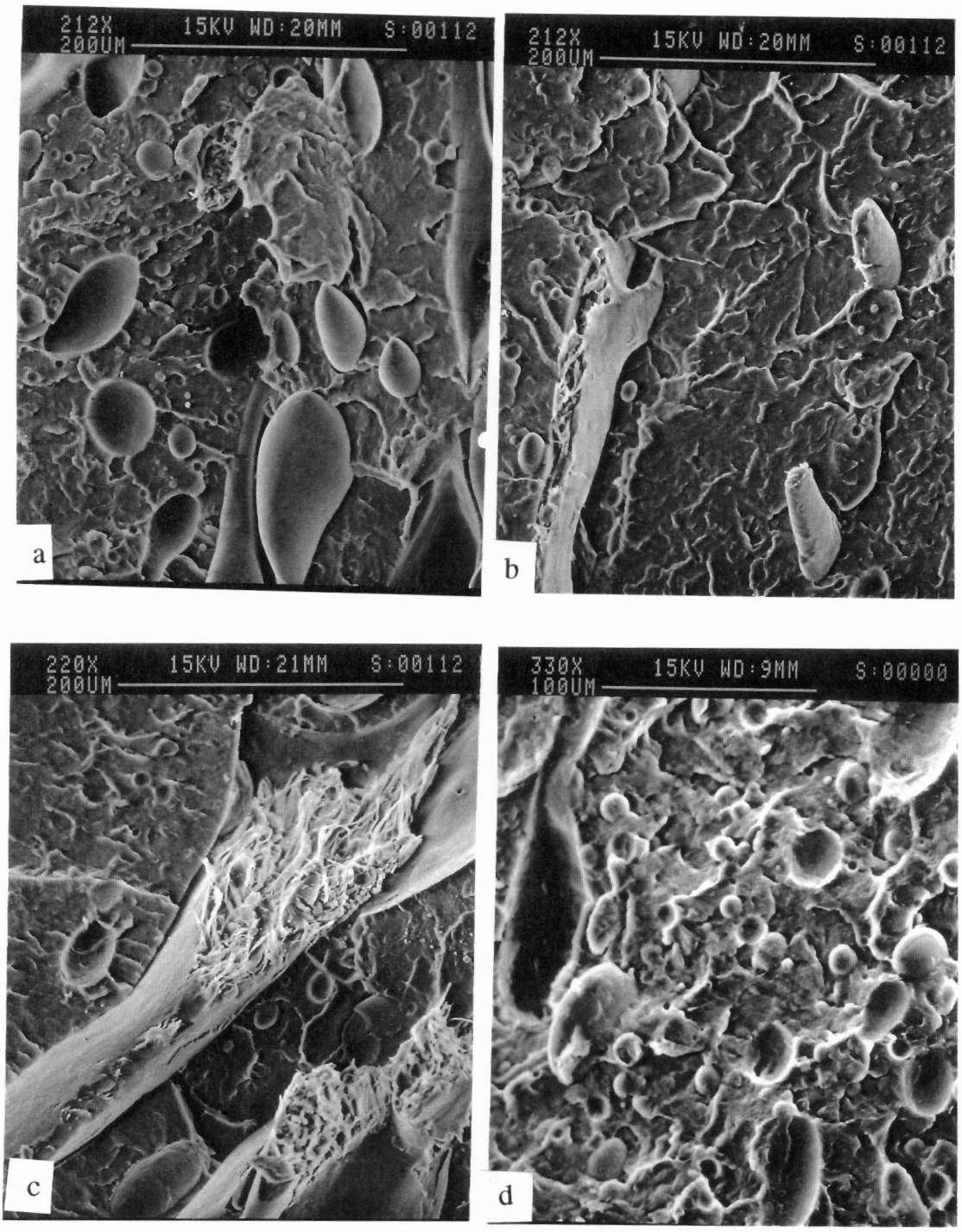

Fig. 3-6 SEM micrographs of the core of a PP(MAP)/LC3000 70/30 sprue: (a) 5 wt% MAP; (b) 10 wt% MAP; (c) 20 wt% MAP; (c) 50 wt% MAP.

the VB blend has not yet been sufficiently reduced to affect the modulus. Increasing the concentration of MAP beyond 50 wt% would be one means to determine if a drop in the modulus of VB blends also occurs. It would be expected based on the photomicrograph that a decrease in modulus is imminent.

In Figs. 3-10a through 3-10c, the fracture surfaces for the LC3000 blends with 0, 20, and 50 wt% MAP, respectively, are shown. Because of the large diversity in phase sizes, a much lower magnification is used in these photomicrographs, 40 versus 180. Again, it is suspected that the viscosity ratio, approximately 0.008, is too low to permit a fine dispersion of LC3000 in the PP(MAP) matrix. At 0 wt% MAP little organization is observed in the LC3000 phase. It appears that more LCP is near the skin versus the core. At 20 wt% MAP, a pattern emerges as apparently more LCP is dispersed within the core of the tensile bar. Finally at 50 wt% MAP, a fine dispersion exists with LC3000 evenly distributed throughout the sample. This concentration leads to the highest strength and elongation for the LC3000 blend. It is possible that since more specific surface area exists for the dispersed blend that a higher amount of interaction on a volume basis exists thus strengthening the blend.

The next figure illustrates the morphology of these blends within plaques. The fracture surfaces are along the machine direction and all samples have been etched to reveal more of the LCP structure. The morphology of VA blends with 0 and 30 wt% MAP are shown in Figs. 3-10a and 3-10b, respectively. These photomicrographs are typical for all the blends studied. At 0 wt% MAP, a course structure is observed with small ribbon-like morphology in the core which gradually thickens as the skin is approached. A much finer structure is observed at 30 wt% MAP with fine fibers in the middle half of the plaque which gradually make a transition to thicker fibers and ribbons until only ribbons or films are observed near the skin. The reason for the

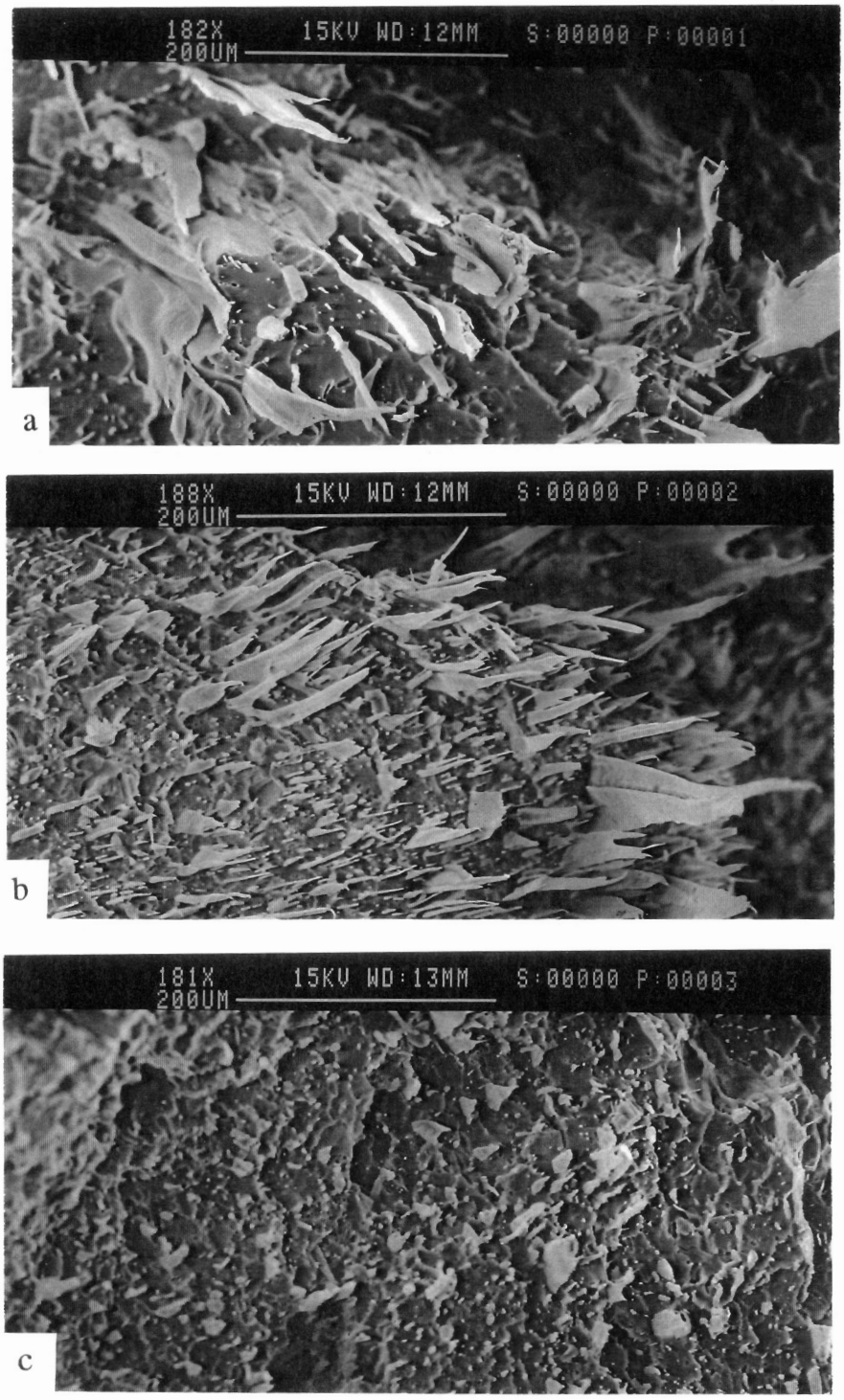

Fig. 3-7 SEM micrographs of a PP(MAP)/VA 70/30 tensile bar: (a) 0 wt% MAP; (b) 20 wt% MAP; (c) 50 wt% MAP.

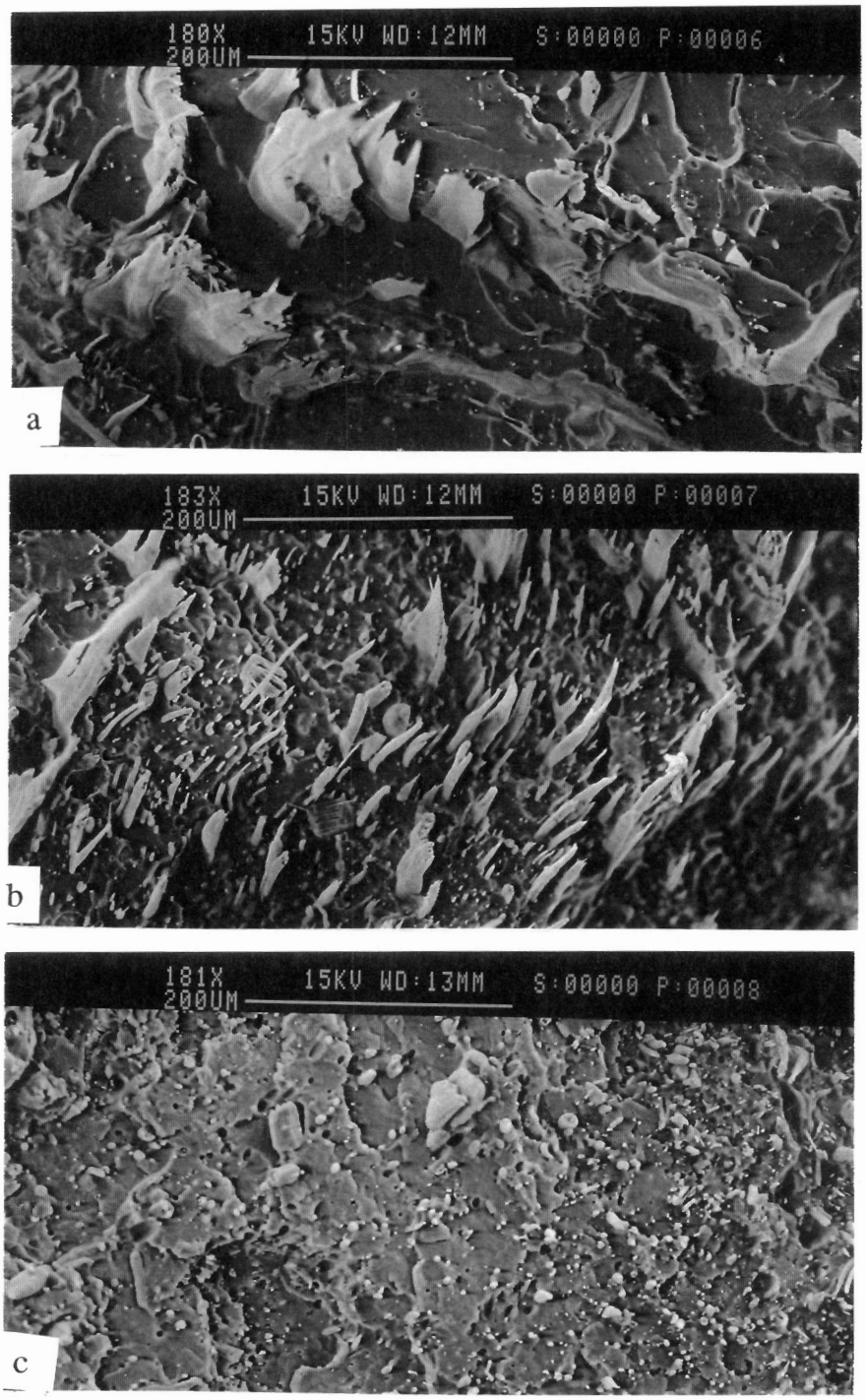

Fig. 3-8 SEM micrographs of a PP(MAP)/VB 70/30 tensile bar: (a) 0 wt% MAP; (b) 20 wt% MAP; (c) 50 wt% MAP.

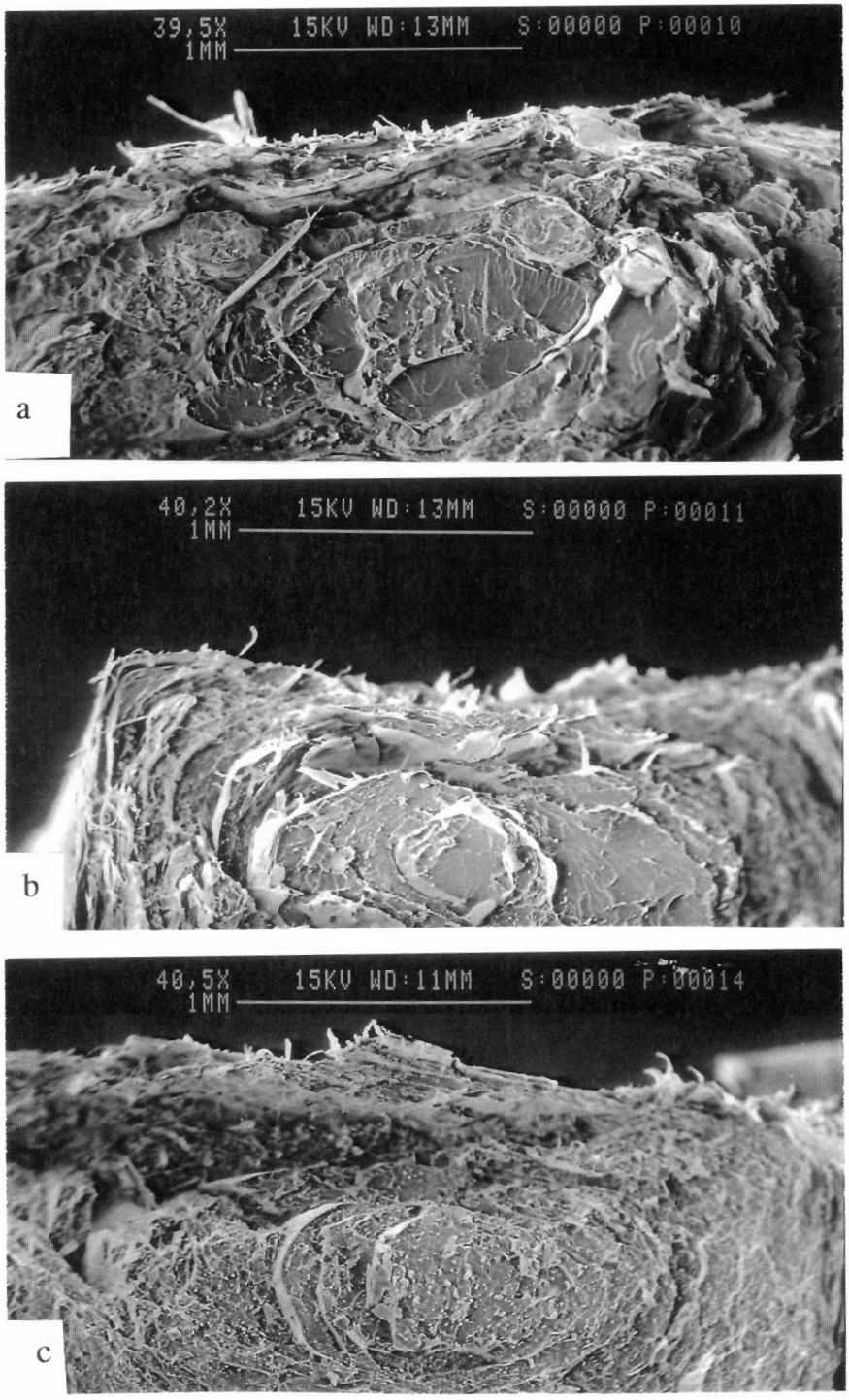

Fig. 3-9 SEM micrographs of a PP(MAP)/LC3000 70/30 tensile bar: (a) 0 wt% MAP; (b) 20 wt% MAP; (c) 50 wt% MAP.

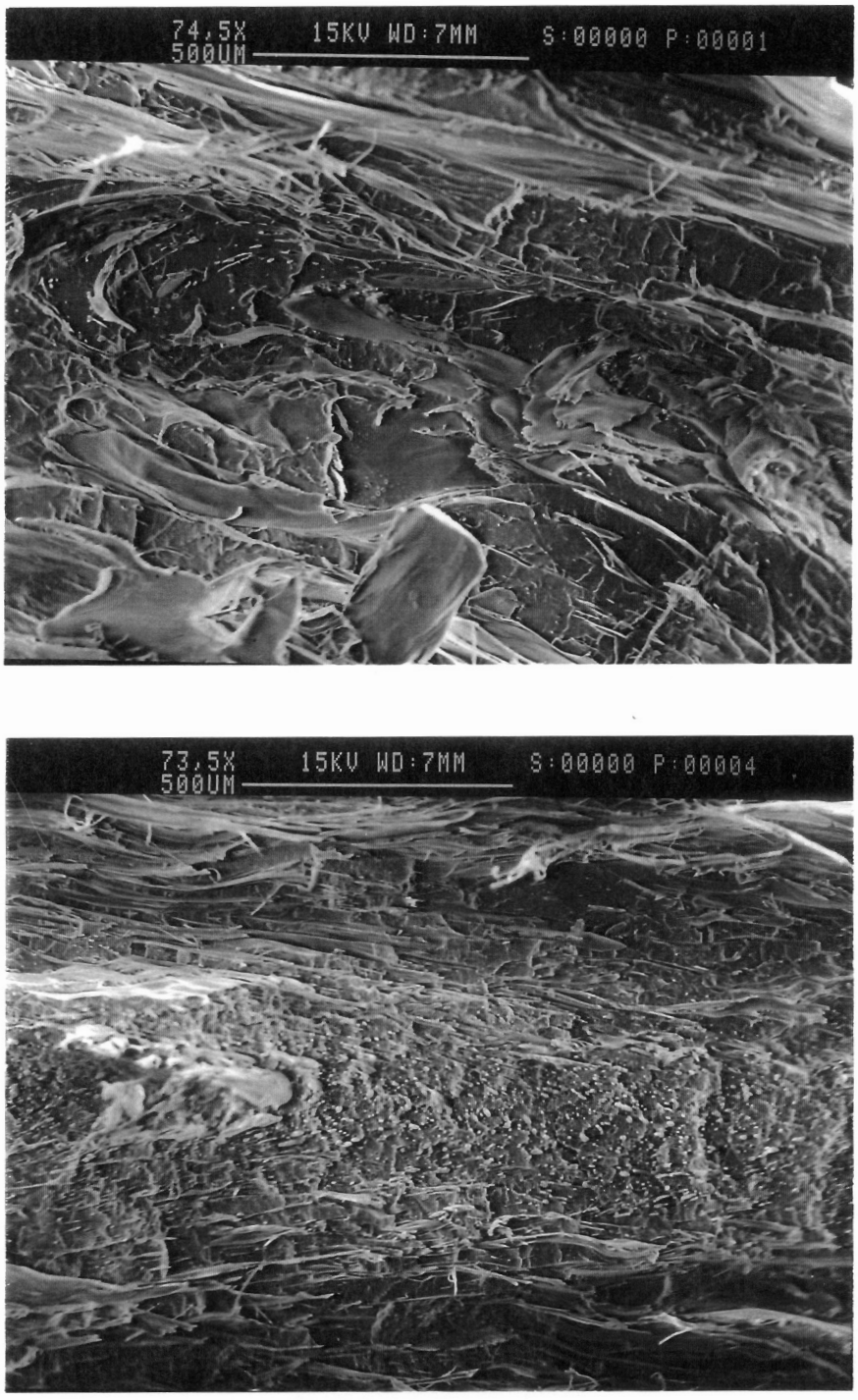

Fig. 3-10 SEM micrographs of a PP(MAP)/VA 70/30 plaque: (a) 0 wt% MAP; (b) 30 wt% MAP.

progressive variation in the morphology is related to whether material experienced the fountain flow at the advancing front or whether the material experienced primarily shear flow. The presence of MAP in this plaque obviously acts to finely disperse the LCP within the matrix. The VB and LC3000 morphologies are very similar to that of the VA blends and will not be shown here. It is obvious from these figures that MAP does act to disperse and reduce the size of the LCP phase. It also appears that eventually the aspect ratio can be decreased leading to a reduction in properties.

3.4.3 Interfacial Properties

Two of the three common characteristics of a compatibilizer are reduced interfacial tension and improved adhesion. These changes can be either measured or derived by various techniques. Often the interfacial tension for polymer melts which are assumed to behave as isotropic Newtonian fluids can be measured by permitting an equilibrium between the two liquids to occur over the course of hours [7,8]. However, when working with two polymers that have marginally overlapping temperatures, equilibrium would not be reached before degradation becomes rampant. This is the situation for blends of PP with either VA or VB. Accordingly, an alternative technique which can be extrapolated to the melt is more suitable. Such a technique which is widely used was proposed by Wu [44]. It consists of measuring the contact angle of two or more liquids on the surface of solid polymers. The liquids must have known polar and dispersive components of the surface tension. Then two equations relating surface tension and interfacial tension may be used to determine the surface tension of the solid and from this the interfacial tension between polymers [25]. The first equation relates the contact angle of a liquid on a solid substrate to the surface and interfacial tension by a force balance. This relationship

is known as Young's equation [42] and is written as

$$\gamma_{12}=\gamma_2-\gamma_1\cos\theta \tag{3-1}$$

where γ_{12} refers to the interfacial tension, γ_1 and γ_2 refers to surface tension for the liquid and solid, respectively. This equation is used in conjunction with the Harmonic mean equation [9,44] which relates the interfacial tension to the polar and dispersive components of the liquid and solid. This equation may be written as

$$\gamma_{12}=\gamma_1+\gamma_2-4\frac{\gamma_1^d\gamma_2^d}{\gamma_1^d+\gamma_2^d}-4\frac{\gamma_1^p\gamma_2^p}{\gamma_1^p+\gamma_2^p} \tag{3-2}$$

where superscripts d and p designate the dispersive and polar components of the surface tension and their sum equals the surface tension, i.e. $\gamma = \gamma^d + \gamma^p$. A minimum of two liquids is required to find the polar and dispersive components of the solid surface tension. If more than two liquids are used then a statistical fitting of the data is necessary. In this work, three liquids were used and the above equations were solved using a nonlinear least squares fit. From these results, the interfacial tension at room temperature can be calculated from the above and this may be extrapolated to the melt temperature using the average gradient of interfacial tension with temperature as discussed by Wu [44]. Once having obtained the interfacial tension at room temperature, the work of adhesion may be calculated from a standard equation [42]

$$W_a=\gamma_{s1}+\gamma_{s2}-\gamma_{12} \tag{3-3}$$

where 's' in the subscripts is a reminder that these are solid polymer surface tensions.

When using these techniques, it should be noted that there are some theoretical compromises or concerns. The first concern is that surface orientation of the plaques used for contact angles measurement introduces some errors because the surface energy of a oriented and

unoriented surfaces differ for LCPs [36]. The second concern is that reactions may occur between the two polymers especially with the use of a compatibilizer. If reactions at the interface occur the contact angle method would lead to over estimation of the interfacial tension.

With these potential shortcomings mentioned, the contact angle for PP, PP(MAP) with 10% MAP, and the three LCPs are listed in Table 3-4. In addition, the calculated surface tension of these polymers and the percent dispersive surface tension are listed in the last two columns. It is clear from the range of contact angles and knowledge that these three liquids have a range of dispersive components between 30 and 60% of their surface tension that a range of data is generated thus allowing the data to be statistically fitted.

The calculated surface tension for PP is 25.6 mJ/m^2. This compares favorably with the reported value for PP of 29.4 mJ/m^2 [46]. However, the dispersive component for PP should nearly equal the surface tension since this is an apolar polymer, and hence there is some discrepancy. The measurement of the dispersive component, 82% in this work, may be low as the result of additives within the matrix. The introduction of 10 wt% MAP to PP increases the surface tension of the matrix by 1.4 mJ/m^2 and decreases the dispersive component. These trends would be expected for addition of a polar component into an apolar polymer. For the LCPs, the surface tension ranges between 34.9 and 40.4 mJ/m^2. Since LC3000 is composed of 40% PET and it is an ester, comparison to the surface tension of PET [44] indicates that the value of 40.4 mJ/m^2 for LC3000 is comparable to that of 42.1 mJ/m^2 for PET. From the surface tension data, the interfacial tension at room temperature may be calculated from the harmonic mean equation. Values of the calculated interfacial tension for PP and PP/MAP matrices are shown in Table 3-5. It is clear that the addition of 10 wt% MAP significantly lowers the interfacial tension.

In the prior section, it was shown that MAP reduces the phase size. Reduced interfacial

Table 3-4 Contact angle data for neat polymers measured with water, formamide, and ethylene gylcol and the resulting surface tension.

Material	θ_{water}	θ_{form}	$\theta_{eth\ gyl}$	γ (mJ/m^2)	γ^d/γ x10^2
PP	99.2 (4.6)	84.0 (2.6)	71.6	25.6	82.0
PP/BP 90/10	90.2 (3.9)	76.7 (3.3)	65.5	27.0	63.5
VA	78.0 (2.8)	56.4 (2.5)	52.7	34.9	54.6
VB	76.81 (3.2)	52.5 (1.4)	47.6	37.5	61.6
LC3000	67.1 (2.2)	49.3 (1.8)	46.2	40.4	46.3

tension and reduced phase size are in accord since the size of a drop and it's interfacial tension can be related through the critical Weber number [10]. This dimensionless number relates the hydrodynamic stress, $\eta\dot{\gamma}$, tending to deform and break a droplet to the interfacial stress, γ_{12}/R. This ratio is typically written as $R\eta\dot{\gamma}/\gamma_{12}$ where R is the drop size, η is the viscosity, $\dot{\gamma}$ is the shear rate, and γ_{12} is the interfacial tension. For a given shear rate and viscosity a lowering of the interfacial tension would necessarily cause a reduction in the drop size to maintain a constant critical Weber number. Thus, the reduced phase size and reduced interfacial tension agree with the trends predicted from fluid mechanical theories thereby providing additional support for the claim that MAP reduces interfacial tension.

The next point that can be established is the work of adhesion between the phases. This information was also calculated from the contact angle data. The results are shown in Table 3-5. For all the blends, the addition of 10 wt% MAP increases the work of adhesion. Three different indirect methods have now indicated that adhesion between the phases is improved. These three methods are the work of adhesion, reduced fiber pullout as shown in prior studies [29,30], and improved tensile properties. This establishes, albeit indirectly, that TP/LCP blends enhanced adhesion.

Thus, compatibilization of TP/LCP blends may be characterized similarly with that of compatibilized TP blends which show decreased interfacial tension, improved dispersion, and enhance adhesion. However, two distinct differences do exist. The first is that the morphology for TP/LCP blends must exhibit LCP structures with high aspect ratios to obtain reinforcement of the TP matrix. Second, instead of improving the impact strength and toughness, a compatibilizer for TP/LCP blends acts to improve the tensile properties of the blend. Thus, compatibilization of TP/LCP blends is similar to that of compatibilization of TP blends, but

Table 3-5 Interfacial tensions and work of adhesion for PP/LCP and PP(MAP)/LCP blends.

	Interfacial Tension (mJ/m^2)		Work of Adhesion (mJ/m^2)	
	PP	PP/MAP	PP	PP/MAP
VA	6.3	1.5	54.2	60.4
VB	5.1	1.7	58.0	62.8
LC3	11.2	4.5	54.8	62.9

because high aspect ratio LCP structures are required for reinforcement, the morphology of in situ composites is drastically different from the droplet morphology of TP blends. This requirement apparently limits the amount of compatibilizer that can be used.

3.4.4 Interfacial Reaction

The occurrence of a reaction or an interaction such as hydrogen bonding at the interface are two possible mechanisms to explain why MAP acts to enhance the mechanical properties of these blends. To distinquish between these two possibilities, comparison of the relative change in the maleic anhydride content in test and control samples was pursued. As discussed in the experimental section, a matrix consisting of PP(MAP) with 70 wt% MAP was prepared for the test and control samples. This mateial is referred to as the precursor. The control is prepared by reextruding the precursor at the temperatures and residence time at which a test sample is prepared. The test sample is an extruded blend prepared from the precursor by adding 30 wt% LCP. Thus, the control separates the effect of time and temperature on maleic anhydride from the effect of reaction of maleic anhydride with the LCP that may occur in the test sample.

The relative amount of maleic anhydride in these samples was determined from FTIR spectra. It is well known that maleic anhydride displays a strong carbonyl absorption peak at 1784 cm^{-1}. Additionally, it is known that maleic anhydride is in equilibrium with it's acids, maleic and fumaric. A shift in equilibrium to the acid form causes a shift in the carbonyl absorption from 1784 to 1714 cm^{-1}. Hence, drying the sample for three days is an important method to form a large ratio of anhydride to acid functionalities. Analysis of the change in the anhydride content from the precursor to the control samples was performed via two methods. The first method was to calculate the ratio of the area under the 1784 cm^{-1} absorption peak to the

area under the 1220 cm^{-1} absorption peak which was reported as a CH wag for PP [39]. This provides a relative concentration of maleic anhydride to PP in each of the samples. A ratio of this relative concentration for the control sample to the precursor sample thereby provides a percentage of maleic anhydride remaining in the control sample. The second method was to measure the peak height at 1784 cm^{-1} and the film thickness to obtain, via the Beer Lambert law, the product of the extinction coefficient and the concentration. A ratio between the test and control samples could then be calculated to obtain the percentage of maleic anhydride concentration remaining in the test sample. This latter method was employed because the presence of LCP particles in some test samples distorts the internal peaks needed for the former method. Comparison of these methods shows some discrepancy exists with higher values obtained from the internal reference method, i.e. 2 to 10% higher values.

Several reactions are possible within these blends. It is known that maleic anhydride grafted PP can react with the amine ends of nylon 6 [4]. While VB has an amine ingredient, p-amino phenol, it would be expected that the high reactivity of the amine would lead to their consumption prior to fully consuming the phenol. Thus, it is doubtful that more than trace amounts of amine would exist in the LCP, so the amine ends would not be available for reaction with the maleic anhydride. Two of the LCPs are copolyesters, and reactions such as acidolysis might occur between the maleic anhydride and the ester moieties. However, this reaction usually requires catalysts to speed the reaction [43]. Thus, at least two types of reactions are possible but for reasons outlined above they are not expected.

In Table 3-6, the relative change of maleic anhydride content for control and test samples are reported. The melt temperature and the reference sample identification are listed as well as the residual percentage of maleic anhydride as determined by two methods. Inspection of the first

Table 3-6 Ratio of maleic anhydride content in extract to maleic anhydride content in precursor or control sample.

	Melt Temp	Reference Sample	Beer Lambert Law	1220 cm^{-1} reference
PP/MAP	260	250°C Precursor	84.9	87.0
PP/MAP	295	250°C Precursor	55.9	67.7
PP(MAP)/VA	295	295°C Control	99.2	106.0
PP(MAP)/VB	295	295°C Control	98.7	n.a.
PP(MAP)/LC3000	250	260°C Control	114.0	n.a.

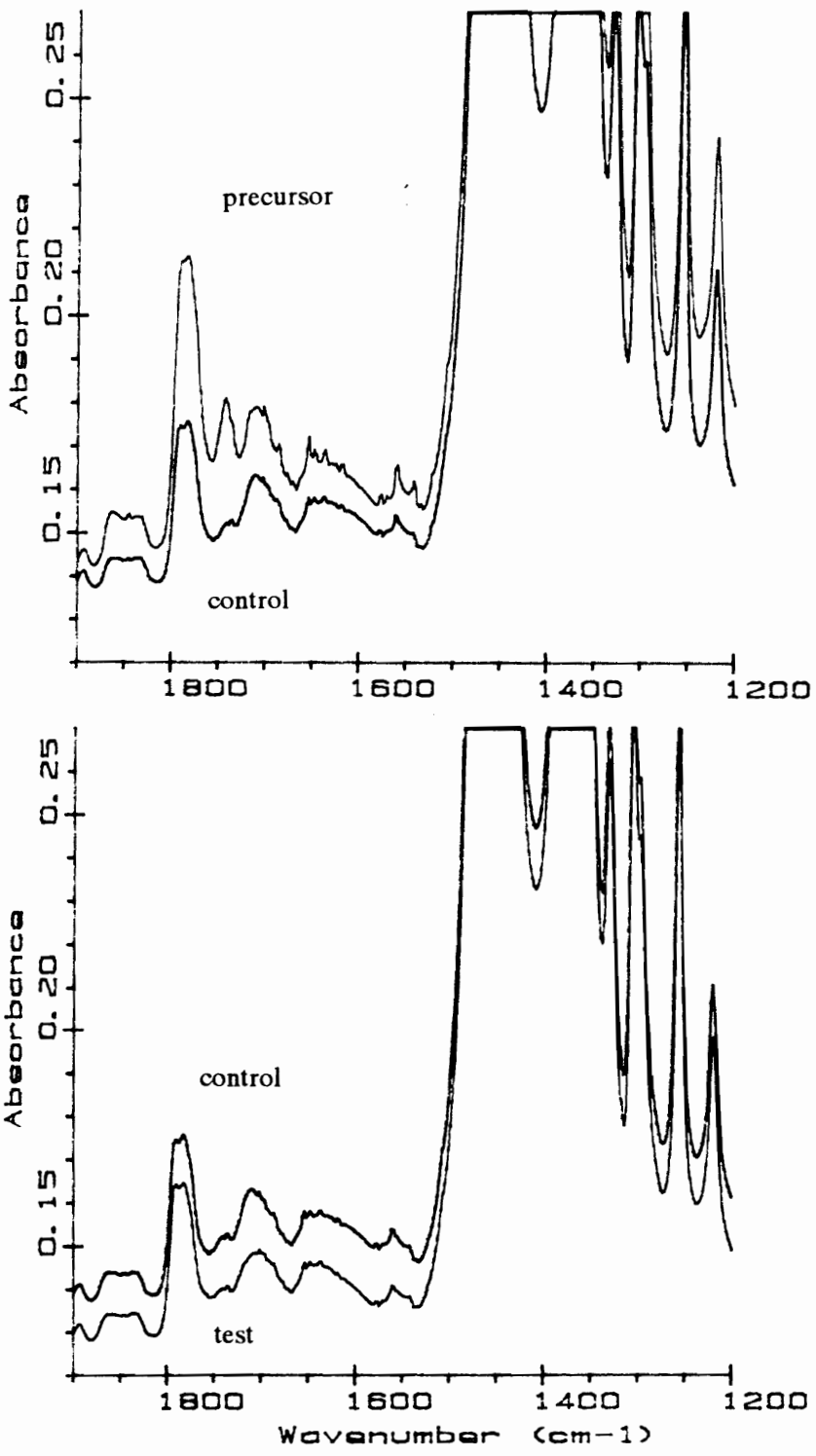

Fig. 3-11 FTIR spectra for precursor and control (extruded at 295°C) (a), and control (extruded at 295°C) and VA test samples (b).

entry in Table 3-6 shows that PP/MAP extruded a second time to produce a control sample made at 260°C shows a drop in the maleic anhydride content to 84.9 or 87.0% (the value depending upon the method). This percentage falls to 55.9 or 67.7% when the precursor is extruded a second time at 295°C. The discrepancy between these methods is in the range of 2 to 10% with the internal reference method always indicating a higher maleic anhydride content. Because of particles in the VB and LC3000 blends, only the thickness method could be used with these samples. However, few particles existed in the VA blend. Comparison of the spectra for the precursor and control samples and for the control and VA test samples is shown in Fig. 3-11. In Fig. 3-11a, the anhydride absorption at 1784 cm^{-1} is clearly reduced while in Fig. 3-11b there is no change in the absorption for the anhydride. Also shown in Fig. 3-11a is an absorption at 1745 cm^{-1}. This wavenumber is associated with PP, and PP is undergoing some change. The assignment for the wavenumber could not be found, but no change at the reference wavenumber of 1220 cm^{-1} occurred.

It is clear from Fig. 3-11 and Table 3-6 that both methods indicate that little if any maleic anhydride is consumed in blending it with VA. Instead, the change in maleic anhydride content results from degradation as indicated by comparison of the spectra of precursor and control samples. This conclusion can also be reached with the other two LCP blends. It should be mentioned that the greater than 100% residual maleic anhydride content in the LC3000 blend is believed to be the result of extruding the blend at a lower temperature than the temperature at which the control was made. The difference between extrusion temperatures of test and control samples occurred because of the poor operating performance of the control at the higher temperature. Thus, this work answers the question of whether maleic anhydride reacts with the LCP. However, since maleic anhydride degrades, it is possible that reactions between LCP and

some of the degradation products occur although this route seems doubtful.

3.5 Conclusions

The addition of MAP to the PP phase leads to significant mechanical property improvements in PP/LCP blends. The tensile strength for all three PP/LCP blends increases as the content of MAP is increased. A possible plateau in the tensile strength of VA blends occurs, and a decrease in the modulus occurs at the highest MAP concentration. This indicates that unlimited increase in the mechanical properties of these blends does not occur. However, significant increases in the strength can occur, and these increases are dependent upon the particular LCP. It does appear that the properties of the copoly(ester-amide), VB, which can undergo strong hydrogen bonding, are strongly affected by the concentration of MAP. The tensile strength of this blend increases without limit in the range of MAP investigated, and the modulus shows large increases for both tensile bar and plaque specimens.

The compatibilization of PP/LCP blends shows that these blends also demonstrate reduced interfacial tension, increased dispersion, and enhanced adhesion which are characteristic of compatibilized TP blends. However, differences exist between compatibilized TP blends and compatibilized TP/LCP blends. First, use of MAP in these PP/LCP blends leads to improved tensile properties as opposed to improved impact strength and toughness in TP blends. Second, the addition of MAP to these blends leads to a finer dispersion of LCP within the matrix but with a more fibrillar structure being formed which leads to reinforcement of the matrix. As shown by PP/VA blends, there is a point where mechanical properties diminish, and at this point the morphology appears to exhibit LCP structures with lower aspect ratios. Finally, it can be stated

that maleic anhydride does not directly react with the LCP, and based on the significant enhancements with PP/VB blends it is believed that an interaction such as hydrogen bonding is the mechanism leading to the compatibilization of LCP blends.

3.6 Acknowledgements

The authors would like to thank Joseph Humink of BP Chemicals for supplying the development grade maleic anhydride grafted polypropylene. This work was supported by the Army Research Office, (grant number DAAL03-91-G-0166), and their support is sincerely appreciated.

3.7 References

1. P.J. Barham and A. Keller, "Review: High-strength Polyethylene Fibres From Solution and Gel Spinning," J. Mater. Sci. 20, 2281 (1985).
2. S.L. Kwolek, P.W. Morgan, J.R. Schaefgen, in Encyclopedia of Polymer Science, H.F. Mark, Ed., John Wiley & Sons, New York (1987).
3. Modern Plastics Encylopedia , McGraw Hill, New York, 1991.
4. N.G. Gaylord, "Compatibilizing Agents: Structure and Function in Polyblends," J. Macromol. Sci., Chem., A26(8), 1211 (1989).
5. A.Y. Coran and R. Patel, Rubber Chem. Technol., 56, 1045 (1983).
6. R.L. Markham, "Introduction to Compatibilization of Polymer Blends", Advances in Polymer Technology, 10(3), 231 (1990).
7. S.H. Anastasiadis, I. Gancarz, and J.T. Koberstein, "Interfacial Tension of Immiscible Polymer Blends: Temperature and Molecular Weight Dependence," Macromolecules, 21, 2980 (1988).
8. H.T. Patterson, K.H. Hu, and T.H. Grindstaff, "Measurement of Interfacial and Surface Tensions in Polymer Systems," J. Polymer Sci.: Part C, 34, 31 (1971).
9. S. Wu, "Calculation of Interfacial Tension in Polymer Systems," J. Polym. Sci.: Part C, 34, 19 (1971).
10. G.I. Taylor, "The Formation of Emulsions in Definable Fields of Flow," Proc. Roy. Soc. A146, 501 (1934).
11. S. Tomotika, "On the Instability of a Cylindrical Thread of a Viscous Liquid Surrounded by Another Viscous Fluid," Proc. Roy. Soc., 150, 322 (1935).
12. A.J. East, L.F. Charbonneau, and G.W. Calundann, "Thermotropic Poly(ester-amides)

Based On Naphthalene Monmers," Mol. Cryst. Liq. Cryst., 157, 615 (1988).
13. D. Done and D.G. Baird, "The Effect of Thermal History on the Rheology and Texture of Thermotropic Liquid Crystalline Polymers," Polym. Eng. Sci., 27(11), 816 (1987).
14. D. Done and D.G. Baird, "Solidification Behavior and Recovery Kinetics of Liquid Crystalline Polymers," Polym. Eng. Sci., 30(16), 989 (1990).
15. D.N. Lewis and J.F. Fellers, "Processing of Polymer Liquid Crystals," in High Modulus Polymers, A. Zachariades and R.S. Porter, Eds., Marcel Dekker, New York, 1988: pg. 1.
16. Y. Ide and Z. Ophir, "Orientation Development in Thermotropic Liquid Crystal Polymers," Poly. Eng. Sci., 23(5), 261 (1983).
17. T-S. Chung, "Fluid Behavior and Orientation Developments During Extrusion of Liquid Crystal Polymeric Rods," J. Polym. Sci.: C Polym. Lett., 24, 299 (1986).
18. T-S. Chung, "Production of Ultrahigh Modulus Liquid Crystal Polymer Rods," J. Polym. Sci. Part B: Polym. Phys., 26, 1549 (1988).
19. S. Kenig, "Orientability of Liquid Crystal Polymers in Elongational Flow," Poly. Eng. Sci., 27(12), 887 (1987).
20. S. Kenig, "Shear-Induced Orientation in Liquid Crystalline Polymers," Poly. Eng. Sci., 29(16), 1136 (1989).
21. P. Zhuang, T. Kyu, and J.L. White, "Characteristics of Hydroxybenzoic Acid - Ethylene Terephthalate Copolymers and Their Blends With Polystyrene, Polycarbonate, and Polyethylene Terephthalate," Poly. Eng. Sci., 28(17), 1095 (1988).
22. A. Kohli, N. Chung, and R. A. Weiss, "The Effect of Deformation History on the Morphology and Properties of Blends of Polycarbonate and a Thermotropic Liquid Crystalline Polymer," Polym. Eng. Sci., 29(9), 573 (1989).
23. A. Siegmann, A. Dagan, and S. Kenig, "Polyblends Containing a Liquid Crystalline Polymer," Polymer, 26, 1325 (1985).
24. M.R. Nobile, E. Amendola, and L. Nicolais, "Physical Properties of Blends of Polycarbonate and a Liquid Crystalline Copolyester," Polym. Eng. Sci., 29(4), 244 (1989).
25. K.G. Blizard and D.G. Baird, "The Morphology and Rheology of Polymer Blends Containing a Liquid Crystalline Copolyester," Poly. Eng. Sci., 27(9), 653 (1987).
26. K.G. Blizard, C. Federici, O. Federico, and L.L. Chapoy, "The Morphology of Extruded Blends Containing a Thermotropic Liquid Crystalline Polymer", Poly. Eng. Sci., 30(22), 1442 (1990).
27. H.J. O'Donnell, A. Datta, D.G. Baird, "The Effect of Compatibilization on the Properties of Blends of TLCPs with Polypropylene," Annual Technical Conference of the Society of Plastic Engineers (ANTEC'92), 50, 2248 (1992).
28. H.J. O'Donnell, H.H. Chen and D.G. Baird, " ," Annual Technical Conference of the Society of Plastic Engineers (ANTEC '93) 51, 1711 (1993).
29. A. Datta, "The Effect of Compatibilization on Blends of Polypropylene with a Liquid Crystalline Polymer ," Polymer 34(4), 759 (1993).
30. A. Datta "Compatibilization of Thermoplastic Composites Based on Blends of Polypropylene with Two Liquid Crystalline Copolyesters," submitted to Polymer.
31. H.J. O'Donnell and D.G. Baird, submitted to The International Journal of Polymer Processing.

32. M.T. Heino and J.V. Seppala, "Studies on Compatibilization of Blends of Polypropylene and a Thermotropic Liquid Crystalline Polymer," J. Appl. Polym. Sci., 47, 1677 (1993).
33. C. Carfagna, E. Amendola, L. Nicolais, D. Acierno, O. Francescangeli, B. Yang, "Blends of a Polyetherimide and a Liquid Crystalline Polymer: Fiber Orientation and Mechanical Properties," J. Appl. Polym. Sci., 43, 839 (1991).
34. F.P. La Mantia, M. Saiu, A. Valenza, M. Paci, and P.L. Magagnini, "Relationships Between Mechanical Properties and Structure for Blends of Nylon-6 with a Liquid Crystal Polymer," Eur. Polym. J., 26(3), 323 (1990).
35. S. Meretz, M. Kwiatkowski, G. Hinrichsen, "Production and Characterization of Finely-Dispersed Mixtures of Liquid Crystalline with Conventional Polymers," Intern. Polym. Proc., VI, 239 (1991).
36. A.M. Seeboth, "Relation Between Polymer Surface Tension and Orientation of Thermotropic Liquid Crystals," Die Angewandte Makromol. Chemie, 196, 101 (1992).
37. R.H. Olley, D.C. Basset, and D.J. Bludell, Polymer, 27, 344 (1986).
38. D.H. Kaelble, P.J. Dynes, and E.H. Cirlin, "Interfacial Bonding and Environmental Stability of Polymer Matrix Composites," J. Adhesion, 6, 23 (1974).
39. S. Krim, "Infrared Spectra of High Polymers," Adv. Polym. Sci., 2, 51 (1960).
40. R.M. Jones, Mechanics of Composite Materials, Hemisphere Publishing, New York, 1975.
41. L.E. Nielsen, Mechanical Properties of Polymers and Composites, Vol 2., Marcel Dekker, New York, 1974.
42. A.W. Adamson, Physical Chemistry of Surfaces, 4th Ed., John Wiley & Sons, New York, 1982.
43. A.M. Kotliar, "Interchange Reactions Involving Condensation Polymers," J. Polym. Sci.: Macromol. Rev. 16, 367 (1981).
44. S. Wu, Polymer Interface and Adhesion, Marcel Dekker, New York (19__).
45. Z. Tadmor, "Molecular Orientation in Injection Molding," J. Appl. Polym. Sci., 18, 1753 (1974).
46. S. Wu, in Polymer Handbook, J.Brandrup and E.H. Immergut, Ed., Wiley Interscience, New York, 1989.

4.0 The Effect of Injection Molding Conditions on the Mechanical Properties of an In Situ Composite: I. Polypropylene and a LCP Based on HBA/HNA [1]

4.1 Introduction

Improving the mechanical properties of polymers has been a continual goal in the research and development of polymers. Several approaches have been employed to accomplish this goal. These approaches include the development of new polymers, the blending of polymers to achieve additive or synergistic results, and the reinforcement of polymers with fillers or fibers. Of the three approaches, development of new polymers is a costly route to improved properties. The latter two approaches, polymer blends and reinforcement of polymers, are generally the preferred methods. One method that combines these two approaches is the blending of a thermoplastic (TP) matrix and a liquid crystalline polymer (LCP). These blends can offer higher mechanical properties than other blends because the mechanical properties of neat LCPs are significantly greater than those of TP matrices. The use of TP/LCP blends also avoids the processing disadvantages such as high pressures and equipment erosion that occur when processing fiber-reinforced polymers. The resulting mechanical properties of TP/LCP blends are not the product of simply mixing the polymers but the product of a processing method that forms a reinforcing fiber-like LCP structure within the blend. Consequently, these blends are often termed in situ composites.

There have been a limited number of studies concerned with how polymer processing

---

[1] This paper is being submitted to Polymer Engineering Science.

variables such as deformation, stress, and temperature affect the mechanical properties of TP/LCP blends. The majority of processing studies have been confined to the capillary extrusion process [20-27] while in a few studies the sheet extrusion process was investigated [27,28]. The resulting processing / property relationships vary on a case by case basis. Review of the important process variables in the capillary extrusion of TP/LCP blends can provide some insight into the variables that may be of importance in injection molding TP/LCP blends.

Studies of the capillary extrusion process have concentrated on investigating the effect of draw ratio on the mechanical properties of extrudates [20-24]. The draw ratio has been found to improve the strand modulus in several studies. Nobile et al. [20] in studying a blend of 90 wt% polycarbonate (PC) and 10 wt% poly(ethylene terephthalate) / p-hydroxybenzoic acid (PET/PHB) found that the modulus of PC and the blend increased with draw ratio until the modulus reached a plateau beyond a draw ratio of 100. At a processing temperature of 220°C, the modulus of the drawn blend exceeded that of the PC matrix (4.1 versus 3.1 GPa, respectively). Dutta et al. [21] investigated the effect of draw ratio on the blend of 80 wt% PC and 20 wt% of a liquid crystalline (LC) copolyester. They found a seven fold increase in the modulus of the blend at a draw ratio of over 900. La Mantia et al. [23] also found that the draw ratio was effective in increasing the modulus. In studying a blend of nylon 6 and Vectra B950, they found that strands of nylon 6 displayed a 40% increase in modulus as the draw ratio was increased from 1 to 100. Addition of 10 wt% LCP raised the modulus of the drawn strands an additional 69%.

In studies where the draw ratio did not significantly increase the modulus, it was found that flow deformation into or within the die was responsible for generating high mechanical properties. Crevecoeur [27] studied the extrusion of a poly(phenylene ether) / polystyrene (PS)

matrix blended with Vectra B950 and found that drawing had only a minor influence on the modulus. The modulus obtained from undrawn strands extruded from a die with a L/D ratio of 2 was nearly equal to the value calculated from the law of mixtures. Drawn strands showed only a slight increase in the modulus. Thus, the flow into the die created nearly all the reinforcement by the LCP that could be expected based on the rule of mixtures. Basett and Yee [22] found that the shear rate within the die was a dominate processing variable in obtaining high mechanical properties. Extruding PS and a blend of 60 wt% PS and 40 wt% Vectra B900 through a die with a L/D ratio equal to 33 they found several results. First, drawing of PS or PS / Vectra B900 was not effective in increasing the modulus of the fibers. Second, increasing the shear rate within the die from less than 500 s^{-1} to greater than 1400 s^{-1} increased the modulus of the blend. Unfortuately, no comparison was made to the rule of mixtures to aid in judging how effective the shear rate was in obtaining reinforcement by the LCP.

The similarity of processing temperatures for TP resins and LCPs has also been shown by Blizard et al. [24] to be an important variable in obtaining high mechanical properties. They studied the capillary extrusion of two LCPs which differed in the melting and crystallization temperatures by 60°C. Drawing of the LCP which exhibited the higher crystallization temperature did not result in large increases in modulus. Examination of the morphology indicated that the LCP was not deformed into long fibrils during extrusion. Thus, they concluded that freezing of the LCP occurred prior to significant deformation during drawing.

Some TP/LCP blends which have significantly different melting points can be blended and the strands drawn by use of a novel mixing process [48]. This mixing process plasticates each polymer at its respective processing temperature followed by mixing of the two streams in a series of static mixers. Examination of the strand morphology showed that fibrils were created

at concentrations as low as 2 wt%.

Even when the TP and LCP have overlapping temperatures, the processing temperature of the blend relative to the melting point of the LCP may be an important variable as shown by Nobile et al. [20]. In capillary extrusion of PC with 10 wt% PET/PHB, drawing did not significantly raise the modulus of the blend processed at 260°C. The modulus of strands processed at this temperature were only 0.5 GPa greater than the matrix. Contrarily, when the blend was processed at 220°C, the modulus of the drawn strand rose 1.2 GPa over the modulus of the matrix. Concurrent with decreased extrusion temperature and increased modulus was a change in morphology from droplets to a fibrillar morphology.

In all of the studies cited above development of a fibrillar morphology was essential for achieving reinforcement of the matrix. Development of this morphology may depend on several factors. These factors include the flow field (extension or shear flows), the magnitude of the rate of deformation, and the concentration of the dispersed phase. The effect of flow field and concentration were examined by Blizard and Baird [26] in a study of capillary extrusion of PET/HBA blended with either polycarbonate or nylon 6,6. The morphology generated in dies of small, 7.8, and large, 21.4, L/D ratios at several LCP concentrations was examined. Extrusion of the blend with 10% LCP through a small L/D ratio die generated a droplet morphology. However, upon increasing the concentration to 30%, a fibrillar morphology was created. This transition was believed to be caused by the ease of deforming the relatively larger phase sizes created by an increased rate of coalescence that occurs at 30% LCP. In larger L/D dies, a droplet morphology was found at both concentrations. A possible explanation for the formation for the formation of droplets in the larger L/D die was that the fibrous structure generated in the entrance flow of the die undergoes breakup in shear flow as the residence time

increases in the larger L/D ratio die.

Fibrillar morphologies were also shown to be generated in a blend with low LCP content by extruding the blend at high shear rates. Beery et al. [25] studied the skin morphology of PC blended with 10 wt% of a LCP based on hydroxynaphthoic acid and hydroxybenzoic acid. This extrusion was performed with a capillary die with a L/D ratio of 33. At low shear rates, i.e. 13.5 and 135 s^{-1}, a droplet morphology was observed with some extended droplets observed at the latter shear rate. When the shear rate was increased to 1350 s^{-1}, a fibrous morphology was observed for LCP structures which were greater than approximately one micron while droplets were observed for submicron particles. At the highest shear rate, 5400 s^{-1}, nearly the entire region was fibrous.

While the above studies have investigated processing / property relationships for capillary extrusion of TP/LCP blends, no studies have been conducted on processing / property relationships for the injection molding process. The processing / property relationship for the injection molding of neat LCPs may, however, indicate important factors to consider. Two studies have been reported. The first study was performed by Jackson and Kuhfuss [15], and they showed that the flexural properties of PET/PHB are extremely sensitive to the mold thickness. In fact, as the mold thickness decreases the moduli rose almost exponentially in the machine direction. Unfortunately, there was little change in the transverse direction properties, and so mechanical anisotropy was created. The second study was performed by Garg and Kenig [42]. They showed that the flexural modulus could be varied by approximately 10% by changing the mold temperature. Observation of the morphology of the skin layer of the specimen were related to the calculated frozen layer thickness as derived by Dietz et al. [41]. They found that as the frozen layer became thicker the modulus became greater.

Based on the above review, several questions can be raised regarding the injection molding of TP/LCP blends. First, are the mechanical properties of TP/LCP blends sensitive to injection molding variables such as fill time and mold temperature? Second, can higher properties be obtained from thinner molds in a manner parallel to that observed for neat LCPs? Third, are the mechanical properties and morphology controlled by the stresses and/or heat transfer within the mold?

Thus, the objective of this paper is to determine if the mechanical properties of an injection molded TP/LCP blend are sensitive to the injection molding conditions (i.e. injection time, mold temperature, and mold thickness). It is also desired to determine if the mechanical properties can be correlated to the dimensionless groups that are related to droplet deformation (Weber number) and heat transfer (Graetz number) during the filling stage of injection molding. In the future, this work will be expanded to other PP/LCP blends in hopes of finding common conditions for injection molding of PP/LCP blends [10,11].

4.2 Experimental

4.2.1 Materials

The polypropylene (PP) used in this study was Profax 6823, a fractional melt flow index (MFI) polymer, and it was purchased from Himont, Inc. The maleated PP was a development grade maleic anhydride grafted polypropylene (MAP) supplied by BP Chemicals, Inc. with a melt flow index of 50. This material was used because it enhances mechanical properties of the blend as discussed in prior publications [6-9]. The LCP was Vectra® A950 purchased from Hoescht Celanese, and hereafter it will be referred to as VA. This LCP is a

copolyester of 73% hydroxybenzoic acid (HBA) and 27% hydroxynaphthoic acid (HNA). The blend was composed of 70 wt% of PP/MAP mixture (containing 10 wt% MAP) and 30 wt% VA. It will be designated as PP(MAP)/VA 70(10)/30.

4.2.2 Rheology

The steady shear viscosity was determined using the Instron capillary rheometer (ICR) with a single capillary of diameter 0.36 mm and a L/D ratio of 74. No end corrections were applied to the data, but the wall shear rate was corrected by means of the well known Rabinowitsch method [4]. Because the test times were in excess of five minutes and an inert atmosphere was not available for the ICR, it is believed that significant degradation of PP/MAP occurred before completion of the tests performed at 295°C. Consequently, PP/MAP was tested at 250, 265, and 285°C and the viscosity was shifted to 295°C using an Arrhenius activation energy, E, of 88 kJ/mol. This value was obtained from a least squares regression where the intercept was not forced to zero so that a better correlation was obtained.

The rheological behavior for VA cooled from the melt temperature to temperatures below the melting point was determined on the Rheometrics Mechanical Spectrometer (RMS 800) in the oscillatory dynamic mode at 1 rad s^{-1}. Parallel plate fixtures with a diameter of 25.4 mm and a gap of approximately 1.5 mm were used for all tests. A nitrogen purge provided an inert atmosphere for all tests conducted on the RMS 800. The measurement was conducted by preheating the sample at the test temperature for five minutes followed by decreasing the temperature at a rate of 5°C per minute. The tests were stopped when the transducer torque approached the transducer torque design limit.

4.2.3 Injection Molding

Dried PP/MAP pellets were physically mixed with 30 wt% dried VA pellets immediately before molding on a Arburg Allrounder, model 221-55-250, injection molder. The molds were 76 by 76 mm rectangular cavities with thicknesses of 1.0, 1.5, and 2.3 mm. Each mold had a film gate which created two dimensional rectilinear flow throughout the cavity. These molds were equipped with heating rods to obtain either a 50 or 70°C mold temperature. The mold temperature was also lowered to 20°C by removing the heating rods and installing water lines for cooling. Mold temperatures were kept within ± 2°C. The injection molder barrel temperatures were set to 160°C in the first zone, 295°C in the second zone, and 295°C in the third zone while the nozzle temperature was set to 280°C. The injection pressure and hold pressure were set to 800 and 600 psi for all runs. The injection speed setting was varied to obtain a range of injection times. The injection time was measured as the travel time for the screw to move from the retracted position to the fully injected position. The volumetric flow rate was calculated by assuming a constant screw injection speed and dividing the volume including the sprue and gate volume, 78.5 mm^3, by the fill time. The fill time is the time for polymer to flow from the entrance of the mold to the point where the mold is filled. It was calculated from the injection time by subtracting the time the screw advances from the retracted position to the point where polymer began entering the mold. The time for the screw to travel from the retracted position to the pressurization point was approximately 35% of the injection time. The average velocity within the mold was then calculated by dividing the volumetric flow rate by the cross sectional area of the mold.

Neat PP/MAP was molded with the same temperature profile as described for the blend. However, neat VA could not easily be molded at the same melt temperature because of rapid

freezing within the mold. Consequently, higher injection molder temperatures were used. The temperature profiles were 220, 310, 330°C in the first through third zones, respectively, while the nozzle temperature was set at 310°C.

4.2.4 Mechanical Testing

All samples were tested in the flexural mode and selected samples were tested in the tensile mode on a Instron mechanical tester, model 4204. The specimens were prepared by cutting 10 by 76 mm long strips from the 76 by 76 mm plaques in either the machine or transverse direction followed by sanding to minimize the cutting marks. Tensile specimens were tested at a crosshead speed of 1.27 mm/min while flexural specimens were tested at a rate of 1.0 %/min. An extensiometer, Instron model 2630-25, was used for all tensile tests except for determination of the strength and elongation of neat PP. A minimum of five samples was tested, and the average value and standard deviation were calculated from the data.

4.2.5 Morphological Studies

Fracture surfaces of plaque samples obtained approximately 13 mm from the end of the plaque were prepared by cryogenic fracture in liquid nitrogen followed by coating with gold on a SPI sputter coater. Fracture surfaces were viewed on a Cambridge stereoscan S200 scanning electron microscope (SEM) using an accelerating voltage of 15 KV. The plaques were fractured in the machine direction which provides a view along the flow direction. These plaque samples were etched in hypochloric acid as described by Olley et al. [29] for 15 minutes to better reveal the LCP morphology. Specimens were also prepared by microtoming the plaques in the machine direction and observing the two phase structure in transmission mode on a Olympus BH2 optical

microscope at 37.5 magnification.

4.3 Results and Discussion

The mechanical properties of the PP(MAP)/VA blends molded at several different injection times are presented first. Data for all three mold thicknesses at one mold temperature are given. Both tensile and flexural data are presented. Second, the morphology is examined to determine if the structure in plaques possessing higher properties have a uniquely different structure from that of plaques possessing lower properties. For instance, the plaques possessing higher properties may exhibit higher aspect ratio fibrils or a finer dispersed phase size. Third, the rule of mixtures is used to estimate how efficiently the LCP reinforces the PP matrix. Fourth, the rheology of the neat polymers and the blend will be presented. The steady shear data is necessary for determination of the shear stresses in the mold while the dynamic cooling behavior indicates how sensitive the rheology of the LCP is to cooling. Finally, the flexural moduli of these blends are related to the stress and heat transfer that existed during the filling stage. Comparison of the flexural moduli to the stress and heat transfer may indicate that one mechanism is a primary influence on the mechanical properties of the blend.

4.3.1 Mechanical Properties of the Blend

Typical mechanical properties of the blend processed at various injection times and in all three molds are shown in Tables 4-1 to 4-3. Both the flexural and tensile properties are shown. Flexural moduli that are higher than the tensile moduli reflect a higher stiffness near the skin relative to the average stiffness of the specimen. Likewise, if the flexural modulus increases to

a greater extent than the tensile modulus as an injection condition such as fill time is increased then the skin region is being reinforced more effectively than the core.

In Table 4-1, the properties of plaques of 1.0 mm thickness are shown. Only the flexural moduli are affected by the injection time with much higher properties, e.g. 5.08 GPa, resulting from the higher injection speed. This indicates that any change in structure should be occurring primarily near the skin while the bulk of the sample is unchanged. The properties for plaques of 1.5 mm thickness are shown in Table 4-2. Here, both the flexural and tensile moduli change with injection time. However, instead of the highest properties occurring at the shortest injection times, the opposite occurs. The higher properties occur at the longest injection time, 5 s. The flexural moduli increase from approximately 3.9 to 5.2 GPa, and the tensile moduli increase from approximately 2.9 to 4.7 GPa. Since both the tensile and flexural moduli change by the same degree, any change in the structure of the plaque is anticipated to occur over much of the thickness. The same trends occur with the properties for plaques of 2.3 mm thickness as shown in Table 5.3. Here, the flexural moduli increased from 2.62 GPa to 4.08 GPa and the tensile moduli increased from 2.12 to 3.08 GPa while the injection time is increased from 1.3 to 7.8 seconds. It should be noted that injection times of seven seconds are exceedingly long for injection molding, and hence these trends would not normally be encountered in molding of a small laboratory specimen.

It is informative to inspect this data in graphical form where the flexural modulus, which varies with injection speed in all three molds, is plotted against the fill time. This data is shown in Fig. 5-1. While the flexural modulus increases with the fill time for the 1.5 and 2.3 mm thick plaques, the opposite trend is found for the 1.0 mm thick plaque. There does not appear to be any consistency once the mold thickness is changed. However, it must be pointed out that when

the mold thickness is changed, corresponding changes occur in the stress and heat transfer. Since these variables do not scale similarly, some differences always occur when the mold thickness is changed. In a latter section, the stress and heat transfer will be examined to determine if one of these variables dominates when maximum flexural moduli occur.

Before leaving this section it should also be noted that the transverse flexural properties were measured and found to be unaffected by changes in the injection speed. The average modulus for the 1.0 mm thick plaques was approximately 1.5 GPa and the average modulus for 1.5 and 2.3 mm thick plaques was 1.4 GPa.

4.3.2 Morphology

The morphology of plaques with the highest and lowest moduli are examined in this section in hopes of finding a morphological difference that could account for the property differences created by varying the injection times. Since the 1.0 and 2.3 mm thick plaques exhibit the greatest variation in properties, the morphology of these plaques is examined.

At the onset, there are only three factors which should affect the moduli in this composite-like structure. The first factor is the orientation of the LCP which leads to high modulus fibrils or ribbons. The second factor is the aspect ratio of the fibers or ribbons. From composite theory [27], a reinforcing fiber needs an aspect ratio of at least 100 in order to follow the rule of mixtures. The third factor is the local concentration of the reinforcing LCP. If flow migration occurs [30], then higher or lower flexural moduli could result depending upon the direction of migration of the reinforcing phase. The orientation indicated from WAXS analysis showed little difference between plaques of high and low moduli. Therefore, in this study, the two phase structure of the blend is examined which provides information about the latter two

Table 4-1 Machine direction properties for PP(MAP)/VA blend in 1.0 mm mold at 50°C mold temperature and various injection times.

Injection Time (s)	Flex Modulus (GPa)	Flex Strength (MPa)	Tensile Modulus (GPa)	Tensile Strength (MPa)	Elongation at Yield (%)
0.8	5.08 (0.37)	64.5 (2.5)	3.13 (0.33)	35.4 (2.6)	1.48 (0.23)
1.3	4.80 (0.53)	62.6 (2.9)	3.36 (0.40)	40.9 (4.8)	1.71 (0.22)
2	3.56 (0.35)	55.5 (1.7)	3.53 (0.22)	35.9 (3.5)	1.60 (0.31)
3	3.43 (0.27)	58.1 (2.5)	2.96 (0.19)	36.5 (1.1)	1.85 (0.20)
3.7	3.87 (0.51)	56.7 (3.5)	3.14 (0.29)	35.5 (2.3)	1.85 (0.31)

Table 4-2 Machine direction properties for PP(MAP)/VA blend in 1.5 mm mold at 50°C mold temperature and various injection times.

Injection Time (s)	Flex Modulus (GPa)	Flex Strength (MPa)	Tensile Modulus (GPa)	Tensile Strength (MPa)	Elongation at Yield (%)
.8	4.10 (0.07)	61.7 (1.1)	3.09 (0.43)	31.5 (1.0)	1.59 (0.25)
1.3	3.93 (.33)	55.6 (1.1)	2.80 (0.21)	31.6 (1.3)	1.93 (0.24)
2.1	3.89 (.64)	56.6 (2.9)	2.90 (0.34)	31.9 (1.7)	1.70 (0.33)
3	4.25 (0.30)	59.5 (1.5)	2.90 (0.29)	33.9 (1.8)	1.72 (0.20)
4	4.44 (.21)	56.2 (1.1)	3.34 (0.10)	31.5 (1.6)	1.51 (0.21)
5	5.20 (0.33)	61.4 (2.7)	4.68 (0.38)	35.6 (2.0)	1.07 (0.11)

Table 4-3 Machine direction properties for PP(MAP)/VA blend in 2.3 mm thick mold at 50°C mold temperature and various injection times.

Injection Time (s)	Flex Modulus (GPa)	Flex Strength (MPa)	Tensile Modulus (GPa)	Tensile Strength (MPa)	Elongation at Yield (%)
1.3	2.62 (.17)	54.8 (1.7)	2.12 (0.20)	28.6 (2.1)	2.60 (0.18)
3	2.78 (.17)	53.4 (1.1)	2.31 (0.07)	31.1 (1.9)	2.28 (0.23)
4	3.16 (.29)	52.8 (2.4)	2.67 (0.16)	31.2 (2.1)	1.82 (0.12)
5.2	3.87 (0.21)	56.1 (2.0)	2.98 (0.20)	32.2 (1.8)	1.52 (0.22)
6.3	3.91 (0.35)	54.9 (1.4)	3.31 (0.15)	31.4 (0.2))	1.35 (0.12)
7.8	4.08 (0.53)	56.7 (1.4)	3.08 (0.23)	30.9 (2.1)	1.60 (0.21)

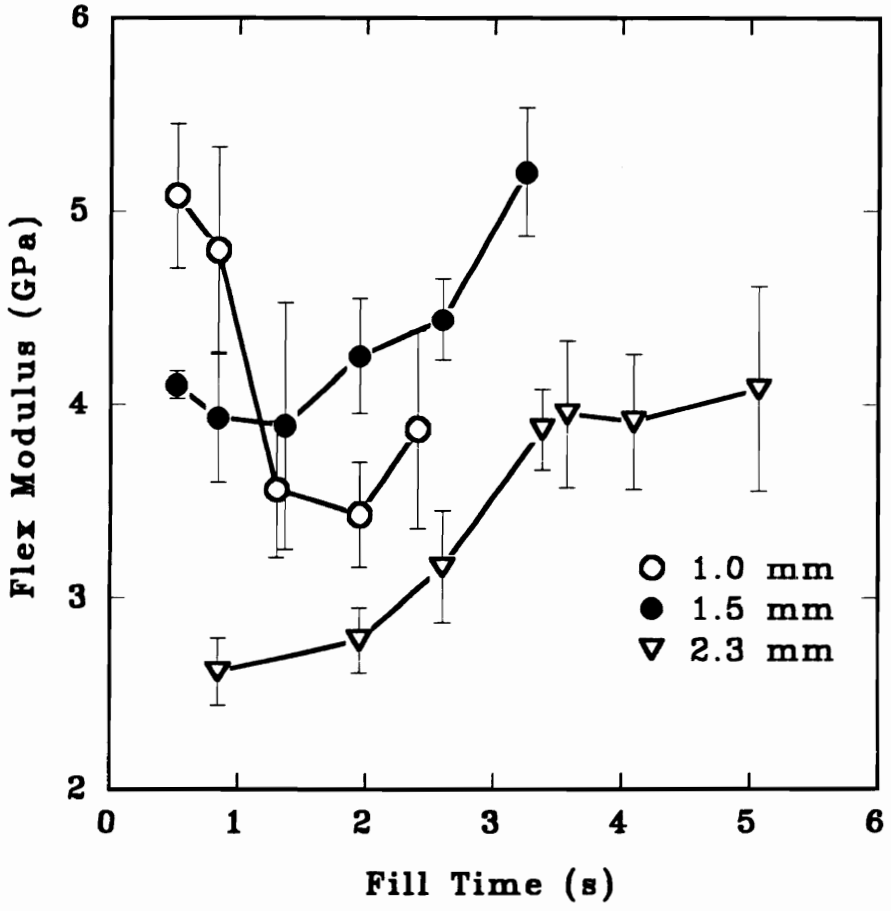

Fig. 4-1 Flexural modulus versus fill time for PP(MAP)/VA 70(10)/30 for 1.0, 1.5, and 2.3 mm thick plaques made with a 50°C mold temperature.

factors.

The first two SEM photomicrographs of two 1.0 mm thick plaques are shown in Figures 4-2 and 4-3. These plaques have flexural moduli of 3.4 and 5.1 GPa, respectively. In Fig. 4-2, the entire plaque cross sectional area and a magnified view of the skin / subskin region as seen along the machine direction is shown. From these photomicrographs, it appears that high aspect ratio VA fibrils or ribbons are absent. In contrast, Fig. 4-3 shows many long ribbons of VA of both large and small thicknesses. In the skin / subskin photomicrograph, several very straight and long ribbons of VA are present. The presence of these ribbons is probably the cause for the greatly improved properties.

The structure of 2.3 mm thick plaques was examined by both scanning electron and optical microscopy techniques. Fig. 4-4 shows the fracture surfaces for a plaque with a flexural modulus of 2.6 GPa. Despite the low modulus, both the photomicrographs of the entire specimen cross sectional area and the magnified skin / subskin region show long fibers or ribbons. Comparison to a plaque with a flexural modulus of 4.1 (Fig. 4-5) shows that in this plaque long fibers or ribbons also exist. However, a greater difference exists than is shown by these photomicrographs. Optical microscopy of microtomed samples reveal more contrast between the structures. In Fig. 4-6, a section of the plaque with a modulus of 2.6 GPa is shown. The area shown is from 0.31 to 1.05 mm from the core with the skin (not shown) located at 1.15 mm. The dark areas are the LCP fibers or ribbons. From this figure long straight structures do not exist. In contrast, the same cross sectional area for the second plaque with a flexural modulus of 4.1 GPa is shown in Fig. 4-7. Almost the entire area is composed of extended long fibers or ribbons. Some of the thinner structures can be measured and aspect ratios of 80 are found in this photograph. This rigid structure that exists even near the core, provides a possible explanation

of why the tensile moduli follows the flexural moduli. In this case, it is not just the skin or subskin that is affected in the thick plaque but nearly the entire specimen. Thus, examination of the morphology indicates that higher moduli are the result of straighter higher aspect ratio LCP structures.

In revisiting the photomicrographs of the 1.0 mm thick plaques, it is now obvious that the morphology of this thickness plaque (Fig. 4-3) is very different from the morphology in the 2.3 mm thick plaque (Fig 4-5). In the 1.0 mm thick plaque, a more diverse LCP structure is observed with a wavy LCP morphology near the core. In contrast, the morphology of the 2.3 mm thick plaque shows a much more uniform morphology with a smooth morphological change from fibrils or ribbon near the skin to larger less deformed LCP structures near the core. It appears that in these two plaques of different thickness that different LCP structures are formed during injection molding. The differences in morphology may be related to the differences in the stress and heat transfer for these two molds that existed during mold filling. This matter will discussed in a latter section.

4.3.3 Rule of mixtures

It is of interest to determine if higher properties of the blend can be obtained from thin molds. This interest is based on the expectation that higher properties can be obtained from neat VA made in thin molds. If higher properties of neat VA are obtained in thin plaques then it is expected that the higher properties of VA will lead to higher properties of the blend. However, while the blend properties may be higher in thinner molds, there is a desire to determine how efficiently the LCP is reinforcing the blend. The rule of mixtures provides a widely accepted method for calculating the upper bound of moduli for a two phase system. The moduli for the

neat components are required to apply this rule to the blend.

Since the properties for neat LCPs depend intimately on how the polymer is processed [16,18,19] there can be a question as to which properties to use for the rule of mixtures. For a LCP fiber-reinforced composite, the modulus of the fiber-spun LCP would be appropriate to use in estimation of the properties of the composite. However, since the LCP fibrils within the blend are generated during injection molding it is appropriate to use the modulus of neat LCP which was injection molded.

The flexural properties for neat VA for three mold thicknesses and three mold temperatures are shown in Table 4-4. Observing the properties of the 2.3 mm thick plaques, it can be seen that the modulus rose slightly (from 10.0 to 11.0 GPa) with the lowering of the mold temperature while the strength was not affected. The moduli in the 1.5 mm thick plaques are substantially higher than those of the 2.3 mm thick plaques (13.1 versus 10.3 GPa, respectively, at a 50°C mold temperature), and the moduli also showed a slight increase as the mold temperature is lowered. Again, no change in strength occurs. In the thinnest plaque, 1.0 mm, significantly higher moduli are obtained (17.4 GPa) with the same slight increase in moduli as the mold temperature is decreased. Thus, the mold thickness is a primary variable influencing the flexural modulus of the neat LCP while the mold temperature is a secondary variable in agreement with past investigations [15,42].

The flexural properties for neat PP are shown in Table 4.5. There is no change in the moduli with a decrease in the mold temperature at any of the thicknesses. There is, however, a slight increase in the flexural moduli from 1.3 GPa for the 2.3 mm thick plaque to 1.8 GPa for the 1.0 mm thick plaque. This increase in modulus is probably the result of higher stresses which orient a flexible chain polymer and more rapid quenching in the thinner mold which

consequently retains the generated orientation. As occurred for the LCP, there is no change in the strength of PP with changes in either the mold temperature or the thickness.

Using the rule of mixtures which considers the components of the blend as behaving in a parallel structural arrangement [31], the component moduli may be combined to predict the modulus of the blend. These calculations using data from the 50°C mold temperature series yield moduli of 5.24, 4.21,and 3.29 GPa for the 1.0, 1.5 and 2.3 mm thick plaques. Comparison to the highest flexural moduli for the blends, 5.08, 5.20, 4.08 GPa. in the 1.0, 1.5, and 2.3 mm thick plaques, respectively, indicate good agreement between prediction and data for the 1.0 mm thick plaques while the moduli for the 1.5 and 2.3 mm thick plaques exceed the rule of mixtures. Based on data in Tables 4-1 to 4-3, the reinforcement effectiveness of VA clearly depends upon the injection time which indicates that the stress and heat transfer may be a controlling factor in obtaining a reinforced morphology.

4.3.3 Rheology

Before analyzing the trends in the flexural properties with respect to the stresses in the mold, the viscosity of the blend at the appropriate shear rates for injection molding are presented. Additionally, it is of interest to determine the isothermal viscosity ratio of these materials and to present the temperature sensitivity of the VA rheology as neat VA cools from the melt. The former information provides a reference for comparison with other systems to be studied [10,11]. The latter data provides an indication of how sensitive the deformation of VA will be during the filling stage to the melt temperature.

The steady shear viscosity for PP/MAP, neat VA, and the PP(MAP)/VA blend at 295°C are shown in Fig. 4-8. The steady viscosity data will be used in this work because of the high

Fig. 4-2 SEM photomicrograph of 1.0 mm thick plaque with a flexural modulus of 3.4 GPa molded in 2.8 seconds: (a) entire plaque; (b) skin/subskin region.

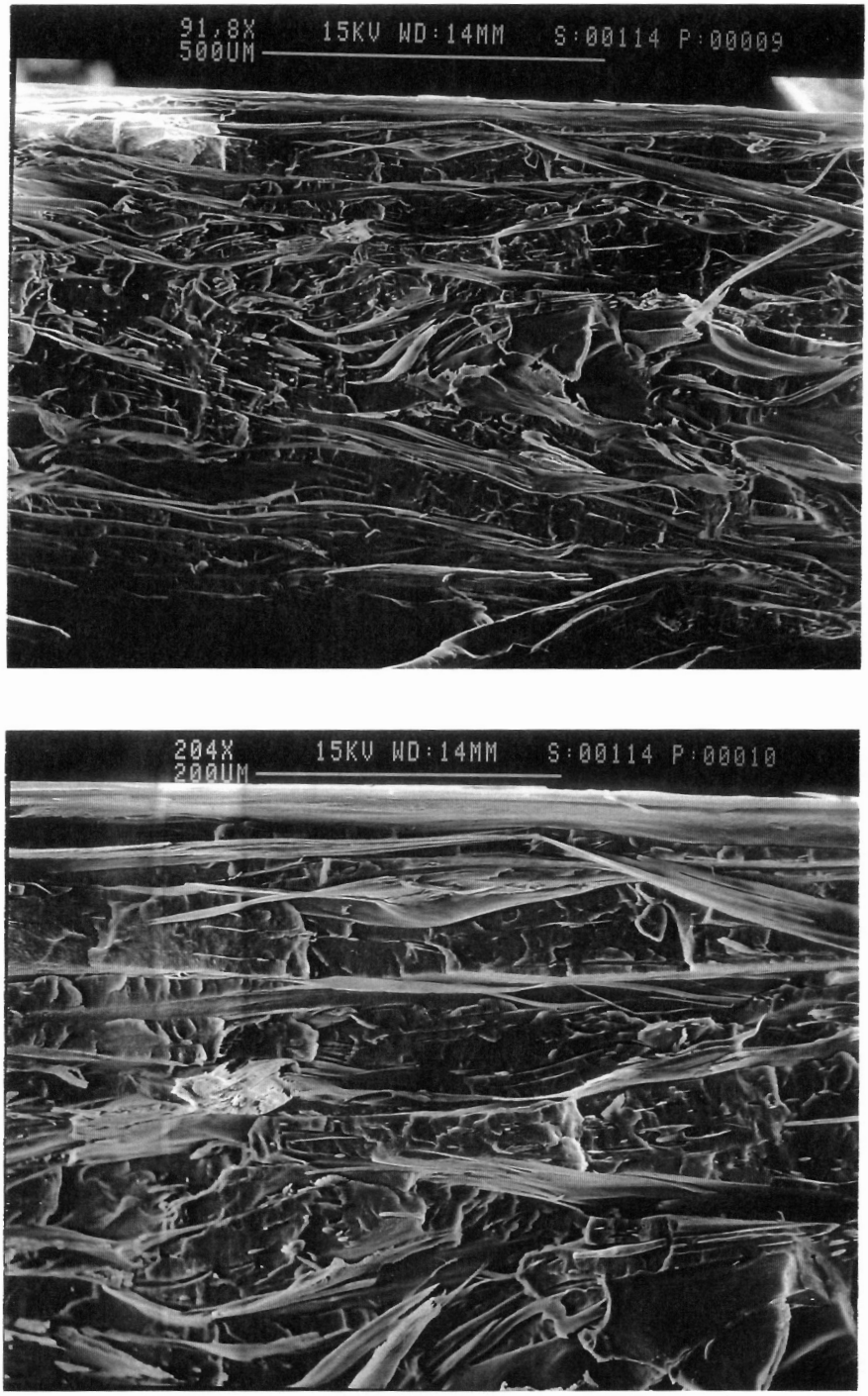

Fig. 4-3 SEM photomicrograph of 1.0 mm thick plaque with a flexural modulus of 5.1 GPa molded in 0.8 seconds: (a) entire plaque; (b) skin/subskin region.

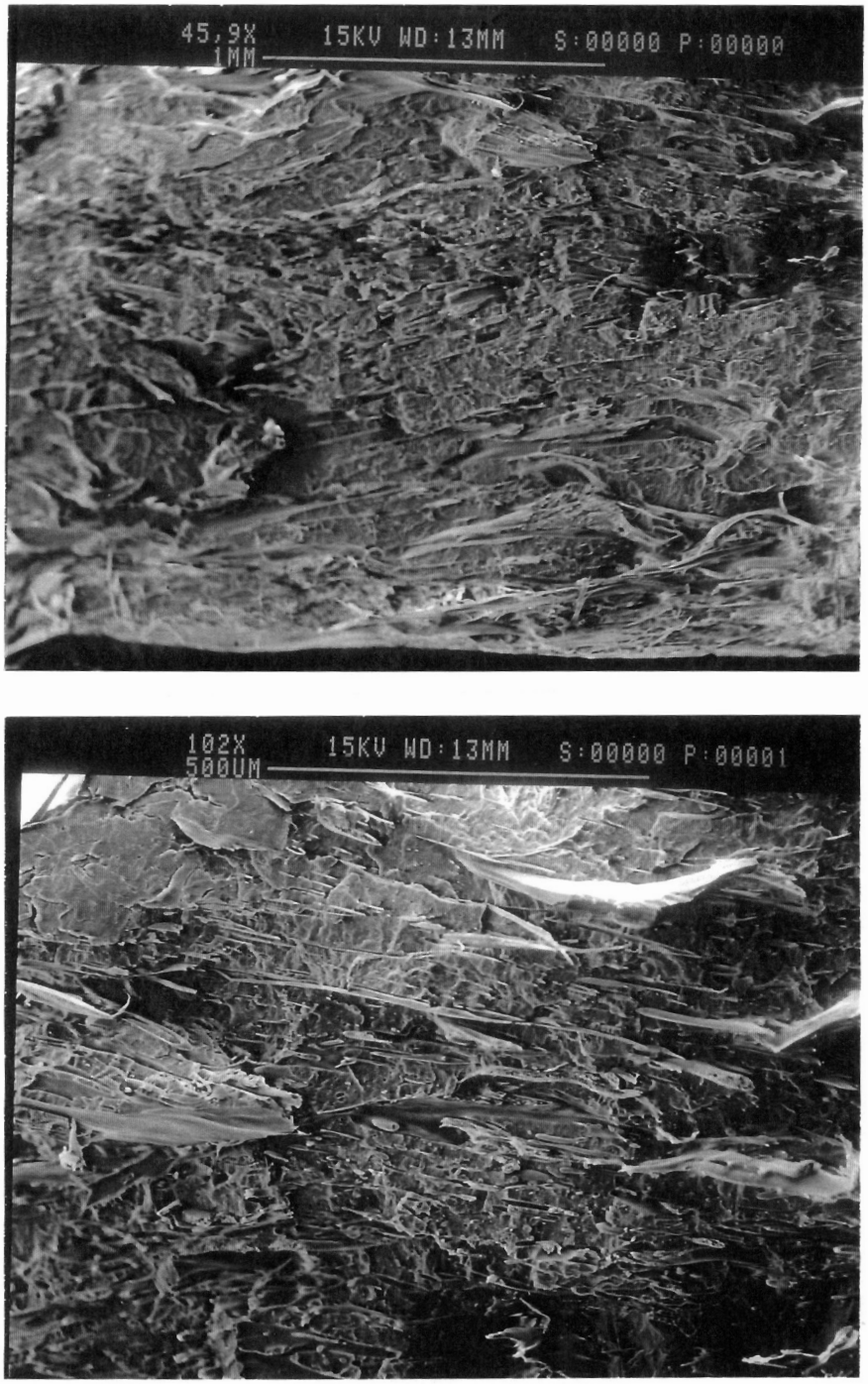

Fig. 4-4 SEM photomicrograph of 2.3 mm thick plaque with a flexural modulus of 2.6 GPa molded in 1.3 seconds: (a) entire plaque; (b) skin/subskin region.

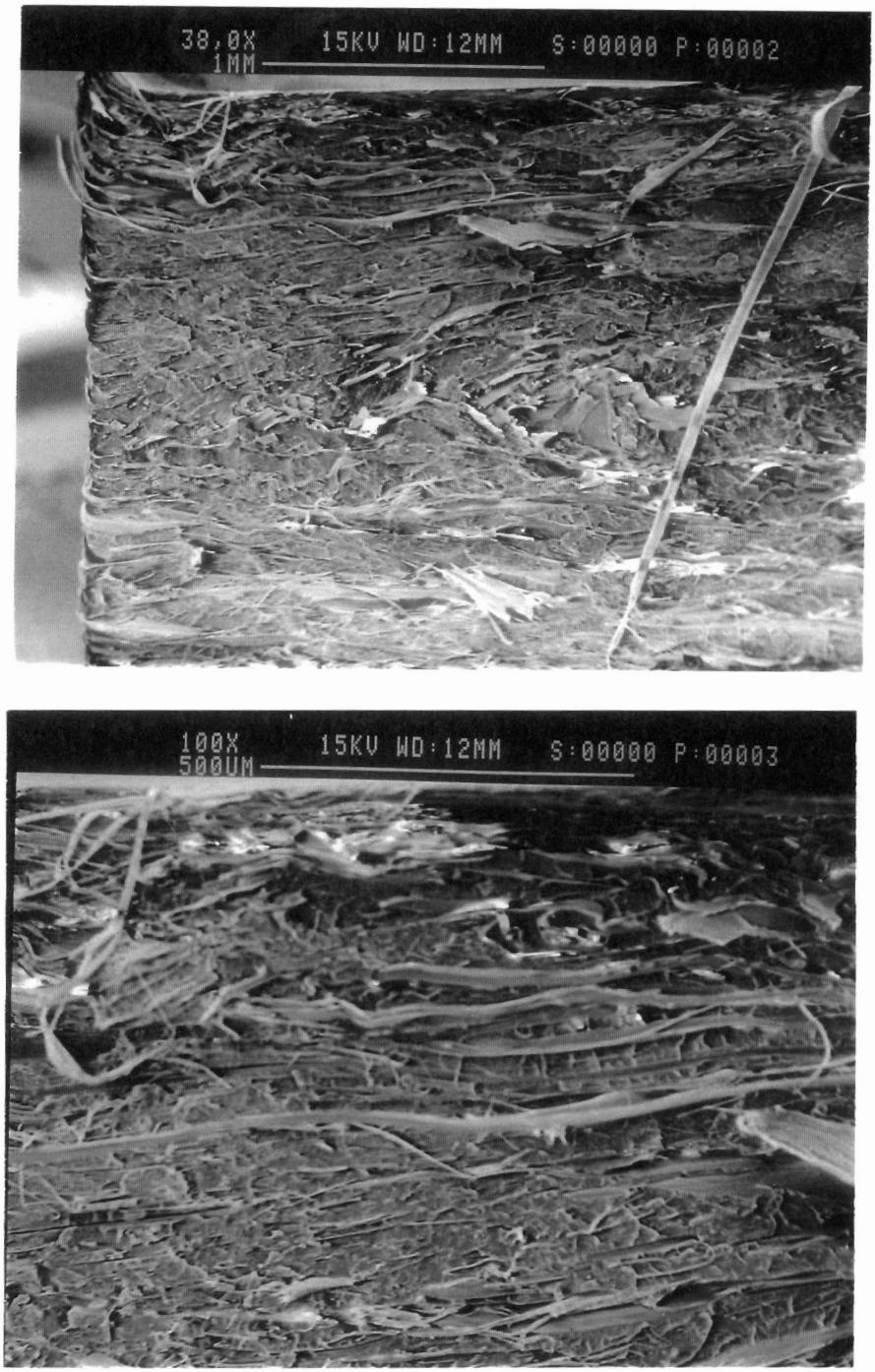

Fig. 4-5 SEM photomicrograph of 2.3 mm thick plaque with a flexural modulus of 4.1 GPa molded in 7.8 seconds: (a) entire plaque; (b) skin/subskin region.

Fig. 4-6 Optical photograph of 2.3 mm thick plaque with a flexural modulus of 2.6 GPa molded in 1.3 seconds: (a) entire plaque; (b) skin/subskin region.

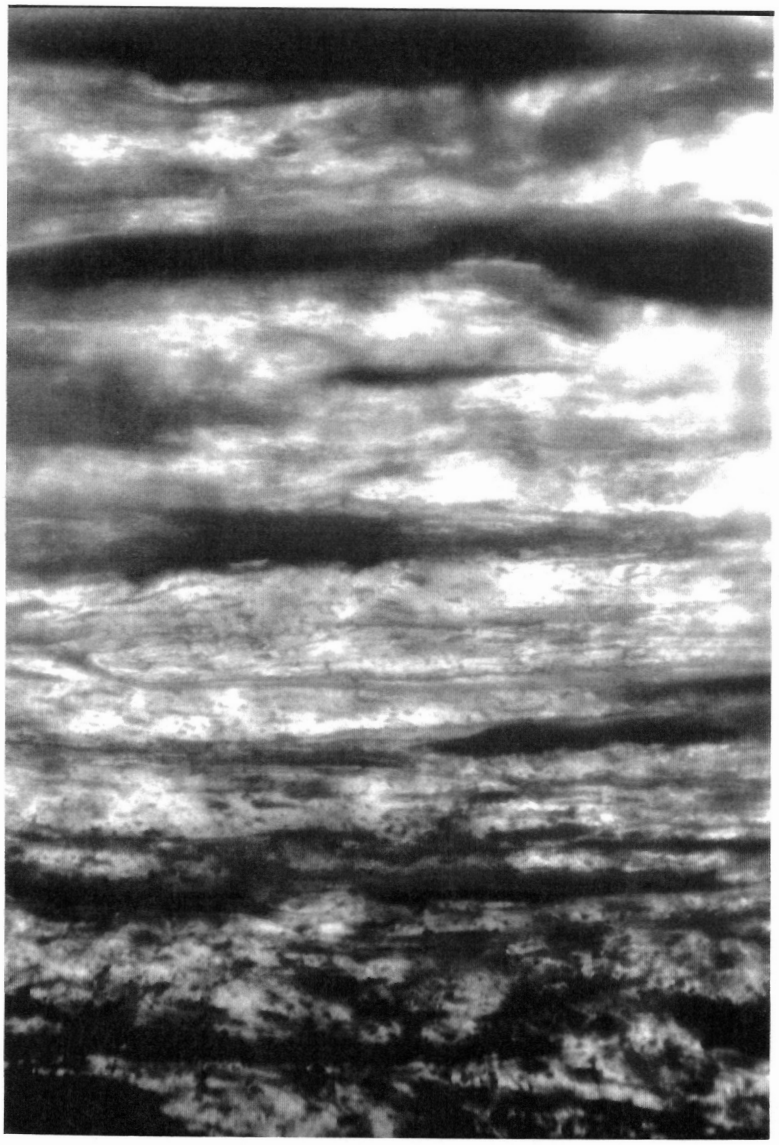

Fig. 4-7 Optical photograph of 2.3 mm thick plaque with a flexural modulus of 4.1 GPa molded in 7.8 seconds: (a) entire plaque; (b) skin/subskin region.

Table 4-4 Machine direction flexural properties for neat VA in 1.0, 1.5, and 2.3 mm thick plaques molded at 20, 50, and 70°C mold temperatures.

Thickness (mm)	Mold Temperature (°C)	Modulus (GPa)	Strength (MPa)
1.0	20	29.2 (2.1)	311.1 (12.0)
	50	32.5 (3.4)	310.6 (60.7)
	70	29.3 (1.3)	316.6 (10.4)
1.5	20	27.5 (0.9)	308.8 (8.5)
	50	20.7 (1.2)	257.5 (10.4)
	70	23.1 (3.5)	257.7 (41.6)
2.3	20	20.3 (1.1)	244.6 (13.7)
	50	19.65 (1.26)	242.5 (10.7)
	70	16.5 (1.8)	212.5 (17.2)

Table 4-5 Machine direction flexural properties for PP in 1.0, 1.5, and 2.3 mm thick plaques molded at 20, 50, and 70°C mold temperatures.

Thickness (mm)	Mold Temp. (°C)	Modulus (GPa)	Strength (MPa)
1.0	20	1.73 (0.13)	42.4 (2.6)
	50	1.96 (0.09)	45.3 (1.5)
	70	1.85 (0.09)	42.3 (1.5)
1.5	20	1.73 (0.08)	49.5 (0.9)
	50	1.68 (0.04)	49.6 (1.7)
	70	1.79 (0.09)	47.4 (0.9)
2.3	20	1.17 (0.09)	44.5 (2.2)
	50	1.31 (0.10)	48.5 (2.1)
	70	1.33 (0.07)	45.6 (0.9)

shear rates experienced in injection molding. For the blend, the power law constants, m and n, where $\eta = m\dot{\gamma}^{n-1}$, are 117 and 0.604, respectively. The power law model is used to calculate the shear stress in the mold where shear rates range between 70 and 4000 s^{-1}. The viscosity ratio of VA to PP/MAP, η_{VA}/η_{PP}, is also calculated from the steady viscosity data. For shear rates of 100 and 1000 s^{-1}, the viscosity ratio is 0.33 and 0.42, respectively, which is close to a viscosity ratio of unity that is often cited for dispersing polymers [48].

The cooling behavior of VA when cooled from 295°C and 300°C are shown in Fig 4-9. The temperature of 295°C was chosen because it is the processing temperature used in this study. The latter temperature provides a reference that indicates how different the rheology of VA can become with a few degrees change in temperature. Several points can be made from this data. First, the data indicates that VA cooled from 295°C behaves more elastically ($G' > G''$) than VA cooled from 300°C, and thus VA may not be completely melted. The dynamic viscosity, $|\eta^*| = (G'^2+G''^2)^{1/2}/\omega$ where ω is the frequency, remains about a half an order of magnitude higher for VA tested at 295°C than for VA tested at 300°C until the temperature reaches about 265°C when the torque exceeds the transducer limit. This indicates that to ensure that VA will deform and create a reinforced morphology when VA is processed from a 295°C melt temperature that limiting the cooling during the filling stage may be an important factor to control.

4.3.4 Effect of Stress on the Flexural Modulus

The most obvious influence of stress on the structuring of TP/LCP blends is deformation of the LCP phase which leads to formation of reinforcing fibrils. Taylor [14] showed that deformation of a Newtonian droplet in Newtonian fluid is related to the Weber number. The Weber number is a dimensionless number that is the ratio of the shear or extensional stress to the

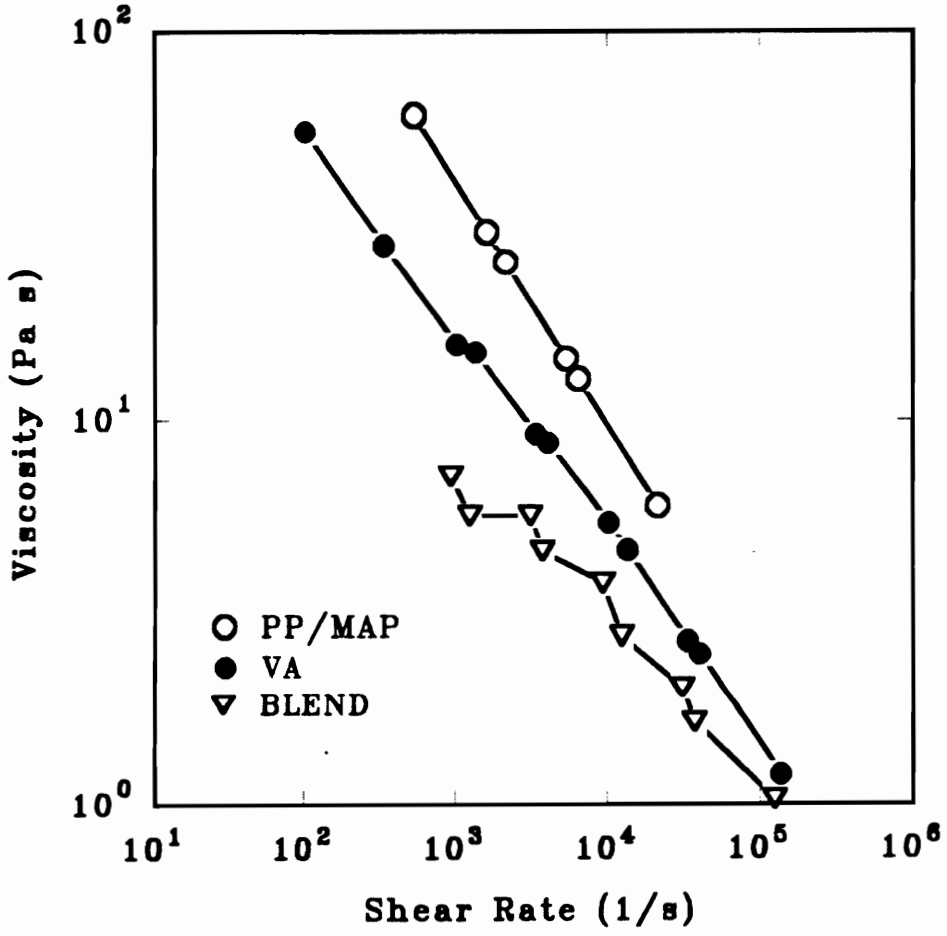

Fig. 4-8 Shear viscosity for PP/MAP 90/10, neat VA, and PP(MAP)/VA 70(10)/30 measured at a 295°C melt temperature.

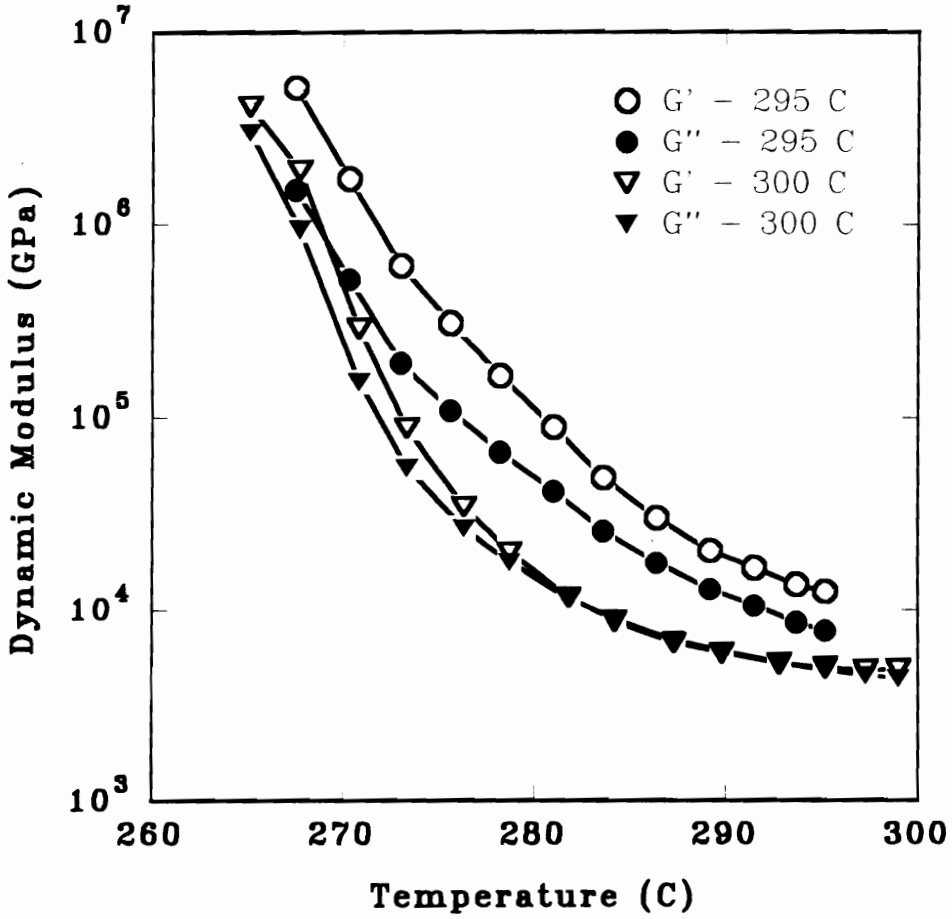

Fig. 4-9 Storage and loss moduli for neat VA cooled at 5°C from 295 and 300°C. Measured at 1 rad/s.

surface stress, σ_{12}/R, where σ_{12} is the interfacial tension and R is the drop radius. From the work of Elemans [44], it is expected that affine deformation of a droplet occurs when the Weber number is twice the value of the Weber number that causes a droplet to undergo breakup into two or more drops. Since the initial radius of a droplet is constant, the Weber number scales directly with the stress. Thus, a critical stress would be expected when affine deformation occurs, and it is believed that the large deformations that occur with affine deformation would lead to reinforcing fibrils and hence to higher mechanical properties of the blend.

Since the Weber number is directly proportional to the stress, and it is difficult to assign an average radius, R, to the LCP morphology, the flexural modulus will be compared directly to the stress to determine if higher stresses lead to higher moduli. During the filling of a mold, two flow fields exist which lead to two stresses that can be correlated with the flexural modulus. At the advancing front, a planar extensional flow (or hyperbolic stagnation flow) exists while upstream of the advancing front a shear flow exists. The shear stress that exists upstream of the advancing front may be approximated for this mold by calculating the shear stress for flow of a power law fluid between parallel plates. The shear stress accordingly can be calculated from the following equation:

$$\tau_{zy} = m \left[\frac{U}{H}\left(\frac{1+2n}{n}\right)\right]^n \left(\frac{y}{H}\right) \qquad (4\text{-}1)$$

where U is the average velocity, H is the half thickness of the mold, and y is the distance from the centerline of the mold.

Calculation of the extensional stress is more difficult because the extensional viscosity is not known. However, it may be approximated by using the Trouton ratio ($\eta_e/\eta_0=3$) for the extensional viscosity, η_e. In this case, the zero shear viscosity, η_0, will be replaced by the

power law viscosity at 100 s^{-1}. The extensional stress may then be estimated using this extensional viscosity and the extensional rate at the advancing front for a power law fluid as proposed by Tadmor [32]. This approach yields the following stress at the advancing front:

$$\tau_{zz} = -\frac{mnU}{4(1+n)H} \tag{4-2}$$

For $n < 1$, the extensional stress will increase to a greater degree than the shear stress as the average velocity increases.

The flexural modulus versus the extensional stress for the blend molded into plaques of three different thickness is shown in Fig. 4-10. While the modulus increases with stress for plaques of 1.0 mm thickness, the opposite trend occurs for the thicker plaques. Both the 1.0 and 1.5 mm thick plaques yield approximately the same maximum flexural modulus yet high stress exists when maximum properties occur in the 1.0 mm thick plaque while low stress exists when maximum properties occur in the 1.5 mm thick plaque. This indicates that extensional stress does not affect mechanical properties in the same manner for all three molds, and some other variable is influencing the development of the structure and mechanical properties of the blend. The same trend is observed in Fig. 4-11 where the flexural modulus is plotted versus the shear stress. The relationship between modulus and shear stress is very similar to that observed in Fig. 4-10 for modulus versus extensional stress. However, as in the case for extensional stress, no consistent relationship is observed from this data.

4.3.4 Effect of Heat Transfer on the Flexural Modulus

Any effect of heat transfer on the properties of TP/LCP blends is believed to be related to maintaining a molten LCP phase during the filling stage. The LCP must be molten to deform

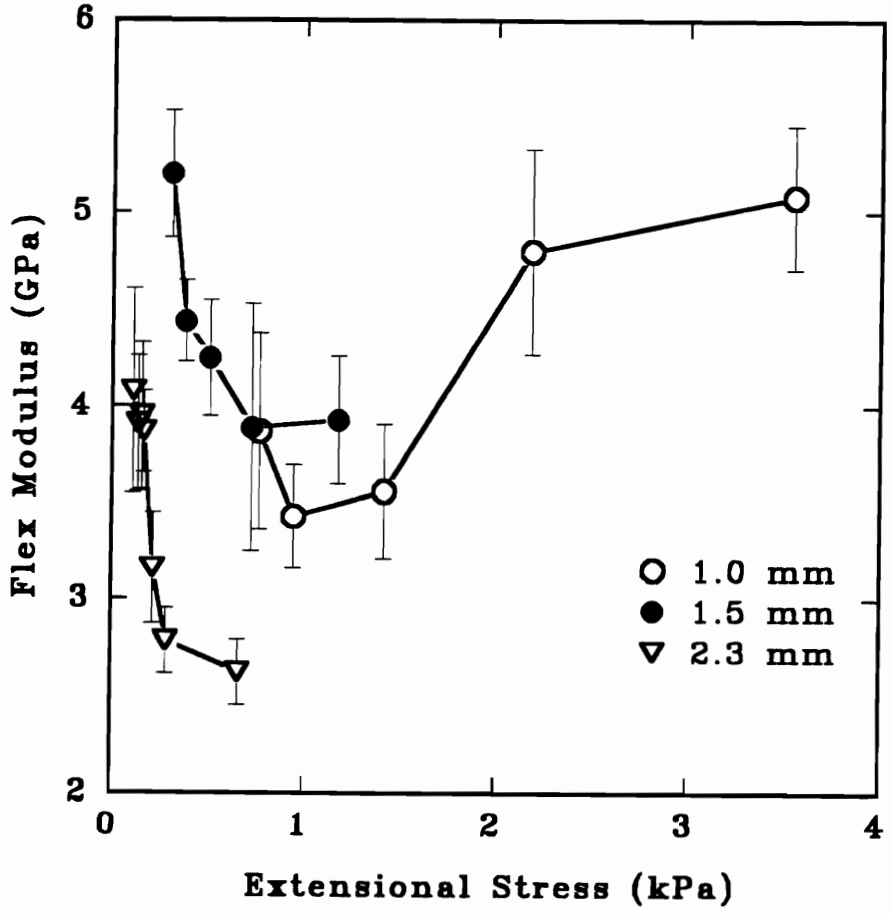

Fig. 4-10 Flexural modulus versus extensional stress for PP(MAP)/VA 70(10)/30 for 1.0, 1.5, and 2.3 mm thick plaques made with a 50°C mold temperature.

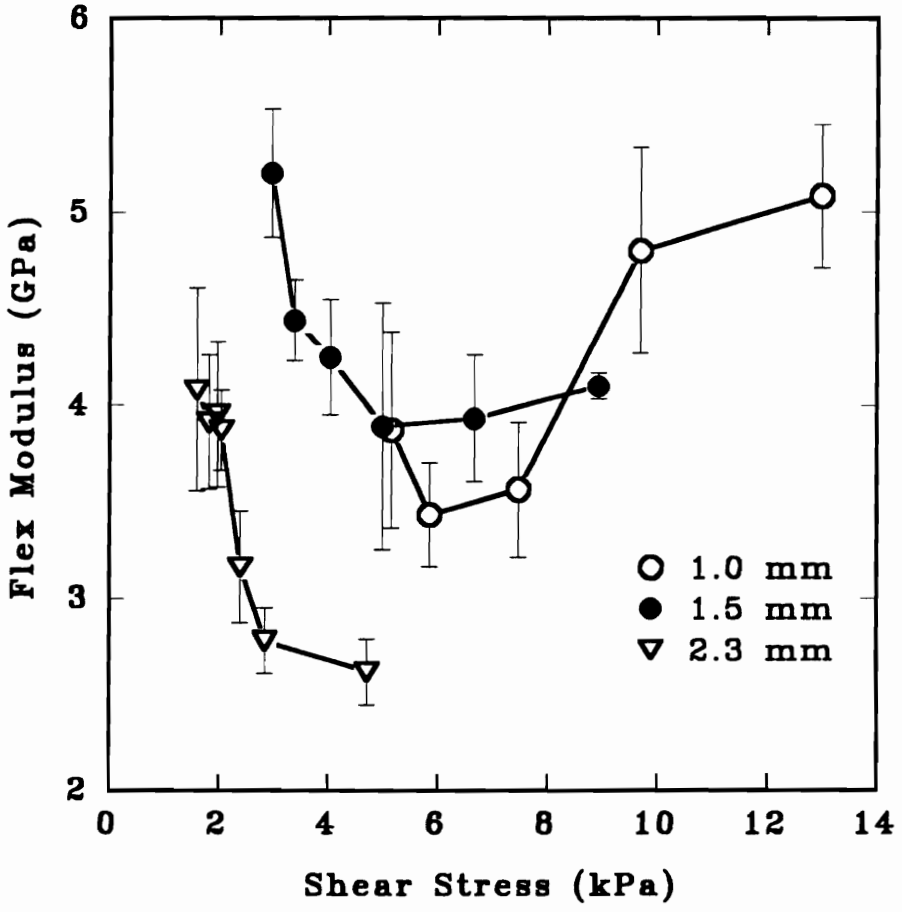

Fig. 4-11 Flexural modulus versus shear stress for PP(MAP)/VA 70(10)/30 for 1.0, 1.5, and 2.3 mm thick plaques made with a 50°C mold temperature.

and extend so that fibrils are formed while at the same time cooling must also lead to reducing the temperature of the LCP to the point where rapid solidification occurs upon cessation of flow. Similar situations have been discussed for both neat VA [17] and for TP/LCP blends [24,20]. The initial rheological properties of VA, shown in Fig. 4-9, shows that VA is already solid-like at 295°C since $G' > G''$. The role of heat transfer in this situation may be to maintain the temperature of VA just above the point where resistance to deformation increases.

Instead of calculating the transient temperature profile and correlating this large volume of data to the mechanical properties, a correlation of the flexural modulus to dimensionless variables was pursued. The appropriate dimensionless number for heat transfer may be obtained from dimensional analysis or by dimensionalizing and simplifying the equations of motion and energy. The latter approach is pursued in the Appendix where the fountain flow at the advancing front is ignored to permit simplification of the problem. This approach yields an equation which is an extension for a power law fluid of the Graetz-Nusselt problem. The only dimensionless number for this problem is the Graetz number, $UH^2/\alpha L$, where α is the thermal diffusivity and L is the mold length. The Graetz number indicates the magnitude of heat convected in the down channel direction to the heat conducted in the transverse direction. Accordingly, a high Graetz number, $Gz \gg 1$, indicates that little transverse cooling occurs while a small Graetz number, $Gz < 1$, indicates that a large degree of transverse cooling occurs. Comparison of the flexural moduli versus the Graetz number should indicate if heat transfer is important in this process.

To calculate the Graetz number, the thermal diffusivity of the blend is required. The values of the thermal diffusivity for PP, VA, and the blend are presented in Table 4-6. The values for PP and VA were obtained from references [46] and [47], respectively. The blend thermal properties were estimated from the individual components properties by a series model

[3], although little difference exists using the series or parallel model.

A second heat transfer method was also investigated which calculated the thickness of the skin that was frozen against the wall during the filling of the mold. Data for this method was generated by varying the mold temperature. While this method will be discussed later in this section, the data will be presented in the figures where the flexural modulus is compared to the Graetz number. This method of presentation should indicate if the modulus is dependent on the mold temperature.

The relationship between the flexural modulus and the Graetz number for plaques of 1.0 mm thickness is shown in Fig. 4-12. The flexural modulus increases from approximately 3.5 to 5 GPa as the Graetz number increases. At a Graetz number around 10 to 17, maximum flexural moduli are obtained. Little difference is observed between the properties of the 1.0 mm thick plaques made at the three different mold temperatures. This indicates that freezing of the skin layer during mold filling is not significantly affecting the mechanical properties.

The trend for the 1.5 mm thick plaques is opposite to the trend for the 1.0 mm thick plaques. For the 1.5 mm thick plaques, higher moduli occur with a decrease in the Graetz number as shown in Fig. 4-13. The maximum moduli occur for a Graetz number around 5 to 8. The same trend occurs for the moduli for plaques of 2.3 mm thickness as shown in Fig. 4-14 where the moduli significantly increase as the Graetz number decreases. The maximum moduli occur for a Graetz number around 5 to 12 which is similar the value of the Graetz number where maximum properties were obtained for the 1.5 mm thick plaque. In Figures 4-12 and 4-14, the change in mold temperature does not significantly affect the flexural modulus. Thus, it appears that mold temperature changes used in this study do not significantly change the LCP structure at the skin.

Table 4-6 Thermal properties for PP [46], VA [47], and PP(MAP)/VA 70(10)/30 estimated from series model [3].

	PP[1]	VA[2]	PP(MAP)/VA
Density (kg/m^3)	930	1400	1071
Thermal Conductivity (W/mK)	0.117	0.322	0.136
Thermal Diffusivity (10^8 m^2/s)	7.0	6.4	6.86

[1] Data for 25°C. [2] Data for 250°C.

The commonality among the moduli of plaques of different thickness versus the Graetz number can be observed in Fig. 4-15 for plaques made at a mold temperature of 50°C. This figure reproduces a portion of the data that was presented in Figures 4-12 to 4-14 to illustrate a common feature. At first since the trends are again opposite for the 1.0 mm thick plaques versus the 1.5 and 2.3 mm thick plaques, there appears to be no relationship between the flexural modulus and the heat transfer. It should be pointed out though that the flexural modulus changes from lower to higher properties for the three plaques of different thicknesses over a narrow range of the Graetz number (near a value of 10). This indicates that the transient temperature profiles are similar when the mechanical property changes occur.

The cooling behavior for VA, shown in Fig. 4-9, may be responsible for the sensitivity of the mechanical properties to the Graetz number. At a 295°C melt temperature, VA appears to be near a solid-like state. It is believed that VA is undergoing solidification in the molds when the Graetz number falls below 10. At a Graetz number above 10, VA remains in a molten state.

The difference between obtaining higher moduli at Graetz numbers below 10 versus obtaining higher moduli above a Graetz number of 10 may be related in part to the different stresses and rate of deformations that exist in filling the three molds of different thicknesses. As shown in section 4.3.1 and 4.3.2, both mechanical property differences and morphological differences exist between the plaques formed under high stresses in the 1.0 mm thick mold and plaques formed under low stresses in the thicker 1.5 and 2.3 mm molds. It is speculated that for $Gz > 10$ in the 1.0 mm mold, VA is in a molten state that permits rapid deformation at the advancing front where large extension rates exist. In the thicker molds, slower rates of deformation occur and for $Gz < 10$, VA is able to deform followed by rapid solidification upon

cessation of flow.

It is appears doubtful because of the complex behavior of the flexural modulus versus the stress and Graetz number that the molds could be scaled to different thicknesses and yield the same properties. For instance, by increasing the stress in the thicker plaques, the same properties that where obtained in the 1.0 mm thick would not be achieved in the thicker plaques because of changes in the stress and heat transfer that are not similar. By increasing the stress in the thicker mold, the Graetz number would no longer be equivalent to the Graetz number that existed in the thinner mold, and the point where solidification occurs would be shifted thus changing the reinforcing morphology. The cooling of the plaques of different thicknesses upon cessation of flow would also be different, thus, leading to differences in morphology and properties. This latter point can be illustrated by examining the solution of the heat conduction equation for the temperature in a slab [13]. The calculation of the temperature in a slab should closely approximate the temperature within a plaque during the cooling stage. As an example, for a slab initially at 295°C, the temperature reaches 200°C at one third the distance into the slab after 0.25 and 1.4 seconds for slabs of 1.0 and 2.3 mm thickness, respectively. While these are relatively short times, the morphology may still relax or undergo interfacial instabilities that cause breakup [45,43] thereby resulting in reduced moduli in the thicker plaques. Thus, unique properties and morphologies will be created in different molds for TP/LCP blends. However, a common condition for obtaining the optimum properties from any thickness plaque appears to be that the LCP is processed near a $G' - G''$ crossover point coupled with filling conditions that create a long fibrous morphology near the skin of the plaque.

The second heat transfer analysis mentioned above is the calculation of the thickness of polymer frozen at the mold wall during the filling of the mold. The calculated frozen skin layer

has been related to the flexural moduli for both TP matrices [41] and neat LCPs [42]. As performed by others [41,42], this analysis is undertaken by varying the melt and/or mold temperature. Because VA is just melted at 295°C and PP degrades rapidly above 295°C the melt temperature was not varied. Instead, the mold temperature was set at three different values to provide a variation in the frozen skin layer. The equation for calculation of the frozen layer thickness as derived by Dietz is shown below.

$$d=2\left(\frac{T_s-T_w}{T_m-T_w}\right)(\alpha t_c)^{1/2} \tag{4-3}$$

where d is the frozen layer thickness, Ts, Tw, and Tm are the solidification, wall, and melt temperatures, respectively. This equation may be made dimensionless by the substitution of ½L/U for the contact time, t_c, of polymer in the center of the mold, and by using the definition for the Graetz number. These substitutions lead to the form of this equation used in this work.

$$\frac{d}{H}=2^{\frac{1}{2}}\left(\frac{T_s-T_w}{T_m-T_w}\right)(Gz)^{-1/2} \tag{4-4}$$

Analysis of the data with this approach did not show the same relationship between flexural modulus and the frozen layer thickness for any two sets of data [12]. The reason for the lack of fit of this model may indicate that the skin region is not being greatly modified. Indeed, the flexural modulus does not change as the mold temperature is changed thereby supporting the supposition that the skin region is not modified by mold temperature. Instead, the subskin region may be undergoing more change then the rapidly solidified skin. Some insight into this possibility can be obtained by examination of the steady state solution of the Graetz-Nusselt problem for power law fluid [2]. This is the steady state solution for the simplified model proposed in the Appendix. For a Graetz number of 10 and a dimensionless thickness (y/H) and

length (z/L) of 0.447 and 0.5, respectively, the dimensionless temperature (Θ), is calculated to be 0.9. The actual melt temperature at this point for mold temperatures of 20 and 70°C are 267.5 and 272.5°C, respectively. Thus, the inner half of the mold is still relatively hot and not effected by a 50°C change in the mold temperature. For the transient case that occurs during mold filling, hot melt would be expected over a wider region than occurs in the steady state case indicating that the mold temperature would have even less influence on the temperature over a wide region in the center of the mold. Thus, the lack of influence of the mold temperature on the flexural modulus indicates that changes in structure are not occurring in the skin and the flat temperature profile in the core indicates that the structural changes are not occurring in the core. However, large temperature gradients can occur in the subskin, and this is the region in which large structural changes where observed in Figures 4-6 and 4-7. In fact, from the steady state solution it can be observed that a change in Graetz number is associated with large changes in the temperature profile in the subskin region. It is expected that the LCP passing through the advancing front at a temperature near to the melt temperature cools quickly upon leaving the front. The actual temperature history that the deformed LCP undergoes probably leads to differences in the resulting morphology and mechanical properties, and this temperature history is greatly influenced by the Graetz number.

4.4 Conclusions

In this study it has been shown that the mechanical properties of these blends are sensitive to both the injection speed and the mold thickness. The flexural modulus of the blend increases as the mold thickness decreases in a manner parallel to the change in the flexural modulus of neat

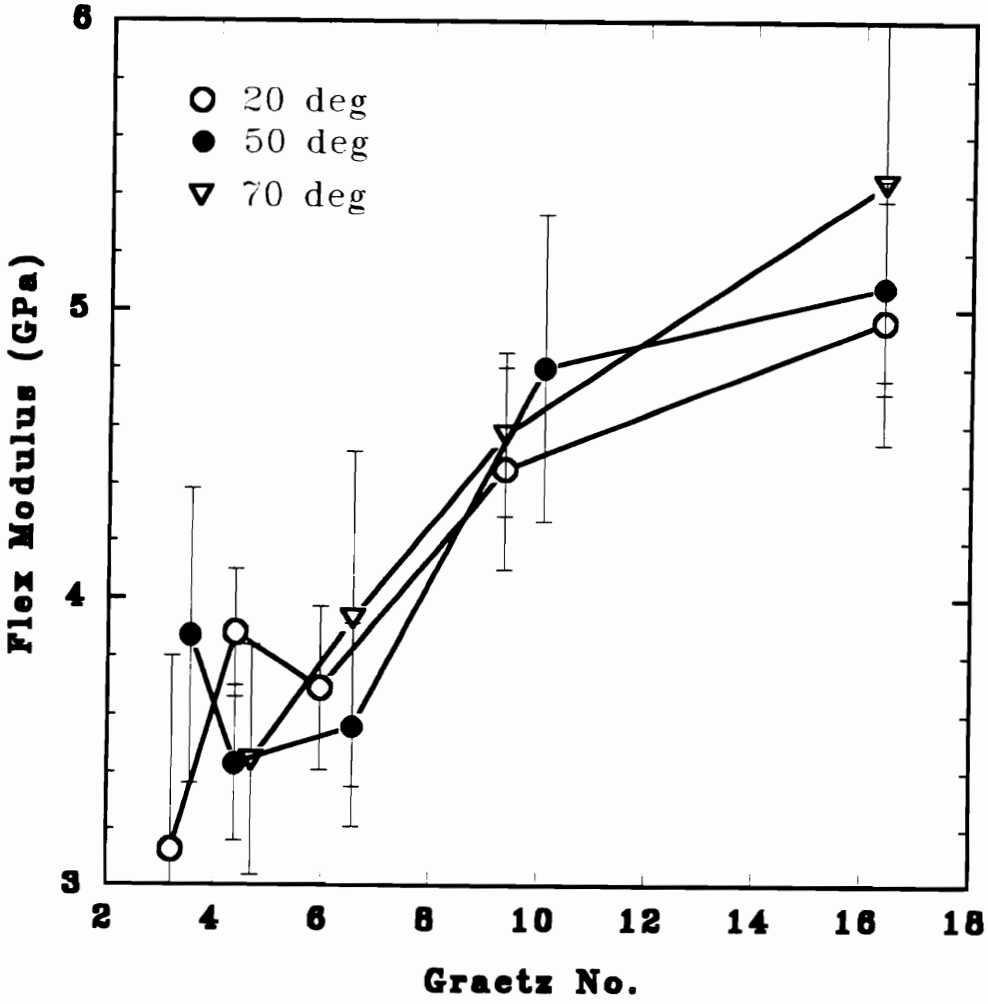

Fig. 4-12 Flexural modulus versus Graetz number for 1.0 mm thick plaques of PP(MAP)/VA 70(10)/30 molded at 20, 50, and 70°C mold temperatures.

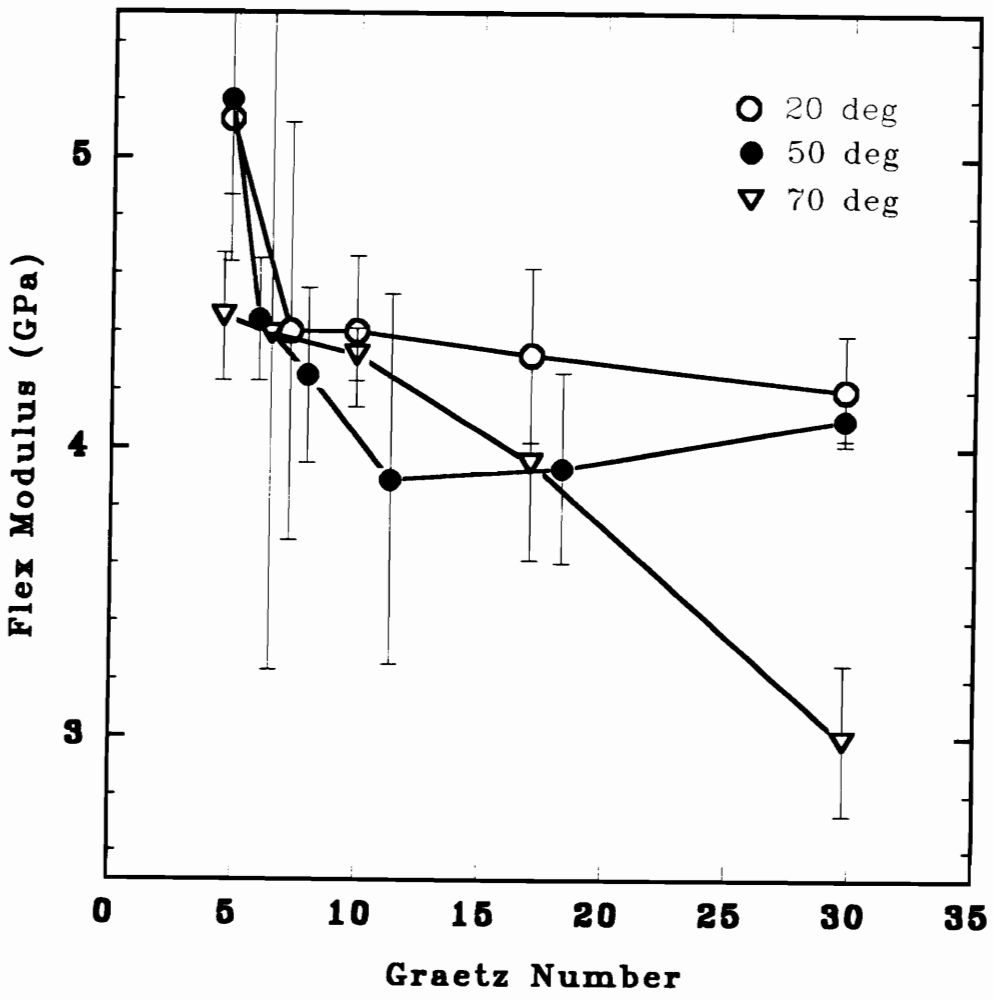

Fig. 4-13 Flexural modulus versus Graetz number for 1.5 mm thick plaques of PP(MAP)/VA 70(10)/30 molded at 20, 50, and 70°C mold temperatures.

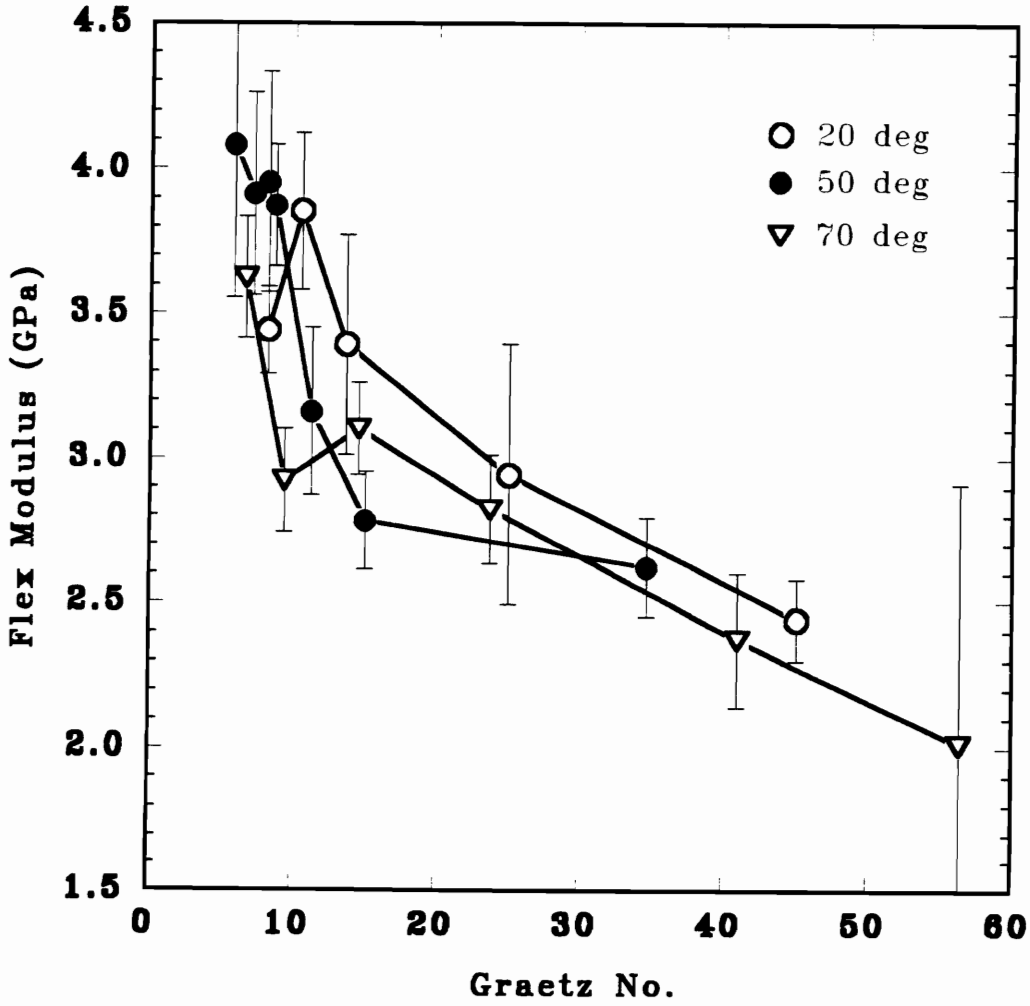

Fig. 4-14 Flexural modulus versus Graetz number for 2.3 mm thick plaques of PP(MAP)/VA 70(10)/30 molded at 20, 50, and 70°C mold temperatures.

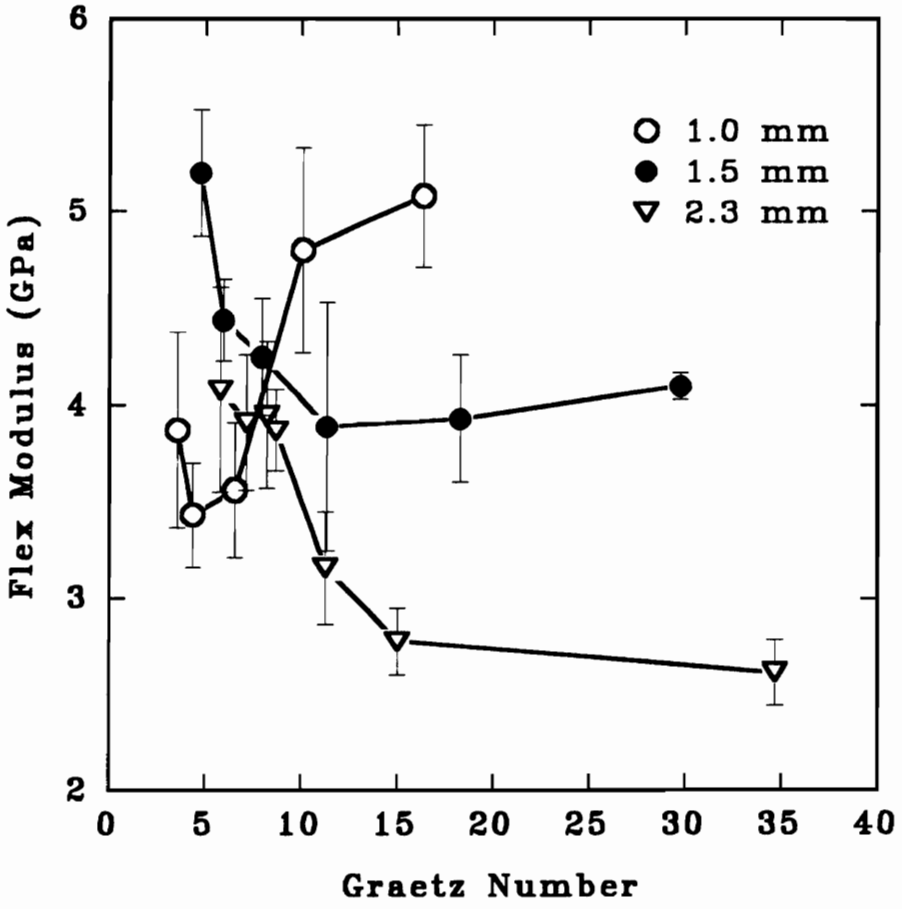

Fig. 4-15 Flexural modulus versus Graetz number for 1.0, 1.5, and 2.3 mm thick plaques of PP(MAP)/VA 70(10)/30 molded at 50°C mold temperatures.

VA as the mold thickness is decreased. The flexural modulus of the blend in the three molds of different thicknesses either meets or exceeds the flexural modulus calculated from the rule of mixtures. Thus, there is an advantage of using this blend in thinner molds. It has also been shown that the injection speed is a critical variable that influences the mechanical properties of these blends. A narrow range of fill times were found where optimum mechanical properties were obtained. However, there was no consistency among the relationships between the modulus and the fill time for the three molds. The optimum properties were obtained at short times for the thin molds and long times for the thicker molds.

Relating the mechanical properties to dimensionless groups which are related to droplet deformation and heat transfer did not lead to a finding a single mechanism that controls the structure and properties of the blends. It was presumed that reinforcement of the matrix should occur as the stress increases leading to large deformation of the LCP phase. However, reinforcement of the matrix occurred at high stresses in the 1.0 mm thick mold and at low stresses in the thicker (1.5 and 2.3 mm) plaques. Thus, there was not a consistent relationship between stress and the mechanical properties. Correlating the flexural moduli to the Graetz number also failed to demonstrate that the optimum properties occur at the same heat transfer condition.

While there was no consistent relationship of the flexural moduli with heat transfer, there was a similarity at the point where the flexural moduli changed from low to high moduli for all three molds. This transition occurred at a Graetz number of 10. For the thinner plaques, the higher moduli occurred when molding was performed with a Graetz number greater than 10. Contrarily, for the thicker plaques, the transition in moduli occurred when the Graetz number was less than 10. It was speculated that VA undergoes solidification during mold filling for a Graetz

number below 10. In the slow filling of the thicker molds the LCP deforms and quickly solidifies. However, in the thinner molds the velocities are much greater, and the LCP must remain fluid-like to undergo the higher rate of deformations that occur in the advancing front. Consequently, the Graetz number must be above 10 to permit rapid deformation. This study indicates that the morphology and mechanical properties will be different in every mold having a different thickness. This is attributable to the differences in the stresses and heat transfer that occur during the filling stage as well as the cooling and freezing that occurs during the cooling stage. For this blend it does appear that optimum mechanical properties can be found by changing the injection molding variables so that the Graetz number is in the vicinity of 10. In the future, studies will be conducted to examine the influence of similar variables on the mechanical properties of two other LCP blends [10,11] in an attempt to find common factors that influence the mechanical properties of injection molded PP/LCP blends.

4.5 Acknowledgements

This work was supported by the Army Research Office (grant number DAAL03-91-G-0166), and their support is sincerely appreciated.

4.6 Appendix A: Equation of Motion and Energy for Injection Molding

The simplified equations of motion and energy for the mold filling stage of injection molding is presented in this section. Since the molds used in this study have a film gate, the velocity has only two components, an down channel velocity that transports polymer into the mold and a transverse component that is large only at the advancing front. By neglecting the fountain flow at the advancing front, the velocity vector may be simplified to one component: the down channel velocity component. This simplification has been used by others in modeling nonisothermal one-dimensional flow into cold molds [33,34,35,36,37]. The equation of motion and energy as well as the power law constitutive equation are shown below.

$$\rho \frac{\partial u}{\partial t} = \frac{\partial \tau_{zy}}{\partial y} - \frac{\partial P}{\partial z} \tag{4A-1}$$

$$\rho C_p \left(\frac{\partial T}{\partial t} + u \frac{\partial T}{\partial z}\right) = k\left(\frac{\partial^2 T}{\partial y^2} + \frac{\partial^2 T}{\partial z^2}\right) + \tau_{zy} \frac{\partial u}{\partial y} \tag{4A-2}$$

$$\tau_{zy} = m\left(\left|\frac{\partial u}{\partial y}\right|\right)^{n-1} \frac{\partial u}{\partial y} \tag{4A-3}$$

where z is the down channel direction, and y is the mold thickness direction with the origin on the center line of the mold. Since semicrystalline polymers can undergo crystallization near the cold mold, this phenomena could also create differences in the microstructure. However, due to the complexities of nonisothermal crystallization and the need to kept this analysis simple, this phase change will not be considered. It is anticipated that crystallization will be more important in the packing and cooling stage in any event. After substituting the power law constitutive equation into the equations of motion and energy, these equations can be converted into

dimensionless form by the following substitutions:

$$\upsilon = u/U;\ \ \xi = y/H;\ \ \zeta = (H/L)(z/H);\ \ \tau = (U/L)t;\ \ \Pi = (L/H)(\eta_0 U/H)P$$

In the above, U is the average velocity, H is the half height of the mold, L is the mold length and η_0 is defined as $m(U/H)^{n-1}$. These substitutions will permit analysis with a few dimensionless numbers as shown below.

$$Re\frac{\partial \upsilon}{\partial \tau} = \frac{\partial}{\partial \xi}\left(\left|\frac{\partial \upsilon}{\partial \xi}\right|^{n-1}\frac{\partial \upsilon}{\partial \xi}\right) - \frac{\partial \Pi}{\partial \zeta} \tag{4A-4}$$

$$Gz\left(\frac{\partial \Theta}{\partial \tau} + \upsilon\frac{\partial \Theta}{\partial \zeta}\right) = \frac{\partial^2 \Theta}{\partial \xi^2} + \frac{H}{L}\frac{\partial^2 \Theta}{\partial \zeta^2} + Br\left|\frac{\partial \upsilon}{\partial \xi}\right|^{n-1}\frac{\partial \upsilon}{\partial \xi} \tag{4A-5}$$

where the Re is a modified Reynold number, $\rho UH^2/\eta_0 L$, Gz is the Graetz number, $UH^2/\alpha L$, Br is the Brinkman number, $\eta_0 U^2/k\Delta T$, and α and k are the thermal diffusivity and conductivity, respectively. Equations (4A-4) and (4A-5) may be simplified considerably by evaluating the values of these dimensionless numbers and neglecting terms where the dimensionless number is much less than unity. The thermal properties of PP and VA are given in Table 4-5. The thermal properties for the blend are estimated from the individual components properties by a series model [2] although little difference exists between estimates using the series or the parallel model. For a nominal condition, the following values are typical: U=0.10 m/s, $H=0.75\times10^{-4}$ m, and $L=7.6\times10^{-2}$ m. Using these values, the modified Reynolds number is much less than unity. Hence, the equation of motion can be treated as a psuedo-steady state problem. The Graetz number which indicates the magnitude of convective heat transfer in the down channel direction versus the conductive heat transfer in the transverse direction is greater than unity and hence must be retained. The second term on the right hand side may be neglected because of the high mold

aspect ratio. Finally, the Brinkman number which indicates the magnitude of heat generation versus heat conduction is much less than unity and therefore, the last term in the energy equation may be neglected. This leaves only one dimensionless number, the Graetz number, and the temperature will be uniquely specified for given dimensionless coordinates and time by the Graetz number.

$$0 = \frac{\partial}{\partial \xi}\left(\left|\frac{\partial \upsilon}{\partial \xi}\right|^{n-1}\frac{\partial \upsilon}{\partial \xi}\right) - \frac{\partial \Pi}{\partial \zeta} \tag{4A-6}$$

$$Gz\left(\frac{\partial \theta}{\partial \tau} + \upsilon\frac{\partial \theta}{\partial \zeta}\right) = \frac{\partial^2 \theta}{\partial \xi^2} \tag{4A-7}$$

It should be realized that these equations are coupled through the viscosity. As a first approximation, the viscosity will be assumed independent of temperature, an assumption used by others for simplification of the problem [38,39,40,41]. This approximation uncouples the equations. The result is a Graetz-Nusselt problem for a power law fluid. A steady state solution for this problem has been presented by Richardson [2].

Now these simplified equations can be considered when the mold thickness and injection speeds are varied. From the substitutions used to obtain the dimensionless variables it can seen that the mold aspect ratio is intimately involved in these equations. In fact, from similarity analysis, if one were interested in scaling up a mold, it would be preferred to use the same aspect ratio for each mold and thereby maintain the same stress and residence time. However, practical problems may exist with the fitting of different length molds on the same injection molder.

The shear stress, residence time, and Graetz number can be compared for molds of the same aspect ratio and for molds of the same length. The shear stress for flow between parallel plates can be derived from the above equation of motion as outlined by Middleman [1] yielding

the following expression for the shear stress.

$$m[\frac{U}{H}(\frac{1+2n}{n})]^n \ (\frac{y}{H}) \qquad \text{(4A-8)}$$

The residence time in the mold is given by L/U. These expressions indicate that the stress and residence time in geometrically similar molds will be identical. However, comparison to the Graetz number, $UH^2/\alpha L$, indicates that either the Graetz number can be maintained similar or the stress and residence time, but not both. In the molds to be studied, the mold length is maintained constant, and hence, only one of these three variables can remain constant. For this situation, the resident time scales with 1/U, the stress scales with U/H, and the Graetz number scales with UH^2. Thus, if one of these three variables significantly controls the structure and properties of these blends, it should be observable from the range of variables studied.

4.7 Appendix B: Strain in Fountain Flow

The rise in flexural moduli with decreased mold thickness is a relationship which has not been explained in the literature. It is desired to determine if the mold aspect ratio or thickness may be responsible for this relationship. One method to determine if the fountain flow is affected by these variables is to derive the relationship between strain and the mold geometry. Strain is taken as the important parameter that is related to the modulus of LCPs based on prior research [16,18,19].

The strain may be calculated from a continuum mechanics viewpoint with the use of the finite strain tensor [4] which is shown below

$$\gamma_{ij}^{[0]} = \sum_{m=1}^{3} \frac{\partial x_m}{\partial x_i} \frac{\partial x_m}{\partial x_j} - \delta_{ij} \tag{4B-1}$$

where $\partial\vec{x}'$ is a differential material vector representing the length and orientation of material at time t′ while $\partial\vec{x}$ is the deformed differential material vector at time t. As discussed in reference [5], the change in the squared length of the material between time t′ and t can be obtained from the finite strain tensor

$$\partial\vec{x} * \partial\vec{x} - \partial\vec{x}' * \partial\vec{x}' = \partial\vec{x}' * \vec{\gamma}^{[0]} * \partial\vec{x}' \tag{4B-2}$$

The strain may then be found from the above by dividing it by the square of the initial length yielding the following relationship

$$\left(\frac{\partial\vec{x} * \partial\vec{x} - \partial\vec{x}' * \partial\vec{x}'}{\partial\vec{x}' * \partial\vec{x}'}\right)^{1/2} = (\partial\vec{n} * \vec{\gamma}^{[0]} * \partial\vec{n})^{1/2} \tag{4B-3}$$

where ∂n is a unit vector oriented in the direction of ∂x′. The term on the left hand side is the engineering strain. Thus, the strain is related to the finite strain tensor. Calculation of the finite

strain tensor will indicate if the mold thickness or aspect ratio effect the strain.

The starting point to calculate the finite strain tensor is to derive the displacement functions $\vec{x}=\vec{x}(\vec{x}',t',t)$ [4]. The kinematics for fountain flow are given by Tadmor as

$$\begin{aligned} v_x &= -\dot{\epsilon}x \\ v_y &= \dot{\epsilon}y \\ v_z &= 0 \end{aligned} \tag{4B-4}$$

This may be transformed into polar coordinates as outlined in reference [4] to yield the following relationship

$$v_r = -\dot{\epsilon}\, r \cos\theta \tag{4B-5}$$

$$v_\theta = \dot{\epsilon}\, r \sin 2\theta \tag{4B-6}$$

The displacement functions in polar coordinates may now be obtained by integrating equations (4B-5) and (4B-6) to obtain

$$r = -r' \exp(-\cos 2\theta\ \epsilon(t,t')) \tag{4B-7}$$

$$\tan\theta = \tan\theta' \exp(2\ \epsilon(t,t')) \tag{4B-8}$$

where

$$\epsilon(t',t) = \int_{t'}^{t} \dot{\epsilon}(t'')\, dt'' \tag{4B-9}$$

At this point the strain rate is required. It is this term which introduces any geometric dependence of the strain to the mold geometry. Again from Tadmor's analysis, the strain rate for a power law fluid is given by

$$-\dot{\epsilon} = U\frac{n}{4(1+n)H} \tag{4B-10}$$

and performing the integration indicated in equation (4B-9), the Hencky strain is obtained

$$-\epsilon = \frac{Un(t-t')}{4(1+n)H} \tag{4B-11}$$

If (t-t′) equals the time a particle spends in the fountain flow then as suggested by Tadmor, this time equals (or is at least proportional to) 2H/U. This yields another form of the Hencky strain

$$-\epsilon = \frac{n}{2(1+n)} \tag{4B-12}$$

which is independent of either mold thickness or aspect ratio. At this point, the finite strain tensor and the strain can be calculated. However, since the objective of this analysis was to determine if a geometric dependence existed, it is now clear that the strain in the fountain flow is independent of mold thickness or aspect ratio, and a full solution for the strain in not required.

4.8 References

1. S. Middleman, Fundamentals of Polymer Processing, McGraw Hill, New York (1977).
2. S.M. Richardson, "Extended Leveque Solution or Flows of Power Law Fluids in Pipes and Channels," Int. J. Heat Mass Transfer, 22, 1417 (1979).
3. M.O.W. Richardson, Polymer Engineering Composites, Applied Science Publishers, London, 1977.
4. R.B. Bird, R.C. Armstrong, and O. Hassager, Dynamics of Polymeric Liquids, Vol 1, John Wiley & Sons, New York, 1987.
5. D. Frederick and T.S. Chang, Continuum Mechanics, Scientific Publishers, Cambridge, 1972.
6. H.J. O'Donnell, A. Datta, D.G. Baird, "The Effect of Compatibilization on the Properties of Blends of TLCPs with Polypropylene," Annual Technical Conference of the Society of Plastic Engineers (ANTEC'92), 50, 2248 (1992).
7. A. Datta, "The Effect of Compatibilization on Blends of Polypropylene with a Liquid Crystalline Polymer," Polymer 34(4), 759 (1993).
8. A. Datta "Compatibilization of Thermoplastic Composites Based on Blends of Polypropylene with Two Liquid Crystalline Copolyesters," submitted to Polymer.
9. H.J. O'Donnell, H.H. Chen and D.G. Baird, Annual Technical Conference of the Society of Plastic Engineers (ANTEC '93) 51, 1711 (1993).
10. H.J. O'Donnell and D.G. Baird, "The Effect of Injection Molding Conditions on the Mechanical Properties of an In Situ Composite: II. Polypropylene and a poly(ester-amide) LCP" submitted to International Journal of Polymer Processing.
11. H.J. O'Donnell and D.G. Baird, "The Effect of Injection Molding Conditions on the Mechanical Properties of an In Situ Composite: III. Polypropylene and a Copolyester LCP Based on PET/PHB," submitted to International Journal of Polymer Processing.
12. H.J. O'Donnell, Ph.D. Dissertation, Virginia Polytechnic Institute and State University, Blacksburg, VA, 1994.
13. J.P. Holman, Heat Transfer, 4th ed., McGraw Hill, New York (1976).
14. G.I. Taylor, "The Formation of Emulsions in Definable Fields of Flow," Proc. Roy. Soc., A146, 501 (1934).
15. W.J. Jackson and H.F. Kuhfuss, J. Polym. Sci., Polym. Chem. Ed., 14, 2043 (1976).
16. Y. Ide and Z. Ophir, "Orientation Development in Thermotropic Liquid Crystal Polymers," Poly. Eng. Sci., 23(5), 261 (1983).
17. T-S. Chung, "Production of Ultrahigh Modulus Liquid Crystal Polymer Rods," J. Polym. Sci.: Part B: Polym. Phys., 26, 1549 (1988).
18. S. Kenig, "Orientability of Liquid Crystal Polymers in Elongational Flow," Poly. Eng. Sci., 27(12), 887 (1987).
19. S. Kenig, "Shear-Induced Orientation in Liquid Crystalline Polymers," Poly. Eng. Sci., 29(16), 1136 (1989).
20. M.R. Nobile, E. Amendola, and L. Nicolais, "Physical Properties of Blends of Polycarbonate and a Liquid Crystalline Copolyester," Polym. Eng. Sci., 29(4), 244

(1989).
21. D. Dutta, H. Fruitwala, A. Kohli, and R.A. Weiss, "Polymer Blends Containing Liquid Crystals: A Review," Polym. Eng. Sci., 30(17), 1005 (1990).
22. B.R. Bassett and A.F. Yee, "A Method of Forming Composite Structures Using In Situ-Formed Liquid Crystal Polymer Fibers in a Thermoplastic Matrix," Poly. Eng. Sci., 11(1), 10 (1990).
23. F.P. La Mantia, M. Saiu, A. Valenza, M. Paci, and P.L. Magagnini, "Relationships Between Mechanical Properties and Structure for Blends of Nylon-6 with a Liquid Crystal Polymer," Eur. Polym. J., 26(3), 323 (1990).
24. K.G. Blizard, C. Federici, O. Federico, and L.L. Chapoy, "The Morphology of Extruded Blends Containing a Thermotropic Liquid Crystalline Polymer", Poly. Eng. Sci., 30(22), 1442 (1990).
25. D. Beery, S. Kenig, And A. Siegmann, "Structure Development During Flow of Polyblends Containing Liquid Crystalline Polymers," Poly. Eng. Sci., 31(6), 451 (1991).
26. K.G. Blizard and D.G. Baird, "The Morphology and Rheology of Polymer Blends Containing a Liquid Crystalline Copolyester," Poly. Eng. Sci., 27(9), 653 (1987).
27. G. Crevecoeur, "In-Situ Composites, Blends of Thermotropic Liquid Crystalline Polymers in a Thermoplastic Matrix," Ph.D. Dissertation, Katholieke Universiteit Leuven, Holland, 1991.
28. D.G. Baird, T. Sun, D.S. Done, and G.L. Wilkes, "In Situ Formation of Reinforced Thermoplastic Composites," J. Thermoplastic Composite Materials, 3,81 (1990).
29. R.H. Olley, D.C. Basset, and D.J. Bludell, Polymer, 27,344 (1986).
30. F. Gauthier, H.L. Goldsmith, and S.G. Mason, "Particle Motions in NonNewtonian Media. II Poiseuille Flow," Trans. Soc. Rheol., 15(2), 297 (1971).
31. R.A. Dickie "Mechanical Properties of Multiphase Polymer Blends," in Polymer Blends, Vol. 1, D.R. Paul and S. Newman, Ed., Academic Press, New York (1978).
32. Z. Tadmor, "Molecular Orientation in Injection Molding," J. Appl. Polym. Sci., 18, 1753 (1974).
33. D.H. Harry and R.G. Parrott, "Numerical Simulation of Injection Mold Filling," Polym. Eng. Sci., 10, 209 (1970).
34. G. Williams, and H.A. Lord, "Mold Filling Studies for the Injection Molding of Thermoplastic Materials. Part I," Polym. Eng., 15(8), 553 (1975).
35. G. Williams, and H.A. Lord, "Mold Filling Studies for the Injection Molding of Thermoplastic Materials. Part II," Polym. Eng., 15(8), 569 (1975).
36. J.L. Berger and C.G. Gogos, "A Numerical Simulation of the Cavity Fillihg Process with PVC in Injection Molding," Polym. Eng. Sci., 12, 102 (1973).
37. P.C. Wu, C.F. Huang, and C.G. Gogos, Polym. Eng. Sci., 14, 223 (1974)
38. H. Janeschitz-Kriegl, "Injection Moulding of Plastics II. Analytical Solution of Heat Transfer Problem," Rheol. Acta, 18, 693 (1979).
39. S.M. Richarson, "Injection Moulding of Thermoplastics. II. Freezing Off in Cavities," Rheol. Acta, 24, 509 (1985).
40. K.M.B Jansen and J. van Dam, "An Analytical Solution for the Temperature Profiles During Injection Molding Including Dissipation Effects," Rheol. Acta, 31, 592 (1992).
41. W. Dietz, J.L. White, and E.S. Clark, "Orientation Development and Relaxation in Injection Molding of Amorphous Polymers," Polym. Eng. Sci., 18(4), 273 (1978).

42. S.K. Garg and S. Kenig, "Development of Orientation During Processing of Liquid Crystalline Polymers," in High Modulus Polymers, A.E. Zachariades, R.S. Porter, Eds., Marcel Dekker; New York, 1988: pg. 71.
43. J.J. Elmendorp, "Dispersive Mixing in Liquid Systems," in Mixing in Polymer Processing, C. Ramwendaul, Ed., Marcel Dekker, New York, 1991.
44. P.H.M. Elemans, "Modelling of the Processing of Incompatible Polymer Blends," Ph.D. Dissertation, Univ. of Eindhoven, Eindhoven, Netherlands, 1989.
45. S. Tomotika, "On the Instability of a Cylindrical Thread of a Viscous Liquid Surrounded by Another Viscous Fluid," Proc. Roy. Soc., 150, 322 (1935).
46. Modern Plastic Encyclopedia, McGraw Hill, New York, 1991.
47. Private communications with Hoescht Celanese Technical Service.
48. A.M. Sukhadia, "The In-Situ Generation of Liquid Crystalline Polymer Reinforcements in Thermoplastics, Ph.D. Dissertation, Virginia Tech, Blacksburg, 1991.

5.0 The Effect of Injection Molding Conditions on the Mechanical Properties of an In Situ Composite: II. Polypropylene and a Liquid Crystalline Copoly(ester-amide) [1]

5.1 Introduction

Reinforcement of thermoplastic (TP) resins with liquid crystalline polymers (LCPs) is a relatively new type of polymer blend. When the blend is processed in a manner to create a reinforcing fibrous LCP structure within the TP matrix, the resulting tensile properties are improved, and the material is termed an in situ composite. The key to obtaining this reinforcing fibrous structure in TP/LCP blends is in the process. Several studies have related the capillary extrusion process to the resulting properties of strands [15-22]. The findings from these studies vary on a case by case basis. Often, it is found that the drawing of strands leads to fibrous morphologies and greatly increased moduli [15,16,18]. In some studies, it was found that drawing was not effective in increasing the modulus of strands [17,22,19]. Two reasons were found for why drawing did not increase the modulus. First, a fibrous morphology may be created upon entering the die and no further increase in fibrillation occurs with drawing [17,22]. Second, a fibrous morphology may not occur because the LCP solidifies before significant drawing occurs [19]. The melt temperature has also been shown to affect mechanical properties and morphology. A fibrous morphology and higher mechanical properties were found when a TP/LCP blend was processed near the melting point of the LCP. When the processing temperature was increased by 30°C, lower mechanical properties and a droplet morphology

[1]This chapter is being submitted to International Journal of Polymer Processing

occurred [15]. The above studies have indicated that deformation, flow field, and temperature are important factors that contribute to the formation of in situ composites.

While studies have been conducted on the capillary extrusion process, only one study has been conducted on the injection molding process. In this study, the effect of injection molding conditions on the mechanical properties of polypropylene (PP) with a liquid crystalline (LC) copolyester was investigated [7]. The fill time and mold thickness were found to be important variables that affected the flexural properties of the blend. It was found that the flexural modulus of the blend increased as the mold thickness decreased in a manner parallel to the behavior of LCPs. Comparison of the blend modulus to the modulus calculated from the rule of mixtures showed good agreement which indicated that the LCP was efficiently reinforcing the matrix. The relationship between the fill time and flexural modulus varied with the mold thickness. For the thinnest mold (1.0 mm) it was found that the modulus increased with a decreased fill time while for the thicker molds (1.5 and 2.3 mm) the modulus reached a maximum at longer fill times. The change in the flexural modulus with a change in fill time or mold thickness was related to solidification of the LCP.

It is of interest to determine if behavior similar to the processing / property relationships determined in the first paper for a PP / LC copolyester blend is duplicated in a PP / LC poly(ester-amide) [7]. This comparison will indicate if similar mechanisms lead to a fibrillar structure in both PP/LCP blends. However, a difference between the prior study and this study is the mixing of the blend. In a prior paper, it was shown that mixing prior to injection molding increased the tensile strength of the blend [6]. Since higher tensile strength is preferred, the blend was prepared by mixing in an extruder prior to injection molding samples.

The goal of this study is to determine if the mechanical properties of an injection molded

PP / LC poly(ester-amide) blend are sensitive to the injection molding conditions (i.e. injection time, mold temperature, and mold thickness). It is also desired to determine if the mechanical properties can be correlated to the dimensionless groups that relate to droplet deformation (Weber number) and the heat transfer (Graetz number) during the filling stage of injection molding. In the future, this work will be expanded to another PP / LC copolyester blend [8] in hopes of finding common mechanisms that control the formation of fibrillar morphologies and high mechanical properties in injection molded PP/LCP blends.

5.2 Experimental

5.2.1 Materials

The polypropylene (PP) used in this study was Profax 6823, a fractional melt flow index polymer, and it was purchased from Himont, Inc. The maleated PP was a development grade maleic anhydride grafted polypropylene (MAP) with a melt flow index of 50 supplied by BP Chemicals, Inc. This material was used because it enhances mechanical properties of the blend as discussed in prior publications [3-6]. The LCP was Vectra® B950 purchased from Hoescht Celanesse, and hereafter it will be referred to as VB. The LCP is a copoly(ester-amide) based on hydroxynaphthoic acid, terephthalatic acid, and aminophenol. The blend was composed of 70 wt% of PP/MAP mixture (containing 10 wt% MAP) and 30 wt% VB. It will be designated as PP(MAP)/VB 70(10)/30.

5.2.2 Rheology

The steady shear viscosity was determined using the Instron capillary rheometer (ICR)

with a single capillary of diameter 0.36 mm and a L/D ratio of 74. No end corrections were applied to the data but the wall shear rate was corrected by means of the well known Rabinowitsch method [2]. Because the test times were in excess of five minutes and an inert atmosphere was not available for the ICR, it is believed that significant degradation of PP/MAP occurred before completion of the tests performed at 295°C. Consequently, PP/MAP was tested at 250, 265 and 285°C and the viscosity was shifted to 295°C using an Arrhenius activation energy, E, of 88 kJ/mol. This value was obtained from a least squares regression where the intercept was not forced to zero so that a better correlation was obtained.

The rheological behavior for VB cooled from the melt temperature to temperatures below the melting point was determined on the Rheometrics Mechanical Spectrometer (RMS 800) in the oscillatory dynamic mode at a rotational frequency of 1 rad s^{-1}. Parallel plate fixtures with a diameter of 25.4 mm and a gap of approximately 1.5 mm were used for all tests. A nitrogen purge provided an inert atmosphere for all tests conducted on the RMS 800. The measurement was conducted by preheating the sample at the test temperature for five minutes followed by decreasing the temperature at a rate of 5°C per minute. The tests were stopped when the transducer torque approached the limit of the transducer.

5.2.3 Blend Preparation

The blend was prepared for injection molding by one of two methods. In one method dried pellets of extruded PP/MAP and dried pellets of VB were tumbled in a container to mix pellets immediately prior to injection molding. Samples prepared in this manner are termed tumbled blends. In another method, dried pellets of PP/MAP and VB were extruded in a Killian extruder having a 25.4 mm diameter screw with a L/D ratio of 24 and a 3:1 compression ratio.

The blend was extruded at 50 rpm with the barrel temperatures of 125, 290, 295°C and a die temperature 200°C. Samples prepared in this manner are termed premixed blends. Tumbled and premixed blends were made from 70 wt.% PP/MAP (with 10 wt.% MAP) and 30 wt.% VB. This material was dried prior to being injection molded.

5.2.4 Injection Molding

Injection molding was performed on an Arburg Allrounder, model 221-55-250. Three molds were used which produced 76 by 76 mm rectangular plaques of 1.0, 1.5, and 2.3 mm thicknesses. Each mold had a film gate which created two dimensional rectilinear flow throughout the cavity. These molds were equipped with heating rods to obtain either a 50 or 70°C mold temperature. The mold temperature was also lowered to 20°C by removing the heating rods and installing water lines for cooling. Temperatures were kept within ± 2°C. The injection molder barrel temperatures were set to 160°C in the first zone, 295°C in the second zone, and 295°C in the third zone while the nozzle temperature was set to 280°C. The injection pressure and hold pressure were set to 800 and 600 psi, respectively, for all runs. The injection speed setting was varied to obtain a range of injection times. The injection time was measured as the travel time for the screw to move from the retracted position to the fully injected position. The volumetric flow rate was calculated by assuming a constant screw injection speed and dividing the volume including the sprue and gate volume, 78.5 mm^3, by the fill time. The fill time is the time for polymer to flow from the entrance of the mold to the point where the mold is filled, and it was calculated from the injection time by subtracting the time the screw advances from the retracted position to the point where polymer began entering the mold. The time for the screw to travel from the retracted position to the pressurization point was approximately 35%

of the injection time. The average velocity within the mold was then calculated by dividing the volumetric flow rate by the cross sectional area of the mold.

5.2.4 Mechanical Testing

All samples were tested in the flexural mode, and selected samples were tested in the tensile mode on a Instron mechanical tester, model 4204. The specimens were prepared by cutting 10 by 76 mm long strips from the 76 by 76 mm plaques in either the machine or transverse direction followed by sanding to minimize the cutting marks. Tensile specimens were tested at a crosshead speed of 1.27 mm/min while flexural specimens were tested at a rate of 1.0 %/min. An extensiometer, Instron model 2630-25, was used for all tensile tests except for determination of the strength and elongation of neat PP. A minimum of five samples was tested, and the average value and standard deviation were calculated from the data.

5.2.6 Morphological Studies

Fracture surfaces of plaque samples obtained approximately 13 mm from the end of the plaque were prepared by cryogenic fracture in liquid nitrogen followed by coating with gold on a SPI sputter coater. Fracture surfaces were viewed on a Cambridge stereoscan S200 scanning electron microscope (SEM) using an accelerating voltage of 15 KeV. The plaques were fractured in the machine direction which provides a view along the flow direction. These plaque samples were etched in hypochloric acid as described by Olley et al. [23] for 15 minutes to better reveal the LCP morphology. All photomicrographs presented in this chapter were obtained from the SEM.

5.3 Results and Discussion

The mechanical properties of the premixed PP(MAP)/VB blend are presented and related to processing conditions. First, the mechanical properties versus injection times, mold temperatures, and mold thicknesses are presented. Second, the flexural modulus is related to the stress and heat transfer that exist during mold filling. Lastly, the processing / property relationships for this blend are compared to the relationships found in a prior study for the blend of PP and a LC copolyester.

5.3.1 Mechanical Properties of the Blend

The flexural and tensile properties of PP(MAP)/VB are presented in Tables 5-1 to 5-3. Both the flexural and tensile properties are presented because the flexural modulus is sensitive to the stiffness of the skin while the tensile modulus reflects the average stiffness of the cross sectional area. Thus, differences between the flexural and tensile modulus indicate differences between the skin and the core of a plaque. For in situ composites, flexural moduli that are higher than tensile moduli indicate that the skin is reinforced more efficiently than the core. It is expected in a study of the effect of processing conditions on the mechanical properties of an in situ composite that the flexural and tensile moduli may change to different degrees which reflect a different degree of change in the structure of the skin and core.

The flexural and tensile properties for 1.0 mm thick plaques of PP(MAP)/VB as function of injection time are shown in Table 5-1. The flexural modulus increased from 3.3 to 3.7 GPa as the injection time was decreased from 4 to 0.65 seconds. Similar changes occurred in the tensile modulus as the modulus increased from 2.86 to 3.39 GPa and the injection time decreased

from 4 to 0.65 seconds. Both flexural and tensile moduli increased to the same degree which indicated that the skin and core changed to the same degree. Little change occurred in the flexural and tensile strength as the injection time was varied.

The flexural and tensile properties for 1.5 mm thick plaques of PP(MAP)/VB as a function of injection time are shown in Table 5-2. The flexural modulus of the 1.5 mm plaques increased as the injection time was decreased. A plateau in the flexural modulus of approximately 4.8 GPa occurred at an injection time of 2.7 seconds. A similar trend occurred for the tensile modulus, but the tensile modulus reached a maximum of 4.74 GPa at 2.7 seconds then decreased to 4.18 GPa as the injection time decreased to 1.0 seconds. Based on the standard deviation, there may be little difference between these values and a plateau in the tensile modulus may exist. Little change occurred in the flexural strength as the injection time was varied, but the tensile strength decreased as the injection time increased. Comparison of the mechanical properties of the 1.0 and 1.5 mm thick plaque (Tables 5-1 and 5-2) indicate that the flexural and tensile moduli of the 1.5 mm thick plaque were approximately 1 GPa greater than the flexural and tensile moduli of the 1.0 mm thick plaque.

The flexural and tensile properties for 2.3 mm thick plaques of PP(MAP)/VB as function of injection time are shown in Table 5-3. There was a maximum in the flexural modulus of 4.86 GPa at 2.1 seconds, and the modulus decreased as the injection time was either increased or decreased. The tensile modulus also reached a maximum 4.31 GPa at 5 seconds. However, based on the standard deviations and calculation of confidence limits, it is possible that a plateau in the tensile modulus existed for all injection times that were less than 5 seconds. The flexural strength did not change with a change in the injection time, but the tensile strength decreased as the injection speed was increased beyond 7.7 seconds.

In all molds, similar processing / property relationships was found. The flexural modulus was greater than the tensile modulus, thus indicating that the LCP reinforced the skin preferentially over the core. The flexural and tensile modulus vary with injection time, and higher properties occurred at shorter injection times. The flexural strength was not significantly affected by the injection speed, and the tensile strength decreased as the injection time increased.

A difference between the properties of the blend made in these molds was that the modulus can change dramatically with mold thickness. The maximum flexural moduli in the 1.0, 1.5 and 2.3 mm thick plaques are 3.8, 5.1, and 4.9 GPa, respectively. Based on a study showing that the modulus of neat LCPs increases as the mold thickness decreases, the trend of the flexural modulus of the blend with mold thickness is unusual [12].

To investigate the efficiency of LCP reinforcement of the matrix, the flexural properties of neat polymers were obtained from plaques made in the three molds. The flexural moduli of the neat polymers were used in the rule of mixtures to predict the upper limit of the flexural modulus of the blend. The flexural moduli for neat VB as a function of mold temperature and mold thickness are shown in Table 5-4. The lowest moduli were obtained in the thickest plaque, 2.3 mm where the flexural moduli is approximately 19 GPa. For the 1.5 mm thick plaque, the modulus increased slightly to approximately 23 GPa. A much greater increase in the flexural modulus occurred in the 1.0 mm thick plaque. Here the flexural modulus is approximately 30 GPa. Thus, the flexural properties of neat VB increased with a decrease in mold thickness as found for other LCP [12,7]. The flexural properties for PP were reported in reference [7]. The flexural moduli for PP in a 2.3, 1.5, and 1.0 mm thick plaque are 1.4, 1.7, and 1.8 GPa, respectively. These values for the flexural moduli of PP and the values of the flexural moduli of neat VB made at a 50°C mold temperature were used to calculate the upper limit of the

flexural moduli of the blend from the rule of mixtures. This calculation yielded moduli of 5.4, 6.0, and 8.7 GPa for the blend of 2.3, 1.5, and 1.0 mm thick plaques, respectively. The maximum flexural properties for the blend reported in Tables 5-1 to 5-3 are 4.9, 5.1, and 3.8 GPa for the 2.3, 1.5, and 1.0 mm thick plaques, respectively. Only the modulus of the thickest plaque, 2.3 mm, is close to the modulus predicted from the rule of mixtures. The difference between predicted and actual modulus increases as the mold thickness decreases. This is in sharp contrast from the earlier study with a LC copolyester where the moduli of three different thickness plaques were approximately equal to the moduli calculated from the rule of mixtures [7]. The reason for inefficient reinforcement of the matrix is not known. However, based on a study with another LCP, the properties of the blend may be very sensitive to the viscosity ratio and the melt temperature [8]. A limited study of the effect of melt temperature is included later in this paper.

5.3.2 Morphology

The two phase structure of plaques with the highest and lowest moduli were examined to determine if a change in the morphology of the LCP phase can be correlated to the mechanical properties. The 1.0 and 2.3 mm thick plaques were examined to investigate the change in morphology of the thickest and thinnest plaques.

There are three factors which should affect the moduli in this composite-like structure. The first factor is the orientation of the LCP which leads to high modulus fibrils or ribbons. The second factor is the aspect ratio of the fibers or ribbons. From composite theory, a reinforcing fiber needs an aspect ratio of at least 100 in order to follow the rule of mixtures [22]. The third factor is the distribution of reinforcing LCP. If flow migration occurs, then higher or lower

Table 5-1 Machine direction mechanical properties of 1.0 mm plaques of premixed PP(MAP)/VB 70(10)/30 molded at various injection speeds (50°C mold temperature).

Injection Time (s)	Flex Modulus (GPa)	Flex Strength (MPa)	Tensile Modulus (GPa)	Tensile Strength (MPa)	Elongation at Yield (%)
.65	3.71 (.18)	54.2 (1.2)	3.39 (0.18)	31.9 (2.2)	1.51 (0.11)
1.4	3.82 (.18)	56.3 (1.6)	3.55 (0.13)	32.8 (0.6)	1.32 (0.19)
2	3.33 (.57)	53.6 (3.2)	3.28 (.10)	31.2 (0.7)	1.52 (0.12)
3	3.60 (.14)	54.8 (1.4)	3.20 (0.24)	29.5 (1.0)	1.40 (0.11)
4	3.30 (.26)	52.9 (2.6)	2.86 (0.38)	26.2 (2.4)	1.88 (0.79)

Table 5-2 Machine direction mechanical properties of 1.5 mm plaques of premixed PP(MAP)/VB 70(10)/30 molded at various injection speeds (50°C mold temperature).

Injection Time (s)	Flex Modulus (GPa)	Flex Strength (MPa)	Tensile Modulus (GPa)	Tensile Strength (MPa)	Elongation at Yield (%)
1	5.10 (.35)	60.5 (2.6)	4.18 (0.29)	36.5 (2.8)	1.25 (0.09)
2.1	4.54 (.23)	55.4 (2.0)	4.34 (0.24)	33.9 (1.5)	1.09 (0.13)
2.7	4.91 (.46)	55.9 (2.4)	4.74 (0.28)	34.3 (3.1)	0.94 (0.13)
4.1	4.06 (.19)	49.5 (1.3)	3.53 (0.18)	32.7 (1.2)	1.87 (0.49)
5	4.39 (0.07)	54.9 (1.3)	3.88 (0.10)	34.9 (1.0)	1.51 (0.18)
8.3	3.77 (0.13)	51.5 (1.4)	3.09 (0.19)	27.8 (1.0)	1.49 (0.15)
10.7	3.21 (0.15)	52.1 (1.6)	2.85 (0.18)	26.3 (1.6)	1.73 (0.87)

Table 5-3 Machine direction mechanical properties of 2.3 mm plaques of premixed PP(MAP)/VB 70(10)/30 molded at various injection speeds (50°C mold temperature).

Injection Time (s)	Flex Modulus (GPa)	Flex Strength (MPa)	Tensile Modulus (GPa)	Tensile Strength (MPa)	Elongation at Yield (%)
.8	3.90 (0.25)	51.6 (1.5)	3.90 (0.76)	36.4 (3.7)	1.35 (0.24)
1.35	4.61 (0.57)	54.5 (2.2)	4.13 (0.73)	34.2 (4.2)	1.15 (0.20)
2.1	4.86 (0.52)	61.7 (2.9)	4.25 (0.68)	36.5 (1.2)	1.24 (0.12)
3.1	4.42. (0.22)	58.9 (1.7)	3.96 (0.21)	36.5 (1.6)	1.25 (0.07)
5	4.45 (0.30)	56.0 (1.9)	4.31 (0.16)	35.0 (4.2)	1.05 (0.15)
7.7	3.90 (.32)	53.4 (.90)	3.77 (.20)	33.6 (2.8)	1.39 (.19)
12.4	3.41 (.20)	52.1 (1.9)	3.31 (.22)	30.2 (2.2)	1.57 (.20)
15.7	3.17 (.20)	53.2 (1.4)	3.28 (.38)	29.9 (1.5)	1.70 (.25)
20	2.91 (.12)	51.3 (1.4)	3.24 (.45)	26.2 (2.1)	1.61 (.29)

Table 5-4 Machine direction flexural properties for neat Vectra® B950 molded into three thicknesses and at three mold temperatures.

Thickness (mm)	Mold Temp (°C)	Modulus (GPa)	Strength (MPa)
1.0	20	29.2 (2.1)	311.1 (12.0)
	50	32.5 (3.4)	310.6 (60.7)
	70	29.3 (1.3)	316.6 (10.4)
1.5	20	27.5 (0.9)	308.8 (8.5)
	50	20.7 (1.2)	257.5 (10.4)
	70	23.1 (3.5)	257.7 (41.6)
2.3	20	20.3 (1.1)	244.6 (13.7)
	50	19.65 (1.26)	242.5 (10.7)
	70	16.5 (1.8)	212.5 (17.2)

flexural moduli could result depending upon the direction of migration of the reinforcing phase [24]. Examination of the morphology will concentrate on relating the LCP phase structure to the properties.

A photomicrograph of a fracture surface from a 1.0 mm thick plaque which was injection molded in 3.5 seconds with a mold temperature of 20°C is shown in Fig. 5-1. The flexural modulus of this plaque was 3.4 GPa, a low modulus for the 1.0 mm thick plaques. The entire cross sectional view of the plaque is shown in the top photomicrograph, Fig. 5-1a, and an enlargement of the skin/subskin region is shown in the bottom photomicrograph, Fig. 5-1b. While a fiber-like morphology is expected for a highly reinforced matrix, large pieces of VB that have not been deformed into high aspect fibrils are seen in Fig. 5-1b. Thus, the lower modulus may be the result of LCP that was not deformed into a fibrous morphology.

In Fig. 5-2, a photomicrograph of a fracture surface from a 1.0 mm thick plaque which was injection molded in 0.8 seconds with a mold temperature of 20°C is shown in Fig. 5-1. The flexural modulus of this plaque was 4.3 GPa, and this value was a maximum for the 1.0 mm thick plaques. The morphology of this plaque is significantly different from the morphology of the plaque shown in Fig. 5-1. A fiber-like morphology is observed in Fig. 5-2 which correlates with the higher modulus for this plaque. In Fig. 5-2a, a fibrous morphology is observed between the skin and the core. It is believed that this morphology is the reason for the higher modulus of this plaque.

A fracture surface from a 2.3 mm thick plaque that was injection molded in 12.4 seconds with a mold temperature of 50°C is shown in the photomicrograph of Fig. 5-3. The flexural modulus of this plaque was 3.4 GPa which was a low value for the 2.3 mm thick plaques. A wavy fibrous structure existed throughout much of the plaque as is shown in Fig. 5-3a. By

examining the skin / subskin region, Fig. 5-3b, a fibrous structure is observed near the skin. However, the fibrous structure lacks long fibrous structures, instead the LCP appear to be wavy and short in length which would not be expected to efficiently reinforce the matrix.

In Fig. 5-4, a photomicrograph of a fracture surface from a 2.3 mm thick plaque which was injection molded in 0.8 seconds with a mold temperature of 20°C is shown. The flexural modulus of this plaque was 4.9 GPa, and this value was a maximum for the 2.3 mm thick plaques. From the view of the entire cross section of the plaque, Fig. 5-4a, long straight fibrous structures are seen in the skin / subskin region. The magnified view of the skin / subskin region is seen in Fig. 5-4b. The structure observed in this figure shows much thicker straighter LCP fibers or ribbons. It is believed that these fibers or ribbons located near the skin are the reason for the higher flexural modulus of this plaque.

In both the 1.0 and 2.3 mm thick plaques, higher flexural moduli occurred with a straight long fibrous LCP structure. Plaques with lower flexural moduli lacked long straight fibers or ribbons, instead either short wavy structures or large undeformed structures were observed. Thus, higher mechanical properties of injection molded in situ composites are related to a straight high aspect ratio reinforcing structure while lower mechanical properties are related to wavy structures or to shorter structures.

5.3.3 Rheology

Investigation of the rheology of the blend and its components may be helpful in analyzing the behavior of the processing / property relationship observed for injection molding of this blend. The type of information gained from investigating the rheology aids in defining the conditions for deformation and breakup of a dispersed phase, and the behavior of the material

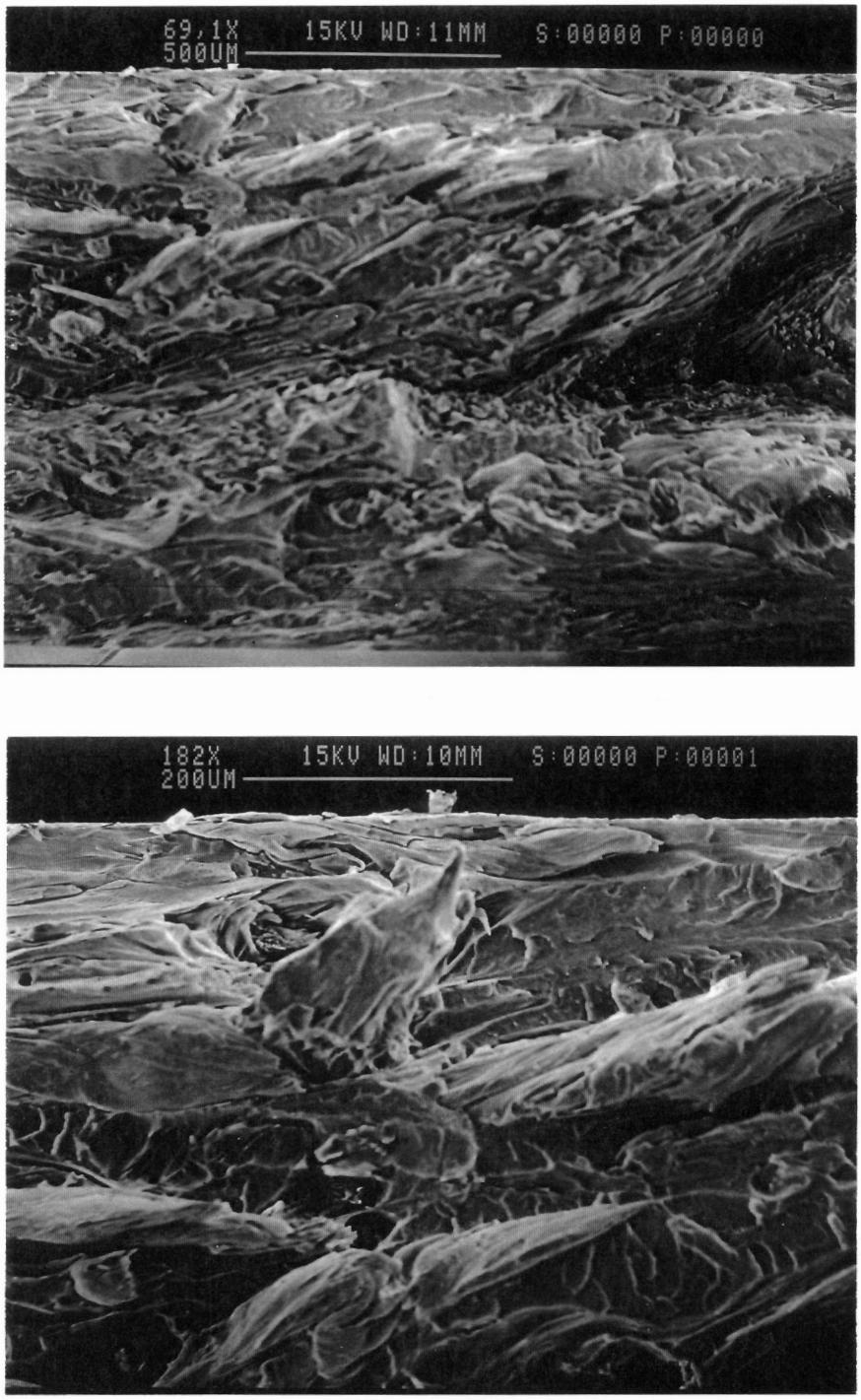

Fig. 5-1 SEM photomicrograph of 1.0 mm thick plaque with a flexural modulus of 3.4 GPa molded in 3.3 seconds: (a) view of entire plaque; (b) view of skin / subskin.

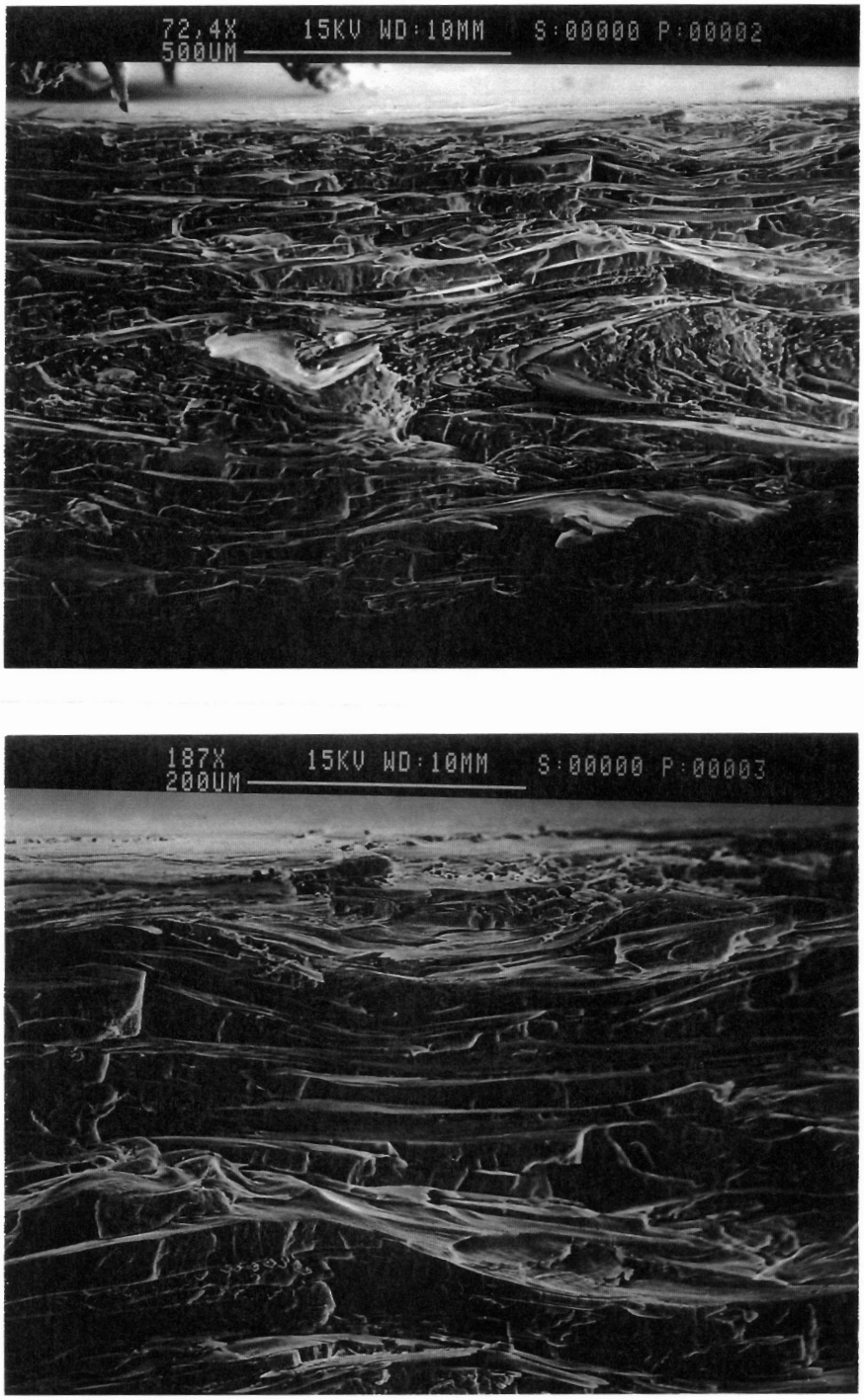

Fig. 5-2 SEM photomicrograph of 1.0 mm thick plaque with a flexural modulus of 4.3 GPa molded in 0.8 seconds: (a) view of entire plaque; (b) view of skin / subskin.

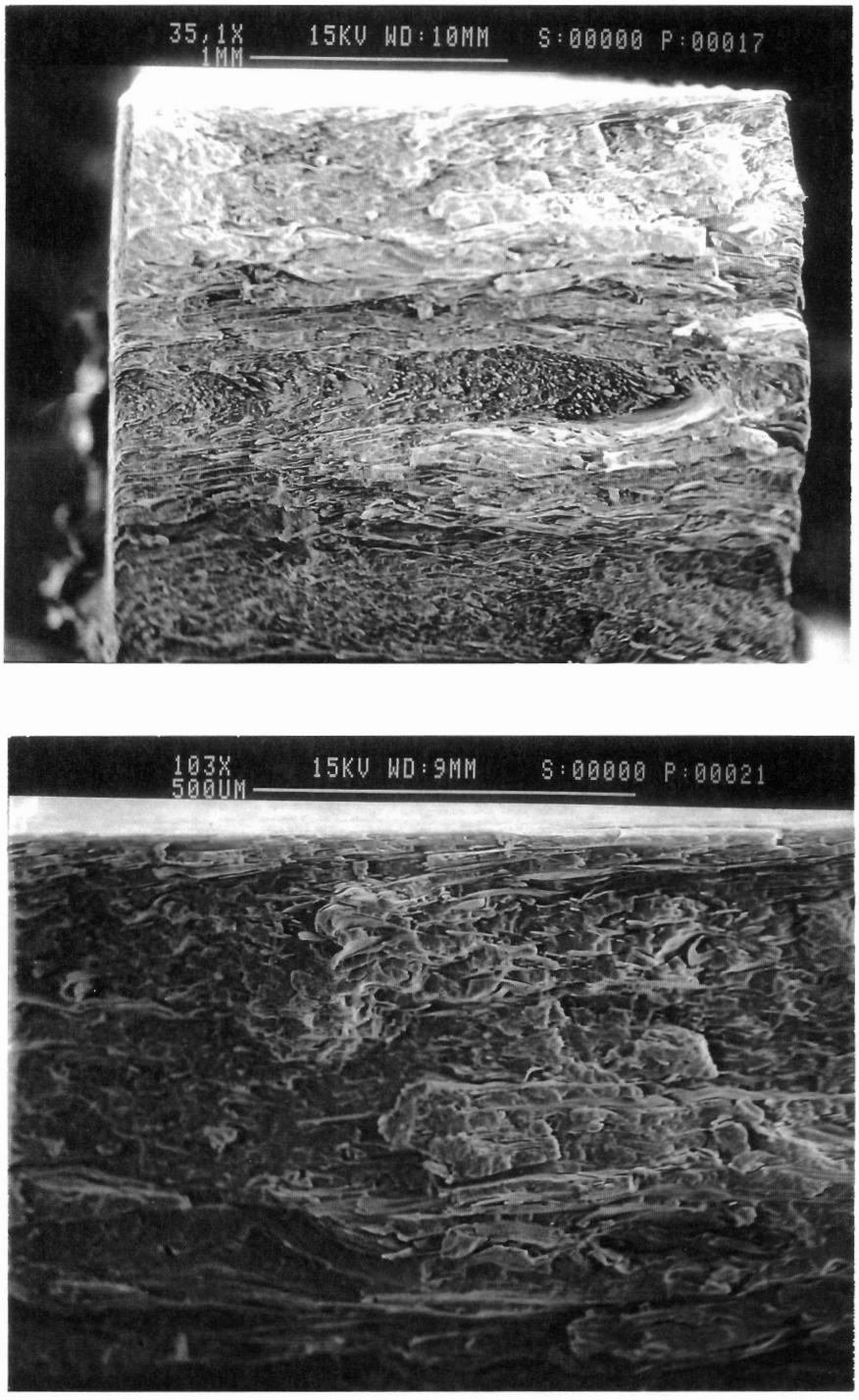

Fig. 5-3 SEM photomicrograph of 2.3 mm thick plaque with a flexural modulus of 3.4 GPa molded in 12.4 seconds: (a) view of entire plaque; (b) view of skin / subskin.

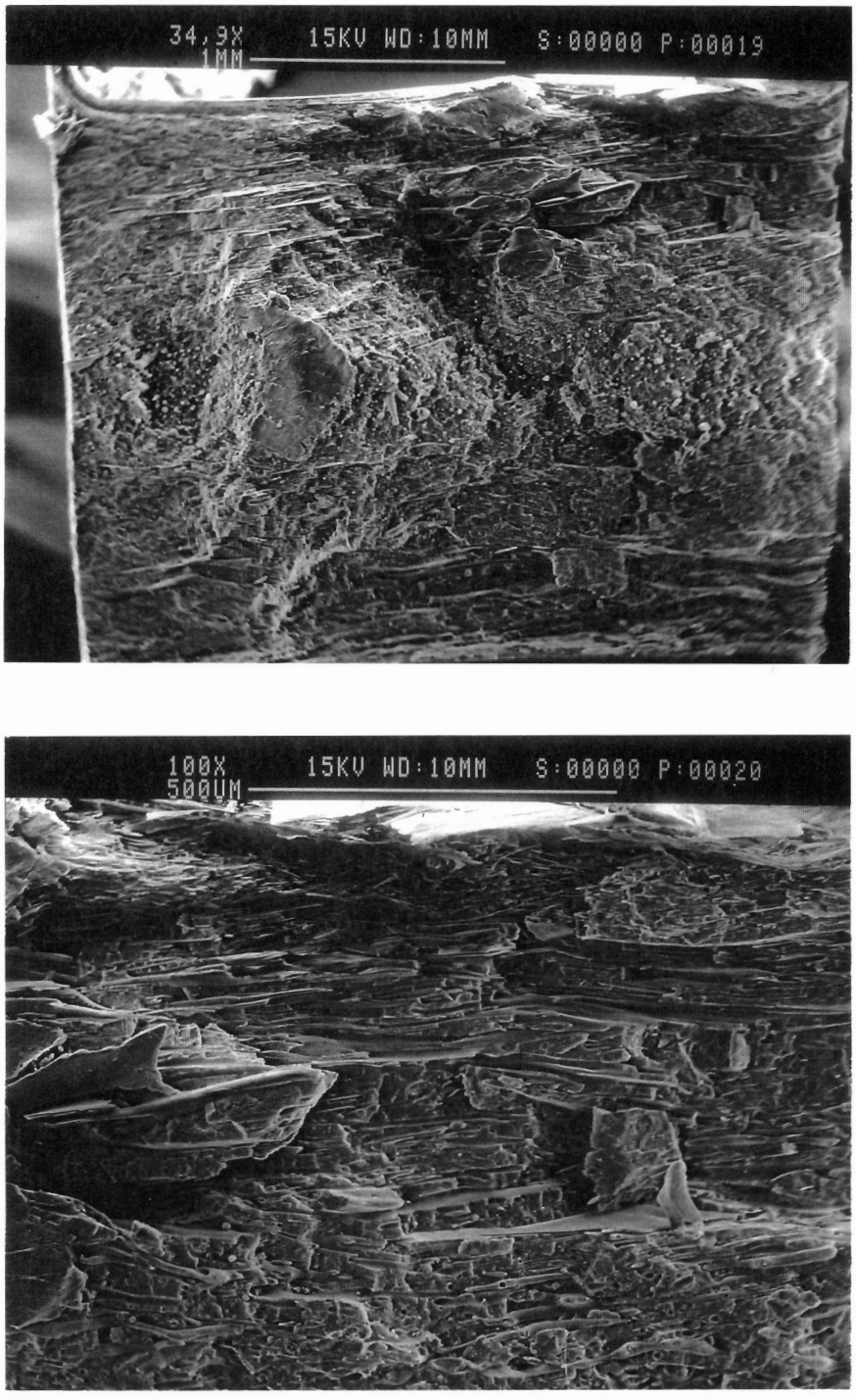

Fig. 5-4 SEM photomicrograph of 2.3 mm thick plaque with a flexural modulus of 4.9 GPa molded in 2.1 seconds: (a) view of entire plaque; (b) view of skin / subskin.

during cooling aids in the analysis of heat transfer and solidification. The cooling and solidification of a LCP has been shown to lead to higher moduli in thick extruded strands [14]. Thus, examination of the cooling behavior of the LCP may be valuable in relating processing conditions to the properties of the blend.

Deformation of the dispersed phase depends on a dimensionless number, called the Weber number, which is ratio of the hydrodynamic stress on a droplet to the surface stress on the droplet. The Weber number is defined as $R\eta\dot{\gamma}/\sigma_{12}$ where R is the drop radius, η is the matrix viscosity, $\dot{\gamma}$ is the shear rate, and σ_{12} is the interfacial tension. For a given type of flow field and viscosity ratio (ratio of droplet to matrix viscosity), a critical Weber number exists where droplets begin to breakup. When the Weber number equals or exceeds this critical value, a droplet undergoes deformation and breakup into two or more droplets. Knowledge of the stress and the viscosity ratio aid in characterizing this blend and it provides a reference for other systems that have been studied [7,8].

To calculate the stress, the viscosity of the blend is required. The viscosity for the blend was fitted to a power law model, and the power law constants (m and n) are 1122 Pa s^n and 0.471, respectively, where $\eta = m\dot{\gamma}^{n-1}$. The viscosity ratio was calculated from the viscosities of PP(MAP) 90/10 and neat VB which where also fitted to a power law model. The power law constants, m and n, for PP(MAP) 90/10 are 3126 Pa s^n and 0.373, respectively, and the power law constants, m and n, for neat VB are 132 Pa s^n and 0.745, respectively. The viscosity ratios can now be calculated at a shear rate greater than 100 s^{-1} where the power law model is valid. For the injection molding conditions used in this study, the shear rates at the wall are between 70 and 4000 s^{-1}. Two viscosity ratios at shear rates near these limits were calculated. The viscosity ratio at 100 and 1000 s^{-1} is 0.23 and 0.55, respectively.

The cooling behavior of VB was determined at 291, 293, and 295°C to show the sensitivity of VB to the melt temperature. The storage and loss moduli for these experiments are shown in Fig. 5-5. At an initial melt temperature of 295°C, the loss modulus is nearly an order of magnitude greater than the storage modulus as is typical for a melt. The storage and loss moduli finally approach each other near 250°C. At an initial melt temperature of 293°C, the storage and loss moduli are approximately an order of magnitude different as was observed when the initial melt temperature was 295°C. However, as the sample cools below 293°C the storage and loss moduli only differ by half an order of magnitude. This indicates that VB is solidifying as it cools. At an initial melt temperature of 291°C, the moduli approach each other rapidly and the rate of rise in the value of the modulus increases over that observed at the higher melt temperatures. Thus, solidification is occurring more rapidly at 291°C.

This data indicates that the rheology of VB is very sensitive to a few degrees Centigrade drop in the melt temperature. Thus, a processing temperature lower than 295°C may not allow deformation of VB prior to solidification. This data can also be compared to a LC copolyester studied previously, and comparison indicates that these LCPs have different rheological behaviors [7]. The LC copolyester was processed at melt temperature where $G' > G''$, which indicated a more solid-like behavior than can be obtained from VB. Additionally, as the LC copolyester was cooled the difference between G' and G'' remained nearly constant indicating that although the viscosity was rising solidification was not rapid. The cooling behavior of VB, therefore, indicates that its rheology is substantially different from that of the LC copolyester studied previously [7].

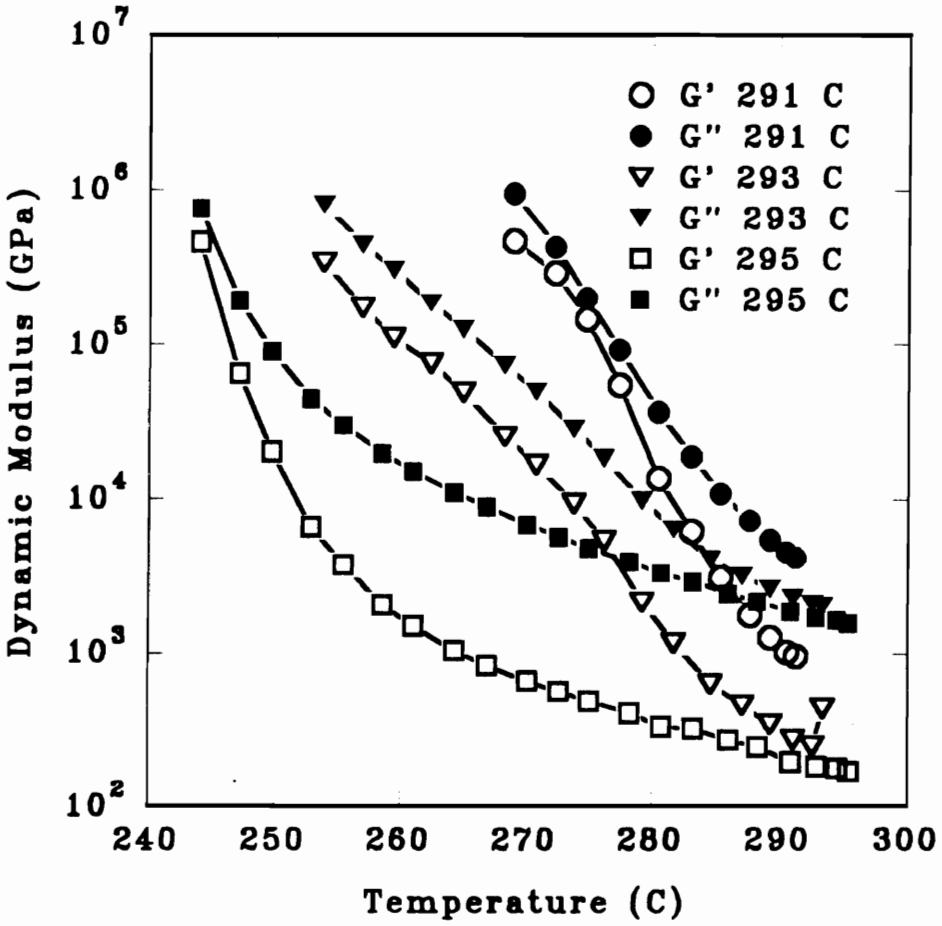

Fig. 5-5 Storage and loss moduli for neat VB cooled at 5°C/min. from 291, 293 and 295°C. Measured at 1 rad/s.

5.3.4 Effect of Stress on the Flexural Modulus

As discussed above, the deformation of dispersed droplets is related to the Weber number. To create a reinforcing structure, the LCP phase must undergo deformation that leads to a fibrous structure. From the work of Elemans [28], it is expected that affine deformation of a droplet occurs when the Weber number is twice the critical Weber number. Thus, the Weber number should be an important parameter in relating the process variables to the mechanical properties. Since the Weber number is related to the initial drop radius which does not change, the Weber number scales with the stress. Hence, for convenience the flexural modulus was related to stress instead of the Weber number.

Two types of flows exist during the filling of a mold. At the advancing front, a planar extensional flow (or hyperbolic stagnation flow) exists while upstream of the advancing front a shear flow exists. These two flows generate two types of stresses, shear stress and extensional stress which can be correlated to the flexural modulus of the blend. The shear stress may be approximated for this mold by calculating the shear stress for flow of a power law fluid between parallel plates which is given below:

$$\tau_{zy} = m \left[\frac{U}{H}\left(\frac{1+2n}{n}\right)\right]^n \left(\frac{y}{H}\right) \qquad \text{(5-1)}$$

where U is average velocity, H the half height of the mold, y is the distance from the centerline of the mold, and z is the flow direction. Calculation of the extensional stress is more difficult because the extensional viscosity is not known. However, it may be approximated by using the Trouton ratio ($\eta_e/\eta_0=3$) for the extensional viscosity, η_e. In this case, the zero shear viscosity, η_e, will be replaced by the power law viscosity at 100 s^{-1}. The extensional stress may then be estimated by using this extensional viscosity and the extensional rate at the advancing front for

a power law fluid as proposed by Tadmor [25]. This approach yields the following stress at the advancing front:

$$\tau_{zz} = -\frac{mnU}{4(1+n)H} \tag{5-2}$$

For $n < 1$, the extensional stress will increase to a greater degree than the shear stress as the average velocity increases.

The flexural modulus of the blend versus the extensional stress at the advancing front for 1.0, 1.5, and 2.3 mm thick plaques is shown in Fig. 5-6. For the thinnest mold, 1.0 mm, as the stress increased the moduli rose slightly. The properties of the 1.0 mm thick plaques were substantially below the flexural modulus calculated from the rule of mixtures. It appears that extensional stress did not significantly affect the modulus. The mechanical properties of the 1.5 and 2.3 mm thick plaques were strongly influenced by the extensional stress. As the stress increased, the modulus increased to a maximum. A similar trend is observed between the flexural modulus and the shear stress as shown in Fig. 5-7.

Although the modulus increased with both extensional and shear stress, the modulus of the 1.5 and 2.3 mm thick plaques did not rise at the same value of stress. If deformation of the LCP phase is the controlling factor, it is expected that the increase in the modulus should occur at the same value of stress or equivalently at the same value of the Weber number. The difference in the range of extensional or shear stress where the flexural modulus increased indicates that droplet deformation was not the sole factor which controlled the deformation the LCP phase.

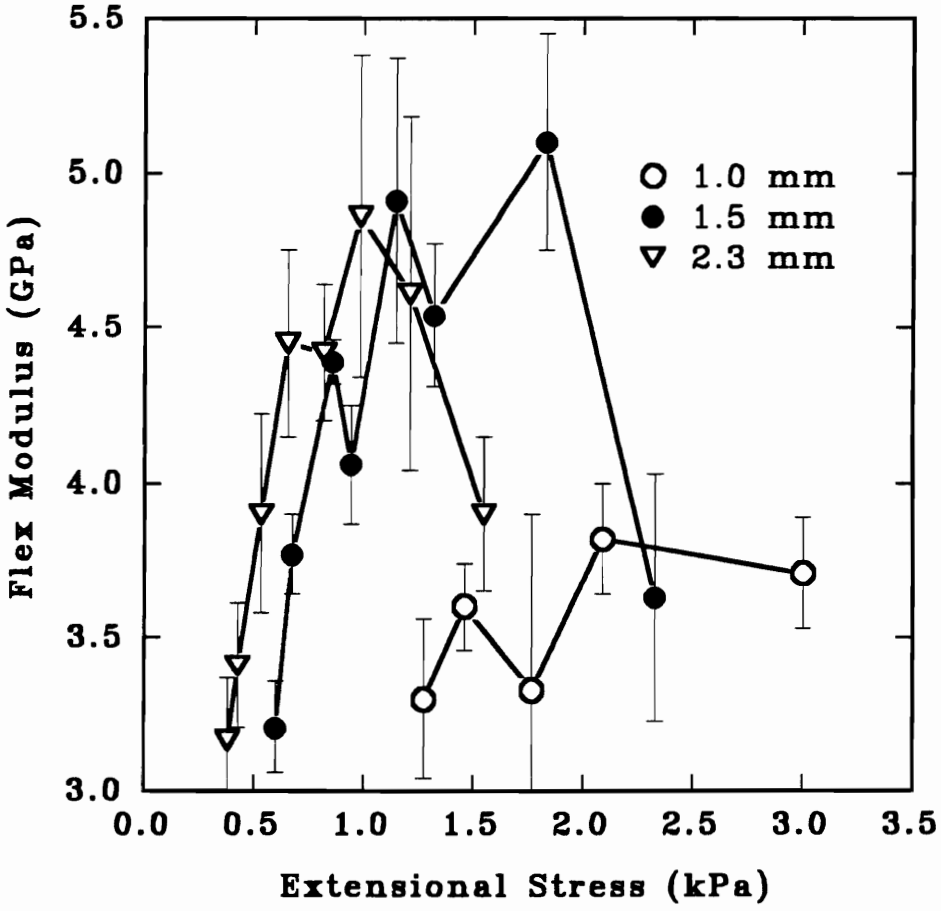

Fig. 5-6 Flexural modulus versus the extensional stress (1.0, 1.5 and 2.3 mm thick plaques shown).

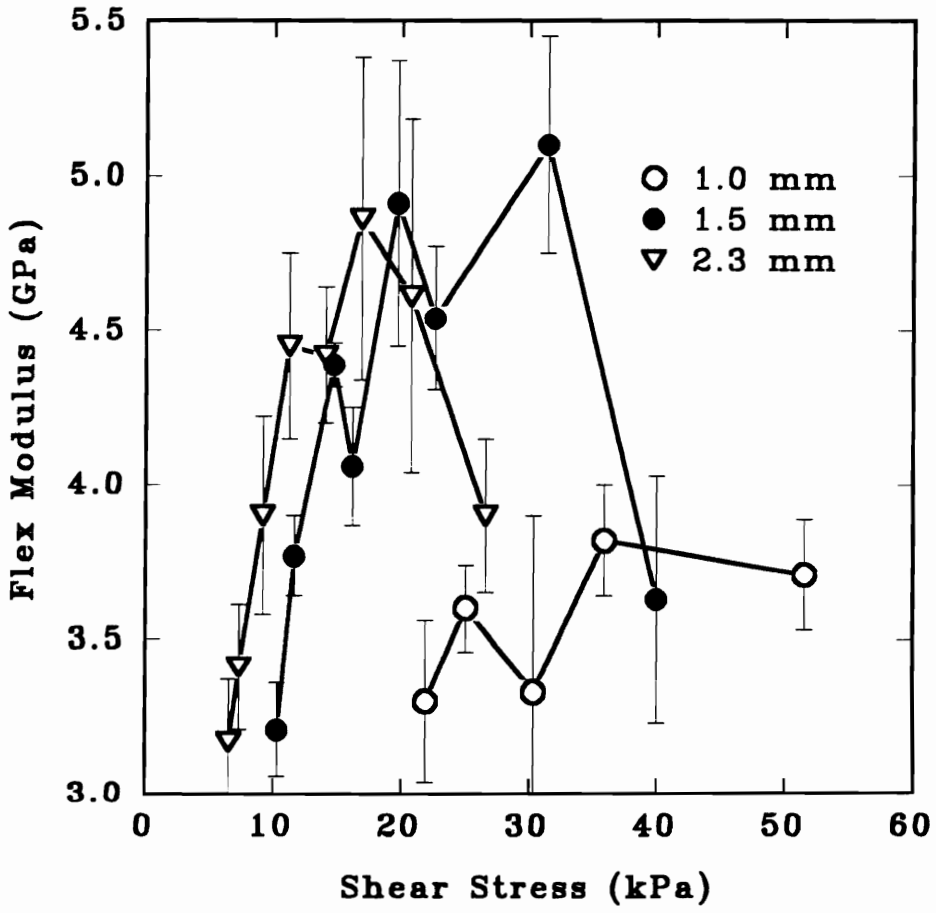

Fig. 5-7 Flexural modulus versus the shear stress (1.0, 1.5 and 2.3 mm thick plaques shown).

5.3.5 Effect of Heat Transfer on the Flexural Modulus

The effect of heat transfer on the properties of TP/LCP blends is believed to be related to the onset of LCP solidification upon cessation of flow. During mold filling, the LCP phase must be maintained in a molten state to permit deformation that leads to the formation of fibrils. At the same time, cooling must occur to reduce the temperature of the LCP to the point where rapid solidification occurs upon cessation of flow. Similar conditions have been discussed for both a neat LCP [14,13] and for TP/LCP blends [19,15].

Instead of calculating the transient temperature profile and correlating this large volume of data to the mechanical properties, a correlation of the flexural modulus to dimensionless variables was pursued. The appropriate dimensionless number may be obtained from dimensionless analysis or by simplifying the equations of motion and energy. The latter approach was pursued elsewhere where the fountain flow at the advancing front was ignored to permit simplification of the problem [8]. This approach yielded a equation which is an extension for a power law fluid of the Graetz Nusselt problem. The only dimensionless number for this problem was identified as the Graetz number, $UH^2/\alpha L$, where α is the thermal diffusivity, and L is the mold length. The Graetz number indicates the magnitude of heat convected in the down channel direction to the heat conducted in the transverse direction. Accordingly, a high Graetz number, $Gz \gg 1$, indicates that little transverse cooling occurs while a small Graetz number, $Gz < 1$, indicates that a large degree of transverse cooling occurs. Comparison of the flexural moduli versus the Graetz number should indicate if heat transfer is important in this process.

To calculate the Graetz number, the thermal diffusivity of the blend is required. The values of the thermal diffusivity for PP, VB, and the blend are presented in Table 5-5. The values for PP and VB were obtained from references [29] and [30], respectively. The blend thermal properties

were estimated from the individual components properties by a series model, although little difference existed using the series or parallel model [1].

A second heat transfer method was also investigated which calculated the thickness of the skin that was frozen against the wall during the filling of the mold. Data for this method were generated by varying the mold temperature. While this method will be discussed later in this section, the data was presented in the figures where the flexural modulus was compared to the Graetz number. This method of presentation should indicate if the modulus was shifted by the mold temperature.

The flexural modulus of 1.0 mm thick plaques made at 20, 50, and 70°C mold temperatures versus the Graetz number is shown in Fig. 5-8. The flexural modulus rose slightly as the Graetz number increased. For the plaques made with a 20°C mold temperature, the modulus rose sharply at a Graetz number of 5. The difference between the flexural modulus of the plaques made at a 20°C mold temperature and the plaques made at higher mold temperatures may be related to freezing of a greater percentage of the oriented melt which is located near the skin [26].

The flexural modulus of 1.5 mm thick plaques made at 20, 50, and 70°C mold temperatures versus the Graetz number is shown in Fig. 5-9. There was little difference among the moduli of the plaques made at the different mold temperatures. The flexural modulus rose as the Graetz number increased. The modulus reached a plateau at a Graetz number between 5 and 10.

Similar behavior was observed for plaques of 2.3 mm thickness as shown in Fig. 5-10. There was little difference between the moduli versus Graetz number for plaques made at the different mold temperatures. The modulus rose as the Graetz number increased to a value of 10. The flexural modulus reached a maximum and then decreased as the Graetz number increased beyond 30. This decline in modulus was believed to be related to the small amount of transverse

Table 5-5 Thermal properties for PP [29], neat VB [30], and PP(MAP)/VB 70(10)/30 as estimated from series model.

	PP[1]	VB[2]	PP(MAP)/VB
Density (kg/m^3)	930	1400	1071
Thermal Conductivity (W/m K)	0.117	0.23	0.131
Thermal Diffusivity (10^8 m^2/s)	7.0	5.4	6.5

[1] Data for 25°C; [2] Data for 250°C

cooling that occurs during rapid filling of a mold. The resulting melt at the end of the filling stage is hotter than if the mold was filled slowly. Consequently, the morphology has more time to relax with a resulting loss in modulus.

A similar feature is shown in Figures 5-8 through 5-10. As the Graetz number increased the flexural modulus increased. This is similar to the behavior observed between the flexural modulus and the extensional or shear stress. However, the rise in the flexural modulus for the three plaques of different thickness occurred at different stresses. Comparison of Figures 5-8 through 5-10 shows that the flexural modulus rose at approximately the same value of the Graetz number, 10. Thus, the flexural properties were affected by the heat transfer that occurred during mold filling. The nature of the effect of heat transfer on the properties of the blend was believed to be related to the solidification of the LCP. At a Graetz number below ten, it is speculated that the LCP begins solidifying, and deformation of the LCP phase becomes difficult. In order to obtain a reinforcing morphology, higher stresses are then required to deform the solidifying LCP which also leads to higher Graetz numbers and less solidification. Thus, it is believed that heat transfer and stress are coupled through the solidification process.

The second heat transfer analysis that was mentioned above is the calculation of the thickness of polymer frozen at the mold wall during the filling of the mold. The calculated frozen skin layer has been related to the flexural moduli for both TP matrices [26] and neat LCPs [27]. As performed by others, this analysis is undertaken by varying the melt and/or mold temperature [26,27]. Because VB is just melted at 295°C and PP degrades rapidly above 295°C the melt temperature was not varied. Instead, the mold temperature was set at three different values to provide a variation in the frozen skin layer. The equation for calculation of the frozen layer thickness as derived elsewhere [7] is shown below:

$$\frac{d}{H}=2^{\frac{1}{2}}\left(\frac{T_s-T_w}{T_m-T_w}\right)(Gz)^{-1/2} \qquad \textbf{(5-3)}$$

where d is the frozen layer thickness and Ts, Tw, and Tm are the solidification, wall, and melt temperatures, respectively. Comparison of the flexural modulus to d/H should indicate if a correlation exists.

Analysis of the data with this approach showed that the flexural modulus could increase as the frozen layer decreased. The reason for the lack of fit of this model indicates that the morphology of the skin region is not affected by the mold temperature. It was discussed in a prior paper, that most morphological changes occur in the subskin region which is affected to a greater extent by the Graetz number [7]. This is also observed in Figures 5-1 to 5-4 for the PP(MAP)/VB blend. Thus, this heat transfer analysis as well as the morphology indicates that the subskin region in the PP(MAP)/VB blend is significantly affected by how the blend is processed.

5.3.6 Effect of Mixing Upon the Tensile Modulus

As mentioned in the introduction, mixing of PP(MAP)/VB prior to injection molding leads to a significant rise in the tensile strength of tensile bars [6]. Accordingly, this blend was mixed in an extruder prior to injection molding the plaques. Since the processing / property behavior of this blend is different from that found with a PP / LC copolyester blend, the effect of mixing on the mechanical properties of the PP(MAP)/VB blend is examined to determine if a tumbled blend has a significantly different processing / property relationship [7]. The flexural and tensile properties of this material are reported in reference [9]. The largest differences were observed in the two thicker plaques. To examine this difference, the flexural modulus versus the shear stress for tumbled and premixed blends are shown in Fig. 5-11 for the 1.5 mm plaques. Similar trends

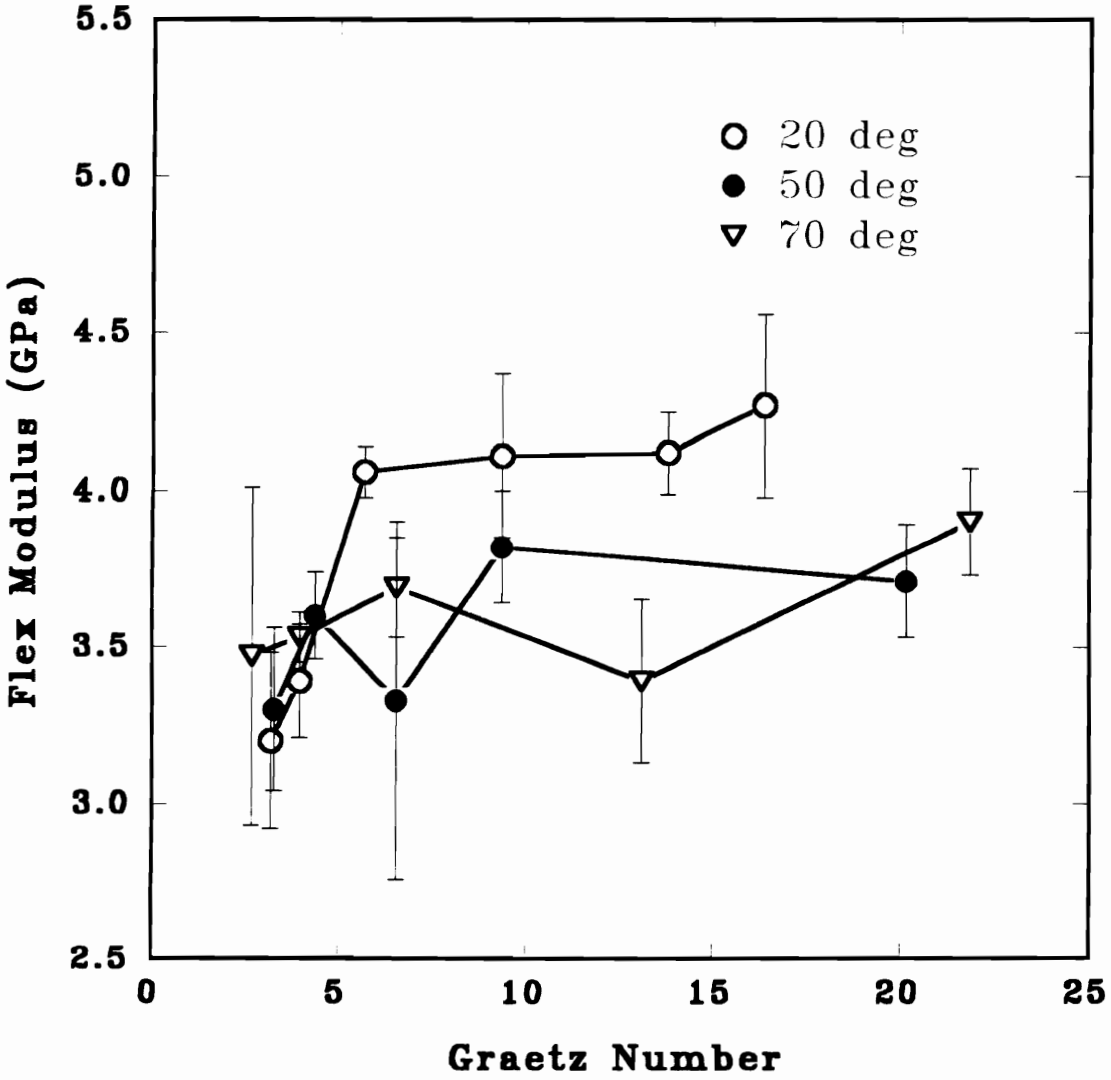

Fig. 5-8 Flexural modulus versus the Graetz number for 1.0 mm thick plaques made at 20, 50, and 70°C mold temperatures.

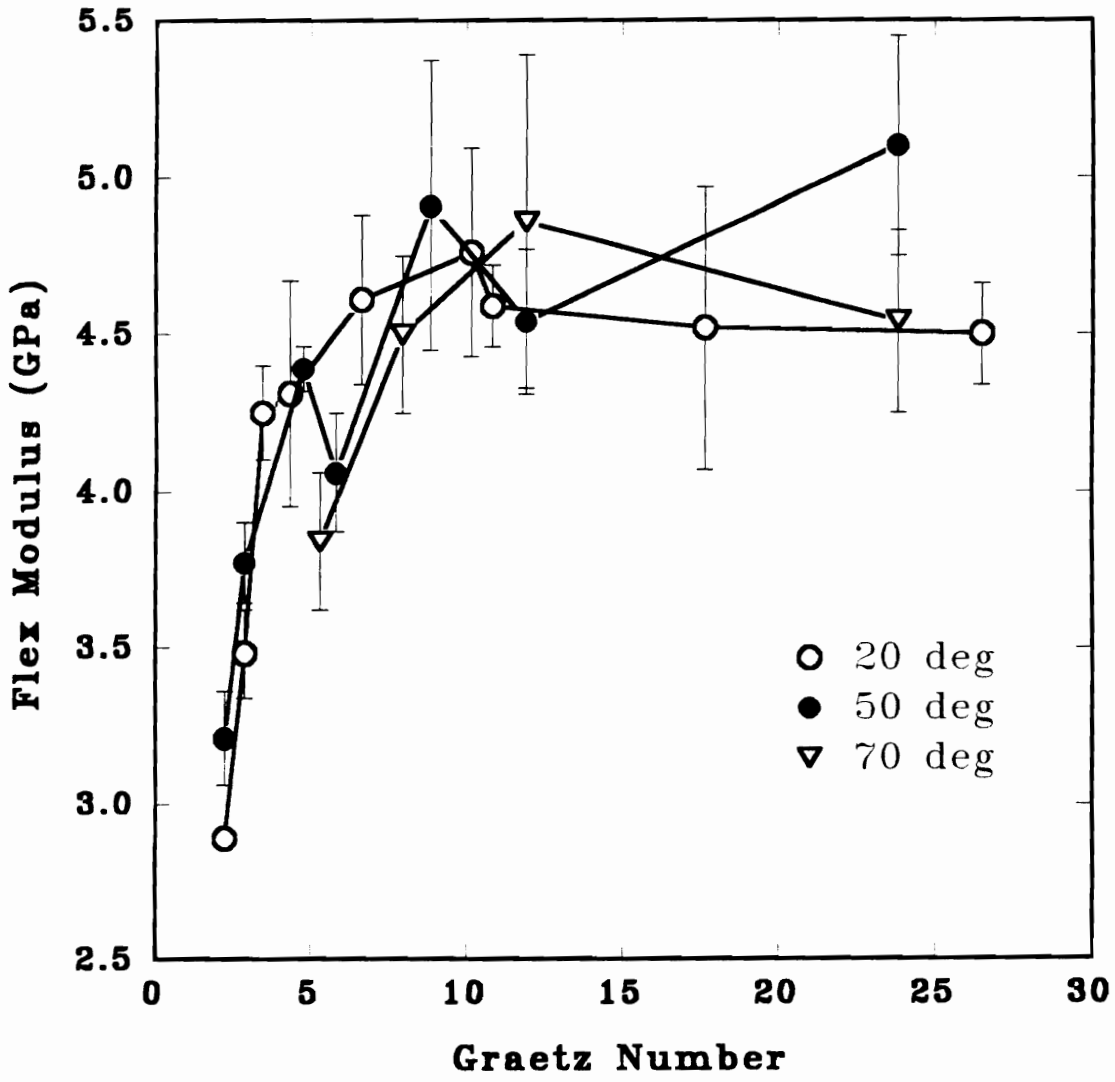

Fig. 5-9 Flexural modulus versus the Graetz number for 1.5 mm thick plaques made at 20, 50, and 70°C mold temperatures.

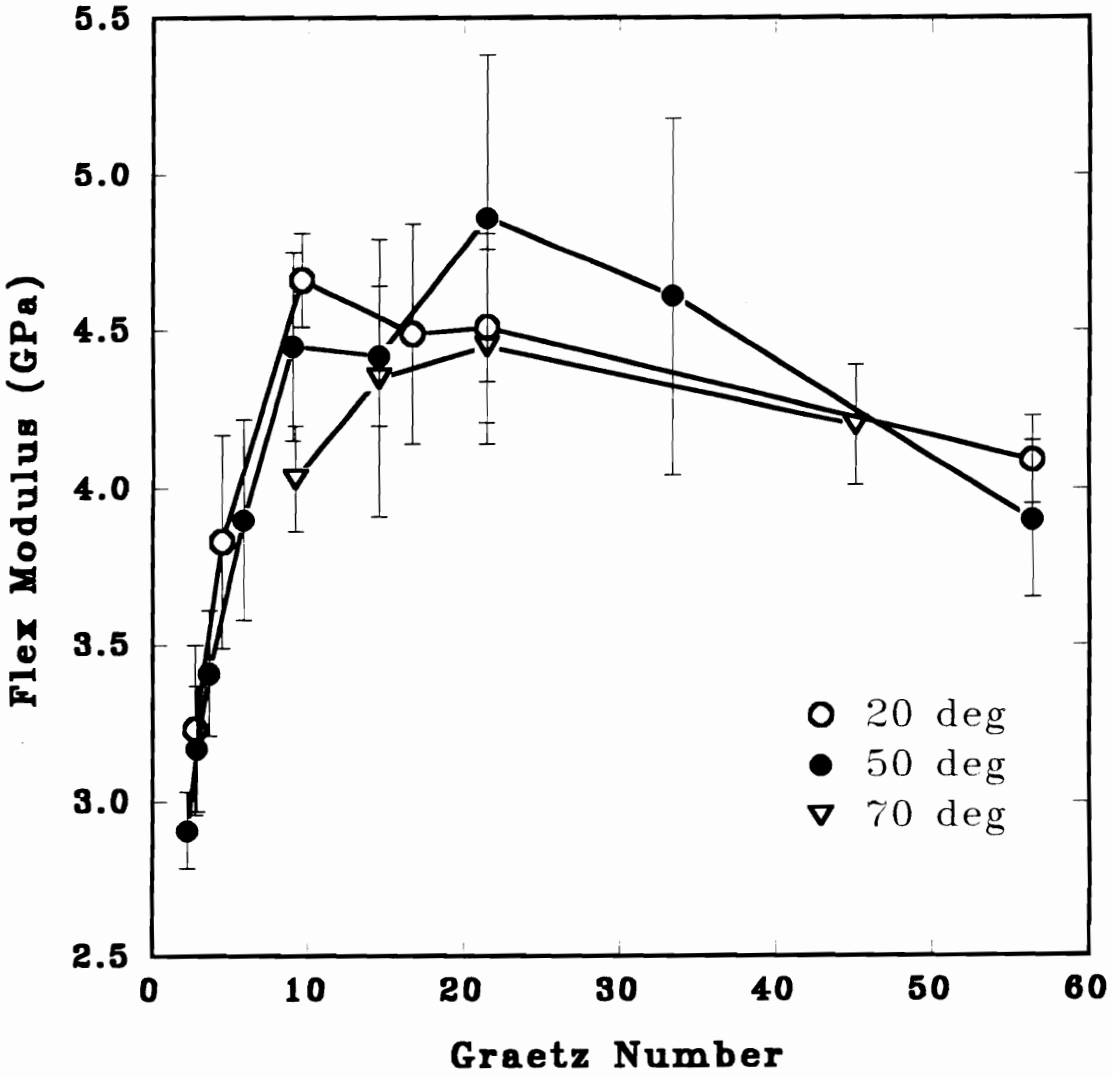

Fig. 5-10 Flexural modulus versus the Graetz number for 2.3 mm thick plaques made at 20, 50, and 70°C mold temperatures.

between the modulus and the stress occurred between premixed and tumbled blends, but the flexural moduli of the tumbled blend rose to slightly higher values, and this rise occurred at a lower value of the shear stress. The flexural modulus versus shear stress for tumbled and premixed plaques of 2.3 mm thickness are shown in Fig. 5-12. The same difference between the tumbled and premixed blend was observed, but the differences were larger.

The difference between the flexural modulus versus shear stress relationship for tumbled and premixed blends is believed to be related to the dispersed phase size. Although quantifying the sizes of the dispersed phase in this blend is difficult, the premixed sample has a smaller phase size than the tumbled samples. This change in the initial drop size while not affecting the critical Weber number shifts the stress required for the Weber number to equal the critical Weber number. In addition, mixing can lead to the creation of submicron particles that do not deform and reinforce the matrix. Hence, the premixed blend may have a larger percentage of the LCP phase which is not reinforcing the matrix, and this leads to a lower flexural modulus.

While differences in the correlation of the flexural modulus of the tumbled and premixed blends with stress can be explained, the effect of mixing does not substantially change the relationship. The different correlation of the flexural modulus with stress and heat transfer between the VB blend and the LC copolyester blend studied previously is not explained on the basis of mixing [7].

5.3.7 Effect of Melt Temperature on Flexural Properties

In a prior study, it was determined that the heat transfer controlled the development of the structure of Vectra A950 (VA) in a PP matrix [7]. The heat transfer was related to a dimensionless group, the Graetz number, and at a Graetz number of ten the flexural modulus

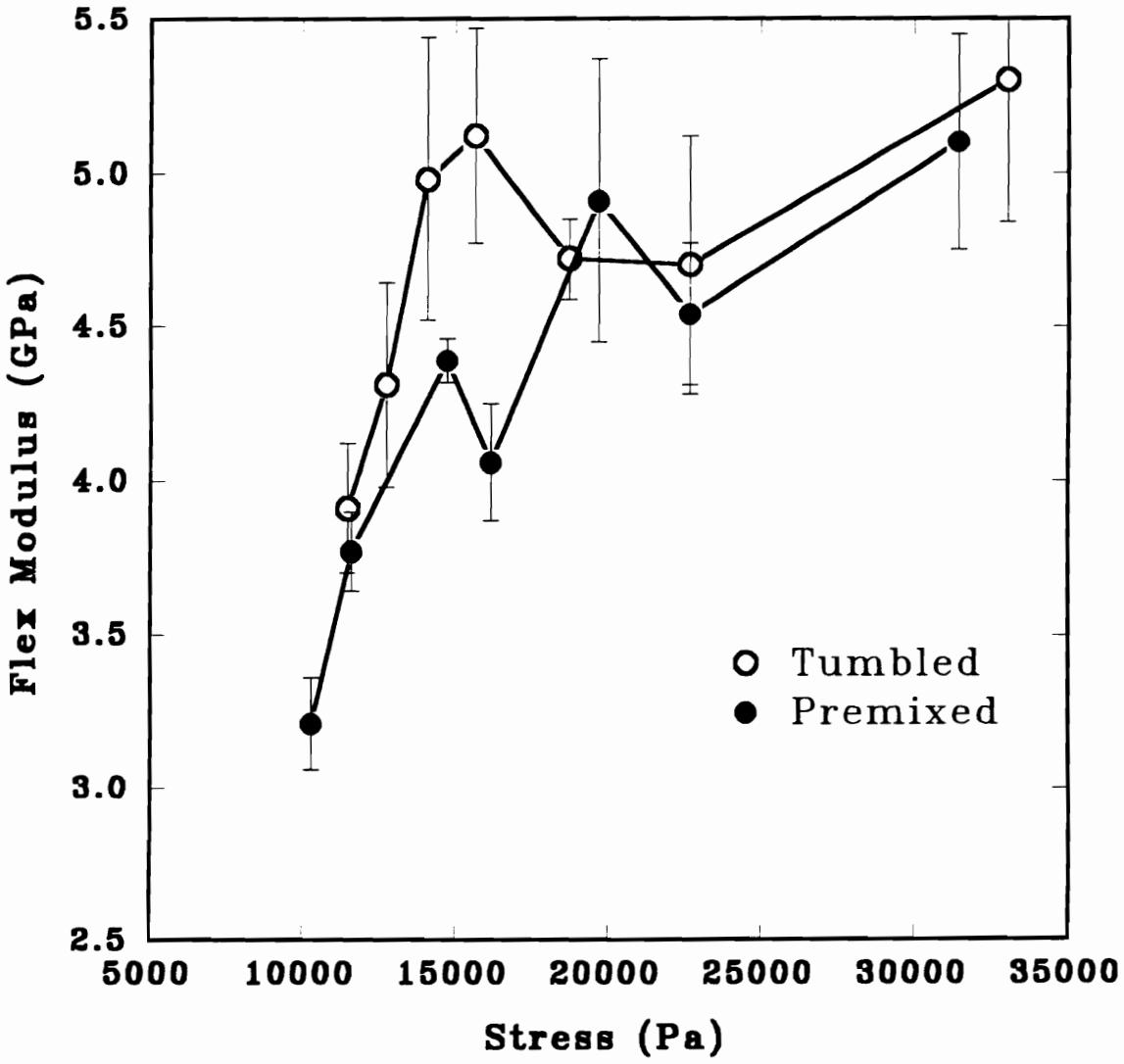

Fig. 5-11 Flexural modulus versus the shear stress for 1.5 mm thick plaques of tumbled and premixed blends.

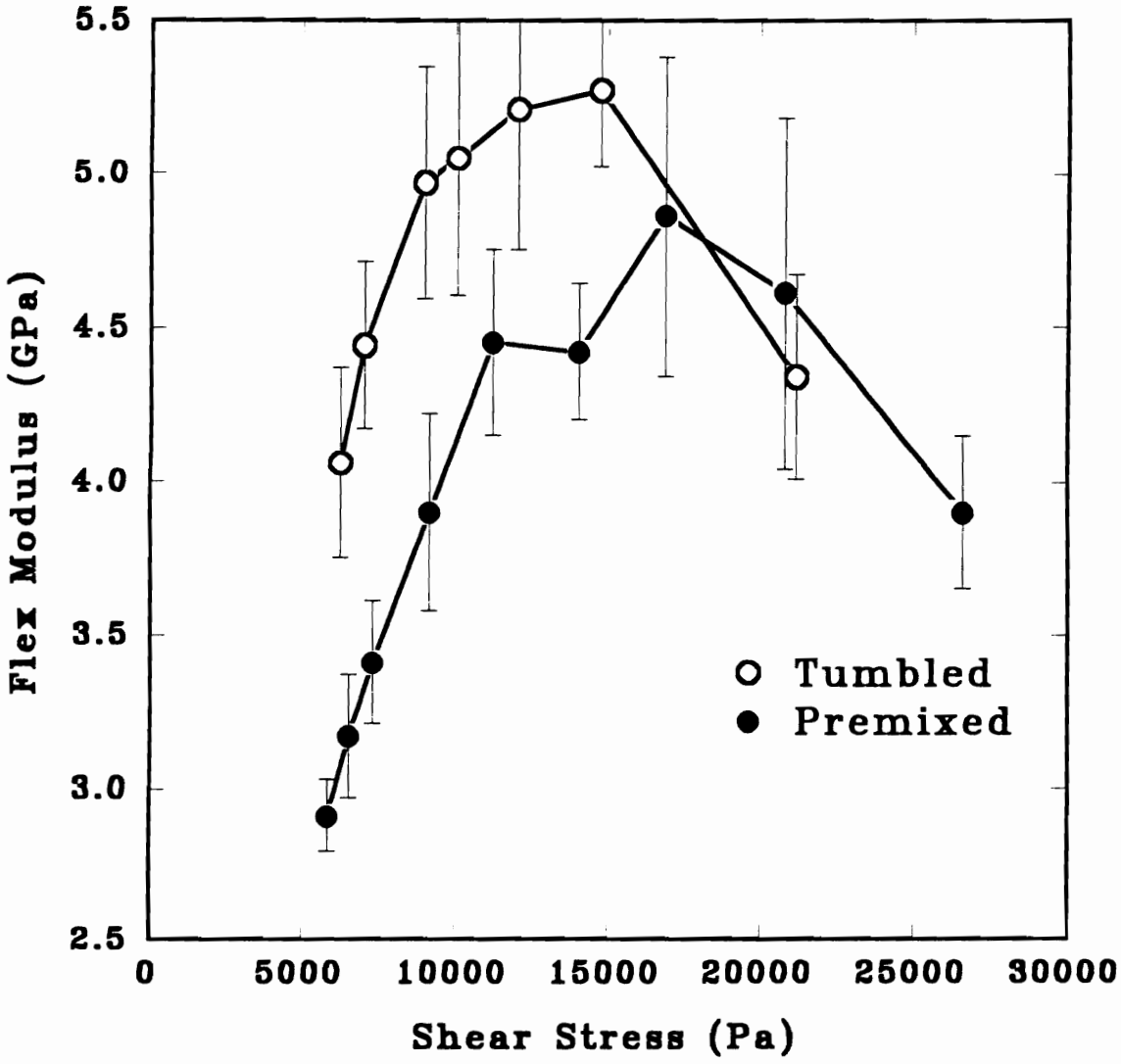

Fig. 5-12 Flexural modulus versus the shear stress for 2.3 mm thick plaques of tumbled and premixed blends.

reached a maximum value. It was speculated based on the relatively low Graetz number and the fact that at the melt temperature the storage modulus, G', of the LCP slightly exceeded the loss modulus, G'', that solidification was involved in this process. The initial rheological condition at the melt temperature, $G' > G''$, combined with transverse cooling condition was believed to lead to the deformation of the LCP phase into a reinforcing structure which quickly solidified upon cessation of flow.

To determine if the melt temperature can change the processing / property relationship for the PP(MAP)/VB blend, the properties of the blend molded at a second melt temperature were investigated. While the storage and loss moduli of VB during cooling, shown in Fig. 5-5, differed from the storage and loss moduli of VA which was presented in a prior study [7], a melt temperature of 292°C was chosen for two reasons. First, the storage and loss moduli began to converge as the melt temperature was lowered from 293 to 291°C, and the condition where $G' = G''$ was approached. Second, based on Fig. 5-5, the VB appears to solidify rapidly at a melt temperature of 291°C and so a higher temperature, 292°C was chosen. This temperature should allow the LCP to deform before solidifying.

A comparison of the flexural modulus versus the Graetz number for tumbled blends processed at injection molding barrel temperatures of 292 and 295°C are shown in Figures 5-13 to 5-15. The flexural modulus versus the Graetz number for 1.0 mm thick plaques is shown in Fig. 5-13. Between a Graetz number of 5 and 10, the flexural modulus of the blend processed at a 292°C barrel temperature increased from approximately 3.6 to 4.1 GPa. This was similar to the behavior observed for VA blends. In contrast, the flexural modulus of the blend processed at a 295°C barrel temperature did not rise until the Graetz number exceeded 20. In either case, the moduli were significantly lower than the value predicted from the rule of mixtures. The flexural

modulus versus the Graetz number for 1.5 mm thick plaques is shown in Fig. 5-14. There was a maximum in the flexural modulus for a Graetz number between 5 and 12 for the blend processed at 292°C. This was similar to the behavior of the PP(MAP)/VA blend studied previously [7]. However, the flexural modulus of the blend processed at a 295°C barrel temperature was greater than the blend processed at a 292°C barrel temperature, and so no improvement in the modulus was obtained by using a melt temperature of 292°C barrel temperature. The flexural modulus versus the Graetz number for the 2.3 mm thick plaques is shown in Fig. 5-15. Again, a maximum in the flexural modulus occurred near a Graetz number of 10 for the blend processed at a 292°C barrel temperature. The flexural modulus for the blend processed at a 295°C barrel temperature was significantly greater than the modulus for the blend processed at a 292°C barrel temperature.

Obviously, the melt temperature did not by itself lead to moduli that meet the rule of mixtures. It did indicate that the processing / property relationship was similar to that observed for PP(MAP)/VA, and therefore the initial melt temperature did significantly influence the processing behavior of the blend [7]. Based on a study with a second LC copolyester, it was shown that even if the blend was processed at the optimal melt temperature, the viscosity ratio can dramatically affect the resulting properties [8]. The viscosity ratio of the PP(MAP)/VB blend was shown to be between 0.2 and 0.6 which was thought to be near optimum [31]. It is possible that another viscosity ratio may lead to flexural moduli meeting the moduli calculated from the rule of mixture, but it is more likely that the material characteristics of VB are responsible for the observed behavior. The difference in the cooling behavior for VB where $G' > G''$ for all melt temperatures was different from the cooling behavior for two LC copolyester where the melt temperature can change the rheology of the LCP from liquid-like, $G' < G''$, to solid-like, behavior [7,8]. Additionally, for VB the storage and loss moduli approach the cross over point, more quickly

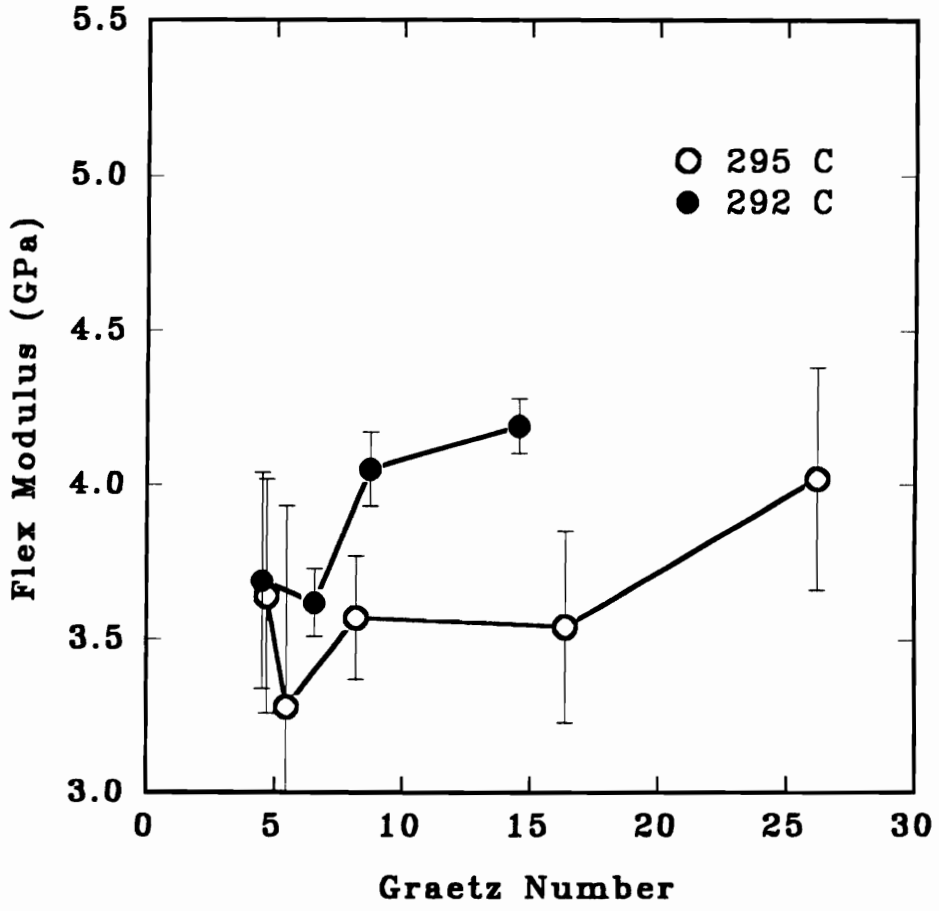

Fig. 5-13 Flexural modulus versus the Graetz number for 1.0 mm thick plaques of tumbled blends made at 292 and 295°C injection molder barrel temperatures.

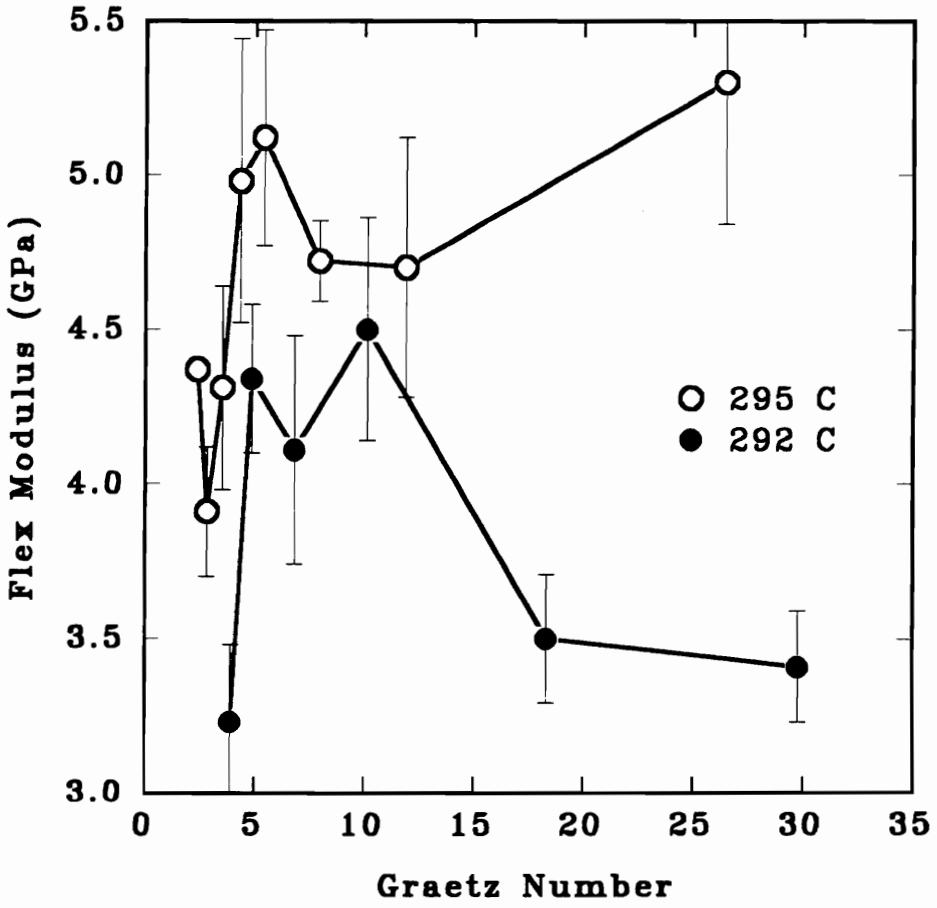

Fig. 5-14 Flexural modulus versus the Graetz number for 1.5 mm thick plaques of tumbled blends made at 292 and 295°C injection molder barrel temperatures.

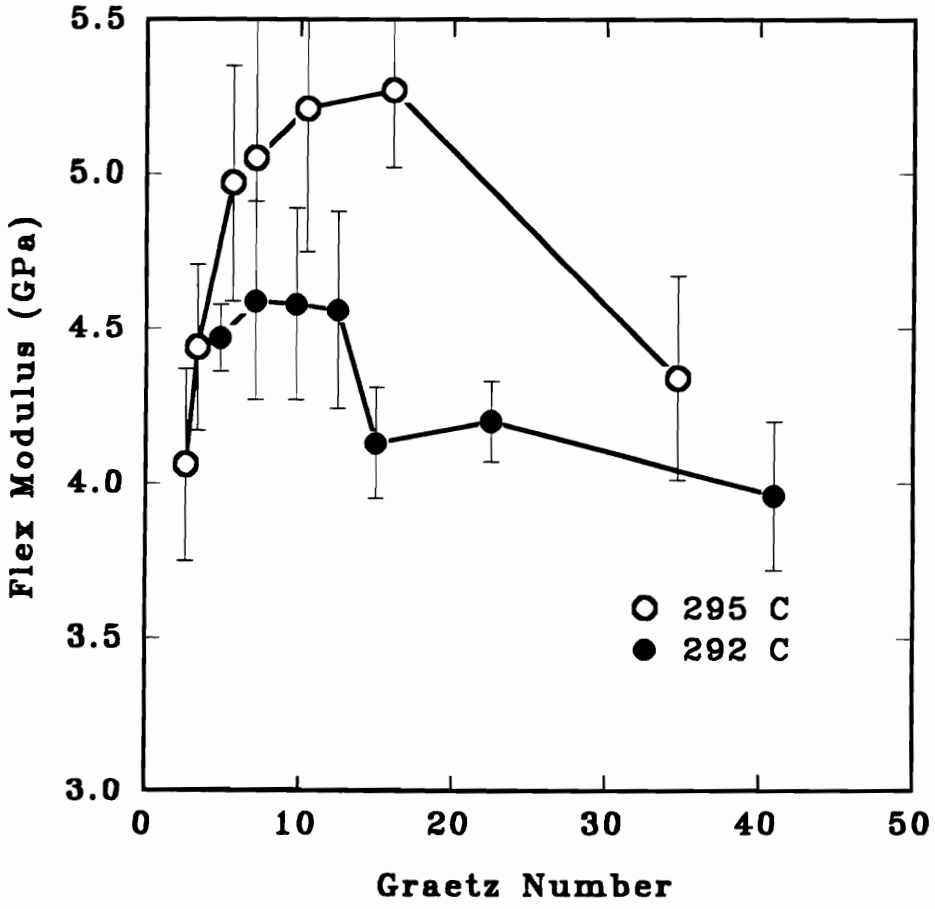

Fig. 5-15 Flexural modulus versus the Graetz number for 2.3 mm thick plaques of tumbled blends made at 292 and 295°C injection molder barrel temperatures.

than occurs for the two copolyesters LCPs [7,8]. This indicates that VB was solidifying more quickly than the LC copolyesters. The behavior of the storage and loss moduli where $G' \sim G''$ at the initial melt temperature as well as the behavior of the storage and loss moduli during cooling was believed responsible for the ability of the LCP to deform into a reinforcing morphology followed by rapid solidification, and this mechanism leads to flexural properties that meet the moduli predicted by the rule of mixtures.

5.4 Conclusions

The mechanical properties of a premixed PP(MAP)/VB are sensitive to the fill time and mold thickness. Based on higher properties of thinner plaques of neat VB, it was expected that higher properties of the blend would be obtained in the thinner plaques. However, significantly lower properties were obtained from 1.0 mm thick plaques. The highest properties were obtained from the 1.5 and 2.3 mm thick plaques. The flexural modulus obtained from plaques of 1.0, 1.5, and 2.3 mm thickness were all lower than the flexural modulus predicted from the rule of mixtures. The difference between the actual modulus and the modulus calculated from the rule of mixtures became greater as the mold thickness decreased thus demonstrating less efficient reinforcement of the matrix by the LCP as the mold thickness decreased.

The flexural and tensile moduli were shown to be very sensitive to the fill time, and the moduli increased as the fill time decreased. The moduli reached a maximum at short fill times where the stresses during mold filling were the greatest.

The flexural properties of the blend could not be directly related to the stress or equivalently the Weber number which is related to the deformation of a dispersed phase. While the flexural

moduli increased as the stress increased, the increase in the modulus did not occur at the same stress or Weber number. For deformation of the LCP to be the controlling factor in attainment of high mechanical properties the moduli should increase at the same value of the Weber number. This indicated that another mechanism as affecting the mechanical properties.

Correlation of the flexural modulus with the Graetz number showed that the modulus increased at the same Graetz number (10) independent of the plaque thickness. It is believed that solidification of VB is the primary factor controlling the development of a reinforcing morphology and high mechanical properties. Solidification leads to a coupling of the effect of stress and heat transfer. Increasing the injection speed increases the stress on a cooling LCP phase which leads to deformation of a more viscous droplet. Simultaneously, the melt remains near the initial melt temperature as the injection speed increases which leads to a lower rate of solidification.

Comparison of the processing / property relationships for blends of PP(MAP)/VB and PP(MAP)/VA which were studied in a previous paper showed that the flexural modulus versus Graetz number relationship is different. For the thicker plaques of PP(MAP)/VA, the flexural moduli reached a maximum at a Graetz number of 10 instead of reaching a broad maximum or plateau beyond a Graetz number of 10 as occurs for the PP(MAP)/VB blend. This processing / property difference was related to the LCP rheology. When the storage and loss moduli are nearly equal, similar processing / property relationship are obtained for PP(MAP)/VB and PP(MAP)/VA. However, the maximum flexural moduli are not obtained under these conditions for PP(MAP)/VB. It is believed that the rheological characteristics of VB (i.e. more rapid solidification of this LC poly(ester-amide) versus the behavior for LC copolyesters) are responsible for the flexural moduli of the blend being less than the moduli predicted from the rule of mixtures.

5.5 Acknowledgements

This work was supported by the Army Research Office (grant number DAAL03-91-G-0166), and their support is sincerely appreciated.

5.6 References

1. M.O.W. Richardson, Polymer Engineering Composites, Applied Science Publishers, London, 1977.
2. R.B. Bird, R.C. Armstrong, and O. Hassager, Dynamics of Polymeric Liquids, Vol. 1, John Wiley, New York, 1987.
3. H.J. O'Donnell, A. Datta, D.G. Baird, "The Effect of Compatibilization on the Properties of Blends of TLCPs with Polypropylene," Annual Technical Conference of the Society of Plastic Engineers (ANTEC'92), 50, 2248 (1992).
4. A. Datta, "The Effect of Compatibilization on Blends of Polypropylene with a Liquid Crystalline Polymer ," Polymer 34(4), 759 (1993).
5. A. Datta "Compatibilization of Thermoplastic Composites Based on Blends of Polypropylene with Two Liquid Crystalline Copolyesters," submitted to Polymer.
6. H.J. O'Donnell, H.H. Chen and D.G. Baird, Annual Technical Conference of the Society of Plastic Engineers (ANTEC '93), 51, 1711 (1993).
7. H.J. O'Donnell and D.G. Baird, "The Effect of Injection Molding Conditions on the Mechanical Properties of an In Situ Composite: I. Polypropylene and a LC copolyester Based on HNA/HBA," submitted to Polym. Eng. Sci.
8. H.J. O'Donnell and D.G. Baird, "The Effect of Injection Molding Conditions on the Mechanical Properties of an In Situ Composite: III. Polypropylene and," submitted to International Journal of Polymer Processing.
9. H.J. O'Donnell, Ph.D. Dissertation, Virginia Polytechnic Institute and State University, Blacksburg, VA, 1994.
10. J.P. Holman, Heat Transfer, 4th ed., McGraw Hill, New York (1976).
11. G.I. Taylor, "The Formation of Emulsions in Definable Fields of Flow," Proc. Roy. Soc., A146, 501 (1934).
12. W.J. Jackson and H.F. Kuhfuss, J. Polym. Sci., Polym. Chem. Ed., 14, 2043 (1976).
13. D. Done and D.G. Baird, "Solidification Behavior and Recovery Kinetics of Liquid Crystalline Polymers," Polym. Eng. Sci., 30(16), 989 (1990).
14. T-S. Chung, "Production of Ultrahigh Modulus Liquid Crystal Polymer Rods," J. Polym. Sci.: Part B: Polym. Phys., 26, 1549 (1988).
15. M.R. Nobile, E. Amendola, and L. Nicolais, "Physical Properties of Blends of Polycarbonate and a Liquid Crystalline Copolyester," Polym. Eng. Sci., 29(4), 244 (1989).
16. D. Dutta, H. Fruitwala, A. Kohli, and R.A. Weiss, "Polymer Blends Containing Liquid Crystals: A Review," Polym. Eng. Sci., 30(17), 1005 (1990).
17. B.R. Bassett and A.F. Yee, "A Method of Forming Composite Structures Using In Situ-

Formed Liquid Crystal Polymer Fibers in a Thermoplastic Matrix," Poly. Eng. Sci., 11(1), 10 (1990).
18. F.P. La Mantia, M. Saiu, A. Valenza, M. Paci, and P.L. Magagnini, "Relationships Between Mechanical Properties and Structure for Blends of Nylon-6 with a Liquid Crystal Polymer," Eur. Polym. J., 26(3), 323 (1990).
19. K.G. Blizard, C. Federici, O. Federico, and L.L. Chapoy, "The Morphology of Extruded Blends Containing a Thermotropic Liquid Crystalline Polymer", Poly. Eng. Sci., 30(22), 1442 (1990).
20. D. Beery, S. Kenig, And A. Siegmann, "Structure Development During Flow of Polyblends Containing Liquid Crystalline Polymers," Poly. Eng. Sci., 31(6), 451 (1991).
21. K.G. Blizard and D.G. Baird, "The Morphology and Rheology of Polymer Blends Containing a Liquid Crystalline Copolyester," Poly. Eng. Sci., 27(9), 653 (1987).
22. G. Crevecoeur, "In-Situ Composites, Blends of Thermotropic Liquid Crystalline Polymers in a Thermoplastic Matrix," Ph.D. Dissertation, Katholieke Universiteit Leuven, Holland (1991).
23. R.H. Olley, D.C. Basset, and D.J. Bludell, Polymer, 27, 344 (1986).
24. F. Gauthier, H.L. Goldsmith, and S.G. Mason, "Particle Motions in Non-Newtonian Media. II Poiseuille Flow," Trans. Soc. Rheol., 15(2), 297 (1971).
25. Z. Tadmor, "Molecular Orientation in Injection Molding," J. Appl. Polym. Sci., 18, 1753 (1974).
26. W. Dietz, J.L. White, and E.S. Clark, "Orientation Development and Relaxation in Injection Molding of Amorphous Polymers," Polym. Eng. Sci., 18(4), 273 (1978).
27. S.K. Garg and S. Kenig, "Development of Orientation During Processing of Liquid Crystalline Polymers," in High Modulus Polymers, A.E. Zachariades, R.S. Porter, Eds., Marcel Dekker, New York, 1988: pg. 71.
28. P.H.M. Elemans, "Modelling of the Processing of Incompatible Polymer Blends," Ph.D. Dissertation, Univ. of Eindhoven, Eindhoven, Netherlands, 1989.
29. Modern Plastics Encyclopedia, McGraw Hill, New York, 1991.
30. Private communications with Hoescht Celanese Technical Service.
31. A.M. Sukhadia, "The In-Situ Generation of Liquid Crystalline Polymer Reinforcements in Thermoplastics, Ph.D. Dissertation, Virginia Tech, Blacksburg, 1991.

6.0 The Effect of Injection Molding Conditions on the Mechanical Properties of an In Situ Composite: III. Polypropylene and a Liquid Crystalline Copolyester Based on PET/PHB [1]

6.1 Introduction

Improving the mechanical properties of polymers has been a continual goal in the research and development of polymers. Several approaches have been employed to accomplish this goal. These approaches include the development of new polymers, the blending of polymers to achieve additive or synergistic results, and the reinforcement of polymers with fillers or fibers. Of the three approaches, development of new polymers is a costly route to improved properties. The latter two approaches, polymer blends and reinforcement of polymers, are generally the preferred approaches. One method that combines these two approaches is the blending of a thermoplastic (TP) matrix and a liquid crystalline polymer (LCP). These blends can offer higher mechanical properties than other blends because the mechanical properties of neat LCPs are much greater than TP matrices. The use of TP/LCP blends also avoids the processing disadvantages such as high pressures and equipment erosion that occur when processing fiber-reinforced polymers. The resulting mechanical properties of the blend are not, however, the product of simply mixing the polymers but the product of a processing method that forms a reinforcing fiber-like LCP structure within the blend. Consequently, these blends are often termed in situ composites.

---

[1] This chapter is being submitted to International Journal of Polymer Processing.

Studies of how the extrusion process affects the mechanical properties of strands and sheets of in situ composites have been conducted in the past [1-9]. However, until recently [15,16], no studies have been conducted on the effect of injection molding conditions on the mechanical properties of in situ composites. Obviously, if mechanical properties of injection molded specimens are sensitive to the conditions under which they are processed then various results can be reported for the same material. This is certainly an unwanted situation.

In previous studies [15,16], the effect of fill time, mold temperature, and mold thickness were determined for two TP/LCP blends. These blends consisted of polypropylene reinforced with either Vectra A950 [15] or Vectra B950 [16] both of which were purchased from Hoescht Celanese, Inc. It was determined that fill time and mold thickness significantly affected the mechanical properties of the blend. For PP/Vectra A950 blends, the study showed that there was no consistency in the relationship among the fill times and optimum flexural modulus for each of the three molds of different thicknesses. For the thinnest mold, the highest flexural moduli were obtained when short fill times were used. Contrarily, for the thicker molds, the highest flexural moduli were obtained when longer fill times were used. Attempts to correlate the conditions when maximum moduli were obtained to the stress and heat transfer (Graetz number) occurring in the filling stage were not successful. It was noted, however, that the mechanical properties changed from low to high values near the same Graetz number. The Graetz number is indicative of the magnitude of heat convected in the down channel direction versus the heat convected in the cross channel direction. It was also noted from the rheology of Vectra A950 measured during cooling of the LCP from the melt temperature that the storage modulus was greater than the loss modulus at the melt temperature. This suggested that Vectra A950 at 295°C was behaving in a solid-like manner. Thus, it was speculated that solidification of the LCP

during filling of the mold was a critical factor in obtaining high moduli in the blend.

A similar study was performed for blends of PP with Vectra B950 [16]. At a melt temperature of 295°C, the flexural modulus reached the highest values in all thickness molds when shorter fill times were used. The increase in moduli as the fill time decreased was related to deformation of the LCP phase. However, the point where properties changed to maximum values did not occur at the same magnitude of stress as would be expected based on droplet deformation theories [19]. Instead, the change in mechanical properties occurred at approximately the same Graetz number. This suggested that solidification of the LCP may have occurred as the stress decreased leading to the lower mechanical properties. When the stress increased so that simultaneously the Graetz number equaled or exceeded 10, Vectra B950 was in a liquid-like state necessary for obtaining high aspect ratio fibrils which lead to high mechanical properties in the blend. The storage and loss moduli of Vectra B950 measured during cooling of the LCP from a temperature of 295°C showed that the loss modulus was greater than the storage modulus at the initial melt temperature. This indicated that Vectra A950 at 295°C was behaving in a liquid-like manner. It was determined that the cooling behavior of Vectra B950 was very sensitive to a 2 to 4°C decrease in the initial melt temperature. The storage modulus approached the loss modulus when an initial melt temperature below 295°C was used. Thus, to determine if a similar modulus versus fill time behavior could be duplicated for the Vectra B950 blend as was observed for the Vectra A950 blend, the melt temperature was decreased to 292°C. The result indeed showed that similar behavior of the flexural modulus versus the fill time was found for the Vectra B950 blend as was observed for the Vectra A950 blend. Thus, a rheological condition for the LCP where storage and loss moduli are equivalent at the initial melt temperature is a key in affecting the process / property relationships in the

injection molding of TP/LCP blends.

It is anticipated that the mechanical properties of the blend studied in this work, PP and a LCP based on poly(ethylene terephthalate) and hydroxybenzoic acid (PET/PHB), may be influenced by the fill time, the melt temperature and the viscosity ratio. The fill time was shown to cause large changes in the flexural moduli of other PP/LCP blends as discussed above. Accordingly, it may also influence the mechanical properties of this blend. The melt temperature has been shown to be an important variable in the capillary extrusion of a blend of PET/PHB and a TP resin where the highest mechanical properties were obtained at a melt temperature of 230°C [1]. Thus, the melt temperature may also exhibit a strong influence on the mechanical properties of this blend. Finally, in a prior paper [15], it was noted that PET/PHB did not disperse well in the PP matrix. It was speculated that the viscosity ratio was too low to generate a finely dispersed morphology. Thus, there is evidence that the viscosity ratio may influence the mechanical properties of this blend.

The objective of this paper is to determine the sensitivity of the mechanical properties of injection molded plaques of a PP - PET/PHB blend to several processing variables (i.e. mold thickness, melt temperature) and material properties (i.e. viscosity ratio, and storage/loss moduli). Additionally, it is desired to determine if the mechanical properties can be correlated to dimensionless groups that are related to droplet deformation (Weber number) and heat transfer (Graetz number) during the filling stage. Finally, it is desired to explain the mechanisms that account for the sensitivity of mechanical properties to processing variables and material properties.

6.2 Experimental

6.2.1 Materials

Two polypropylenes (PP) were used in this study. The first PP was Profax 6823, a fractional melt flow index (MFI) polymer, and it was purchased from Himont, Inc. This polymer was used in prior studies of PP/LCP blends [13-17]. The second PP was Stamylan P supplied by DSM Inc., of the Netherlands. This polymer with a MFI of 45 was selected to obtain a higher viscosity ratio for the blend and to permit injection molding of the blend at 230°C where difficulties were encountered with the Profax PP. In this paper, the Profax 6823 and Stamylan P polymers will be designated as PP1 and PP2, respectively. The maleated PP was a development grade maleic anhydride grafted polypropylene (MAP) supplied by BP Chemicals, Inc. with a melt flow index of 50. This material was used because it enhances the mechanical properties of the blend as discussed in prior publications [10-13]. The LCP was LC3000 supplied by Unitika Ltd. of Japan. This polymer is a copolymer of poly(ethylene terephthalate) and hydroxybenzoic acid (PET/PHB). The blend was composed of 70 wt% of a PP/MAP mixture (containing 10 wt% MAP) and 30 wt% LC3000. It will be designated as PP(MAP)/LC3000 70(10)/30.

6.2.2 Rheology

The steady shear viscosity for PP/MAP, LC3000, and the blend was determined using the Instron capillary rheometer (ICR) with a single capillary of diameter 0.36 mm and a L/D ratio of 74. No end corrections were applied to the data, but the wall shear rate was corrected by means of the well-known Rabinowitsch method [29].

The storage and loss moduli for LC3000 cooled from the melt temperature was determined on the Rheometrics Mechanical Spectrometer (RMS 800) in the dynamic oscillatory mode at a rotational frequency of 1 rad s^{-1}. Parallel plate fixtures with a diameter of 25.4 mm and a gap of approximately 1.5 mm were used for all tests. A nitrogen purge provided an inert atmosphere for all tests conducted on the RMS 800. The measurements were conducted by preheating the sample at the test temperature for five minutes followed by decreasing the temperature at a rate of 5°C per minute. The tests were stopped when the transducer torque approached the transducer torque design limit.

6.2.3 Injection Molding

Dried PP/MAP pellets were physically mixed with 30 wt% dried LC3000 pellets immediately before molding on an Arburg Allrounder, model 221-55-250, injection molder. The molds were 76 by 76 mm thick rectangular cavities with thicknesses of 1.0, 1.5, and 2.3 mm. Each mold had a film gate which created two dimensional rectilinear flow throughout the cavity. Three melt temperatures (230, 250, or 265°C) were used in this study. To obtain these melt temperatures, the three injection molder barrel temperature settings were adjusted. The first temperature zone of the injection molder barrel was set to 160°C for all three melt temperatures. The second and third zone of the injection molder barrel as well as the nozzle temperature were all set to either 230, 250, or 265°C to obtain the desired melt temperatures. The injection pressure and hold pressure were set to 800 and 600 psi for all runs. The injection speed setting was varied to obtain a range of injection times. The injection time was measured as the travel time for the screw to move from the retracted position to the injected position. The volumetric flow rate was calculated by assuming a constant screw injection speed and dividing the volume

including the sprue and gate volume, 78.5 mm^3, by the fill time. The fill time is the time for polymer to flow from the entrance of the mold to the point where the mold is filled. It was calculated from the injection time by subtracting the time for the screw to advance from the retracted position to the point where polymer began entering the mold. The time for the screw to travel from the retracted position to the pressurization point was approximately 35% of the injection time. The average velocity within the mold was then calculated by dividing the volumetric flow rate by the cross sectional area of the mold.

6.2.4 Mechanical Testing

All samples were tested in the flexural mode and selected samples were tested in the tensile mode on an Instron mechanical tester, model 4204. The specimens were prepared by cutting 10 by 76 mm long strips from the 76 by 76 mm plaques in either the machine or transverse direction followed by sanding to minimize the cutting marks. Tensile specimens were tested at a crosshead speed of 1.27 mm/min while flexural specimens were tested at a rate of 1.0 %/min. An extensiometer, Instron model 2630-25, was used for all tensile tests except for determination of the strength and elongation of neat PP or PP(MAP). A minimum of five samples were tested, and the average value and standard deviation were calculated from the data.

6.2.5 Morphological Studies

Fracture surfaces of plaque samples obtained approximately 13 mm from the end of the plaque were prepared by cryogenic fracture in liquid nitrogen followed by coating with gold on a SPI sputter coater. Fracture surfaces were viewed on a Cambridge stereoscan S200 scanning

electron microscope (SEM) using an accelerating voltage of 15 KeV. The plaques were fractured in the machine direction which provides a view along the flow direction. These plaque samples were etched in hypochloric acid as described by Olley et al. [20] for 15 minutes to better reveal the LCP morphology.

6.3 Results and Discussion

The flexural moduli of the PP(MAP)/LC3000 blend versus fill time for both PP1 and PP2 matrices molded at three melt temperatures and in three molds with different thicknesses are presented first. This data indicates the process conditions and material properties that lead to the highest mechanical properties for the blend. Subsequently, the reason for obtaining higher mechanical properties from plaques processed over a range of conditions is sought.

6.3.1 Effect of Processing Conditions

As discussed in the introduction, variables such as the fill time, mold thickness, melt temperature and viscosity ratio may influence the mechanical properties of the blend. To investigate the effect of these variables, plaques of 1.0, 1.5, and 2.3 mm thickness were molded at various fill times and three different melt temperatures. A melt temperature of 230°C was chosen as the lowest temperature because higher mechanical properties were obtained in capillary extrusion at this temperature for a blend of PET/PHB and PC [1]. The other two melt temperatures were chosen as 250 and 265°C. The melt temperature of 265°C was chosen because it was used in prior studies of this blend [10,12,14] while the 250°C melt temperature was arbitrarily chosen as an intermediate temperature. The standard PP used in our laboratory

PP1 was reported as causing a poor dispersion of LC3000 in the matrix [15]. In order to raise the viscosity ratio of the blend and lower the blend viscosity so that injection molding could be performed at 230°C, a lower MFI polymer was used, PP2.

The flexural modulus is used in this study to provide a measure of the effect of process conditions and material properties on the mechanical properties of the blend. In Fig. 6-1, the flexural moduli of the blend molded into 1.0 mm thick plaques are plotted versus the fill time. Four combinations of melt temperatures and PP matrices are presented in the figure. The blend made with PP2 and processed at a 250°C melt temperature showed the highest flexural moduli (5.1 GPa) that increased as the fill time was decreased. At the larger fill times (2 to 3 s), the moduli dropped to values nearly equivalent to those obtained for the other three experimental conditions (3.5 to 4 GPa). The modulus of the blend made with PP2 and processed at a 230°C melt temperature showed no response to the fill time. For the samples made with PP1 there appears to be more variability of the flexural moduli with fill time, and no clear explanation exists at this time for the observed behavior.

In Fig. 6-2, the flexural moduli versus the fill time of the blend molded into 1.5 mm thick plaques are presented. Again, the blend made with PP2 and processed at a 250°C melt temperature showed the highest flexural moduli (3.5 GPa). However, now the maximum moduli occurred at larger fill times (3 to 4 s). The fill time does not appear to have a significant influence on the blends made with PP1 or the blend made with PP2 and processed at a melt temperature of 230°C. The flexural moduli for this latter blend does appear to be 0.3 to 0.5 GPa greater than the moduli for the blend made with PP1. This difference is only slightly greater than the confidence interval of approximately 0.3 GPa. .

In Fig 6-3, the flexural moduli versus the fill time of the blend molded into 2.3 mm thick

plaques are presented. On average, the moduli are lower in the 2.3 mm thick plaque than in the thinner plaques. However, for the blend made with PP2 which was processed at a 250°C melt temperature, the moduli showed a large increase in the flexural moduli from 2.6 to 3.5 GPa as the fill time increased from 3 to 4 seconds. While no large changes in the flexural moduli occurred for the other experimental conditions, there appeared to be a slight increase in the flexural moduli of the blend made with PP2 which was processed at a melt temperature of 230°C. The slight increase in moduli occurred at approximately the same range of fill times as were observed for PP2 which was processed at a melt temperature of 250°C. The increase in modulus was approximately equal to the confidence limits for the data, so it is not possible to confirm that blends with a PP2 matrix processed at a 230°C melt temperature are sensitive to injection times. To investigate the sensitivity of the PP2 blend to injection times and melt temperature, this blend was made at one other melt temperature, 265°C. The flexural moduli for the blend made with PP2 and processed at a 265°C melt temperature did not show a maximum but showed an average moduli of approximately 3.0 GPa [17]. This data indicated that the maximum flexural moduli occur only over a narrow range of the melt temperatures.

The data presented in these three figures indicate that only one set of variables leads to high mechanical properties. The blend made with PP2 and processed at a 250°C melt temperature clearly produced the highest mechanical properties. This indicates that the viscosity ratio and the melt temperature are both important variables. Consequently, the rheology of LC3000 and the blend were investigated to determine if any relationships might explain this behavior. In addition, the maximum properties occurred over a narrow range of fill times, and this range varied as a function of mold thickness. In the 1.0 mm thick mold, the maximum properties occurred at the shortest fill times while the maximum properties occurred at the longest

fill times for the 1.5 and 2.3 mm thick molds. The stresses and heat transfer that occurred during the filling of the three molds varied substantially, and comparison of the stress and heat transfer conditions that existed when maximum moduli occurred are also investigated.

6.3.2 Rheology

The rheology of the PP matrix and neat LC3000 will be examined to provide information that may assist in understanding why variables such as the matrix viscosity and melt temperature affect the mechanical properties of the blend. It is believed that the viscosity ratio and the rheological behavior of the LCP upon cooling will be important data to obtain and to relate to the changes in flexural moduli noted above.

The shear viscosity for the PP1/MAP, PP2/MAP, and neat LC3000 are shown in Fig 6-4. The viscosity of the PP1/MAP and PP2/MAP matrices differ by approximately a half an order of magnitude at 100 s^{-1} while the viscosity of LC3000 is one to two orders of magnitude lower than the PP matrix viscosities. The power law relationship for viscosity was fitted to this data [17] and the ratio of the LC3000 viscosity to the PP matrix viscosity was calculated from the power law model. The viscosity ratio at 100 and 1000 s-1 is shown in Table 6-1. For the PP1/MAP matrix, the viscosity ratio ranges from 0.0049 to 0.016 with the shear rate affecting the viscosity to a greater magnitude than the melt temperature. The viscosity ratio for neat LC3000 and PP2/MAP ranges from 0.032 to 0.084. Since the dispersion of Newtonian liquids in shear flow readily occurs for fluids with a viscosity ratio between 0.1 and 1 [19], the viscosity ratio of the blends is not as close to unity as might be preferred. However, the PP2 is already a low molecular weight polymer, and the viscosity ratio for this polymer does approach the desired value of unity. Thus, it is difficult with PP and LC3000 to obtain a viscosity ratio near

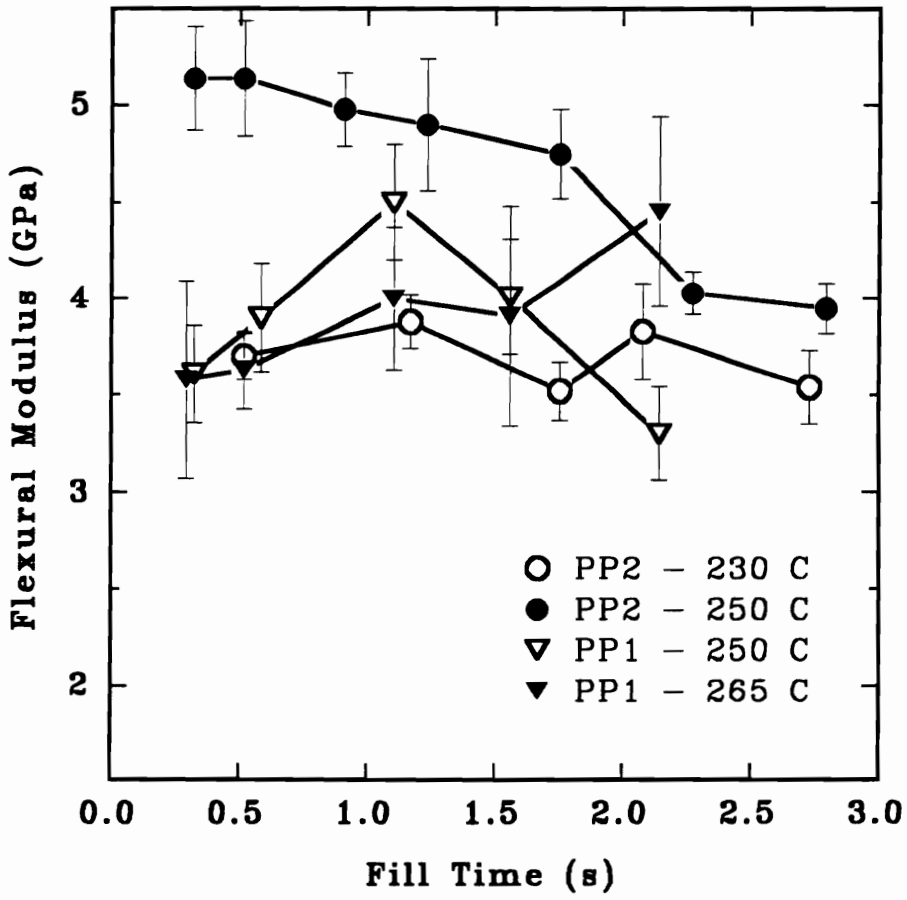

Fig. 6-1 Flexural Modulus versus fill time of 1.0 mm plaques of PP2(MAP)/LC3000 at 230 and 250°C and PP1(MAP)/LC3000 at 250 and 265°C

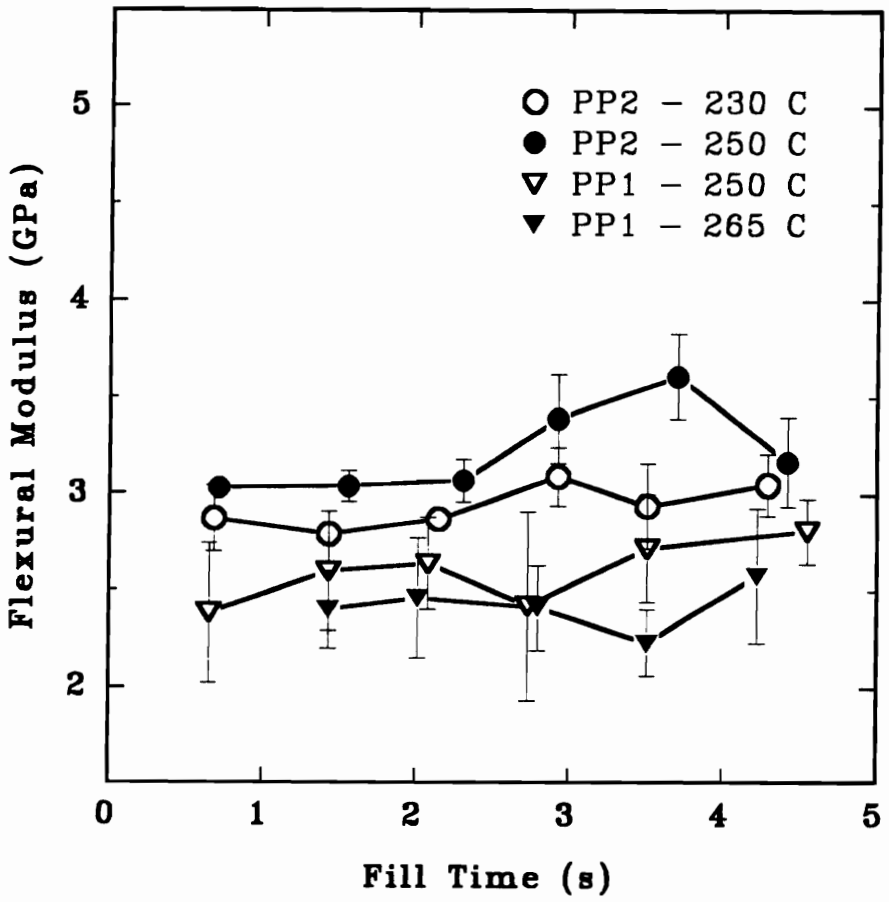

Fig. 6-2 Flexural Modulus versus fill time of 1.5 mm plaques of PP2(MAP)/LC3000 at 230 and 250°C and PP1(MAP)/LC3000 at 250 and 265°C

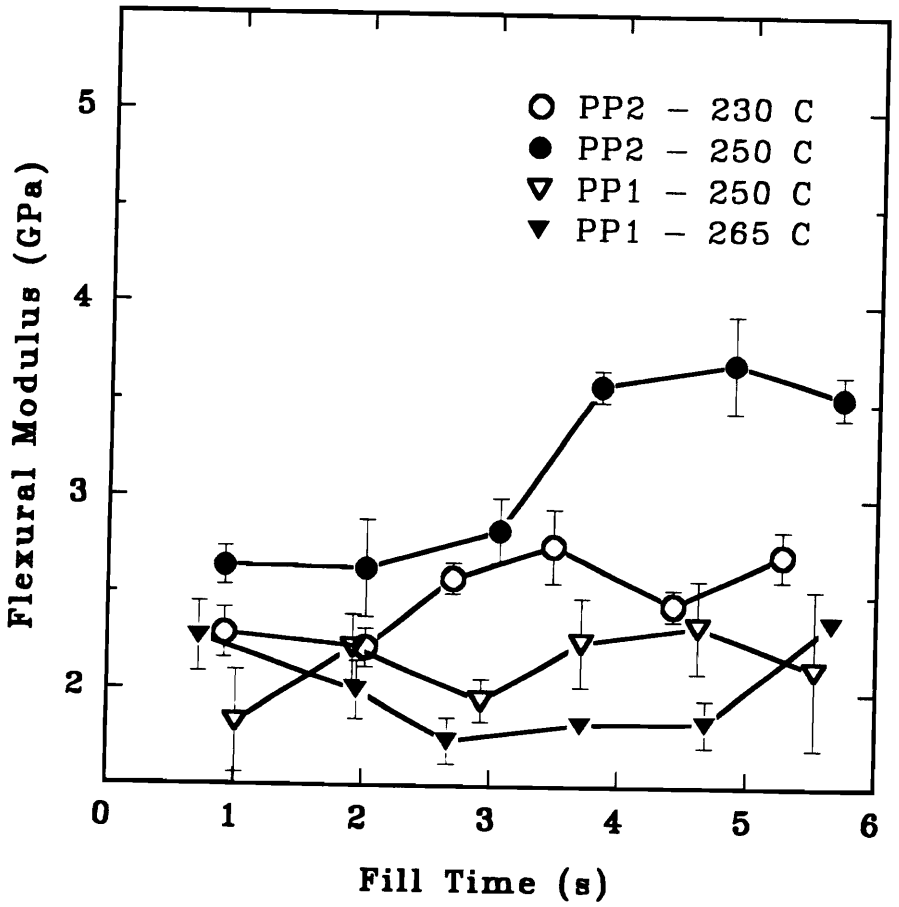

Fig. 6-3 Flexural Modulus versus fill time of 2.3 mm plaques of PP2(MAP)/LC3000 at 230 and 250°C and PP1(MAP)/LC3000 at 250 and 265°C

unity. However, the PP2 matrix does give a more favorable viscosity ratio, and the dispersion of LC3000 within the PP2 matrix is substantially improved.

The melt temperature also had an effect on the mechanical properties of the blend. It was believed that the melt temperature affected the rheology of LC3000 while it did not have a significant effect on the rheology of the PP. This speculation was confirmed by measurement of the complex viscosity or storage, G', and loss, G'', moduli of both the neat PP and the neat LC3000 during the cooling of the melts to temperatures below their respective melting point. The storage and loss moduli for neat LC3000 as it is cooled from melt temperatures of 230, 250, and 265°C are shown in Fig. 6-5. There is little difference among the moduli of LC3000 heated to 230, 250, and 265°C once the temperature falls below 210°C. However, there is a large difference among the moduli at the initial melt temperatures. The largest moduli obviously occur at the lowest melt temperature, 230°C, where the LCP is closest to solidifying. A more significant finding is discovered when the storage and loss moduli at a given melt temperature are compared. At 265°C, the loss modulus is greater than the storage modulus as is typical for a liquid or melt, and the moduli are equal once the melt is cooled to approximately 225°C. At the 250°C melt temperature, the loss modulus is slightly greater than the storage modulus, and at approximately 230°C the moduli are equal. However, at 230°C melt temperature, the storage modulus is greater than the loss modulus. This indicates that LC3000 is behaving in a solid-like manner. The transition from a solid-like ($G' > G''$) to a liquid-like ($G' < G''$) behavior must occur at a melt temperature slightly below 250°C. Thus, when the blend is processed at a 250°C melt temperature, LC3000 is almost behaving in a solid-like manner.

From prior studies on the injection molding of TP/LCP blends [15,16], it was determined that maximum properties could be obtained from the blend when the melt temperature caused the

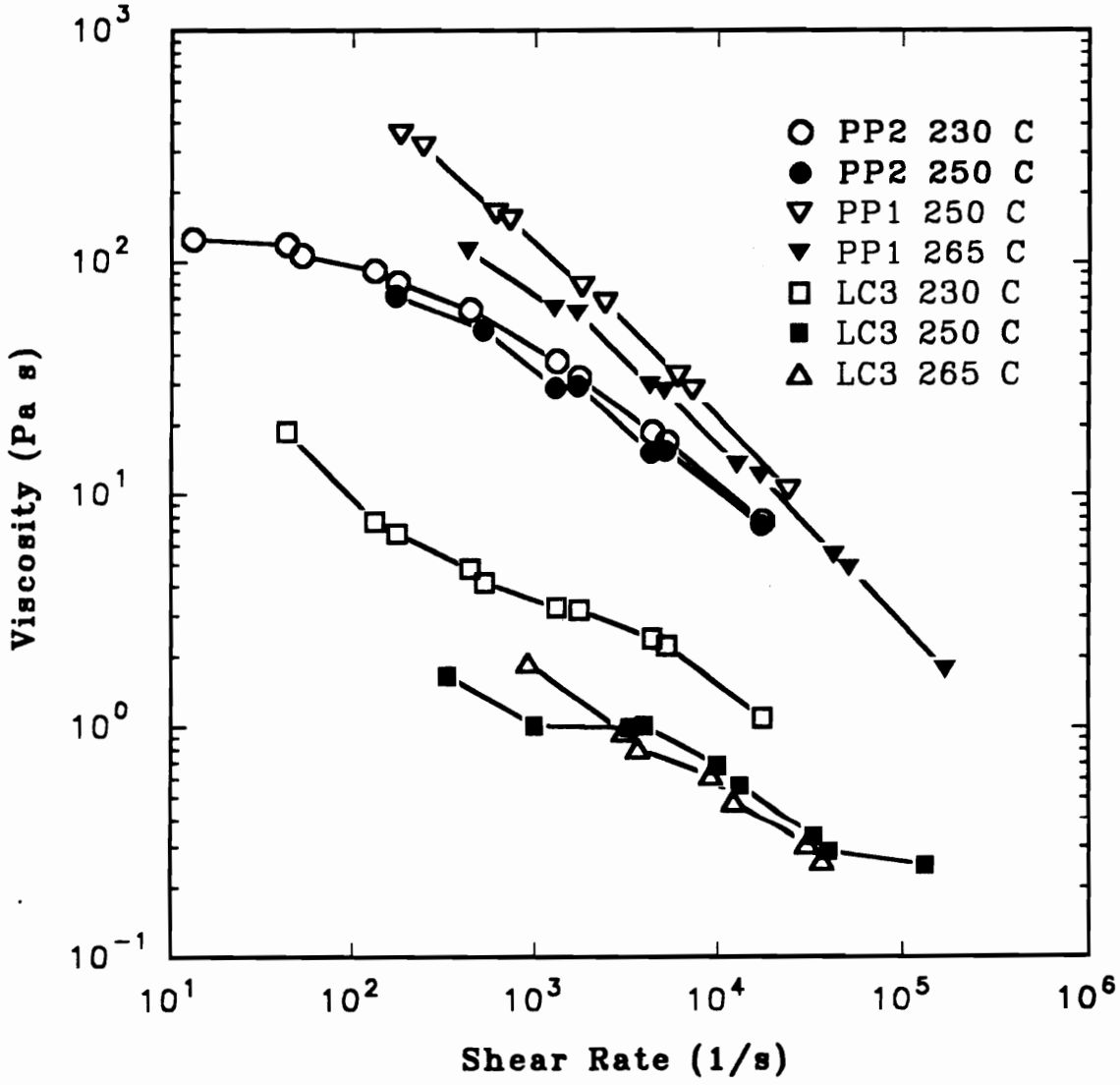

Fig. 6-4 The shear viscosity of PP1/MAP 90/10 at 250 and 265°C, PP2/MAP 90/10 at 230 and 250°C, and neat LC3000 at 230, 250, and 265°C

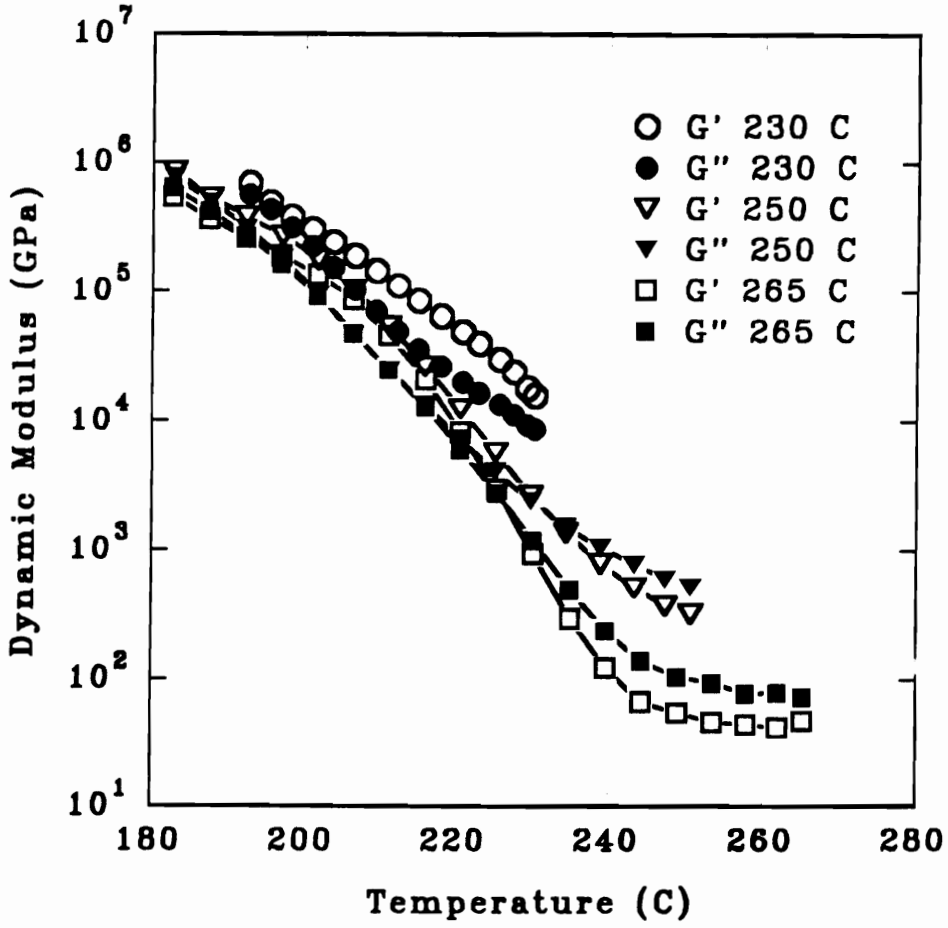

Fig. 6-5 The storage and loss moduli for neat LC3000 cooled at a rate of 5°C/min. from melt temperatures of 230, 250, and 265°C

storage and loss moduli of the LCP to be approximately equivalent. This finding also appears to be true for the PP(MAP)/LC3000 blends. Of the three melt temperatures tested, a melt temperature of 250°C is closest to the condition where $G' \approx G''$, and 250°C is the melt temperature where maximum flexural moduli were obtained. Thus, all three PP/LCP blends studied appear to have the condition $G' \approx G''$ at the melt temperature as a requirement for obtaining a maximum in the mechanical properties as the fill time is varied.

Another aspect that will be investigated is the correlation of the mechanical properties to the stress that occurs during the filling stage. Accordingly, the shear viscosity was required for the blends with PP1 and PP2 matrices. This data was calculated from capillary viscometry measurements, and the viscosity was fitted to the power law model. Little difference in the viscosity of the blends with PP1 and PP2 matrices was observed. The power law parameters are shown in Table 6-2 and there is little difference between the preexponent and exponent for any of the blends.

6.3.3 Mechanical Properties

The effect of several variables including the viscosity ratio and melt temperature has been presented. The PP2(MAP)/LC3000 blend processed at a 250°C melt temperature was found to produce the highest flexural moduli, and the effect of mold thickness and injection time on the flexural and tensile properties of this blend are now presented.

The flexural and tensile properties for the PP2(MAP)/LC3000 blend molded into 1.0 mm thick plaques at a melt temperature of 250°C are shown in Table 6-3. As the injection time is decreased from 4.3 to 0.8 seconds, the flexural modulus increased from 3.95 to 5.14 GPa as shown in Fig. 6-1. The tensile modulus showed only a slight change from 3.76 to 4.11 GPa

Table 6-1 Viscosity ratio for LC3000 and PP1(MAP) or PP2(MAP) 90/10 at various melt temperatures.

Matrix	Melt Temperature °C	Viscosity Ratio at 100 s^{-1}	Viscosity ratio at 1000 s^{-1}
PP2(MAP)	230	0.076	0.084
	250	0.032	0.041
PP1(MAP)	250	0.0049	0.011
	265	0.0066	0.015
	285	0.0085	0.016

Table 6-2 Power law parameters, m and n, for PP1(MAP)/LC3000 at 250 and 265°C and PP2(MAP)/LC3000 at 230 and 250°C.

	Melt Temperature (°C)	m (Pa s^n)	n
PP2(MAP)/LC3000	230	707	0.443
	250	468	0.463
PP1(MAP)/LC3000	250	631	0.449
	265	512	0.460

which just exceeds the confident limit of approximately 0.3 GPa as the injection time was decreased from 4.3 to 0.8 seconds. Since the flexural modulus is more sensitive to the stiffness of the skin region while the tensile modulus reflects the stiffness of the specimen throughout the entire cross sectional area, the higher flexural modulus indicates that the skin region is reinforced to a greater extent than the core. Additionally, since the flexural modulus increased with a decreased injection time while the tensile modulus remained almost unchanged, it is anticipated that the LCP structure near the skin becomes either more fibrous or the existing fibrous morphology increases in aspect ratio. At the same time, the LCP structure near the core remains unchanged. The strength of the plaques did not vary significantly with injection time. The flexural strength increased slightly from 61.4 to 65.2 MPa as the injection time was decreased while the tensile strength decreased from 37.6 to 33.4 MPa which was greater than the confidence limits of approximately 2.2 GPa. The decrease in tensile strength may be the result of a two step failure mechanism where the reinforced skin breaks followed by failure of the less reinforced core, thus resulting in a lower tensile modulus.

The flexural and tensile properties for the PP2(MAP)/LC3000 blend molded into 1.5 mm thick plaques at a melt temperature of 250°C are shown in Table 6-4. The flexural modulus has a maximum value of 3.61 GPa at 5.7 seconds and a minimum value of 3.03 GPa at 1.1 seconds. The tensile modulus has a maximum modulus of 2.96 GPa that also occurred at 5.7 seconds and the modulus has a minimum of 2.17 GPa that occurred at 1.1 seconds. Since both the tensile and flexural moduli increased by approximately the same magnitude, it is anticipated that any change in the LCP structure occurred in the subskin and core rather than in the skin region. Again, the flexural and tensile strength remain almost unchanged. The tensile strength showed a slight increase from 28.1 to 36.4 MPa.

The flexural and tensile properties for the PP2(MAP)/LC3000 blend molded into 2.3 mm thick plaques at a melt temperature of 250°C are shown in Table 6-5. A maximum in the flexural and tensile modulus occurred at longer injection times as was noted for the moduli of the 1.5 mm thick plaques. The maximum in flexural modulus was 3.70 GPa that occurred at 7.5 seconds while the minimum flexural modulus was 2.63 GPa that occurred at 3.1 seconds. The maximum tensile modulus was 3.25 GPa that occurred at 5.9 seconds and the minimum tensile modulus was 2.33 MPa that occurred at 3.1 seconds. Both the flexural and tensile moduli increased by approximately one GPa indicating that any change in the LCP structure occurred over a large cross sectional area of the plaque. The tensile strength showed an increase from 26.6 to 32.8 as the injection time increased from 1.4 to 8.8 seconds. As opposed to the behavior of the tensile strength of the 1.0 mm plaque, the tensile strength of the thicker plaques increases as the modulus increases. This may indicate that if a sharp change in morphology occurred near the skin in the 1.0 mm plaque causing a two step failure mechanism as discussed above then a smooth change in morphology occurs over a large percentage of the plaque thickness in the thicker plaques resulting in a more integral specimen.

While the mechanical properties show maximums at various injection times, it is of interest to determine how efficiently the LCP is reinforcing the matrix. This may be determined by obtaining the properties of the two neat components and calculating the upper bound of the modulus using the rule of mixtures [23]. Shown in Table 6-6 are the flexural properties for neat LC3000 molded into 1.0, 1.5, and 2.3 mm thick plaques. For each mold, plaques of neat LC3000 were made at 230, 250, and 265°C melt temperatures, and little difference between the moduli for a given plaque thickness occurred. There is a significant difference between the moduli of neat LC3000 as the mold thickness is changed. At a 250°C melt temperature, the

moduli are 10.0, 12.4, and 17.5 GPa for the 2.3, 1.5, and 1.0 mm thick plaques, respectively. Thus, the modulus of neat LC3000 increases significantly in thinner molds.

The upper bound of the blend modulus can be calculated from the moduli of neat LC3000 and PP. The flexural moduli for PP were reported in reference [15], and the moduli are 1.3, 1.7, and 1.8 GPa for the 2.3, 1.5, and 1.0 mm thick plaques, respectively. Accordingly, the moduli calculated from the rule of mixtures are 3.2, 4.1, and 5.3 GPa for the 2.3, 1.5, and 1.0 mm thick plaques, respectively. From Tables 6-3 to 6-5, the maximum moduli for the blend are 3.7, 3.6, and 5.1 GPa for the 2.3, 1.5, and 1.0 mm thick plaques, respectively. While there is some variability, the moduli of the PP2(MAP)/LC3000 blends processed with a melt temperature of 250°C fit the rule of mixture prediction indicating that maximum reinforcement of the blend occurred.

6.3.4 Morphology

The effect of processing conditions and matrix viscosity on the mechanical properties of the PP2(MAP)/LC3000 has been presented. It is now desired to relate the differences between the mechanical properties to the observed morphology. The morphology of the thickest (2.3 mm) and the thinnest (1.0 mm) plaques will be examined.

In Fig. 6-6, the photomicrograph of a 1.0 mm thick plaque molded in 0.5 seconds with a flexural modulus of 5.1 GPa is shown. In the top photomicrograph, Fig. 6-6a, the entire 1.0 mm thickness is shown while an enlargement of the skin/subkin region of the plaque is shown in the bottom photomicrograph, Fig. 6-6b. The LCP structure shown in the Fig. 6-6a is composed of many short fibers or ribbons. In the magnified view of the skin/subskin, Fig. 6-6b, long fibers or ribbons are observed near the skin. Short fibers or ribbons occur not far removed

Table 6-3 Machine direction mechanical properties of PP2(MAP)/LC3000 70(10)/30 of 1.0 mm plaques made at a 250°C melt temperature.

Injection Time (s)	Flex Modulus (GPa)	Flex Strength (MPa)	Tensile Modulus (GPa)	Tensile Strength (MPa)	Elongation at Yield (%)
0.8	5.14 (0.30)	65.2 (3.6)	4.11 (0.17)	33.4 (2.0)	1.01 (0.08)
1.4	4.98 (0.19)	63.7 (1.6)	3.97 (0.26)	35.6 (3.5)	1.37 (0.20)
1.9	4.90 (0.34)	65.1 (2.4)	4.06 (0.11)	38.9 (1.4)	1.42 (0.09)
2.7	4.75 (0.23)	64.8 (1.6)	3.71 (0.15)	34.6 (1.8)	1.33 (0.14)
3.5	4.03 (0.11)	60.2 (2.4)	3.98 (0.50)	42.6 (2.4)	1.45 (0.14)
4.3	3.95 (0.13)	61.4 (1.4)	3.76 (0.22)	37.6 (2.9)	1.53 (0.15)

Table 6-4 Machine direction mechanical properties for PP2(MAP)/LC3000 70(10)/30 of 1.5 mm plaques made at a melt temperature of 250°C.

Injection Time (s)	Flex Modulus (GPa)	Flex Strength (MPa)	Tensile Modulus (GPa)	Tensile Strength (MPa)	Elongation at Yield (%)
1.1	3.03 (0.03)	59.7 (1.6)	2.17 (0.13)	28.1 (0.9)	2.10 (0.25)
2.4	3.04 (0.08)	61.7 (2.4)	2.46 (0.16)	30.0 (1.2)	1.99 (0.12)
3.6	3.07 (0.11)	62.7 (2.0)	2.19 (0.10)	31.9 (1.5)	2.50 (0.33)
4.5	3.39 (0.23)	65.0 (1.5)	2.94 (0.14)	35.3 (1.0)	1.99 (0.12)
5.7	3.61 (0.22)	62.1 (2.3)	2.96 (0.11)	36.4 (0.6)	2.19 (0.20)
6.8	3.17 (0.23)	63.7 (0.8)	2.71 (0.14)	35.1 (1.5)	2.36 (0.22)

Table 6-5 Machine direction mechanical properties for PP2(MAP)/LC3000 70(10)/30 of 2.3 mm plaques made at a 250°C melt temperature.

Injection Time (s)	Flex Modulus (GPa)	Flex Strength (MPa)	Tensile Modulus (GPa)	Tensile Strength (MPa)	Elongation at Yield (%)
1.4	2.64 (0.10)	57.4 (1.9)	2.39 (0.21)	26.6 (0.7)	2.17 (0.15)
3.1	2.63 (0.25)	58.2 (1.4)	2.33 (0.16)	27.4 (0.3)	2.13 (0.29)
4.7	2.83 (0.17)	55.2 (2.5)	2.56 (0.16)	29.1 (0.9)	2.24 (0.21)
5.9	3.58 (0.08)	56.8 (1.4)	3.25 (0.13)	31.5 (0.54)	1.66 (0.19)
7.5	3.70 (0.25)	56.3 (1.9)	2.96 (0.21)	32.2 (0.9)	1.91 (0.18)
8.8	3.53 (0.11)	58.1 (2.1)	3.09 (0.15)	32.8 (0.8)	1.90 (0.27)

Table 6-6 Flexural properties for neat LC3000 molded to 1.0, 1.5, and 2.3 mm thick plaques at 230, 250 and 265°C melt temperatures.

Thickness (mm)	Melt Temperature (°C)	Flex Modulus (GPa)	Flex Strength (MPa)
1.0	230	15.79 (0.54)	131.9 (3.3)
	250	17.46 (0.84)	129.1 (3.4)
	265	15.78 (1.06)	124.1 (6.0)
1.5	230	13.36 (0.42)	116.1 (2.2)
	250	12.39 (0.25)	105.3 (1.5)
	265	11.46 (0.36)	99.6 (1.5)
2.3	230	8.83 (0.15)	89.8 (0.3)
	250	10.00 (0.22)	93.2 (1.6)
	265	9.75 (0.23)	92.9 (1.1)

from the skin. Thus, it appears that only the skin is reinforced by the LCP. In Fig. 6-7, the photomicrograph of a 1.0 mm thick plaque molded in 3.5 seconds with a flexural modulus of 4.0 GPa is shown. In contrast to the morphology observed in Fig. 6-6, many long fibers or ribbons are seen in the subskin and short fibers or ribbons are seen near the skin. The long LCP structures that have formed in the subskin would not be expected to increase the flexural modulus as greatly as long fibers in the skin. These fibers or ribbons in the subskin might be expected to increase the tensile modulus. Comparison of the tensile modulus for samples whose morphology is shown in Figures 6-6 and 6-7 shows that little difference exists. It is speculated that a shift in the temperature profile is responsible for the creation of this morphology.

In Fig. 6-8, the photomicrograph of a 2.3 mm thick plaque molded in 1.4 seconds with a flexural modulus of 2.6 GPa is shown. In the top photomicrograph, the entire 2.3 mm thickness is shown while an enlargement of the skin is shown in the bottom photomicrograph. This plaque shows an unusual morphology. As seen in the top photomicrograph, there is a two zone morphology. From the surface of the plaque to approximately 0.29 mm into the plaque a highly fibrous morphology is observed. Just below 0.29 mm from the surface the LCP structure changes sharply from a fibrous to a droplet morphology. Thus, only 13% of the plaque thickness is reinforced by the fibers.

In Fig. 6-9, the photomicrograph of a 2.3 mm thick plaque molded in 7.5 seconds with a flexural modulus of 3.7 GPa is shown. In the top photomicrograph, the entire 2.3 mm thickness is shown while an enlargement of the subskin of the plaque is shown in the bottom photomicrograph. The region near the skin of this plaque shows a fibrous morphology as was observed in Fig. 6-8. However, the fibrous morphology gradually changes to droplets over 25% of the thickness. It is believed that the presence to a greater depth into the plaque of a fibrous

morphology accounts for higher flexural and tensile moduli of this sample.

It was also of interest to examine the morphology of the 2.3 mm thick plaque made at a 230°C melt temperature. This plaque molded in 4.2 seconds with a flexural moduli of 2.5 GPa is shown in Fig. 6-10. The entire 2.3 mm thickness is shown in the top photomicrograph, Fig. 6-10a, while an enlargement of the skin/subskin region is shown in the bottom photomicrograph, Fig. 6-10b. Observing the bottom photomicrograph, fibers appear at 0.25 mm from the surface of the plaque. At the skin, there are many short fibers that would not be expected to efficiently reinforce the plaque. Both Figures 6-7 and 6-10 have shown the presence of fibers in a region away from the skin. This is unusual behavior for injection molded in situ composites. The location of long fibers may be related to the temperature profile in the mold during the filling stage. The plaque shown in Fig. 6-7 was molded more slowly (3.5 s) than the plaque shown in Fig. 6-6 (0.5 s). Accordingly, the temperature near the mold wall is cooler in the former plaque. It is speculated that this shift in temperature causes a shift in the location of the long fibers in the plaque. This mechanism also explain the presence of fibers in the subskin of Fig. 6-10 where the temperature in the core of the mold must be 20°C cooler than in the plaques processed at a 250°C.

6.3.5 Effect of Stress on the Flexural Modulus

The most obvious influence of stress on the structuring of TP/LCP blends is deformation of the LCP phase which leads to formation of reinforcing fibrils. Taylor's analysis showed that deformation of a Newtonian droplet in Newtonian fluid is related to the Weber number [19]. The Weber number is a dimensionless group that is the ratio of the shear or extensional stress to the surface stress, σ_{12}/R, where σ_{12} is the interfacial tension and R is the drop radius. From the

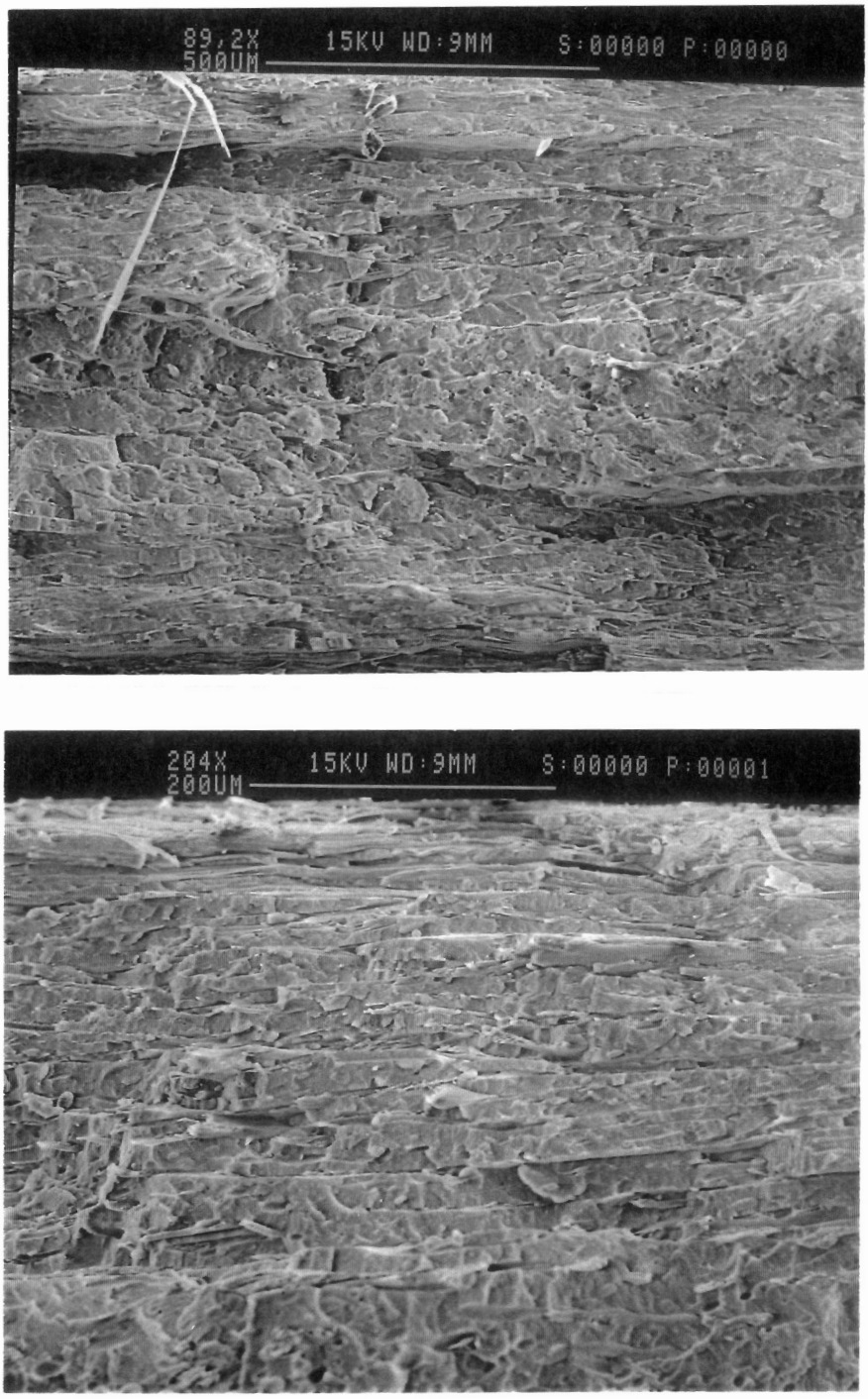

Fig. 6-6 SEM photomicrograph of 1.0 mm thick plaque of PP2(MAP)/LC3000 made at 250°C with a flexural modulus of 5.1 GPa molded in 0.5 seconds: (a) entire plaque; (b) skin/subskin region.

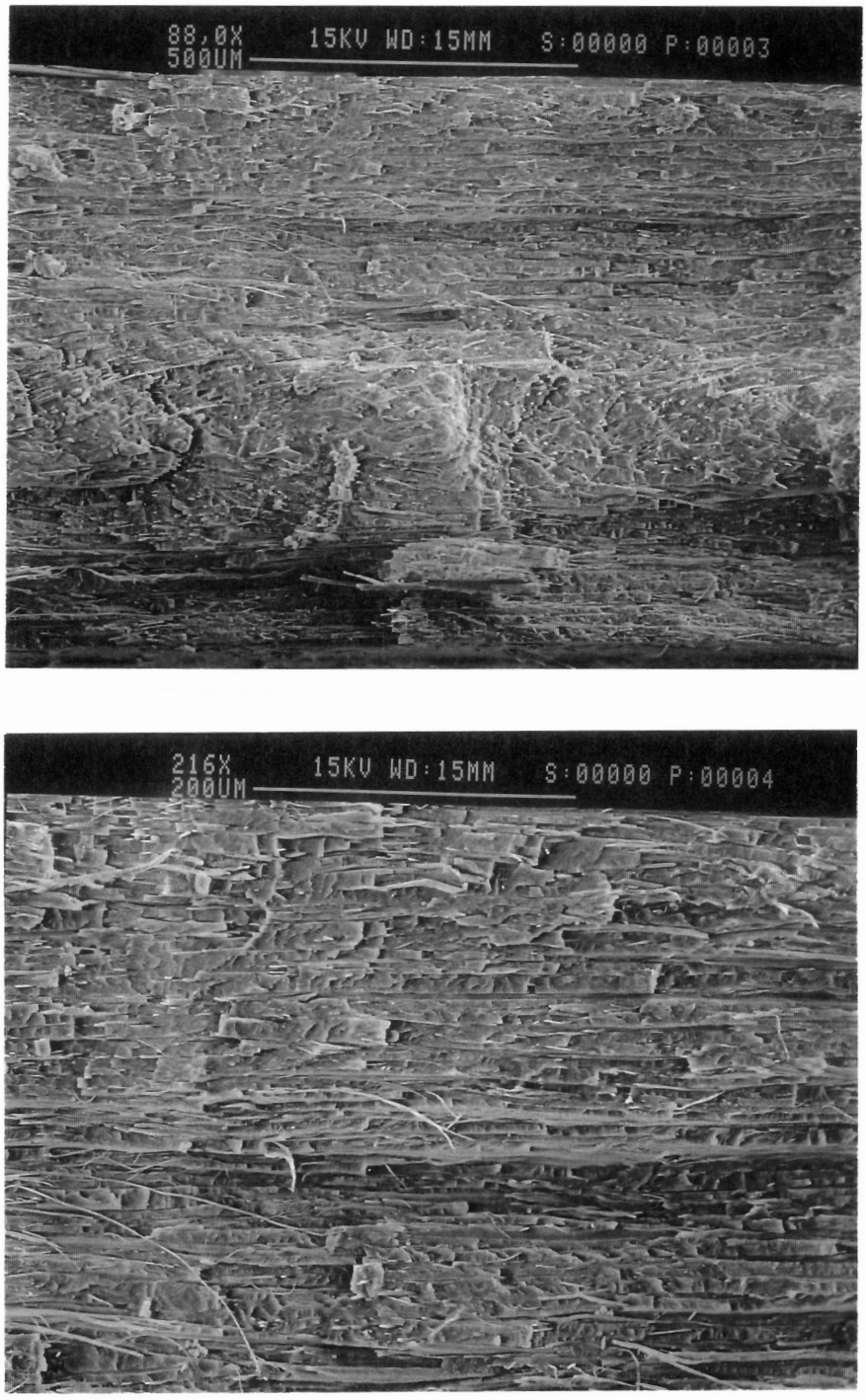

Fig. 6-7 SEM photomicrograph of 1.0 mm thick plaque of PP2(MAP)/LC3000 made at 250°C with a flexural modulus of 4.0 GPa molded in 3.5 seconds: (a) entire plaque; (b) skin/subskin region.

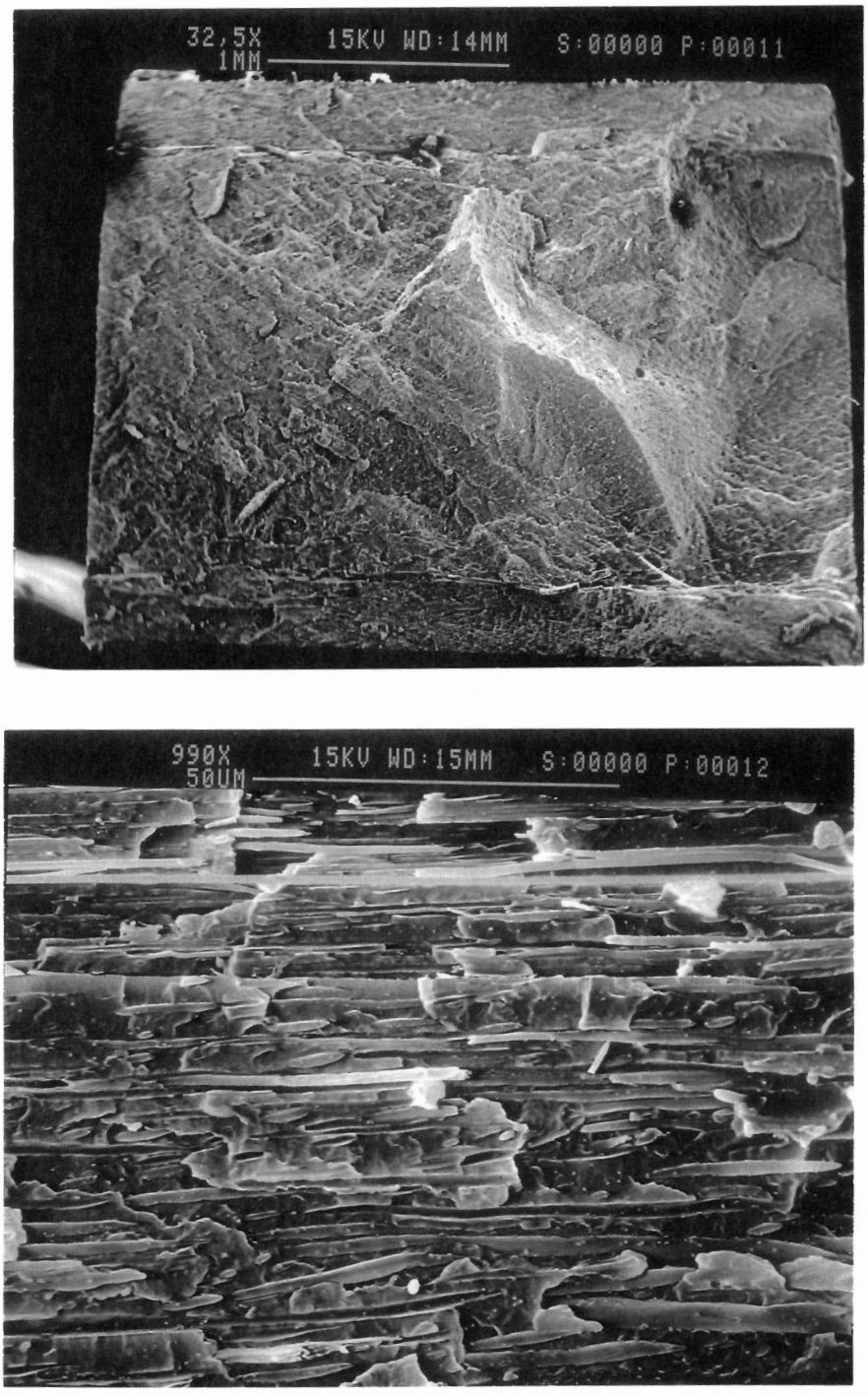

Fig. 6-8 SEM photomicrograph of 2.3 mm thick plaque of PP2(MAP)/LC3000 made at 250°C with a flexural modulus of 2.6 GPa molded in 1.4 seconds: (a) entire plaque; (b) skin/subskin region.

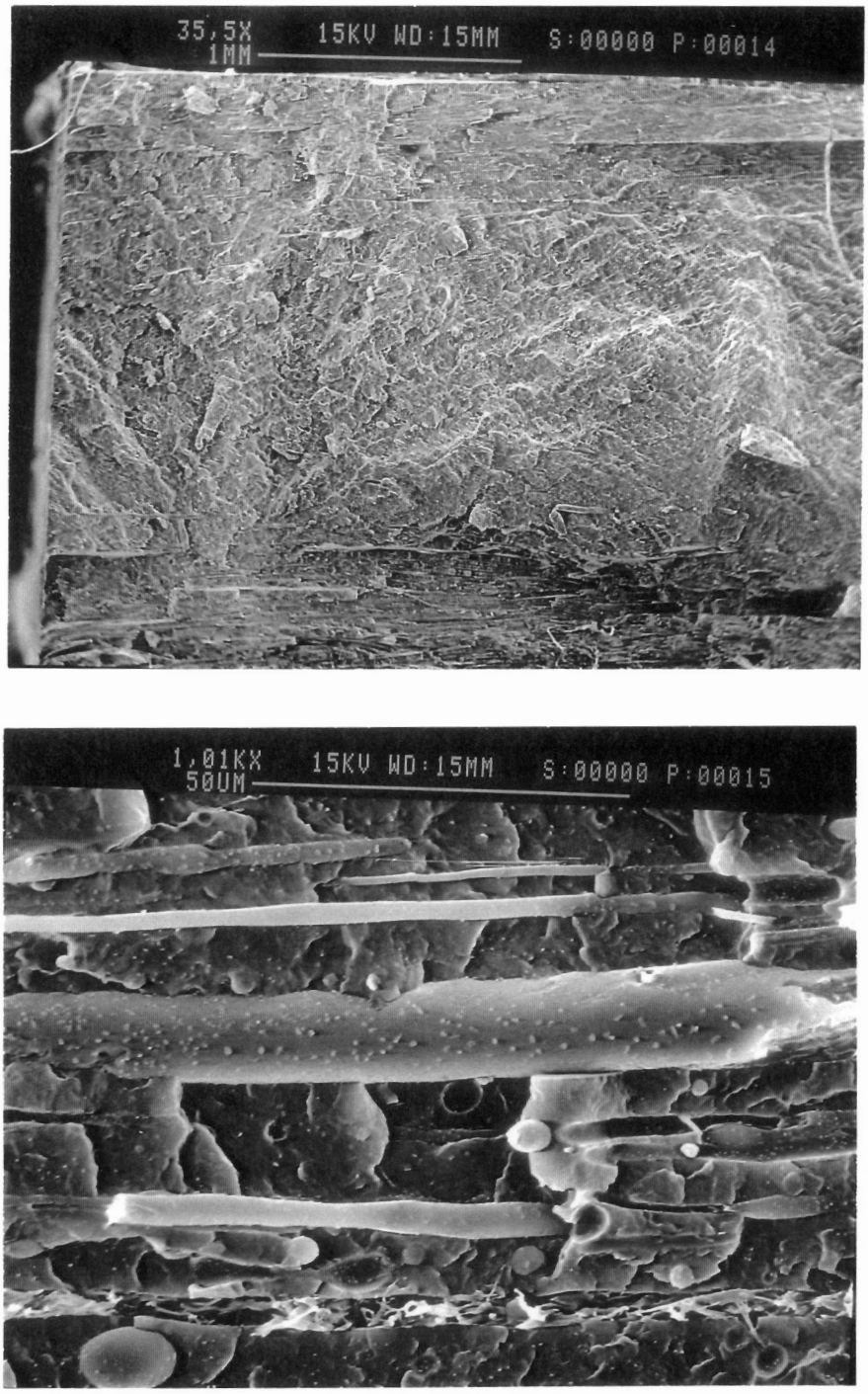

Fig. 6-9 SEM photomicrograph of 2.3 mm thick plaque of PP2(MAP)/LC3000 made at 250°C with a flexural modulus of 3.7 GPa molded in 7.5 seconds: (a) entire plaque; (b) skin/subskin region.

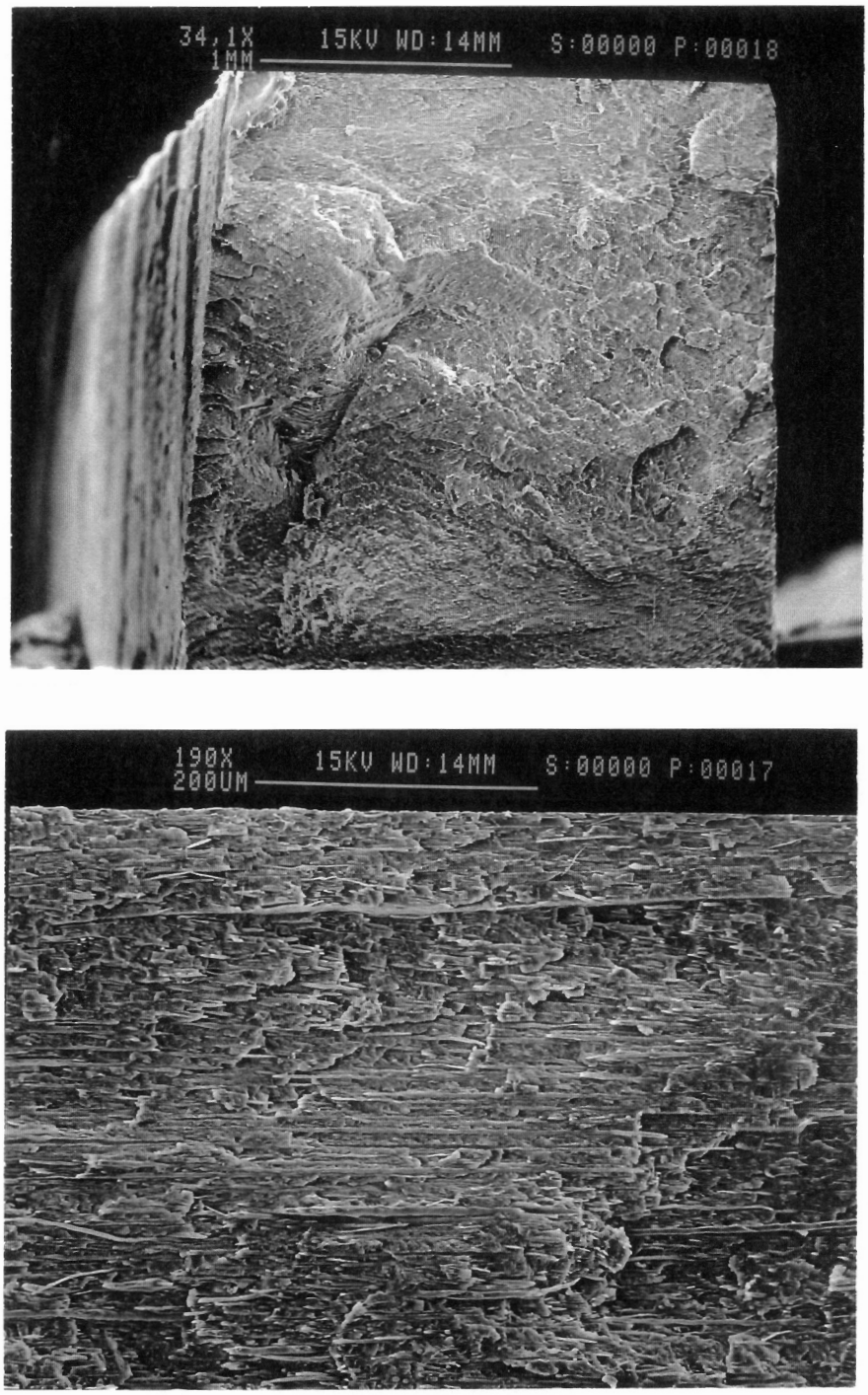

Fig. 6-10 SEM photomicrograph of 2.3 mm thick plaque of PP2(MAP)/LC3000 made at 230°C: (a) entire plaque; (b) skin/subskin region.

work of Elemans [27], it is expected that affine deformation of a droplet occurs when the Weber number is twice the value of the Weber number that causes a droplet to undergo breakup into two or more drops. Since the initial radius of a droplet is constant, the Weber number scales directly with the stress. Thus, a critical stress would be expected when affine deformation occurs, and it is believed that the large deformations that occurs with affine deformation would lead to reinforcing fibrils and hence to higher mechanical properties of the blend.

Since the Weber number is directly proportional to the stress, and it is difficult to assign an average radius, R, to the LCP morphology, the stress will be compared directly to the flexural modulus to determine if higher stresses lead to higher moduli. During the filling of a mold, two flow fields exist which lead to two stresses that can be correlated with the flexural modulus. At the advancing front, planar extensional flow (or hyperbolic stagnation flow) exists while upstream of the advancing front shear flow exists. The shear stress during mold filling may be approximated by calculating the shear stress for flow of a power law fluid between parallel plates. The shear stress accordingly can be calculated from the following equation:

$$\tau_{zy} = m\left[\frac{U}{H}\left(\frac{1+2n}{n}\right)\right]^n \left(\frac{y}{H}\right) \qquad \textbf{(6-1)}$$

where U is the average velocity, H is the half thickness of the mold, and y is the distance from the centerline of the mold.

Calculation of the extensional stress is more difficult because the extensional viscosity is not known. However, it may be approximated by using the Trouton ratio ($\eta_e/\eta_0=3$) for the extensional viscosity, η_0. In this case, the zero shear viscosity, η_0, will be replaced the viscosity at 100 s^{-1} as estimated by the power law model. The extensional stress may then be estimated using this extensional viscosity and the extensional rate at the advancing front for a power law

fluid as proposed by Tadmor [24]. This approach yields the following stress at the advancing front:

$$\tau_{zz} = -\frac{mnU}{4(1+n)H} \qquad (6\text{-}2)$$

For $n < 1$, the extensional stress will increase to a larger degree than the shear stress as the average velocity increases.

The flexural modulus versus extensional stress the for the blend molded into plaques with three different thicknesses is shown in Fig. 6-11. While the modulus increases with stress for plaques of 1.0 mm thickness, the opposite trend occurs for the thicker plaques. Both the 1.5 and 2.3 mm thick plaques yield approximately the same maximum flexural modulus as the extensional stress is decreased. Since both high and low stress can create high mechanical properties, this indicates that extensional stress does not affect mechanical properties in the same manner for the three molds of different thicknesses, and some other variable is influencing the development of the structure and mechanical properties of the blend. The same trend is observed in Fig. 6-12 where the flexural modulus is plotted versus the shear stress. The relationship between the modulus and the shear stress is very similar to that observed in Fig. 6-11 for modulus versus extensional stress. However, as in the case for extensional stress, no consistent relationship is observed from this data.

6.3.6 Effect of Heat Transfer on the Flexural Modulus

Any effect of heat transfer on the properties of TP/LCP blends is believed to be related to maintaining a molten LCP phase during the filling stage where the LCP must deform and extend to form fibrils while at the same time the heat transfer must also lead to reducing the

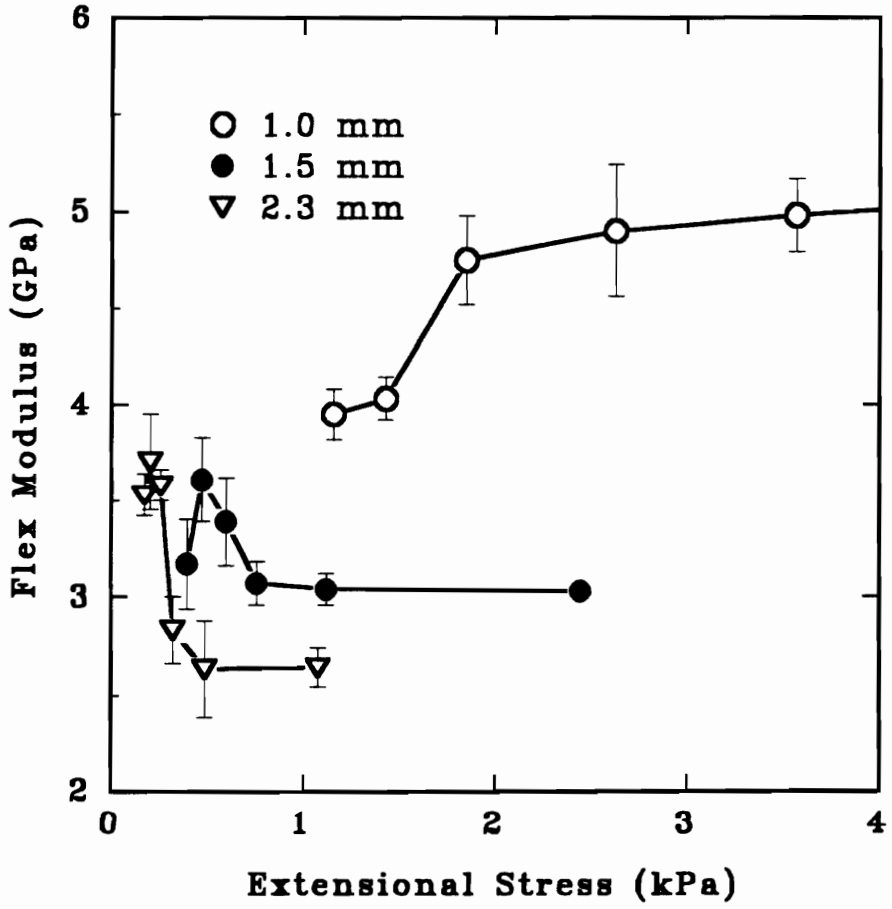

Fig. 6-11 Flexural modulus versus extensional stress for PP2(MAP)/LC3000 70(10)/30 for 1.0, 1.5, and 2.3 mm thick plaques.

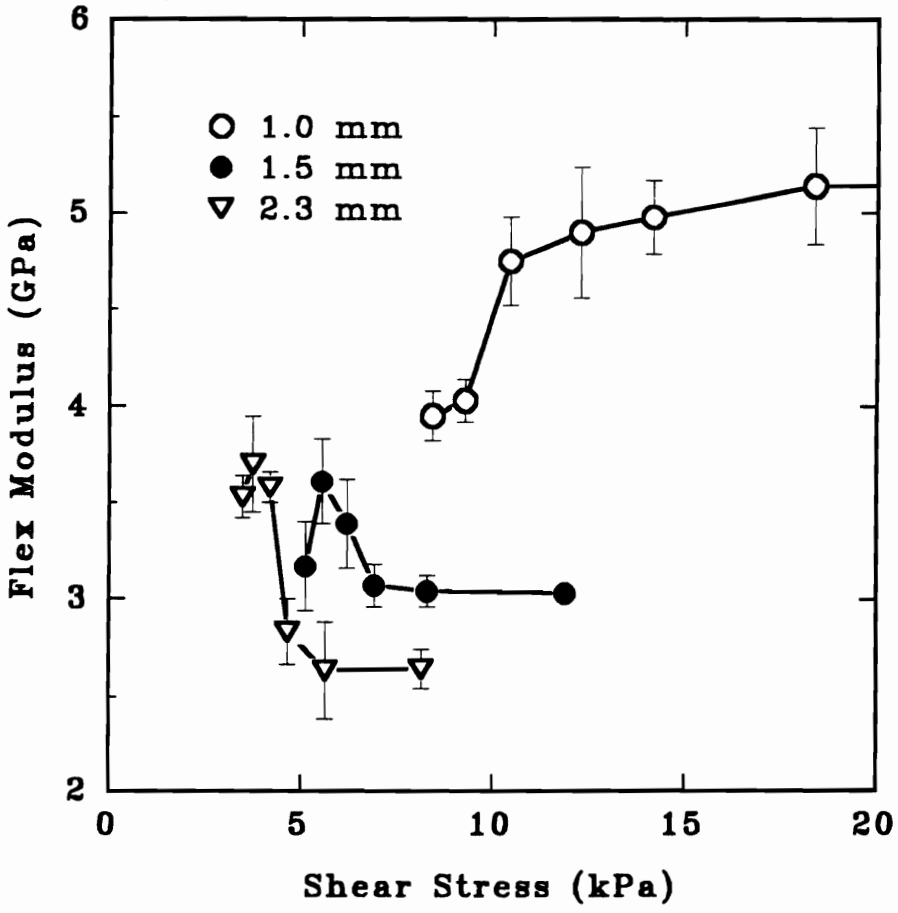

Fig. 6-12 Flexural modulus versus shear stress for PP2(MAP)/LC3000 70(10)/30 for 1.0, 1.5, and 2.3 mm thick plaques.

temperature of the LCP to the point where rapid solidification occurs upon cessation of flow. Similar situations have been discussed for both neat VA [21] and for TP/LCP blends [5,1]. The initial rheological properties of LC3000 at a 250°C melt temperature, shown in Fig. 6-5, indicate that LC3000 is approaching a solid-like state where $G' \approx G''$. The role of heat transfer in this situation may be to maintain the temperature of LC3000 just above the point where resistance to deformation increases.

Instead of calculating the transient temperature profile and correlating this large volume of data to the mechanical properties, a correlation of the flexural modulus to dimensionless variables was pursued. The appropriate dimensionless group may be obtained from dimensionless analysis or by simplifying the equations of motion and energy. The latter approach was pursued in reference [15] where the fountain flow at the advancing front was ignored to permit simplification of the problem. This approach yielded an equation which was an extension for a power law fluid of the Graetz-Nusselt problem. The only dimensionless group which arises for this problem is the Graetz number, $UH^2/\alpha L$, where α is the thermal diffusivity and L is the mold length. The Graetz number indicates the magnitude of heat convected in the flow direction to the heat conducted in the transverse direction. Accordingly, a high Graetz number, $Gz \gg 1$, indicates that little transverse cooling occurs while a small Graetz number, $Gz < 1$, indicates that a large degree of transverse cooling occurs. Comparison of the flexural modulus versus the Graetz number should indicate if heat transfer is important in this process.

The relationship between the flexural modulus and the Graetz number for plaques of 1.0, 1.5, and 2.3 mm thickness is shown in Fig. 6-13. The flexural modulus for the 1.0 mm thick plaque increases from approximately 4.0 to 5.1 GPa as the Graetz number increases. At a Graetz number above 5, maximum flexural moduli are obtained. The trend for the 1.5 mm thick plaques

are opposite to the trend for the 1.0 mm thick plaques. For the 1.5 mm thick plaques, higher moduli occur with a decrease in the Graetz number. The maximum moduli occur for a Graetz number of 5. The same trend occurs for the moduli for plaques of 2.3 mm thickness where the moduli significantly increase as the Graetz number is lowered. The maximum moduli occur for a Graetz number around 5 to 8 which is similar the value of the Graetz number where maximum properties were obtained for the 1.5 mm thick plaque.

The commonality among the moduli of plaques of different thicknesses and the Graetz number can be observed in Fig. 6-13. At first since the trends are opposite for the 1.0 mm thick plaques versus the 1.5 and 2.3 mm thick plaques, there appears to be no relationship between the flexural modulus and the Graetz number. It should be pointed out, however, that the Graetz numbers where the flexural modulus transitions from lower to higher properties for plaques of all three thicknesses occur over a narrow range of the Graetz number (near a value of 5). This indicates that the transient temperature profiles are similar when the moduli change from lower to higher values. Reflecting on the cooling behavior for LC3000 shown in Fig. 6-5 where LC3000 appears to be near a solid-like state at a 250°C melt temperature, it is believed that LC3000 is undergoing solidification in the mold when the Graetz number falls below 5. Contrarily, at a Graetz number above 5, it is believed that LC3000 remains in a molten state during the filling stage.

The difference between obtaining higher moduli at Graetz numbers below 5 versus obtaining higher moduli above a Graetz number of 5 may be related in part to the different stresses and rate of deformation that exist in filling the different thickness molds. As shown in section 6.3.3 and 6.3.4, both mechanical property differences and morphological differences exist between the plaques formed under high stresses in the 1.0 mm thick mold and plaques formed

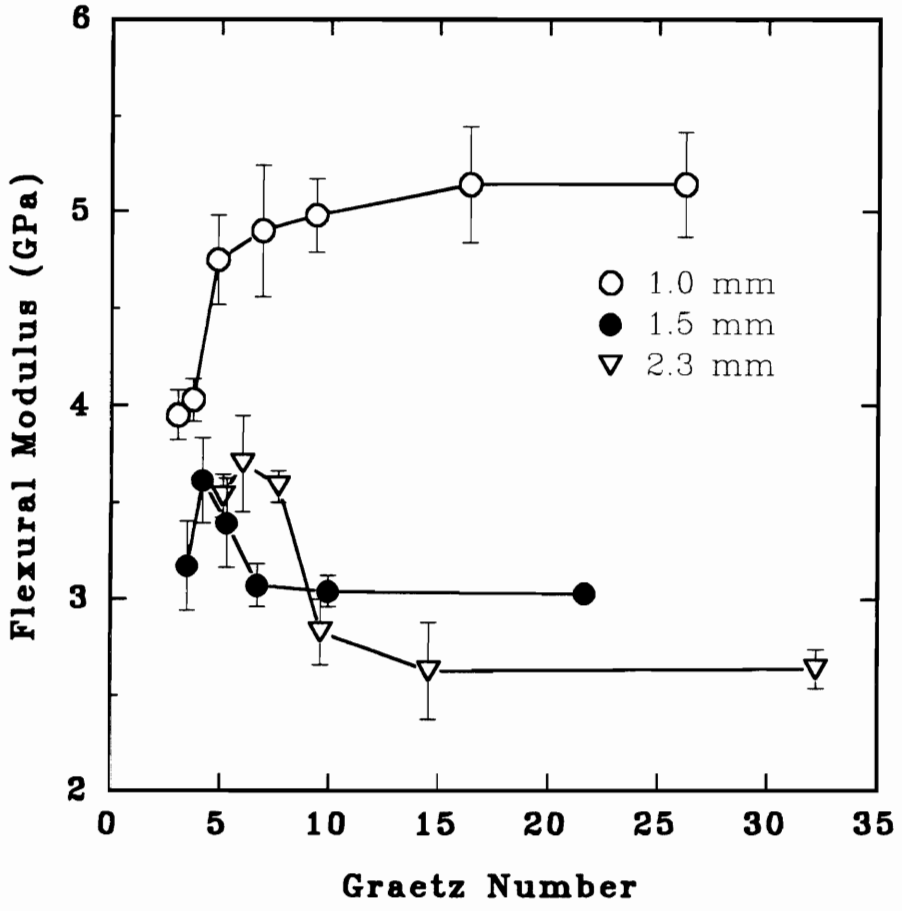

Fig. 6-13 Flexural modulus versus Graetz number for 1.0, 1.5, and 2.3 mm thick plaques of PP2(MAP)/LC3000 70(10)/30.

under low stresses in the thicker 1.5 and 2.3 mm molds. It is speculated that in the mold of 1.0 mm thickness and for $Gz > 5$, LC3000 is in a molten state that permits rapid deformation at the advancing front where large extension rates exists. Contrarily, in the thicker molds, slower deformation occurs and for $Gz < 5$, LC3000 is able to deform at the slower rates followed by rapid solidification upon cessation of flow.

It is appears doubtful because of the complex behavior of the flexural modulus versus the stress and Graetz number that the molds could be scaled to different thicknesses and yield the same properties. For instance, by increasing the stress in the thicker plaques, the same properties that where obtained in the 1.0 mm thick would not be achieved in the thicker plaques because of changes in the stress and heat transfer that are not similar. By increasing the stress in the thicker mold, the Graetz number would no longer be equivalent to the Graetz number that existed in the thinner mold, and the point where solidification occurs would be shifted thus changing the reinforcing morphology. The cooling of the plaques of different thicknesses upon cessation of flow would also be different, thus, leading to differences in morphology and properties. This latter point was discussed in a prior paper [15] where the solution of the heat conduction equation for the temperature in a slab [18] was used to approximate the temperature in the plaque during the cooling stage. As an example, for a slab initially at 250°C, the temperature reaches 200°C at one third the distance into the slab after 0.15 and 0.75 seconds for slabs of 1.0 and 2.3 mm thickness, respectively. While these are relatively short times, the morphology may still relax or undergo interfacial instabilities that cause breakup [28,26] thereby resulting in reduced moduli in the thicker plaques. It appears that unique properties and morphologies will be created in different molds for TP/LCP blends. However, a common condition for obtaining the optimum properties from any thickness plaque appears to be that the LCP is processed near a $G' - G''$

crossover point coupled with a temperature profile during the filling stage that leads to a fibrous morphology near the skin of the plaque.

6.4 Conclusions

This study has shown that the mechanical properties of PP(MAP)/LC3000 blends are sensitive to the injection speed, the mold thickness, viscosity ratio, and the melt temperature. The greatest influence on the mechanical properties of these blends was shown to be the viscosity ratio and the melt temperature. Two matrices were used which provided viscosity ratios of approximately 0.008 and 0.04. The mechanical properties were higher from the blend with a viscosity ratio closer to unity when the melt temperature was 250°C. Since droplet deformation is sensitive to the viscosity ratio and the rheology of LC3000 changes from liquid-like to solid-like near 250°C, these conditions indicate that the extent of deformation of the LCP is being changed by the matrix viscosity and the melt temperature. Under these conditions, it has been shown that the injection speed is a critical variable that influences the attainment of maximum properties. However, there is no consistency between maximum properties and the injection time. In the 1.0 mm thick mold, maximum properties were obtained by short injection times while in the 1.5 and 2.3 mm thick molds maximum properties were obtained by long injection times. The mold thickness was also shown to significantly affect the mechanical properties of the blend. Maximum flexural properties obtained for each thickness plaque approximately equaled the values calculated from the rule of mixtures. The flexural modulus of the blend increases as the mold thickness decreases in a parallel manner to the change in the flexural modulus of neat LC3000 that increased as the mold thickness decreased. Thus, there is an

advantage to using this blend in thinner molds.

Correlation of the mechanical properties of the blend to the stresses that tend to deform LC3000 into reinforcing fibrils and the heat transfer that cools the molten polymer during filling of the mold did not yield a simple relationship. High stresses that were expected to lead to a fibrous LCP structure which reinforced the matrix did not create high mechanical properties in the thicker molds. High stresses did lead to a reinforced skin structure with higher flexural moduli in the thin mold. Since high flexural moduli could be obtain with both high and low stresses no correlation was found. The maximum flexural modulus did not correlate with the Graetz number since maximum flexural moduli occurred at Graetz numbers above 5 in the thin plaques while maximum flexural moduli occurred at Graetz numbers of 5 for the thicker plaques.

A common condition, however, was found between the changes from low to high flexural moduli and the Graetz number. At a Graetz number of 5 the flexural moduli changed from low to high values in all three molds. This indicates that the temperature profile is identical in the three molds when these flexural modulus changes occur. For the thin mold, higher moduli occur when the Graetz number is greater than 5 while for the thicker molds higher moduli occur when the Graetz number is at 5. This behavior can be explained by first noting that the rheology of LC3000 at the optimum melt temperature is near a solid-like state. The relatively low Graetz number indicates that significant cooling occurs during mold filling. Thus, it is believed that for injection molding in the thick plaque the LCP is cooled to a point where solidification occurs quickly when flow ceases. For the thin plaque, however, the high stresses and velocities require large rates of deformation that can only occur with a liquid-like state for the LCP. Thus, the Graetz number must be above 5 to achieve this condition.

6.4 Acknowledgements

This work was supported by the Army Research Office (grant number DAAL03-91-G-0166), and their support is sincerely appreciated.

6.5 References

1. M.R. Nobile, E. Amendola, and L. Nicolais, "Physical Properties of Blends of Polycarbonate and a Liquid Crystalline Copolyester," Polym. Eng. Sci., 29(4), 244 (1989).
2. D. Dutta, H. Fruitwala, A. Kohli, and R.A. Weiss, "Polymer Blends Containing Liquid Crystals: A Review," Polym. Eng. Sci., 30(17), 1005 (1990).
3. B.R. Bassett and A.F. Yee, "A Method of Forming Composite Structures Using In Situ-Formed Liquid Crystal Polymer Fibers in a Thermoplastic Matrix," Poly. Eng. Sci., 11(1), 10 (1990).
4. F.P. La Mantia, M. Saiu, A. Valenza, M. Paci, and P.L. Magagnini, "Relationships Between Mechanical Properties and Structure for Blends of Nylon-6 with a Liquid Crystal Polymer," Eur. Polym. J., 26(3), 323 (1990).
5. K.G. Blizard, C. Federici, O. Federico, and L.L. Chapoy, "The Morphology of Extruded Blends Containing a Thermotropic Liquid Crystalline Polymer", Poly. Eng. Sci., 30(22), 1442 (1990).
6. D. Beery, S. Kenig, And A. Siegmann, "Structure Development During Flow of Polyblends Containing Liquid Crystalline Polymers," Poly. Eng. Sci., 31(6), 451 (1991).
7. K.G. Blizard and D.G. Baird, "The Morphology and Rheology of Polymer Blends Containing a Liquid Crystalline Copolyester," Poly. Eng. Sci., 27(9), 653 (1987).
8. G. Crevecoeur, "In-Situ Composites, Blends of Thermotropic Liquid Crystalline Polymers in a Thermoplastic Matrix," Ph.D. Dissertation, Katholieke Universiteit Leuven, Holland (1991).
9. D.G. Baird, T. Sun, D.S. Done, and G.L. Wilkes, "In Situ Formation of Reinforced Thermoplastic Composites," J. Thermoplastic Composite Materials, 3,81 (1990).
10. H.J. O'Donnell, A. Datta, D.G. Baird, "The Effect of Compatibilization on the Properties of Blends of TLCPs with Polypropylene," Annual Technical Conference of the Society of Plastic Engineers (ANTEC'92), 50, 2248 (1992).
11. A. Datta, "The Effect of Compatibilization on Blends of Polypropylene with a Liquid Crystalline Polymer ," Polymer 34(4), 759 (1993).
12. A. Datta "Compatibilization of Thermoplastic Composites Based on Blends of Polypropylene with two liquid crystalline copolyesters," submitted to Polymer.
13. H.J. O'Donnell, H.H. Chen and D.G. Baird, Annual Technical Conference of the Society of Plastic Engineers (ANTEC '93), (1993).
14. H.J. O'Donnell and D.G. Baird, "In Situ Reinforcement of Polypropylene with LCP: Effect of Maleic Anhydride Grafted Polypropylene," submitted to Polymer.

15. H.J. O'Donnell and D.G. Baird, "The Effect of Injection Molding Conditions on the Mechanical Properties of an In Situ Composite: I. Polypropylene and a Liquid Crystalline Copolyester Based on HBA/HNA," submitted to Polym. Eng. Sci.
16. H.J. O'Donnell and D.G. Baird, "The Effect of Injection Molding Conditions on the Mechanical Properties of an In Situ Composite: II. Polypropylene and a Liquid Crystalline Poly(ester-amide)" submitted to International Journal of Polymer Processing.
17. H.J. O'Donnell, Ph.D. Dissertation, Virginia Polytechnic Institute and State University, Blacksburg, VA, 1994.
18. J.P. Holman, Heat Transfer, 4th ed., McGraw Hill, New York, 1976.
19. G.I. Taylor, "The Formation of Emulsions in Definable Fields of Flow," Proc. Roy. Soc. A146, 501, (1934).
20. R.H. Olley, D.C. Basset, and D.J. Bludell, Polymer, 27, 344 (1986).
21. T-S. Chung, "Production of Ultrahigh Modulus Liquid Crystal Polymer Rods," J. Polym. Sci.: Part B: Polym. Phys., 26, 1549 (1988).
22. F. Gauthier, H.L. Goldsmith, and S.G. Mason, "Particle Motions in NonNewtonian Media. II Poiseuille Flow," Trans. Soc. Rheol., 15(2), 297 (1971).
23. R.A. Dickie "Mechanical Properties of Multiphase Polymer Blends," in Polymer Blends, Vol. 1, D.R. Paul and S. Newman, Ed., Academic Press, New York, 1978.
24. Z. Tadmor, "Molecular Orientation in Injection Molding," J. Appl. Polym. Sci., 18, 1753 (1974).
25. H. Janeschitz-Kriegl, "Injection Moulding of Plastics II. Analytical Solution of Heat Transfer Problem," Rheol. Acta, 18, 693 (1979).
26. J.J. Elmendorp, "Dispersive Mixing in Liquid Systems," in Mixing in Polymer Processing, C. Ramwendaul, Ed., Marcel Dekker, New York, 1991.
27. P.H.M. Elemans, "Modelling of the Processing of Incompatible Polymer Blends," Ph.D. Dissertation, Univ. of Eindhoven, Eindhoven, Netherlands, 1989.
28. S. Tomotika, "On the Instability of a Cylindrical Thread of a Viscous Liquid Surrounded by Another Viscous Fluid," Proc. Roy. Soc., 150, 322 (1935).
29. R.B. Bird, R.C. Armstrong, and O. Hassager, Dynamics of Polymeric Liquids, Vol. 1, John Wiley, New York, 1987.

7.0 Recommendations For Future Work

This study has contributed to the understanding of how to process PP/LCP in situ composites. However, in doing so, this study has uncovered new questions regarding the behavior and the processing / property relationship for these blends. Some of these questions are discussed here with recommendations for future work.

Other compatibilizers, acrylic acid and phenol modified polypropylene, were evaluated in preliminary studies. The properties of TP/LCP blends with fixed content of these compatibilizers were equivalent to the properties of TP/LCP blends with MAP. Hence, determination of property / concentration relationships would be useful to provide a comparison of acrylic acid and phenol modified compatibilizers to MAP.

It was shown that MAP degrades at processing temperatures. Less compatibilizer may be needed if it were thermally stable. Hence, development of a stable compatibilizer lead to improved compatibilization of these blends.

It would also be of interest to design a reactive LCP / compatibilizer system. This type of compatibilized system could potentially be used to increase the mechanical properties in a PP/LCP blend to a greater degree than can be obtained with interactive compatibilizers.

It may be desired to improve the impact properties of PP/LCP blends. This could be done in a standard manner by inclusion of a rubbery phase in either the PP or LCP phase. Use of a compatibilizer would be helpful in attaining the greatest improvement from a toughening phase.

As shown in this study, the relationship between stress, Graetz number, and flexural modulus is complex. If the processing / property relationship for injection molding the blends in mold of different lengths but the same thickness (thin) were studied, a different range of conditions would be obtained. This would extend the relationships obtained in this study. The new information gathered by the above approach would be the processing / property relationship for PP/LCP blends at a reduced stress without changing the Graetz number. Additionally, the solidification of the plaque in the cooling stage would remain constant since the mold thickness remains constant. Because the sample length changes, special flexural testing equipment may be necessary that would permit flexural testing of small specimens (e.g., less than 50 mm).

The formation of long fibrous LCP morphologies was correlated with higher flexural properties in this study. This morphology was formed under a narrow range of heat transfer and melt rheology. It would be of interest to determine how sensitive the deformation of dispersed LCP in a matrix was to the flow field, rate of deformation, and the Graetz number. This study could be accomplished in standard flow visualization equipment such as the slot flow or impinging flow. However, to accomplish the nonisothermal nature of the experiment, the temperature of the entry flow would have to be controlled and analyzed. These experiments could indicate the conditions were fibrillation most readily occurs. These conditions could then be related to numerical simulations of the transient temperature profiles during the filling stage to aid in mold design.

Cooling and solidification of the LCP was found to be a key in obtaining fibrous morphology and high mechanical properties. The solidification process in not understood well at present. It would, therefore, be helpful to study the solidification process. This study might be accomplished by comparing differential thermal analysis to rheological measurements. In

particular, it would be of value to compare the crystallization kinetics of the LC poly(ester-amide) to the LC copolyester. As shown in this study, significant differences exist between these two types of LCPs, and it would be desired to confirm or disprove that crystallization is involved with this process.

Rheological differences between LC copolyesters and LC poly(ester-amides) exist which indicate how a TP/LCP blend behaves during processing. Accordingly, the developers of new LCPs may be able to use the rheological cooling behavior as an aid in deciding upon the most useful chemical structure for processing TP/LCP blends.

Appendix

Table A-1 Comparison of the machine direction flexural properties of PP1 and PP2 of 1.5 mm thick plaques.

	Flexural Modulus (GPa)	Flexural Strength (MPa)
PP2(MAP) 90(10)	1.61 (0.08)	48.5 (1.7)
PP1	1.68 (0.04)	49.6 (1.7)

Table A-2 Tensile properties of PP1 and MAP dogbone specimens.

	Tensile Strength (MPa)	Tensile Modulus (GPa)	Elongation at Yield (%)
PP	36.7 (0.5)	1.37 (0.10)	>9
MAP	30.6 (0.4)	1.37 (0.08)	5.82 (0.13)

Table A-3 Machine direction flexural properties of PP2(MAP)/LC3000 70(10)/30: 2.3 mm thick plaque.

Flexural Properties of DSM(BP)/LC3000 70(10)/30 265°C Melt Temperature 0.09" Plaques		
Injection Time (s)	Modulus (GPa)	Strength (MPa)
1.3	2.04 (0.10)	55.7 (1.5)
2.9	3.01 (0.07)	55.8 (1.4)
4.0	3.23 (0.09)	55.7 (2.1)
5.5	2.60 (0.08)	59.2 (0.7)
7.2	3.02 (0.11)	60.8 (0.6)
9.0	3.05 (0.12)	57.2 (0.8)

Table A-4 Sensitivity analysis of the effect of variations in the ethylene glycol contact angle ($\theta_{ethy\ glyc}$) on the interfacial properties of blends with VA.

	γ (mJ/m2)	γ_d/γ (x100)	γ_{12} (mJ/m2)	W_{ad} (mJ/m2)
$\theta_{ethy\ glyc}+2.8°$				
PP	23.6	74.5	4.5	54.0
PP(MAP)	26.6	61.8	1.4	60.1
$\theta_{ethy\ glyc}+0°$				
PP	25.6	82.0	6.3	54.2
PP(MAP)	27.0	63.5	1.5	60.4
$\theta_{ethy\ glyc}$-2.8°				
PP	26.6	84.3	7.07	54.4
PP(MAP)	26.0	53.5	1.31	59.6

Table A-5 Sensitivity analysis of the effect of a variation of the water contact angle (θ_{water}) on the interfacial properties of blends with VA.

	γ (mJ/m2)	γ_d/γ (x100)	γ_{12} (mJ/m2)	W_{ad} (mJ/m2)
$\theta_{water}+2.8°$				
PP	23.7	61.2	2.4	56.2
PP(MAP)	27.1	68.7	2.2	59.8
$\theta_{water}+0°$				
PP	25.6	82.0	6.3	54.2
PP(MAP)	27.0	63.5	1.5	60.4
$\theta_{water}-2.8°$				
PP	22.9	61.2	2.7	55.1
PP(MAP)	26.6	42.6	2.6	58.9

Table A-6 Machine direction flexural properties for PP(MAP)/VA 70(10)/30 1.0 mm thick plaques.

Mold Temperature	Injection Time (s)	Flex Modulus (GPa)	Flex Strength (MPa)
20°C	0.8	61.3 (2.5)	4.96 (0.42)
	1.4	59.7 (1.9)	4.45 (0.35)
	2.2	54.9 (1.4)	3.69 (0.28)
	3	58.0 (2.2)	3.88 (0.22)
	4.1	52.7 (4.6)	3.13 (0.67)
70°C	0.8	63.3 (4.0)	5.44 (0.68)
	1.4	60.4 (1.8)	4.57 (0.28)
	2	57.1 (2.8)	3.93 (0.58)
	2.8	53.7 (3.3)	3.44 (0.40)

Table A-7 Machine direction flexural modulus for PP(MAP)/VA 70(10)/30 1.5 mm thick plaques.

Mold Temperature	Injection Time (s)	Flex Modulus (GPa)	Flex Strength (MPa)
20°C	.8	4.20 (.19)	55.8 (1.1)
	1.4	4.32 (.30)	57.4 (0.8)
	2.4	4.40 (.26)	58.3 (2.3)
	3.3	4.40 (.72	55.2 (0.8)
	5	5.13 (.49)	59.4 (1.3)
70°C	.8	2.99 (.26)	51.9 (3.0)
	1.4	3.95 (.34)	55.4 (2.0)
	2.4	4.32 (.09)	54.7 (1.0)
	3.7	4.39 (1.16)	58.3 (1.1)
	5.3	4.45 (.22)	57.2 (1.0)

Table A-8 Machine direction flexural modulus for PP(MAP)/VA 70(10)/30 2.3 mm thick plaques.

Mold Temperature	Injection Time (s)	Flex Modulus (GPa)	Flex Strength (MPa)
20°C	1	2.44 (.14)	51.3 (1.9)
	1.8	2.94 (.45)	55.0 (1.1)
	3.3	3.39 (.38)	55.8 (3.2)
	4.3	3.85 (.27)	57.1 (2.9)
	5.5	3.44 (.15)	55.2 (1.5)
70° C	.8	2.01 (.90)	52.8 (2.0)
	1.1	2.37 (.23)	53.7 (2.0)
	1.9	2.82 (.19)	54.0 (2.0)
	3.1	3.10 (.16)	56.0 (2.9)
	4.8	2.92 (.18)	55.5 (.7)
	6.8	3.62 (.21)	55.7 (2.9)

Table A-9 Flexural properties for PP(MAP)/VB 70(10)/30 tumbled blend: 1.0 mm thick plaque.

Injection Time	Modulus (GPa)	Strength (MPa)
Machine Direction		
0.5	4.02 (.36)	51.5 (1.5)
0.8	3.54 (.31)	49.8 (1.8)
1.6	3.57 (.20)	51.4 (1.6)
2.4	3.28 (.65)	49.4 (1.9)
2.8	3.64 (.38)	50.0 (1.9)
Transverse Direction		
0.5	1.52 (.15)	29.5 (4.2)
0.8	1.41 (.21)	31.7 (4.9)
1.6	1.71 (.24)	33.5 (5.6)
2.4	1.63 (.11)	33.1 (2.7)
2.8	1.67 (.15)	33.7 (3.9)

Table A-10 Flexural properties for PP(MAP)/VB 70(10)/30 tumbled blend: 1.5 mm thick plaques.

Injection Time (s)	Flex Modulus (GPa)	Flex Strength (MPa)
Machine Direction		
.9	5.30 (0.46)	50.0 (3.1)
2	4.70 (0.42)	47.5 (2.5)
3	4.72 (0.13)	46.2 (2.9)
4.4	5.12 (0.35)	46.8 (2.8)
5.5	4.98 (0.46)	44.8 (2.9)
6.8	4.31 (0.33)	47.1 (1.6)
8.5	3.91 (0.21)	47.0 (2.1)
10	4.37 (0.47)	46.7 (3.3)
Transverse Direction		
.9	1.80 (.20)	35.1 (3.2)
2.0	1.98 (.43)	35.9 (4.4)
3.0	1.69 (.31)	38.3 (5.9)
4.4	1.59 (.18)	34.8 (3.9)

Table A-11 Flexural properties for PP(MAP)/VB 70(10)/30 tumbled blends: 2.3 mm thick plaques.

Injection Time (s)	Flex Modulus (GPa)	Flex Strength (MPa)
Machine Direction		
1.3	4.34 (0.33)	49.4 (4.8)
2.8	5.27 (0.25)	52.1 (1.4)
4.3	5.21 (0.46)	53.1 (5.6)
6.3	5.05 (0.45)	50.5 (3.2)
8	4.97 (0.38)	54.7 (2.5)
13.5	4.44 (0.27)	41.8 (3.6)
17.3	4.06 (0.31)	41.5 (2.3)
Transverse Direction		
1.3	1.83 (.25)	37.0 (1.2)
4.3	1.83 (.40)	34.2 (2.9)

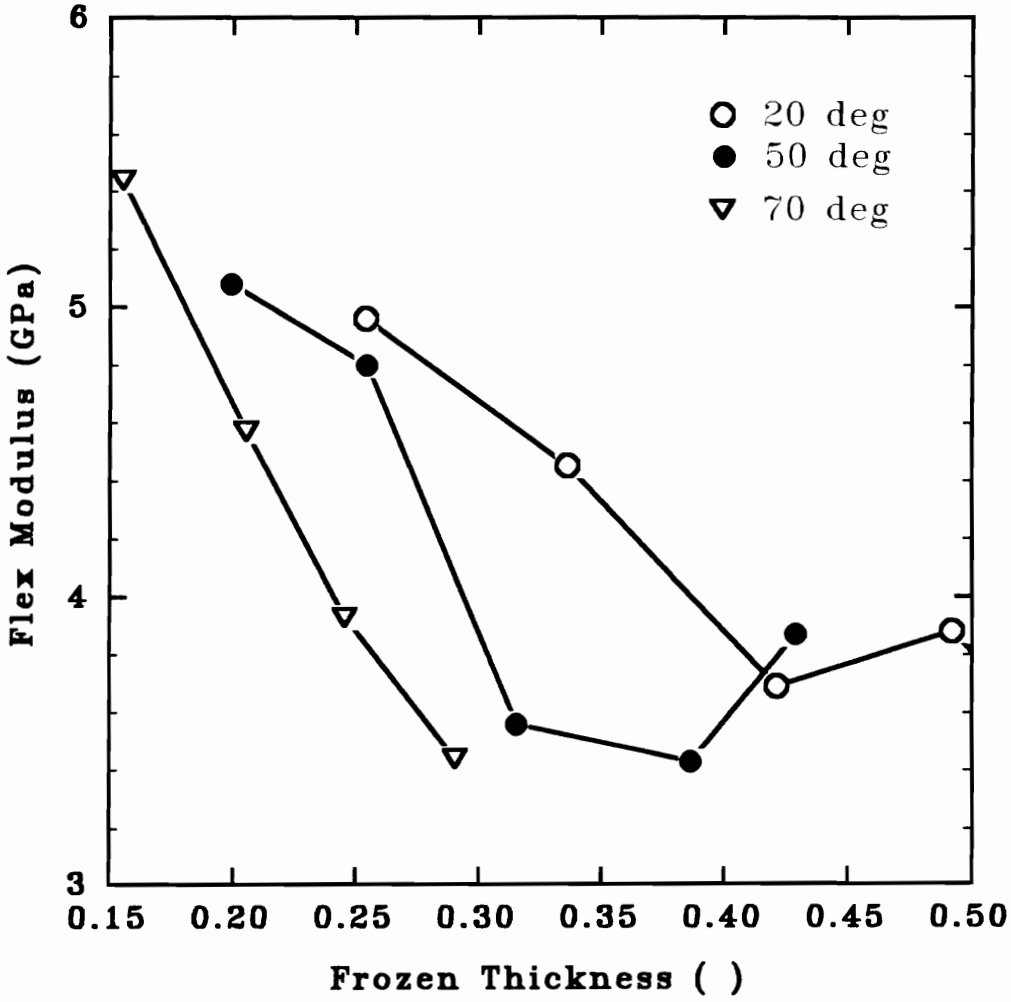

Fig. A-1 Flexural modulus of a 1.0 mm thick plaque of PP(MAP)/VA 70(10)/30 versus the frozen layer thickness.

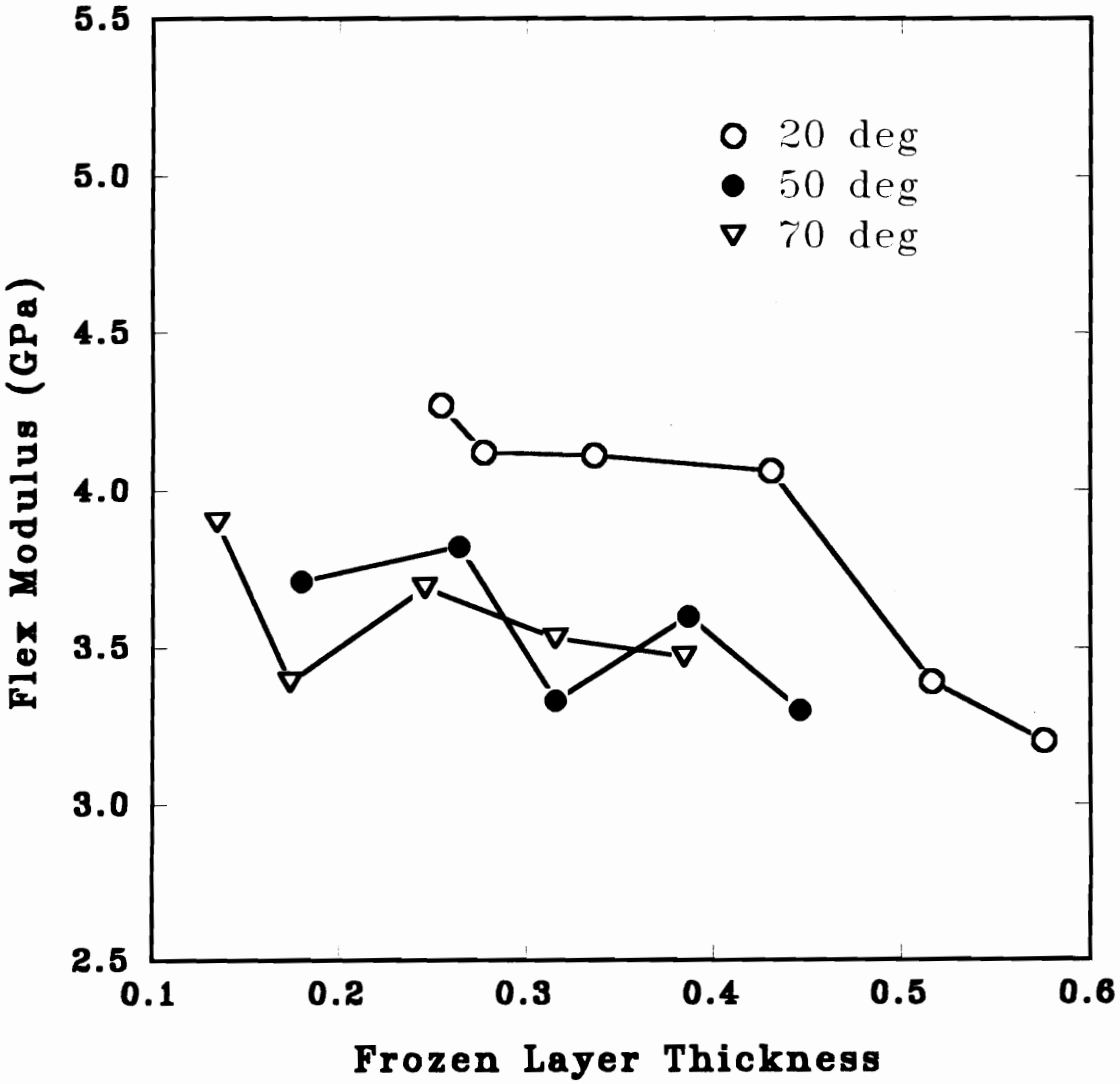

Fig. A-2 Flexural modulus of 1.0 mm thick plaque of PP(MAP)/VB 70(10)/30 versus the frozen layer thickness.

Vita

The author was born in Philadelphia, PA on August 19, 1956. After attending Penn State and graduating with a B.S. in chemical engineering, he joined DuPont. During his twelve years with DuPont, he worked as process engineer in nylon fiber spinning, manufacturing supervisor during the startup of the Kevlar expansion plant, and process / process control engineer in the Kevlar polymer area. After attending a four year part-time program, he received a M.S. in chemical engineering in 1990 from the University of Virginia. In a quest for more knowledge related to polymer science and engineering and with little regard for family stress, he moved his wife and two girls to Blacksburg where he pursued a doctorate in chemical engineering.